UNIVERSIDADE DA CORUÑA

E.T.S.E. CAMIÑOS, CANAIS E PORTOS

Ph.D. Dissertation

Civil Engineering Ph.D. Program

NUMERICAL MODELS OF DIFFUSION AND SORPTION THROUGH THE OPALINUS AND CALLOVO-OXFORDIAN CLAYS

Presented by **Acacia Naves**

Supervised by **Javier Samper**

A Coruña (Spain), April 2011

UNIVERSIDADE DA CORUÑA

E.T.S.E. CAMIÑOS, CANAIS E PORTOS

Tesis Doctoral

Programa de Doctorado de Ingeniería Civil

MODELOS NUMÉRICOS DE DIFUSIÓN Y SORCIÓN EN LAS FORMACIONES ARCILLOSAS OPALINUS CLAY Y CALLOVO-OXFORDIAN CLAY

Presentada por **Acacia Naves García-Rendueles**

Bajo la dirección de **Javier Samper Calvete**

A Coruña, Abril 2011

NUMERICAL MODELS OF DIFFUSION AND SORPTION THROUGH THE OPALINUS AND CALLOVO-OXFORDIAN CLAYS

ABSTRACT

Opalinus and Callovo-Oxfordian clays are being considered as potential host rocks for a deep geological repository of radioactive waste. The diffusion and retention of radionuclides through these argillaceous formations are relevant to assess the performance of the repository. Most of the experimental work in this field has focused on laboratory experiments performed on small samples. In situ diffusion experiments are performed at underground research laboratories to overcome the limitations of laboratory diffusion experiments and to investigate possible scale effects.

Numerical models of different complexity have been used in this dissertation to interpret the field data of the DI-B, DIR and DR in situ diffusion experiments. Dimensionless sensitivities of tracer concentrations have been computed numerically in a systematic and comprehensive manner for different tracers. Computed sensitivities have been used to identify which parameters can be estimated with the least uncertainty from tracer dilution and overcoring data. The main conclusions of the sensitivity analyses include: Tracer concentrations are sensitive to all key parameters. Computed sensitivities are tracer dependent and vary with time. Computed concentrations in the borehole are much less sensitive to changes in model parameters that concentrations along the profiles. The role of anisotropy depends on the design of the experiment and the geological formation.

Synthetic experiments generated with prescribed known parameters have been interpreted automatically with INVERSE-CORE^{2D} and used to determine parameter identifiability in the presence of random errors. They have been used also to evaluate the relevance of experimental uncertainties in the volume of water of the injection system, the presence of the filter and an excavation disturbed zone (EdZ) and those arising from the sampling methods. The main conclusions of the identifiability analyses include: Data noise makes difficult the estimation of clay parameters. Overcoring data allows for a more accurate estimation of the parameters of the undisturbed clay than the tracer dilution data. Small errors in the volume of the circulation system do not affect significantly the estimates of clay parameters. The proper interpretation of in situ diffusion experiments requires accounting for the filter and the EdZ. The effect of water sampling on the relative tracer concentrations depends on the sampling methodology and frequency, the volume of the samples and the volume of the circulation system. These effects of sampling are different in the DIR and DR experiments. These effects should not be neglected without a careful in-depth analysis of the experiment design. The impact on estimates of potential errors on the vertical location of the sampling profiles has been evaluated using actual data of overcoring samples of the DR experiment

for HTO and $^{22}Na^{+}$. Model results indicate that a shift of 2 cm in the vertical position may introduce large errors on parameter estimates.

In addition, conceptual and numerical models of radionuclide diffusion and sorption around the high-level radioactive waste repository have been evaluated for HTO, $^{36}Cl^{-}$, $^{133}Cs^{+}$ and ^{238}U. The following models have been tested: 1) 1D transport perpendicular to the axes of the disposal cells; 2) 1D axisymmetric transport around disposal cells for bounded and unbounded domains (they account for or disregard the boundary effect of the neighbor cell); 3) 2D transport through vertical planes; and 4) 1D vertical transport from the disposal cells into the overlying Oxfordian formation. It can be concluded from the model results that the 1D unbounded model is always acceptable for ^{238}U. It is valid for $^{133}Cs^{+}$ for $t < 10^{4}$ years and for HTO and $^{36}Cl^{-}$ only for $t < 10^{3}$ years where t is the time from the radionuclide release. Computed concentrations with the 1D parallel and the 1D axisymmetric models are markedly different and, therefore, the use of the 1D parallel model for the long-term modeling of radionuclide migration from the repository should be avoided. The 1D vertical model is valid only for conservative radionuclides released instantaneously and leads always to large errors for all radionuclides for a constant concentration.

MODELOS NUMÉRICOS DE DIFUSIÓN Y SORCIÓN EN LAS FORMACIONES ARCILLOSAS OPALINUS CLAY Y CALLOVO-OXFORDIAN CLAY

RESUMEN

Las formaciones arcillosas Opalinus y Callovo-Oxfordian se consideran posibles ubicaciones para albergar un almacenamiento geológico profundo (AGP) de residuos radioactivos. La comprensión de los procesos de difusión y sorción que tienen lugar en estas arcillas es fundamental para la viabilidad y seguridad del AGP. La mayoría de los estudios realizados consisten en ensayos de laboratorio con pequeñas muestras. Los ensayos de difusión in situ que se realizan en los laboratorios subterráneos pretenden superar las limitaciones de los ensayos de laboratorio y estudiar posibles efectos de escala.

En esta tesis se han interpretado con modelos numéricos de diferente complejidad los experimentos de difusión in situ DI-B, DIR y DR. Se han realizado análisis de sensibilidad de las concentraciones de diferentes trazadores a la variación de los parámetros del modelo. A partir de las sensibilidades calculadas se han identificado los parámetros que se pueden estimar con menor incertidumbre a partir de los datos de dilución y de los perfiles de concentraciones medidos en la formación. Las principales conclusiones de los análisis de sensibilidad son: Las concentraciones de un trazador son sensibles a todos los parámetros fundamentales del modelo. Las sensibilidades calculadas dependen del tipo de trazador y varían con el tiempo. Las concentraciones calculadas en el sondeo son mucho menos sensibles a la variación de los parámetros que las concentraciones calculadas en la formación. El papel de la anisotropía depende del diseño del experimento y de la formación geológica.

Se han interpretado automáticamente con el código INVERSE-CORE^{2D} ensayos sintéticos de características similares a los reales y con valores conocidos de los parámetros, para analizar la identificabilidad de los parámetros del modelo a partir de datos con errores. También se han utilizado para evaluar la importancia de las incertidumbres del ensayo, como el volumen total de agua en el sistema, la existencia de una zona alterada por la perforación del sondeo o el efecto del muestreo. Las principales conclusiones de los análisis de identificabilidad son: Los errores en los datos dificultan la estimación de los parámetros de la arcilla a partir de los datos de dilución en el sondeo. Los datos medidos en la formación permiten una estimación más precisa de los parámetros que los datos de dilución. Pequeños errores en el volumen del sistema no afectan significativamente la estimación de los parámetros. Una interpretación adecuada de los ensayos in situ requiere tener en cuenta el filtro y una zona alterada por la perforación del sondeo (EdZ). El efecto del muestreo en las concentraciones depende del método y frecuencia de muestreo, del volumen de las muestras y

del volumen del sistema de recirculación. Se han obtenido conclusiones opuestas acerca de la influencia del muestreo para los experimentos DR y DIR, por lo que ésta no se debe despreciar sin un estudio en profundidad en el que se tenga en cuenta el diseño del ensayo. Se evaluaron también la influencia en los parámetros estimados de posibles errores en la profundidad de los perfiles. Los resultados de las simulaciones realizadas indican que una desviación de 2 cm en la profundidad introduciría importantes errores en los valores estimados de los parámetros.

Además, se han evaluado varios modelos conceptuales de la difusión y sorción de radionucleidos desde un AGP en una formación de este tipo para el HTO, $^{36}Cl^-$, $^{133}Cs^+$ y ^{238}U. Los modelos analizados son los siguientes: 1) Modelo 1D perpendicular a los ejes de las celdas de almacenamiento; 2) Modelo 1D radial alrededor de las celdas para dominios finitos o semi-infinitos, teniendo en cuenta o no el efecto de borde de las celdas vecinas; 3) Modelo 2D a través de planos verticales; y 4) Modelo 1D vertical desde las celdas hacia la formación situada sobre las arcillas. De los resultados de los modelos se puede concluir que: El modelo 1D radial semi-infinito es aceptable siempre para el ^{238}U, para el $^{133}Cs^+$ con $t < 10^4$ años y para el HTO y el $^{36}Cl^-$ si $t < 10^3$ años, donde t es el tiempo desde la liberación de los radionucleidos. Las concentraciones calculadas con los modelos 1D paralelo y 1D radial son muy diferentes, por lo que se deben evitar los modelos 1D paralelos en la simulación a largo plazo de la migración de radionucleidos. El modelo 1D vertical sólo es válido en el caso de un pulso de un radionucleido conservativo, sin embargo lleva a errores importantes en el caso de una liberación constante de cualquier radionucleido.

.

MODELOS NUMÉRICOS DE DIFUSIÓN E SORCIÓN NAS FORMACIÓNS ARXILOSAS OPALINUS CLAY E CALLOVO-OXFORDIAN CLAY

RESUMO

As formacións Opalinus Clay e Callovo-Oxfordian Clay considéranse posibles localizacións para aloxar un almacenamento xeolóxico profundo (AXP) de residuos radioactivos. A comprensión dos procesos de difusión e sorción que teñen lugar nestas arxilas é fundamental para a viabilidade e seguridade do AXP. A maioría dos estudos realizados consisten en ensaios de laboratorio con pequenas mostras. Os ensaios de difusión in situ que se realizan nos laboratorios subterráneos pretenden superar as limitacións dos ensaios de laboratorio e estudar posibles efectos de escala.

Nesta teses interpretáronse con modelos numéricos de diferente complexidade os experimentos de difusión in situ DI-B, DIR e DR. Realizáronse análises de sensibilidade das concentracións de diferentes trazadores á variación dos parámetros do modelo. A partir das sensibilidades calculadas identificáronse os parámetros que se poden estimar con menor incerteza a partir dos datos da dilución e dos perfís de concentracións medidos na formación. As principais conclusións das análises de sensibilidade son: As concentracións dun trazador son sensibles a todos os parámetros fundamentais do modelo. As sensibilidades calculadas dependen do tipo de trazador e varían co tempo. As concentracións calculadas na sondaxe son moito menos sensibles á variación dos parámetros que as concentracións calculadas na formación. O papel da anisotropía depende do deseño do experimento e da formación xeolóxica.

Interpretáronse automaticamente co código INVERSE-CORE^{2D} ensaios sintéticos de características similares aos reais e con valores coñecidos dos parámetros, para analizar a identificabilidade dos parámetros do modelo a partir de datos con erros. Tamén se utilizaron para avaliar a importancia das incertezas do ensaio, como o volume total da auga no sistema, a existencia dunha zona alterada pola perforación da sondaxe ou o efecto da mostraxe. As principais conclusións das análises de identificabilidade son: Os erros nos datos dificultan a estimación dos parámetros da arxila a partir dos datos da dilución na sondaxe. Os datos medidos na formación permiten unha estimación máis precisa dos parámetros que os datos da dilución. Pequenos erros no volume do sistema non afectan significativamente a estimación dos parámetros. Unha interpretación adecuada dos ensaios in situ require ter en conta o filtro e unha zona alterada pola perforación da sondaxe (EdZ). O efecto da mostraxe nas concentracións depende do método e frecuencia de mostraxe, do volume das mostras e do volume do sistema de recirculación. Obtivéronse conclusións opostas acerca da influencia da mostraxe para os experimentos DR e DIR, polo que ésta non se debe desprezar sen un estudo en profundidade no que se teña en conta o deseño do ensaio. Avaliáronse

tamén a influencia nos parámetros estimados de posibles erros na profundidade dos perfís. Os resultados das simulacións realizadas indican que unha desviación de 2 cm na profundidade introduciría importantes erros nos valores estimados dos parámetros.

Ademais, avaliáronse varios modelos conceptuais da difusión e sorción de radionucleidos desde un AXP nunha formación deste tipo para o HTO, $^{36}Cl^{-}$, $^{133}Cs^{+}$ e ^{238}U. Os seguintes modelos foron analizados: 1) Modelo 1D perpendicular aos eixos das celas de almacenamento; 2) Modelo 1D radial ao redor das celas para dominios finitos ou semi-infinitos, tendo en conta ou non o efecto de bordo das celas veciñas; 3) Modelo 2D a través de planos verticais; e 4) Modelo 1D vertical desde as celas cara á formación situada sobre as arxilas. Dos resultados dos modelos pódese concluír que: O modelo 1D radial semi-infinito é aceptable sempre para o ^{238}U, para o $^{133}Cs^{+}$ con $t < 10^4$ anos e para o HTO e o $^{36}Cl^{-}$ se $t < 10^3$ anos, onde t é o tempo desde a liberación dos radionucleidos. As concentracións calculadas cos modelos 1D paralelo e 1D radial son moi diferentes, polo que se deben evitar os modelos 1D paralelos na simulación a longo prazo da migración de radionucleidos. O modelo 1D vertical só é válido no caso dun pulso dun radionucleido conservativo, por outra banda leva a erros importantes no caso dunha liberación constante de calquera radionucleido.

ACKNOWLEDGMENTS

First of all, I would like to thank Professor Javier Samper for the opportunity he provided me to join his research group and performing this dissertation under his supervision. It has been a pleasure and an honor to work with him. Day by day, I have learned hydrogeology from him, but I have learned from his way of working, his effort, his patience and his good taste in well done job. I am convinced that working in this group during the last 8 years have made me grow as a scientist and as a person.

Most of the research presented in this dissertation has been performed within the framework of research projects funded by the European Commission (project FUNMIG), ENRESA (project DI-B), ANDRA (project DIR-MOD), the Consortium of Mont Terri (project DR) and the CICYT (project CGL2006-09080 which had a research scholarship associated). I am grateful for the good job and the support provided by the researchers of other agencies involved in the projects. Among them, I would like to recognize especially Sarah Dewonck and Thomas Gimmi who gave me the opportunity to spend 4 months in their research centers at Bure (France) and PSI (Switzerland), respectively. My stays in France and Switzerland have been very enriching experiences both professionally and personally. They would not have been possible without the collaboration of ANDRA, the PSI and my colleagues in Bure and Willingen.

I would like to thank also all the colleagues with whom I have worked the last five years: Bruno, Alba, Yanmei and Luis, who have lived through the end of this thesis; Jorge Molinero, Changbing, Liange, Mercedes, Chuanhe, Santiago, Diego, Shuping and Hongyun who have been part of our research group in the past; colleagues and friends of the Engineering School with whom I have shared these days.

Finally, I would like to dedicate this dissertation to my friends and, above all, to Jose and my family. You are the best that I have.

AGRADECIMIENTOS

En primer lugar querría agradecer a Javier Samper la oportunidad de trabajar en el grupo de investigación que dirige y de realizar esta tesis doctoral. Ha sido un placer y un honor trabajar con él. Año a año he aprendido hidrogeología a su lado, pero también he aprendido de su modo de trabajar, su esfuerzo, su paciencia y su gusto por el trabajo bien hecho. Estoy convencida que la convivencia con él durante los últimos 8 años me han hecho crecer como científica y como persona.

Este trabajo de investigación aquí presentado ha sido desarrollado en el marco de proyectos de investigación financiados por la Comisión Europea (Proyecto FUNMIG), ENRESA (Proyecto DI-B), ANDRA (Proyecto DIR-MOD), el Consorcio Internacional de Mont Terri (Proyecto DR) y la CICYT (Proyecto CGL2006-09080 al que se le asignó una beca FPI que disfruté durante los últimos cuatro años).

Se agradece el buen hacer y el apoyo facilitado por los investigadores de otros organismos participantes en los proyectos. Entre ellos querría hacer un reconocimiento especial a Sarah Dewonck y Thomas Gimmi que me dieron la oportunidad de integrarme en sus centros durante 4 meses en Francia y en Suiza. Han sido dos experiencias muy enriquecedoras tanto en lo profesional como en lo personal, que no hubieran sido posibles sin la colaboración de ANDRA, el PSI y de mis compañeros en Bure y en Villingen.

También quiero agradecer su colaboración y apoyo a todos los compañeros con los que he convivido durante estos años. A Bruno, Alba, Yanmei y Luis, que han vivido este final de tesis. A los que han formado parte del el grupo y ya no están: Jorge Molinero, Changbing Yang, Liange, Mercedes, Chuanhe, Santiago, Diego, Shuping y Hongyun. Los compañeros y amigos de la Escuela con los que comparto el día a día.

Por último, dedico esta tesis a mis amigos y, sobretodo, a Jose y a mi familia. Sois lo mejor que tengo.

INDEX

NUMERICAL MODELS OF DIFFUSION AND SORPTION THROUGH THE OPALINUS AND CALLOVO-OXFORDIAN CLAYS

1. Introduction and state-of-the-art

Argillaceous formations are being considered as potential host rocks for the deep geological disposal of radioactive waste. The assesment of the performance of such host rocks as geological barriers requires understanding and quantifying radionuclide transport through them. Therefore, careful laboratory, modeling and field studies are required.

Various experimental programs are being carried out at the Mont Terri Underground Research Laboratory (URL) in Switzerland and at the Meuse/Haute-Marne URL in France to study the feasibility of the Opalinus Clay and Callovo-Oxfordian Clay formations to host a radioactive waste repository. Such programs aim at analyzing the hydrogeological, geochemical and rock mechanical properties of the argillaceous formation, evaluating the changes of these properties induced by the excavation of galleries and improving the investigation techniques. Their results are important inputs for evaluating the feasibility and safety of a geological repository for radioactive waste in overconsolidated clay formations.

Clay media usually exhibit extremely low hydraulic conductivities and therefore solute diffusion is the most relevant transport mechanism. A brief review of solute diffusion through clay formations is presented in Appendix 1.

Diffusion and sorption laboratory experiments have enlarged our understanding of these mechanisms and provided a wealth of data on diffusion and sorption parameters. These experiments are often performed on small samples up to 1 cm which may have suffered alterations during their preparation. To overcome the limitations of laboratory experiments and to investigate possible scale effect, various in situ diffusion experiments have been performed at underground laboratories.

In situ diffusion experiments are often carried out in packed-off sections of a borehole. A porous filter is located in the interval which is connected by the flow lines to the gallery of the URL. There, the surface equipment consists in a circuit with a reservoir that allows tracer injection and sampling. The reservoir has a pressure control device to maintain pressure similar to that of local porewater and to prevent any flow between the test interval and the rock surrounding the interval. The system is filled with synthetic water which is continuously circulated by means of a gear pump. Tracers are injected into the system. Then, their dilution is monitored by taking periodic aliquots (dilution data). At the end of the experiment, a volume of rock around the injection interval, where the tracers are expected to have diffused, is removed by overcoring the borehole. The overcore is cut into pieces to collect undisturbed centimeter-sized rock samples in which tracer concentration is measured at the laboratory (overcoring data). Numerical models of in situ diffusion experiments are needed to interpret the dilution and overcoring data and derive diffusion and sorption parameters. Appendix 2 presents a state-of-the-art of the in situ diffusion experiments performed so far within the framework of both experimental programs and the numerical models related to them. Such

compilation is useful to provide the background and the general context of the numerical models developed in this dissertation to interpret the DI-B, the DIR and the DR experiments.

The DI-B experiment was performed to study the transport and retention properties of non-radioactive tracers in Opalinus Clay. It was performed in a borehole drilled in the DI niche at Mont Terri URL. At this location, the bedding dips 32º to the SE. Synthetic porewater of similar composition to porewater was circulated during approximately 5 months to ensure that the solution chemistry and pressure were in equilibrium with the rock. After that, four tracers were injected: HDO, I^-, $^6Li^+$ and $^{87}Rb^+$. The experiment lasted for 417 days. Twelve subcores were drilled from the overcore with different depths and directions and each one was sliced into 1 cm thick samples.

The DIR program includes seven in situ diffusion experiments performed in vertical boreholes at the Bure URL. The DIR in situ diffusion experiments (DIR2001, DIR2002, DIR2003, DIR1001, DIR1002 and DIR1003) were performed as single point dilution tests by injecting tracers into a 1 m long packed-off section of the boreholes. 10 L of synthetic water of similar composition to that expected in the formation were continuously circulated in the system. Once the chemical equilibrium between the synthetic water and porewater was reached, the following tracers were injected: HTO, $^{36}Cl^-$, $^{125}I^-$, $^{22}Na^+$, $^{85}Sr^+$, $^{75}Se^{2+}$ and $^{134}Cs^+$. The decrease of tracer concentrations in the system was monitored for about a year. The design of the EST208 experiment differs from the DIR experiments. EST208 is being performed in a ~550 m deep borehole drilled from ground surface. The set up of the experiment was adapted for this kind of borehole having a 10 m long packed diffusion interval and two hydraulic lines for flux circulation. The system was filled with ~192 L synthetic porewater that has been circulated for several months reaching chemical equilibrium with the formation. HTO, $^{36}Cl^-$ and $^{134}Cs^+$ were injected. Due to the design of the experiment, the overcoring of the rock around the injection interval is not feasible in this case and only dilution data are available.

The DR experiment was performed in a borehole drilled in the DR niche at the Mont Terri URL. The borehole was drilled at an angle of 45º with respect to the tunnel bottom, so it is normal to the bedding. The experiment design was optimized to determine in situ the diffusion anisotropy, having two 15 cm test intervals and a duration between 3 and 4 years. Each injection interval was connected to a surface equipment filled with 30 L of artificial porewater. The following tracers were injected in the upper borehole interval: HDO, $^{60}Co^{2+}$, $^{137}Cs^+$, $^{133}Ba^{2+}$ and $^{152}Eu^{3+}$. Tracers injected in the lower borehole interval include: HTO, I^- (stable), Br^- (stable), $^{22}Na^+$, $^{85}Sr^{2+}$, ^{18}O (water) and $^{75}Se^{4+}$.

2. Methodology

Numerical models of different complexity have been used to interpret the dilution and overcoring data of the DI-B, DIR and DR experiments and derived diffusion parameters.

Model results depend on parameters that may contain uncertainties. Furthermore, the interpretation of diffusion experiments is complicated by several potentially-disturbing effects caused by the presence of the sintered filter, the gap between the filter and the borehole wall and possibly an excavation disturbed zone, EdZ. Dimensionless sensitivities of tracer concentrations in the injection interval and along the overcoring profiles have been computed numerically for tracers

of different characteristics. They have been used to identify the tracer parameters that can be best estimated from tracer dilution or overcoring data.

Synthetic experiments having the same geometric properties as the real experiments have been interpreted and used also to ascertain parameter identifiability in the presence of random errors and to evaluate the effect of experimental uncertainties.

Conceptual and numerical models of radionuclide diffusion and sorption around a high-level radioactive waste repository have been developed and evaluated with the aim of identifying which are the most appropriate assumptions and simplifications.

More details about the objectives and the methodology used in this dissertation can be found in the Appendixes 3 to 10. In the publications involving several authors (Appendix 3 to 6 and 10), the specific contributions of the author of this dissertation are clearly indicated in the front page of each appendix.

3. Conclusions and contributions on the numerical modeling and interpretation of the DI-B experiment

At the end of the DI-B experiment, dilution and overcoring a data were available. Rock samples were taken to obtain concentration profiles at different depths and directions: horizontal and parallel to the bedding, horizontal and across the bedding, perpendicular to the bedding and vertical from the bottom of the borehole. Measured tracer distributions confirmed that the anisotropy in diffusion, which had been previously identified in laboratory experiments, can be observed also in this in situ experiment. Diffusion is fastest and extends furthest along planes parallel to bedding while the slowest diffusion is along the direction perpendicular to bedding.

Contrary to the methods commonly used for the interpretation of in situ experiments which rely on 2-D models and disregard diffusion across bedding, the DI-B experiment was modeled using a fully 3-D anisotropic finite element model which accounts for the anisotropic behavior of diffusion and imposes no restriction for diffusion across the bedding (see Appendix 3). CORE^{3D} was used to simulate the experiment. Model parameters were calibrated by a trial and error method by fitting the model results to measured dilution and overcoring data for HDO and I-. The model provides reliable estimates of effective diffusion coefficients (D_e) and accessible porosities (ϕ_{acc}) for both tracers which are within the range of published values. The numerical model reproduces the general trend of measured data in the borehole and along profiles. However, computed profiles perpendicular to bedding slightly overestimate measured data. It was not possible to improve this fit by varying diffusion parameters without spoiling the fit of the rest of the profiles. Since the influence of anisotropy ratio increases proportional to the angle between the bedding plane and the profile, it has been found that the fit improves for these profiles when the angle decreases 20º (Appendix 4). A sensitivity analysis of the concentrations to changes in key transport parameters was performed to evaluate parameter uncertainties (Appendix 3). The results of the sensitivity runs were expressed in terms of normalized relative sensitivities. Computed concentrations in the borehole are much less sensitive to changes in model parameters than concentrations along overcoring profiles. Computed

concentrations close to the borehole are most sensitive to the accessible porosity while concentrations at distances greater than 0.085 m are most sensitive to the diffusion coefficient parallel to the bedding. Computed concentrations along some profiles are sensitive to the effective diffusion perpendicular to bedding.

$^{6}Li^{+}$ and $^{87}Rb^{+}$ measured concentrations along profiles present strong fluctuations. Thus, the calibration of diffusion parameters was performed from dilution data only (Appendix 4). $^{6}Li^{+}$ behaves in the Opalinus Clay as a weakly-sorbing tracer and the derived parameters agree well with those obtained previously for Na^{+} in Mont Terri. The $^{87}Rb^{+}$ data in the dilution curve shows a lot of fluctuation and do not allow the determination of a unique set of transport and sorption parameters, although a strong sorption has been confirmed.

It has been shown that a simple 2-D model can be safely used to interpret data along central profiles although it may lead to biased estimates when applied to profiles located near the edges of the test interval. Model results have been compared to those computed with a 2-D model performed by J.M. Soler who used CRUNCH. Both models agree in general. However, there are differences in the results of both models which may be due to differences in the geometry (3D / 2D) and the method used to compare model results and the experimental data.

Additional details of the model and the conclusions are presented in Appendices 3 and 4. The papers included in these appendixes are the result of a joint research work containing the contributions from other researchers. My contribution to them includes: The predictive calculations, the sensitivity runs and the parameter calibration for all the tracers performed with the three-dimensional approach using $CORE^{3D}$.

4. Conclusions and contributions on numerical modeling and interpretation of the DIR experiments

Numerical interpretation of the DIR experiments requires the use of 3D models due to the diffusion anisotropy. However, symmetry with respect to the borehole axis allows the use of 2D axi-symmetric models. The relevance of anisotropy for the DIR experiments was unknown a priori and was ascertained with a 2D axisymmetric anisotropic numerical model. The results of the simulations showed that a 1D axisymmetric model can be safely used to interpret tracer dilution data because they are not sensitive to diffusion anisotropy (Appendix 5). On the other hand, the interpretation of the DIR experiments is complicated by several non-ideal effects caused by the presence of a sintered filter, a gap between the filter and borehole wall and an excavation disturbed zone (EdZ). The relevance of such non-ideal effects and their impact on estimated clay parameters was evaluated. Previous studies indicated that tracer dilution curves of in situ DIR experiments cannot be reproduced unless an EdZ is considered. The effect of the filter and the gap was analyzed by comparing tracer dilution curve computed with a detail model which accounts for filter and gap with that computed with a simplified model that does not accounts for them. Failing to account for the filter and the gap may result in significant errors in tracer concentrations.

The extracted samples are replaced with the same volume of synthetic unspiked water. The effect of water sampling is commonly disregarded during the numerical interpretation of such experiments, although it may induce changes in the tracer concentrations and errors in the parameter estimates. Such errors have been analyzed for different tracers of the DIR2003 and EST208 experiments with different geometries and sampling methods by using a numerical model which accounts for sample extraction and sample volume replacement (Appendix 9). The effect of water sampling on the relative tracer concentrations depends on the sampling frequency, the volume of the samples and the volume of the circulation system. Anionic tracers are the most affected by sampling while sorbing tracers are the least influenced. It has been found that water sampling in these experiments may lead to a significant overestimation of diffusion and sorption parameters for the EST208 experiment, and therefore cannot be disregarded.

Normalized dimensionless sensitivities of tracer concentrations at the test interval have been computed numerically (Appendix 5). Tracer concentrations have been found to be sensitive to all key parameters. Sensitivities are tracer dependent and vary with time. Sensitivities have been used to identify which are the parameters that can be estimated with less uncertainty and find the times at which tracer concentrations begin to be sensitive to each parameter. Synthetic experiments having similar parameters and geometry as the real DIR experiments were interpreted automatically with INVERSE-CORE^{2D} and used to evaluate the relevance of non-ideal effects and ascertain parameter identifiability in the presence of random measurement errors. The identifiability analysis of synthetic experiments revealed that data noise makes difficult the estimation of clay parameters. Parameters of the clay and the EdZ cannot be estimated simultaneously from noisy dilution data. Models which disregard the EdZ fail to reproduce synthetic data. The proper interpretation of in situ diffusion experiments requires accounting for the filter, the gap and the EdZ. The estimates of the D_e and the ϕ_{acc} of the clay are highly correlated, indicating that these parameters cannot be estimated simultaneously. The accurate estimation of the D_e and the porosities of the clay and the EdZ is only possible when the standard deviation of the random noise is less than 0.01. Small errors in the volume of the circulation system do not affect the clay parameter estimates. Normalized sensitivities as well as the identifiability analysis of synthetic experiments provided additional insight on the inverse estimation of these diffusion experiments which will facilitate the interpretation of the actual DIR data (not presented in this dissertation).

Additional details of the models and their conclusions are presented in Appendices 5 and 9. The paper included in Appendix 5 is the result of a joint research effort with the contributions from other researchers. My main contribution included: the development of the 2D and 1D forward models, the sensitivity analyses to changes in model parameters and the evaluation of the non-ideal effects in the tracer concentrations and the estimation errors. All the modeling tasks presented in the Appendix 9 were performed by the author of this dissertation with the supervision of her advisor Javier Samper and Sarah Dewonck, who was her co-advisor during her stay at the Meuse/Haute-Marne URL.

5. Conclusions and contributions on numerical modeling and interpretation of the DR experiment

The numerical interpretation of the DR experiment has been performed by using 2D axis-symmetric models which account for the non-ideal effects caused by the sintered filter, the gap between the filter and the borehole wall and the EdZ. Dimensionless sensitivities of tracer concentrations in the injection interval and along the overcoring profiles have been computed numerically for conservative (HDO/ HTO), anionic (Br^-/ I^-), weakly-sorbing ($^{22}Na^+$, $^{133}Ba^{2+}$ and $^{85}Sr^+$) and strongly-sorbing tracers ($^{137}Cs^+$, Cs^+ and $^{60}Co^{2+}$) (Appendix 6). Average relative sensitivities have been computed in a systematic and comprehensive manner for different parameters, tracers and for dilution and overcoring data. Computed sensitivities are tracer dependent, vary with time and are different among different profiles. They have been used to identify which parameters can be estimated with the least uncertainty from tracer dilution and overcoring data. Contrary to dilution data, concentrations along overcoring profiles are sensitive to the effective diffusion normal to the bedding.

Synthetic experiments generated with prescribed known parameters have been interpreted automatically with INVERSE-CORE^{2D} and used to determine parameter identifiability in the presence of random errors and to evaluate the relevance of experimental uncertainties. The identifiability analysis was performed first for HTO and $^{22}Na^+$ from either dilution or overcoring data (Appendix 6). Model results revealed that data noise makes difficult the estimation of undisturbed clay when the tracer dilution data contain noise. Although the parameters of the undisturbed clay and the EdZ cannot be estimated using tracer dilution data, their joint estimation from overcoring noisy data is possible for standard deviations of the noise (σ) up to 0.05. The diffusion anisotropy can be estimated from overcoring data but cannot be estimated from dilution data. Overcoring data allow a more accurate estimation of the parameters of the undisturbed clay than the tracer dilution data. Similar conclusions have been obtained from the identifiability analysis for anionic tracers (not presented in this dissertation). On the contrary, the analysis for strongly sorbing tracers has shown that the parameters of the undisturbed clay cannot be estimated (Appendix 7). Clearly, the noise on data introduces a bias in estimates and the K_d and the D_e of the EdZ cannot be estimated simultaneously from dilution data with $\sigma > 0.05$. The estimates obtained from overcoring data are less affected by data noise than those derived from dilution data.

At the end of the in situ DR experiment both dilution and overcoring data are available. Therefore, the identifiability analysis was improved for HTO and $^{22}Na^+$ by using simultaneously both types of data (Appendix 8). The use of both types of data improves the results derived from only dilution data by reducing estimation errors and allowing the estimation of the diffusion anisotropy and the joint estimation of the parameters of the clay and the EdZ. Synthetic experiments were also used to evaluate the effect of other uncertainties related to the volume of the water in the injection system, V, the D_e of the filter and the existence of an EdZ. Small errors in the volume of the circulation system do not affect significantly the estimates of the clay parameters. The proper interpretation of the in situ DR experiments requires accounting for the filter and the EdZ. Uncertainties in the D_e of the filter lead to significant estimation errors when the inverse runs are

performed from only dilution data. When overcoring data are also used, the effect of the uncertainty in the D_e of the filter is negligible.

It has been found that the conclusions of the parameter identifiability analysis are not affected by the particular sequence of random noise added to synthetic data (Appendix 8). Therefore, they can be extrapolated directly to the interpretation of the actual DR experiment.

The impact on estimates of potential errors on the vertical location of the sampling profiles has been evaluated using actual data of the overcoring samples of the DR experiments for HTO and $^{22}Na^{+}$. Model results indicate that a shift of 2 cm in the vertical position may introduce large errors on parameter estimates.

The effect of water sampling in the tracer concentrations and the parameter estimates has been analyzed for the DR experiment (Appendix 9). In the sampling method used in the Mont Terri URL, sampling volumes are not replaced after aliquoting the solution. In this case, there is no tracer dilution, but the volume in the circulation decreases with time progressively. The effect of water sampling has been computed by using a numerical model which accounts for sample extraction and the changes in the volume of the circulation system. It has been found that water sampling in the DR experiments causes minor changes in the relative tracer concentrations and its effects can be disregarded. This conclusion differs from that derived for the DIR2003 and EST208 experiments and illustrates that the effects of the water sampling should not be neglected without a careful in-depth analysis of the experimental design.

Additional details of the models and their conclusions can be found in Appendices 6, 7, 8 and 9. The paper included in Appendix 6 is the result of a joint research work with the contributions from other researchers. My main contribution included: the development of the numerical model and the sensitivity analysis for the strongly-sorbing tracers. The contents of the other three appendixes have been developed entirely by the author of this dissertation under the supervision of my advisor.

6. Conclusions and contributions on the conceptual and numerical models of solute diffusion and sorption around a HLW repository in clay

The reactive transport models used to simulate solute diffusion and the long-term hydrochemical evolution around radioactive waste repositories often rely on simplifications of the geometry and dimensionality of the problem. On the other hand, detailed three-dimensional flow and transport models are used which often oversimplify the geochemical reactions. Conceptual and numerical models of radionuclide diffusion and sorption around a repository in clay have been developed with the aim of identifying which are the most appropriate assumptions and simplifications (see Appendix 10). The following models of increasing dimensionality have been analyzed: 1) 1D transport perpendicular to the axes of the disposal cells; 2) 1D axisymmetric transport around disposal cells for bounded and unbounded domains (they account for or disregard the boundary effect of the neighbor cell); 3) 2D transport through vertical planes; and 4) 1D vertical transport from the disposal cells into the overlying Oxfordian formation. Model results have been compared for simulation times up to 10^6 years and for the following radionuclides and tracers: HTO,

which is treated here as an ideal and conservative tracer (radioactive decay is neglected), $^{36}Cl^-$ which experiences anion exclusion, $^{133}Cs^+$ which sorbs moderately and ^{238}U which shows a strong sorption capacity. Radionuclides are released into the disposal cell either at a fixed concentration or as an instantaneous unit pulse. There are several stages in the time evolution of radionuclide migration from the disposal cell through the formation. Radionuclides diffuse from the disposal cell into the clay in the first stage in an axisymmetric pattern. This stage lasts until the radionuclide arrives to the middle point between two adjacent cells. Axial symmetry vanishes in the second stage when the radionuclides migrate both in the horizontal and the vertical directions. The third stage takes place at late times when radionuclide migration is mostly vertical and can be approximated with a 1D vertical grid. Model results indicate that the 1D unbounded model is always acceptable for ^{238}U and is valid for $^{133}Cs^+$ for $t < 10^4$ years (where t is the time from the radionuclide release). It is valid for HTO and $^{36}Cl^-$ only for $t < 10^3$ years. These conclusions hold true for both release modes. Computed concentrations with the 1D parallel and the 1D axisymmetric models are markedly different and, therefore, the use of the 1D parallel model for the long-term modeling of radionuclide migration from the repository should be avoided. The 1D vertical model is valid only for conservative radionuclides released instantaneously and leads always to large errors for all radionuclides for a constant concentration.

Additional details of the models and their conclusions are presented in more detail in Appendix 10. My contribution to this Appendix included: the development of the conceptual and numerical models of radionuclide diffusion and sorption of increasing dimensionality, the simulations and the analysis of the model results.

7. Recommendations for future research

Recommendations for future work for the numerical models of in situ diffusion experiments include:

- The evaluation of the sensitivities to changes in several parameters at the same time.
- The interpretation of actual tracer data of the DR experiment using both dilution and overcoring data.
- The exploration of simple models to account for the filter, gap and EdZ, to avoid model "overparameterization".
- The use of reactive transport models to simulate and interpret in situ diffusion experiments performed with geochemically reactive tracers and for the case in which the chemistry of the injection water is changed to create a chemical disturbance.
- The evaluation of other uncertainties.

The numerical models of diffusion from a HLW repository in clay could be extended by accounting for:

- The decay of radionuclides.
- The time evolution of the geochemical conditions using reactive transport models.
- The spatial variability of clay parameters.
- The uncertainties in the boundary conditions of the Callovo Oxfordian clay formation and the porosity of the disposal cells.
- The actual 3D configuration of the repository.

APPENDIX 1

DIFFUSION IN CLAY FORMATIONS

1. SOLUTE TRANSPORT MECHANISMS

This appendix presents a brief review on molecular diffusion through argillaceous formations or media. This review is based on technical reports, manuals of reactive solute transport codes such as CORE (Yang et al., 2003) and reports about clay projects performed by the Research Group of J. Samper for ENRESA (Molinero et al., 2003).

Solute concentration changes in porous media due to several factors. The fundamental processes are advection and hydrodynamic dispersion. Solute sources and sinks, sorption and ion exchange, radioactive decay, chemical reactions and biological processes are also relevant.

Since the chemical species is dissolved in the porewater, the movement of that species depends on the water flow through the porous medium. Notice that the real velocity of the fluid is larger than the average Darcy's velocity because the medium is filled with grains which are not accessible to the fluid.

Hydrodynamic dispersion is caused by the complexity of the porous medium in which the flow takes place. It is a macroscopic process linked to the heterogeneity of the flow inside the microstructures of the formation. In fact, it is the result of the combination of mechanical dispersion and molecular diffusion.

The main interaction between the fluid and the porous medium is mechanical and, as a result of this interaction, the flow changes in magnitude and direction. The tracer particles split up continuously when they are flowing due to the stochastic nature of the porous media and to the heterogeneity of the microscopic velocities. They flow to thinner porous and take up a larger space all the time. This is known as mechanical dispersion and results in a larger spreading than that expected from the mean flow.

Molecular diffusion is caused by a heterogeneous distribution of the tracer in the fluid. Tracer molecules located in the high concentration areas tend to move towards the low concentration areas leading to for a uniform distribution. Even in stationary conditions, the concentration gradient causes the diffusion of the tracer to a larger and larger area.

While mechanical dispersion makes tracer particles move through the porous channels, molecular diffusion tends to homogenize tracer concentration along each pore and between different porous. Mechanical dispersion dominates the hydrodynamic dispersion in most of media; nevertheless molecular diffusion can prevail when the flow is extremely slow.

Argillaceous formations have very low hydraulic conductivity and groundwater flows slowly. So, molecular diffusion dominates solute transport.

2. SOLUTE DIFFUSION

2.1. Diffusion in water

Diffusion in pure water is defined by Crank (1956) as the "process by which matter is transported from one part to another as a result of random molecular motions".

The stochastic study of diffusion shows that the diffusive flux, j_D, that is the amount of ions which diffuses through a unit area per unit time, is proportional to the ion concentration in water, c_i, and the chemical potential of the ion, μ_i :

$$j_D = -k_D c_i \nabla \mu_i \quad (1)$$

where k_D is the factor of proportionality.

Developing the expression of the chemical potential gradient and considering a 1D movement, the Fick's first law is derived:

$$j_D = -D_i \nabla c_i \quad (2)$$

where D_i is the diffusion coefficient of the ion in pure water which depends on its activity coefficient, f_i, and its concentration, c_i.

$$D_i = k_D RT\left(1+\frac{d\ln f_i}{d\ln c_i}\right) \quad (3)$$

The values of the diffusion coefficient in pure water can be correlated with its ionic potential, $|z_i|/r_i$, where z_i and r_i are the electric charge and the radius of the ion (Li and Gregory, 1973). In general, the higher the ionic potential of an ion, the thicker the hydration layer around it and, therefore, the slower the diffusion.

On the other hand, Simpson and Carr (1958) proved that changes in the diffusion coefficient in water with temperature (0-100ºC) and viscosity can be properly described by the Stokes-Einstein's equation:

$$D = \frac{kT}{6\pi\eta r} \quad (4)$$

where k is the Boltzman's constant, h is the water viscosity, r is the radius of the ion and T is the temperature in ºK. The relation between the diffusion coefficients in water of an ion i at different temperatures can be deduced from:

$$\left(\frac{D_i^{0,T1}\eta}{T}\right)_{T1} = \left(\frac{D_i^{0,T2}\eta}{T}\right)_{T2} \quad (5)$$

Thus, the diffusion coefficient in water at a temperature T can be calculated from its value at a reference temperature (25ºC) and the change of water viscosity with temperature (Dorsey, 1940).

The effect of pressure on the diffusion coefficient can be related to the changes in the water viscosity (Benedek y Purcell, 1954). Moreover, there are also changes in water viscosity in the presence of high salinity solutions.

2.2. Diffusion in porous media

Fick's law in 1D can be formulated as:

$$J_A = -D_o\left(\frac{\partial C}{\partial X}\right) \tag{6}$$

where J_A is the diffusive flux, D_o is the diffusion coefficient in free water, C is the concentration and X is the distance.

Chemical species diffuse through the solutions filling the porous medium of a geological formation. They follow irregular paths along the pores and run into the porous walls. Therefore, diffusion in this context is smaller than that through the fluid in which there is not a rock matrix surrounding the solution. These processes which reduce solute diffusion are controlled by porosity, porous size distribution (constrictivity) and tortuosity of the paths.

2.3. Effective diffusion

The effective diffusion coefficient (D_e), known also as intrinsic diffusion coefficient (D_i), is the diffusion coefficient of a chemical species that does not suffer sorption and moves through the porous medium. It can be related to the diffusion coefficient in pure water through:

$$D_e = \phi\left(\frac{\chi}{\tau^2}\right)D_o = \phi D_p \tag{7}$$

where ϕ is the porosity, χ is the constrictivity, τ is the tortuosity, χ/τ^2 is the geometric factor of the porous medi um and D_p is the porewater diffusion coefficient.

Tortuosity (τ) is defined as the average ratio between the length travelled by a species through the microscopic pore channels (L) and the macroscopic distance between two points (x):

$$\tau = \frac{L}{x} \geq 1 \tag{8}$$

The effective diffusion coefficient is a property of the porous media, the porewater and the chemical species. It can be derived from diffusion experiments or calculated from known values of D_o.

It is very difficult to determine experimentally the tortuosity and the constrictivity. Therefore, some authors lump them into a geometric factor denoted by τ which sometimes can be confused with the tortuosity notation defined in Equation (8). This parameter is introduced in Equation (7) leading to:

$$D_e = \phi\tau D_o \tag{9}$$

where the geometric factor τ is always smaller than 1.

Other authors use also the diffusivity, Ψ, which depends only on the properties of the porous medium and is defined as:

$$\psi = \frac{D_e}{D_0} = \phi \frac{\chi}{\tau^2} \tag{10}$$

It should be noticed that a chemical species which suffers anion exclusion, the diffusivity depends not only on the porous medium but also on the type of chemical species.

2.4. Linear sorption

If sorption is instantaneous and linear, the sorption in isotherm can be described by the simple relation $S = K_d C$, where S is the tracer concentration in the solid phase; *C, is* the tracer concentration in the liquid phase; and K_d is the distribution coefficient. The retardation factor R is defined in terms of the distribution coefficient, the porosity and the dry density (ρ_d):

$$R = 1 + \frac{\rho_d K_d}{\phi} \qquad \longrightarrow \qquad R\phi = \phi + \rho_d K_d \tag{11}$$

The term $\phi + \rho_d K_d$ is a dimensionless parameter known as the capacity factor, α, of the porous medium.

2.5. Apparent diffusion

The apparent diffusion coefficient, D_a, is the relevant diffusion coefficient in transient diffusion experiments. D_a is related to D_e through:

$$D_a = \frac{D_e}{\phi R} = \frac{D_p}{R} = \left(\frac{\chi}{\tau^2}\right)\frac{D_o}{R} \tag{12}$$

From Equations (11) and (12) it follows that:

$$D_a = \frac{D_e}{\phi + \rho_d K_d} = \frac{D_e}{\alpha} \tag{13}$$

For a conservative species R = 1, the capacity factor is equal to the porosity and:

$$D_a = \frac{D_e}{\phi} = D_p \tag{14}$$

2.6. Accessible porosity to diffusion

Research on overconsolidated clay formations shows that the porosity available for diffusion transport can be smaller than the value determined from the water content. Accessible porosity is defined as the fraction of the total porosity available for molecular diffusion. Accessible porosity depends on the properties of the solute and the geological formation, and other environmental variables such as ionic strength and pH of the porewater.

Ion exclusion may cause that negatively-charged ions are electrostatically repelled from the vicinity of the clay surface. In addition, some ions may be excluded due to pore size, dead end or blind pores. This motivates the use of the concept of accessible porosity to diffusion.

Henrion et al. (1991) conclude from their studies of bentonite and Boom Clay that there is a reduction of the mobility of the particles when they are compacted because of changes in the porous

media. Moreover, De Preter et al. (1991) have measured in situ the accessible porosity to diffusion of the Boom Clay which is equal to 0.082 for I^- and 0.34 for HTO, while the total porosity of the formation is about 0.4. Other authors have performed measurements in other consolidated clays and obtained similar conclusions (Bourke et al., 1988; Allen et al., 1988).

3. ANION EXCLUSION

Anion exclusion refers to the deficit of anions in the vicinity of the negatively charged clay surfaces. It is also known as anionic repulsion, anionic expulsion or negative adsorption. This deficit of negative charges is caused by electrostatic interactions between anions dissolved in porewater and clay particles. Therefore, it depends on the clay nature, its surface charge and the electrochemical properties of the interstitial water.

There is a large evidence for anion exclusion. Figure 1 shows a typical distribution of ions dissolved in the porewater of a clay. This sketch illustrates the concept of the diffuse double layer. Anions are repelled by negatively charged clay surfaces and are mostly located at the middle of the pores.

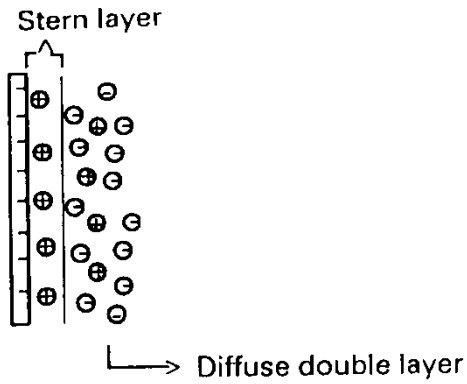

Figure 1 Distribution of ions dissolved in porewater (Corapcioglu and Lingham, 1994).

On the other hand, water velocity inside is largest in the middle of the pore and smallest at the mineral surfaces. The velocity profile inside a pore is shown in Figure 2 . Dissolved anions located in the middle of the pore are transported with a velocity larger than the average velocity. Thus, negatively charged particles can migrate further than other neutral dissolved species travelling with the average water velocity.

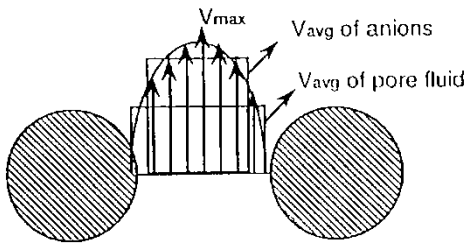

Figure 2 Flow velocity profile in an isolated pore (Corapcioglu and Lingham, 1994).

4. ANISOTROPIC DIFFUSION

Connected pores in a porous medium can be conceptualized as a group of tortuous channels. When the tortuosity depends on the direction, the porous medium is said to be anisotropic.

The anisotropy of the clay formations is well known. There is a large number of scientific publications attesting that hydraulic conductivity is anisotropic (Davis, 1969; Freeze and Cherry, 1979; Domenico and Schwartz, 1990; etc.). On the other hand, clay microstructure consists of tabular minerals that are oriented perpendicular to the largest compacting direction (see Figure 3). A porous system having this kind of microstructure presents little vertical continuity due to the overlap of the tabular mineral grains (Horseman et al., 1996). Besides, clay formations are often characterized by a foliated structure at a scale larger than that of the microstructure due to the existence of discontinuities such as bedding planes. Therefore, argillaceous formations have a microscopic anisotropy (at mineral grain scale) and meso-macroscopic anisotropy (at the scale of the sedimentary or metamorphic structure). Clay mineral orientation tends to be parallel to sedimentary and metamorphic discontinuities according to Morgenstern and Tchalenko (1967). Therefore, tortuosity of clay formations in the direction perpendicular to the bedding is larger than parallel to the bedding due to the overlap of the grains and discontinuities (Figure 3).

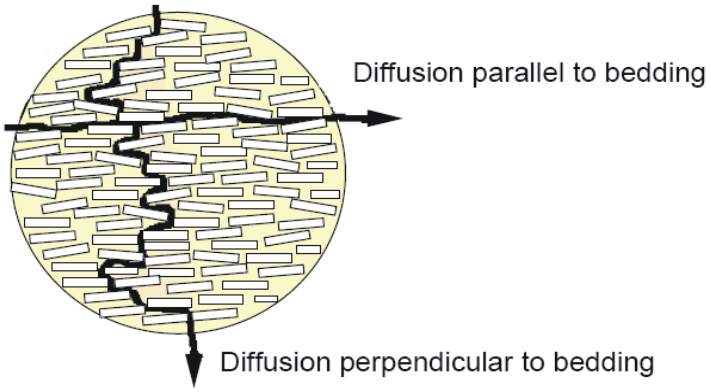

Figure 3 Sketch of the clay mineral tabular structure and representation of the tortuosity of a medium parallel and perpendicular to the bedding planes (Van Loon et al., 2004).

4.1. Formulation of molecular diffusion in an anisotropic porous medium

Fick's law in an isotropic medium is given by:

$$\mathbf{J} = -D\,\mathbf{grad}\,C \tag{15}$$

where ***J*** is the mass flux vector, *D* is the diffusion coefficient, *grad* is the gradient operator and *C* is the concentration.

Fick's law can be generalized to an anisotropic medium. If the coordinates system (x, y, z) coincides with the principal components, then the fluxes are given by:

$$J_x = -D_x \frac{\partial C}{\partial x} \tag{16}$$

$$J_y = -D_y \frac{\partial C}{\partial y} \tag{17}$$

$$J_z = -D_z \frac{\partial C}{\partial z} \tag{18}$$

However, equations (16), (17) and (18) correspond to a problem simplification. In an anisotropic diffusion problem, the components (J_x, J_y, J_z) of the mass flux vector **J** have three components. For example, the component J_x along the *x* axis has three parts J_{xx}, J_{xy} y J_{xz}. Thus, equation (16) becomes:

$$J_x = -D_{xx} \frac{\partial C}{\partial x} - D_{xy} \frac{\partial C}{\partial y} - D_{xz} \frac{\partial C}{\partial z} \tag{19}$$

One can see that J_x depends not only on the concentration gradient in the x direction, but also in the gradient in the y and z directions. In a similar way, the components J_y and J_z are:

$$J_y = -D_{yx} \frac{\partial C}{\partial x} - D_{yy} \frac{\partial C}{\partial y} - D_{yz} \frac{\partial C}{\partial z} \tag{20}$$

$$J_z = -D_{zx} \frac{\partial C}{\partial x} - D_{zy} \frac{\partial C}{\partial y} - D_{zz} \frac{\partial C}{\partial z} \tag{21}$$

The nine components of an anisotropic medium define the diffusion tensor, which in a matrix form is:

$$\begin{pmatrix} D_{xx} & D_{xy} & D_{xz} \\ D_{yx} & D_{yy} & D_{yz} \\ D_{zx} & D_{zy} & D_{zz} \end{pmatrix} \tag{22}$$

The diffusion tensor is a second-order symmetric tensor ($D_{ij} = D_{ji}$), like the hydraulic conductivity tensor. When the principal directions of anisotropy coincide with the coordinate axes, the off-diagonal components are equal to zero. In this case, the tensor is given by:

$$\begin{pmatrix} D_{xx} & 0 & 0 \\ 0 & D_{yy} & 0 \\ 0 & 0 & D_{zz} \end{pmatrix} \tag{23}$$

In summary, the simplified formulation presented in Equations (16), (17) and (18) is a particular case of the general formulation presented in Equations (20), (21) and (22) corresponding to the choice of a coordinate system parallel to the principal directions. The diffusion tensor in a general coordinate system can be obtained from the diffusion coefficient in the principal directions (represented in Figure 4 as an ellipsoid) by rotating the tensor.

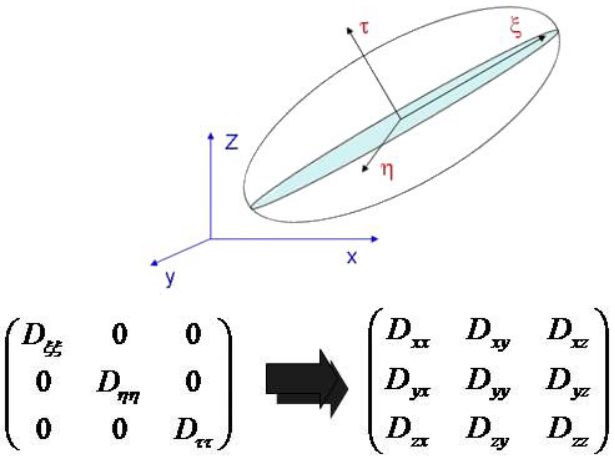

$$\begin{pmatrix} D_{\xi\xi} & 0 & 0 \\ 0 & D_{\eta\eta} & 0 \\ 0 & 0 & D_{\tau\tau} \end{pmatrix} \Rightarrow \begin{pmatrix} D_{xx} & D_{xy} & D_{xz} \\ D_{yx} & D_{yy} & D_{yz} \\ D_{zx} & D_{zy} & D_{zz} \end{pmatrix}$$

Figure 4 Diffusion anisotropy ellipsoid in the principal axes of the rock system and coordinates system (ξ, η, τ) (top). The diffusion tensor is diagonal when it is referred to the principal axes, otherwise it is a full tensor in the coordinate system (x, y, z) (bottom).

4.2. Solute transport equation

The transport equation for a tracer which diffuses into a low permeability anisotropic porous medium is given by Bear (1972):

$$\phi_a R \frac{\partial C}{\partial t} = \nabla \cdot \left(\overline{D_e} \cdot \nabla C \right) \tag{24}$$

where C is tracer concentration, t is time, Φ_a is the accessible porosity, R is retardation factor and $\overline{D_e}$ is the effective diffusion tensor given by (22).

5. REFERENCES

Allen, A.J., Baston, A.H., Bourke, P.J., Jefferies, N.L., 1988. Small angle neutron scattering studies of diffusion and permeation through pores in clays. Nirex Ltd., Harwell, U.K. Nirex Safety Stud. Rep. NSS/R160.

Bear, J., 1972. Dynamics of fluids in porous media. Elsevier. New York.

Benedek, G.B., Purcell, E.M., 1954. Nuclear magnetic resonance in liquids under pressure. *Journal of Chemical Physics* 22, 2003.

Bourke, P.J., Gillin, D., Jefferies, N.L., Lever, D.A., Lineham, T.R., 1988. Mass transfer in the London Clay, Southeastern England. In: *Materials Research Society Proceedings of the 12th International Symposium Science Basis for Nuclear Waste Management in Berlin*, 805-812.

Crank, J. (1956). The mathematics of diffusion. Ed. Oxford University Press.

Corapcioglu, M. Y., Lingam, R. (1994). The anion exclusion phenomenon in the porous media flow; A Review. *Advances in Porous Media*, Elsevier, pp. 151–168.

De Preter, P., Van Loon, L., Maes, A., Cremers, A. (1991). Solid/liquid distribution of radiocesium in Boom Clay. A quantitative interpretation. *Radiochimica Acta* 52, 299–302.

Davis, S.N., 1969. Porosity and permeability of natural materials. In: De Wiest, R.J.M. (Ed.), *Flow through porous media*, New York, Academic Press, p. 53-89.

Domenico, P.A., Schwartz, F.W., 1990. Physical and chemical hydrogeology. John Wiley & Sons Inc., New York.

Dorsey, N.E., 1940. Properties of ordinary water-substance. Reinhold

Freeze, A.R., Cherry, J.A., 1979. Groundwater. Prentice Hall Inc, Englewood Cliffs, NJ (USA).

Henrion, P.N., Put, M.J., Van Gompel, M., 1991. The influence of compaction on the diffusion of non-sorbed species in Boom clay. *Radioactive Waste Management Nuclear Fuel Cycle* 16, 1–14.

Horseman, S.T., Higgo, J.J.W., Alexander, J., Harrington, J.F., 1996. Water, gas and solute movement through argillaceous media. NEA/OECD Report CC-96/1.

Li, Y., Gregory, S., 1973. Diffusion of ions in sea water and in deep-sea sediments. *Geochimica et Cosmochimica Acta* 88, 703-714.

Juanes, R., Samper, J., Molinero, J., 2002. A general and efficient formulation of fractures and boundary conditions in the finite element method. *International Journal for Numerical Methods in Engineering* 54, 1751-1774.

Molinero, J., Samper, J., Montenegro, L., 2003. Actualización de los modelos conceptuales T-H-G para formaciones arcillosas. Informe final de la Subtarea 1.2 del Proyecto Arcillas de ENRESA. Universidade da Coruña.

Morgenstern, N.R, Tchalenko, J.S, 1967. The optical determination of preferred orientation in clays and its application to the study of microstructure in consolidated kaolin. Part I. *Proceedings Royal Society of London* A300, 218-234.

Simpson, J.H., Carr, H.Y., 1958. Diffusion and nuclear spin relaxation in water. *Physical Review* 111, 1201-1202.

Van Loon, L.R., Soler, J.M., 2004. Diffusion of HTO, $^{36}Cl^-$, $^{125}I^-$ and $^{22}Na^+$ in Opalinus Clay: effect of confining pressure, sample orientation, sample depth and temperature. PSI Bericht Nr. 04-03.

Yang, C.B., Juanes, R., Samper, J., Molinero, J., Montenegro, L., 2003. Users manual of CORE^{3D}. Technical report. Universidade da Coruña.

APPENDIX 2

IN SITU DIFFUSION EXPERIMENTS IN OPALINUS AND CALLOVO-OXFORDIAN CLAYS

1. INTRODUCTION

Clay media usually exhibit extremely low hydraulic conductivities and therefore molecular diffusion becomes the most relevant transport process (Appendix 1). Diffusion and sorption laboratory experiments have enlarged our understanding of these processes and provided a wealth of data on diffusion and sorption parameters. These experiments are often performed on small samples up to 1 cm which may have suffered alterations during their preparation. To overcome the limitations of laboratory experiments and to investigate possible scale effect, various in situ diffusion experiments have been performed in underground research laboratories (URL).

This dissertation presents the numerical modeling and interpretation of several in situ diffusion experiments performed within the experimental programs which are being carried out at Mont Terri URL (Switzerland) and at Meuse/Haute-Marne URL (France) to study the feasibility of the Opalinus and Callovo-Oxfordian clays as host formations for radioactive waste disposal, respectively. This appendix compiles a review of the in situ diffusion experiments performed so far within the framework of both experimental programs and of the numerical modeling tasks related to them. Its main objective is to provide the background and the general context of this dissertation.

2. IN SITU DIFFUSION EXPERIMENTS AT MONT TERRI URL

In 1995 several organizations (Nagra, ANDRA, IRSN, BGR, ENRESA, JNC and SCKCEN) decided to start an international research project in the reconnaissance gallery of the Mont Terri motorway tunnel, in north-western Switzerland. The gallery had been constructed in 1989 to investigate geological and geotechnical aspects of the construction of the tunnel. It had been drilled in a Mesozoic shale formation: the Opalinus Clay. Several niches were excavated into the wall of the gallery in 1996 where some experiments were performed (Figure 1). New galleries and niches were excavated in 1998, 2004 and from 2008 to nowadays on the SW side of the gallery to host new experiments (Swisstopo, 2008).

The Opalinus Clay consists on incompetent beds of silty and sandy shales deposited about 180 million years ago in a shallow coastal marine environment of the Jurassic sea (Thury and Bossart, 1999). It can be characterized as an overconsolidated shale formation (present overburden 300 m, estimated overburden in the past at least 1000 m) with 40–80% clay minerals and micas, 10–40% quartz, 5–40% calcite, 1–5% siderite, 0–1.7% pyrite and 0.1-0.5% organic carbon. The overall thickness of the formation is around 104 m and three slightly different facies can be distinguished: a shaly facies, a sandy-limy facies and a sandy facies. In the area where the URL is located, the rock

strata dip with an angle of approximately 45º to the SE and are penetrated by several minor faults. One larger fault zone, the Main Fault, was observed which affects a 1 to 5 m rock thickness.

The Opalinus Clay has extremely low hydraulic conductivities ($2 \cdot 10^{-13}$ to $1 \cdot 10^{-12}$ m/s) and no natural water inflows or wet areas were observed in the URL galleries. Therefore, is expected that the predominant transport process will be diffusion (Vitart and Calmels, 1997).

The first project on diffusion consisted on the analysis of natural profiles of stable isotope and dissolved noble gas contents across the formation, which were an experimental evidence supporting diffusion as the main transport mechanism (See section 2.1). In addition, a new field experiment design was developed which purpose was the in situ determination of the diffusion parameters of the Opalinus Clay (Palut et al., 2003). The feasibility of this new methodology was demonstrated by the DI-Experiment (See section 2.2) and then was improved for each new experiment and adapted to its specific objectives. Table 1 lists the in situ diffusion experiments performed so far at the Mont Terri URL.

Table 1 In situ diffusion experiments performed so far at Mont Terri URL.

DI	Diffusion in rock (preliminary experiment)
FM-C	Flow mechanisms with tracers
DI-A	Long term diffusion
DI-B	Long term diffusion
DI-A2	Long term diffusion of sorbing tracers
DR	Radionuclide diffusion and retention
DR-A	Disturbances, diffusion and retention

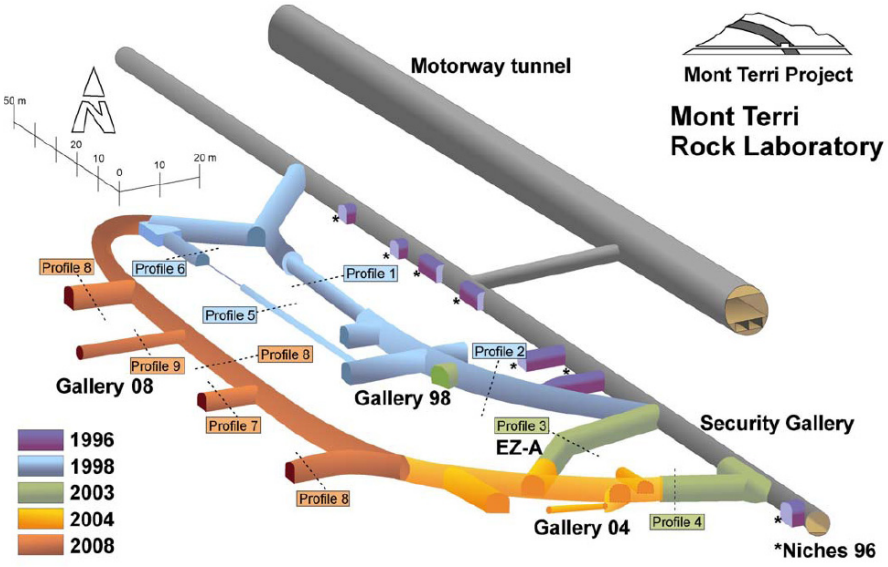

Figure 1 Geometry of the Mont Terri rock laboratory (Swisstopo, 2008).

2.1. Natural profiles of stable isotope and dissolved noble gas contents

Porewater samples across the formation indicated the existence of highly mineralized sodium-chloride waters in the middle of the Opalinus Clay, while the mineralization decreased towards the adjacent aquifers. This fact is consistent with slow diffusion from the saline Opalinus Clay porewater to the young groundwaters of the adjacent limestones and it is an experimental evidence supporting diffusion as the main transport mechanism in Opalinus Clay.

Rübel et al. (1999) measured the porewater content on samples from Mont Terri URL (WS-E diffusion experiment). The D_a of the ^{4}He was estimated from measured concentrations along the formation by fitting an analytical solution of the diffusion equation (Figure 2). The estimate of the D_a is equal to $3.5 \cdot 10^{-11}$ m^2/s which corresponds to $D_e = 5 \cdot 10^{-12}$ m^2/s, assuming an accessible porosity of 15%. Bath et al. (2003) obtained $D_a = 5 \cdot 10^{-8}$ m^2/s improving the porewater characteristics of the adjacent formations in the model. The profiles of δ^{18}O and δD across the formation were also studied (Rübel et al., 2002). Modeling these profiles (Figure 2) further suggested that meteoric waters have been circulating in the adjacent formations since 10 million years ago.

The composition of the porewater samples taken from three boreholes along Mont Terri tunnel was used by Degueldre et al. (2003) to estimate the diffusion coefficients of Na^+, Cl^-, Br^-, I^-, δ^{18}O and δD in Opalinus Clay. Estimates of the D_a are equal to $2.6 \cdot 10^{-11}$ m^2/s for Cl^-, Br^-, I^- and Na^+ and $5.2 \cdot 10^{-11}$ m^2/s for δD and δ^{18}O. These diffusion coefficients are consistent with those obtained at the laboratory.

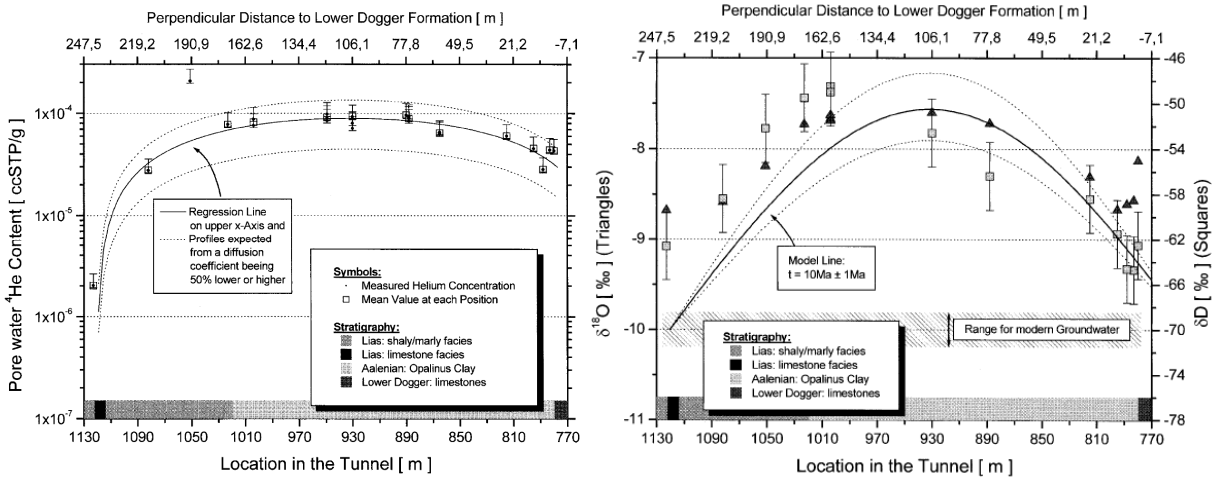

Figure 2 Natural profile of ^{4}He across the Opalinus Clay (left). The square symbols represent the mean value of measured data for all the samples at each position. Natural profiles of δ ^{18}D (triangles) and δD (squares) profiles across the formation (right). Figure extracted from Rübel et al., 2002.

2.2. DI experiment

The DI in situ diffusion experiment was designed to characterize diffusion in the undisturbed rock matrix of Opalinus Clay (Tevissen and Soler, 2003; Palut et al., 2003). The objectives of this experiment were to develop an experimental concept to measure in situ the diffusion parameters, demonstrate its feasibility and to compare its results against those measured on samples at the laboratory.

The in situ experiment was carried out in a 76 mm diameter borehole with a depth sufficient to reach a level of Opalinus Clay as undisturbed as possible (Fierz, 2000a; Palut et al., 2002). Figure 3 shows a schematic experiment layout. It included a packer system capable of isolating a section of the borehole. A porous sintered stainless screen, that was located in it, maintained the mechanical stability for the borehole walls. The borehole equipment also included an additional observation interval to detect a possible leakage and to provide an extra control of the experiment. The packed-off section of the borehole was connected by the flow lines to the gallery. There, the surface equipment consisted in a circuit with a reservoir that allowed tracer injection and sampling. The reservoir had a pressure control device to maintain pressure similar to that of local porewater and to prevent any flow between the test interval and the rock surrounding the interval.

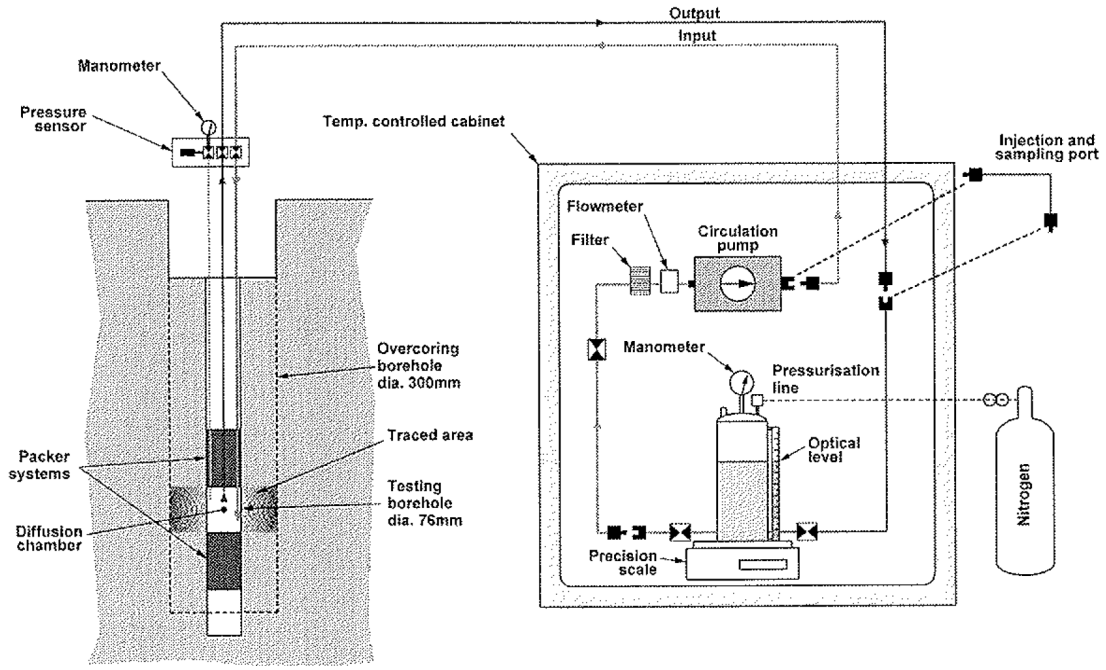

Figure 3 DI experiment design (Tevissen and Soler, 2003).

The interval was filled with synthetic water with a composition close to that of the porewater. Then, the fluid started to continuously circulate by means of a gear pump. After the stabilization of the system, two tracers were added to the circulating fluid (December 1998): tritiated water (HTO) and stable iodine (I^-). Initially, the procedure was intended to maintain the tracer concentrations constant in the interval in order to ensure constant boundary conditions. However,

this requirement was abandoned after 4 months by experimental difficulties. From then, the dilution of the tracers was measured at the interval.

After about 1 year of diffusion (November 1999), the area where the tracers were expected to have diffused was removed by overcoring the borehole (Bossart, 2000; Fierz, 2000b). The overcore was cut into pieces to collect undisturbed centimeter-sized rock samples and to obtain several tracer concentration profiles with different orientations respect to the axis of the borehole and the bedding anisotropy. The concentration of the tracers was measured on each sample at the laboratory.

The DI experiment was interpreted using a three-dimensional model (Montarnal and Lamoreux, 2000; 2001; Palut et al., 2002). The domain consisted in a clay cylinder around the injection chamber. Diffusion was simulated with the finite element code CASTEM 2000 (Verpeaux et al., 1998). The effective diffusion coefficients parallel and perpendicular to the bedding, $D_{e//}$ and $D_{e-|}$, and the accessible porosity, ϕ_{acc}, have been estimated first from the dilution curve and then from the measured concentration profiles. For HTO, the estimates of the $D_{e//}$ and ϕ_{acc} were equal to $5 \cdot 10^{-11}$ m^2/s and 15% respectively fixing an anisotropy ratio of 7, based on experimental data (Pocachard, 1997). Derived parameters for I^- were $D_{e//} = 1.5 \cdot 10^{-11}$ m^2/s and ϕ_{acc} = 12.5%, fixing an anisotropy ratio of 4.4 based on experimental data. There were some uncertainties in results for I^-, for which dilution and overcoring data were not consistent. The simplest hypothesis was to consider that chemical form of some iodide had changed, either associated or not with biological activity, although iodide retention in the rock could not be excluded.

The mean success of the DI experiment was the validation of the experimental concept and of the vast majority of associated techniques. Furthermore, a strong consistency between laboratory and field experiments appears not only from a phenomenological point of view, but also in relation to the values of diffusion parameters. The consistency between laboratory and field data was verified for only one location, therefore an array of tests covering the variations in lithological properties of the formation and different tracers should be performed to be able to extrapolate the results without ambiguity to other situations. The experimental design should be improved to allow for the estimation of the $D_{e-|}$ and to minimize the borehole drilling disturbance.

2.3. FM-C experiment

Within the framework of the FM-C experiment (Flow mechanisms with tracers) several in situ diffusion tests were performed in the Main Fault at Mont Terri URL. An in situ diffusion experiment, similar to the previous DI experiment, was performed. Prior to that, eight in-diffusion and out-diffusion experiments and a cross-hole in situ diffusion experiment were carried out with helium.

The in-diffusion and out-diffusion tests concept consisted in maintaining permanent circulation in a closed circuit that went through a packed-off borehole interval and monitoring the

diffusion of helium into and out of the interval using both helium isotopes (Fierz, 2000c; 2001a). In the in-diffusion experiments, the ^{4}He content which is high in natural groundwater is maintained low in the fluid within the circulation circuit. The increase of ^{4}He corresponds to the diffusion of ^{4}He within the formation water into the interval. In the out-diffusion experiments the fluid is picked with ^{3}He, which content in natural groundwater is very low, and the concentration decrease was monitored in the circuit. These experiments confirmed that in situ helium diffusion tests are feasible at Opalinus Clay and can be replicated. They were useful to optimize the equipment design and experimental methodologies such as the waterproofing of the equipment or the minimization of desaturation during borehole drilling. In addition, they were used to explore the Major Fault zone of Mont Terri URL.

The ^{3}He cross-hole diffusion experiment between two boreholes separated ~26 cm was performed between May 2000 and February 2001. A ^{3}He pulse was injected into the test interval of one of the two boreholes and the decrease of ^{3}He was measured during 13 days. Then, the ^{3}He evolution within the circulation lines was measured at the other borehole, the observation borehole. Results verified the feasibility of this diffusion experiment within a reasonable time frame.

The out-diffusion and in-diffusion in situ experiments were numerically interpreted as pulse experiments (Gómez, 2000). A 2D finite difference model was used, over a domain contained in a vertical radial plane. Some of the experiment could be simulated obtaining a good fit to measured concentrations. The estimate of the D_e for ^{4}He into the fractured zone was 2.1×10^{-10} m^2/s. Derived porosity was larger than the one observed in the formation as it would be expected in the fracture zone. Other experiments could not be modeled with coherent values of the parameters because of desaturation or artificial oversaturation of a zone disturbed by borehole drilling.

The cross-hole in situ experiment was also simulated as a pulse experiment (Gómez et al., 2004) with a 2D finite difference model. The diffusion was assumed horizontal in between the boreholes by neglecting the bedding influence. Measured concentration evolution at injection and observation boreholes were interpreted. The out-diffusion could be simulated for $D_e = 4 \cdot 10^{-10}$ m^2/s. However, the observed values were completely different from any computed concentration at the in-diffusion borehole. This discrepancy was attributed to local heterogeneities around the injection borehole or to an unknown source of ^{3}He not considered in the model.

Finally, an in situ diffusion experiment was performed using HTO and I^- as tracers (Fierz, 2001b; Nussbaum et al., 2001) between June 2000 and February 2001. From the experimental point of view, the experiment was a replica of the DI experiment. However, the DI experiment was carried out in the undisturbed Opalinus Clay matrix while this one was situated within the major fault zone of the laboratory.

Scoping calculations where done by Gómez and Hendricks (2000) for this experiment to evaluate the magnitude of diffusion away from the borehole and the impact of heterogeneity in the experiment results. They used a preliminary 2D model and assumed that diffusion took place along the bedding planes. Results showed that mild heterogeneities were not relevant, while the large heterogeneity produced by the contrast between the rock and the fracture zone has a large impact, channeling most of the diffusion in the fracture itself. On the other hand, they also found that clay anisotropy was significant during modeling.

Therefore, a new 3D model accounting for the fracture and the anisotropy was used to interpret numerically the measured concentrations (Gómez and Guardiola, 2004). For HTO, computed concentrations related to $D_e = 6.8 \cdot 10^{-11}$ m^2/s and $\Phi_{acc} = 0.28$ match very well the measured dilution curve and concentration profiles. However, the first part of the computed profiles seems to be much steeper than the measured curves. This feature could be explained by the effect of the filter or of a disturbed area surrounding the borehole. Calibrated parameters for iodide were $D_e = 2.5 \cdot 10^{-11}$ m^2/s and $\Phi_{acc}=0.05$. The D_e is quite similar to the one derived for HTO. Accessible porosity is much smaller than that for HTO according with the anion exclusion effect. The fit to measured concentrations for iodide is not as good as for HTO.

2.4. DI-A experiment

The DI-A experiment is a long-term in situ diffusion experiment to study the diffusion of sorbing species which, so far, had not been studied at Mon Terri (Wersin et al., 2004; 2006; Van Loon et al., 2004a). Besides the non-sorbing tracers HTO and I^- which were injected to compare with the previous DI experiment, the diffusion of the weakly ($^{22}Na^+$) and more strongly sorbing elements (Cs^+) was investigated.

The experiment took place in a borehole at the DI niche of the Mont Terri URL (shaly facies). Its lay out was similar to that of the DI experiment (Figure 3), but there is a single 1 m long interval isolated with a single packer. The artificial water used in the recirculation system was a synthetic Opalinus Clay porewater (Pearson, 1998). The tracers (HTO, I^-, $^{22}Na^+$ and Cs^+) were injected in the borehole in January 2002. From that moment, the dilution of each tracer in the borehole solution was monitored by regularly sampling aliquots. Cs^+ concentration within the circuit fluid decreased quickly as was expected due to sorption behavior. The weakly sorbing $^{22}Na^+$ revealed a significant lower dilution than Cs^+. The inert tracers HTO and I^- showed less dilution compared to the sorbing tracers. Their behavior was similar to that observed in previous in-situ experiments.

After 292 days of diffusion, the equipment was retrieved and the single packer was removed from the borehole. The lower part of the borehole was immediately filled with quartz sand and epoxy resin mixture to stabilize it. The test interval was then overcored. The entire core was lifted

and cut into core sections at the borehole mouth. After removing, the overcore was reoriented with the help of the bedding planes. The exact depth position of the overcore containing the test interval was localized. Nine profiles were drilled from the overcore at different positions and orientations. They were sliced into wheels of 1 cm thickness and the partly desaturated surface was cut away with a saw. The rock samples were immediately transferred into polyethylene bottles and carried to the laboratory for their analyses. Concentrations were measured on the samples for all the tracers but Cs^+, for which only a few selected samples were analyzed. Measured HTO and I^- concentrations in the overcoring samples closest to the borehole showed clear deviations from the general trend, likely because of the effect of the filter, a borehole disturbed zone or a desaturation during overcoring.

Overcoring data showed a similar distribution of the tracers with depth what indicates that the diffusion occurred relatively homogeneously within the test interval. As expected, the penetration of HTO was largest, reaching about 20 cm. The penetration depths of I^- and $^{22}Na^+$ were very similar (≈10 cm). The smallest penetration of I^- was attributed to anion exclusion. The smaller penetration depth of $^{22}Na^+$ compare to HTO is due to the weak sorption of this cation to the clay. Cs^+ shows the smallest penetration depth of about 3 cm which is explained by the significant sorption of this tracer on the clay matrix. Cs^+ concentrations were also successfully measured along profiles with high resolution methods showing a small-scale heterogeneity of Cs^+ distribution in the rock.

Three independent modeling exercises were performed in order to interpret the dilution and overcoring data from the DI-A experiment and to check the robustness and consistency of the conclusions (Wersin et al., 2006): 1) 2D calculations along the bedding plane performed by J. M. Soler from CSIC-IJA (Spain) using CRUNCH code; 2) 2D modeling using an analytical solution in Laplace space performed by Th. Gimmi from PSI (Switzerland); and 3) 3D calculations performed by A. Cartalade from CEA (France) using CAST3M code.

The results from the field experiment have been interpreted by means of 2D transport calculations including diffusion and sorption by Van Loon (2004a) and Wersin et al. (2004; 2006). Diffusion was assumed to be homogeneous and isotropic. Three types of sorption models were implemented corresponding to: 1) no sorption, s = 0, for HTO and I^-; 2) linear sorption, $s = K_d \cdot c$, for $^{22}Na^+$; and 3) Freundlich isotherm, $s = a \cdot c^b$, for Cs^+, where s is the sorbed tracer concentration (mol/Kg_{solid}) and c is dissolved tracer concentration ($mol/L_{solution}$). Cs^+ was modeled assuming a Freundlich-type behavior based on the batch sorption study of Lauber et al. (2000). Radioactive decay was not explicitly included in the calculations for radioactive tracers (HTO and $^{22}Na^+$); instead, the experimental data were corrected for decay. The reactive transport code CRUNCH (Steefel, 2006) was used for the simulations. Derived diffusion parameters were: $D_e = 5.4 \cdot 10^{-11} m^2/s$ and $\Phi_{acc} = 0.18$ for HTO; $D_e = 1.3 \cdot 10^{-11} m^2/s$ and $\Phi_{acc} = 0.09$ for I^-, were $D_e = 7.2 \cdot 10^{-11} m^2/s$ and $K_d = 0.2$ L/Kg for $^{22}Na^+$, fixing $\Phi_{acc} = 0.18$, and $D_e = 3 \cdot 10^{-10} m^2/s$, $\Phi_{acc} = 0.18$ and $s = 0.186 \cdot C^{0.53}$.

The approach of Th. Gimmi used an analytical solution in the Laplace space of the differential equation which describes conservation of solute mass, including radial diffusion, linear sorption and radioactive decay (Wersin et al., 2006). Only radial diffusion parallel to the bedding was considered. Therefore, the solution was computed in a 2D, axis-symmetric, and semi-infinite domain. An analytical inversion of the analytical solution in Laplace space to the time domain was performed numerically using the Talbot algorithm (Jury and Roth, 1990). Derived parameters were: $D_e = 5.5 \cdot 10^{-11} m^2/s$ and $\Phi_{acc} = 0.17$ for HTO; $D_e = 1.2 \cdot 10^{-11} m^2/s$ and $\Phi_{acc} = 0.09$ for I^- and $D_e = 8.2 \cdot 10^{-11}$ m^2/s and $K_d = 0.13$ L/kg for Na^+. Results for these three tracers also showed fairly good fits to field data. Cs^+, required a more sophisticated sorption model than the linear sorption.

A preliminary fully 3D interpretation of the experiment was performed by Wersin et al. (2006) using CAST3M code (Benet and Mouche, 2000). Thus, the diffusion perpendicular to bedding was not disregarded. Linear sorption was considered and radioactive decay was also included. The derived parameter values for a dip angle of 30° were: $D_{e//} = 6.5 \cdot 10^{-11}$ m^2/s, $D_{e-|} = 1 \cdot 10^{-11}$ m^2/s and $\alpha = 0.2$ for HTO; $D_{e//} = 2 \cdot 10^{-11}$ m^2/s, $D_{e-|} = 3.2 \cdot 10^{-11}$ m^2/s and $\alpha = 0.15$ for I^-; $D_{e//} = 8 \cdot 10^{-11}$ m^2/s, $D_{e-|} = 1 \cdot 10^{-11}$ m^2/s and $\alpha = 0.45$ for $^{22}Na^+$. The uncertainty in the derived diffusion data, especially in α, is relatively large. On the other hand, the results clearly demonstrated the strong effect of anisotropy on diffusion.

The derived diffusion parameters for HTO, I^- and $^{22}Na^+$ in the three approaches were found to be consistent among themselves and with the small-scale lab diffusion measurements performed parallel to the bedding plane (Van Loon and Soler, 2003a) and with batch sorption measurements for Na^+ (Lauber et al., 2000). For Cs^+, the obtained high effective diffusion coefficient (5 times that measured on samples) is in qualitative agreement with the diffusion data reported for the Callovo-Oxfordian formation (Melkior et al., 2005). Their sorption values are lower by a factor of 2 than those from batch experiments, what suggests a slight upscaling effect from batch sorption studies to field conditions leading to slight decrease in sorption capacity of the rock matrix.

After 2005, several modelers developed more complex models of the DI-A experiment that account of heterogeneity of the Opalinus Clay and geochemical reactions. Appelo (2005) used PHREEQC code for the analysis of more complex scenarios than that of uniform diffusion coefficient and porosity: different diffusion coefficients for the clay and a sandy intercalation, perturbed zones with a relatively high diffusion coefficient adjacent to the borehole and dual porosity model zones. Subsequent models of the experiment included anion exclusion, cation exchange capacity, multicomponent interactions, diffusive double layer around the clay particles, heterogeneous distribution of exchange sites and exchange sites with kinetics (Glaus et al., 2007; Appelo and Wersin, 2007; Appelo, 2008a). Another model was presented by Appelo (2008b) including the borehole filter and the annular space between the filter and the borehole wall. The filter poses a resistance to

diffusion of the ions that explains the retarded concentration decrease of Cs^+ and that it has been previously model by decreasing the exchange capacity or combining a heterogeneous distribution of exchange sites and kinetics.

2.5. DI-B experiment

The DI-B in situ diffusion experiment was a long-term and natural-scale test to study the transport and retention properties of selected non radioactive tracers in the Opalinus Clay (Yllera et al., 2002; 2004). It was performed in a 60 cm long packed-off section of a borehole drilled at the DI niche of the URL (shaly facies). At this location, the bedding dips 32º to the SE. The set up was similar to those of the DI and DI-A experiments. It was equipped with a pneumatic single packer system with a stainless steel filter mounted just below at the bottom of the borehole. The filter was connected to three lines for water inflow, water outflow and pressure monitoring in the injection section. The flow lines connected to a surface stainless steel circuit intended to circulate the synthetic porewater and to allow the tracer injection and sampling. The circuit included a system to equilibrate the pressure in the circulation system with the hydraulic pressure of the geological formation and to prevent any flow. The flow-rate, pH, redox potential and conductivity of the solution in the system were also monitored.

Synthetic porewater (Pearson, 1998) was circulated during approximately 5 months prior to tracer injection to ensure that solution chemistry and pressure were in equilibrium with the rock. The total volume of solution in the circulation system was about 30 L. Four tracers were injected to the system in September 2002: HDO, I^-, $^6Li^+$ and $^{87}Rb^+$. The dilution of the tracers at the circuit was monitored by taking periodic aliquots. The experiment lasted slightly over one year (417 days). A volume of rock around the injection interval was successfully overcored after the end of the experiment. Several sandy layers and a small tectonic fracture were observed in the overcore at the upper part of the interval, which are probably characterized by different transport parameters. Twelve subcores were drilled from the overcore with different depths and directions (Figure 4). Profiles 1 to 5 and 9 were horizontal and parallel to bedding; profiles 6 to 8 were also horizontal but perpendicular to bedding; profiles 1 to 5 were at a 32º angle respect to bedding; profiles 10 and 11 were at an angle of 74º with respect to bedding and profile 12 was vertical. Each subcore was sliced into 1 cm thick samples.

Measured dilution trends are tracer dependent (Naves, 2005; Samper et al., 2006). At very early times, concentrations in the reservoir showed a very large dispersion of values possibly due to incomplete mixing of the tracer at the time of sampling. They also presented fluctuations caused by pressure oscillations in the injection system and sporadic clogging of filters along the circuit. However, they did not affect the overall performance of the experiment.

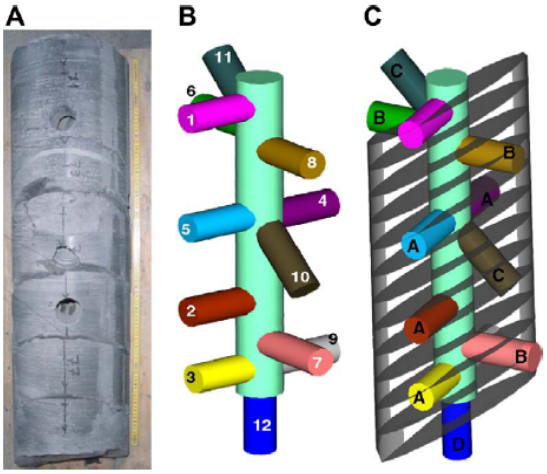

Figure 4 (A) View of overcore of BDI-B3, (B) schematic location of the 12 sampling profiles and (C) types of profiles depending on their orientation with respect to bedding (Samper et al., 2006).

Overcoring data illustrated how diffusion is fastest along planes parallel to bedding while the slowest diffusion occurred along the direction perpendicular to bedding. This confirmed anisotropy in diffusion previously identified in laboratory (Van Loon et al., 2003b; 2004b). A large variability in the profiles for $^{87}Rb^{+}$ was observed possibly due to natural small-scale heterogeneity of the rock regarding sorption properties, alike for other strongly sorbing tracers in previous experiments.

Scoping calculations were performed to improve the final design of the experiment by three teams using different conceptual approaches and numerical codes (Yllera et al., 2002).

Calculations presented by the CSIC-ICTJA team simulated the experiment as a pulse test using GIMRT code (Steefel, 2001). The diffusion was assumed to be homogeneous and isotropic and to take place in a horizontal bedding plane perpendicular to the borehole to be along this plane. Linear sorption was taken into account for $^{87}Rb^{+}$. Results for parameters based on laboratory measurements indicated that the diffusion profile would be measurable in the overcored rock HDO, I^{-} and ^{6}Li after 1 year. In case of $^{87}Rb^{+}$, it was expected a very small diffusion. Simulation of the experiment performed by Ciemat was similar to that of CSIC-ICTJA. The problem was solved using CODE-BRIGHT (UPC) for candidate tracers. Results helped to decide the tracers and the initial tracer mass.

The scoping numerical model performed by UDC team considered a 2D axis-symmetric domain (Molinero and Samper, 2001; 2002). The simulations were performed only for HDO using $CORE^{2D}$ (Samper et al., 2003). Concentration profiles at the end of the experiment were calculated for different values of the parameters and experimental conditions. Derived conclusions were: 1) The consideration of an EdZ does not affect the conclusions; 2) Performing successive additions of the tracers could generate more defined concentration profiles and 3) The effect of clay anisotropy on the diffusion seems to be relevant.

The real experiment data were interpreted numerically with a 2D model by CSIC-ICTJA and a fully 3D model by UDC (Samper et al., 2004; 2006; Soler et al., 2008).

The 2D model of the experiment included diffusion only along the bedding planes and linear sorption for sorbing tracers. Diffusion was assumed to be homogeneous and isotropic. The finite differences reactive transport code CRUNCH (Steefel, 2006) was used for the calculations. Diffusion and sorption parameters were derived from fitting computed to measured concentrations: $D_e = 5 \cdot 10^{-11}$ m^2/s and $\Phi_{acc} = 0.16$ for HDO; $D_e = 1.2 \cdot 10^{-11}$ m^2/s and the $\Phi_{acc} = 0.09$ for I^- and $D_e = 7 \cdot 10^{-11}$ m^2/s and $K_d = 0.24$ L/Kg for $^6Li^+$, fixing $\Phi_{acc} = 0.16$. Clearly, $^6Li^+$ behaved as a weakly sorbing tracer. Estimates are in good agreement with the laboratory results and derived porosity for HDO was identical to the measured average water content porosity. It was not possible to assign a unique value of D_e and K_d to $^{87}Rb^+$, due to the variability displayed between the different measured profiles in the rock. Two sets of results were derived: $D_e = 5 \cdot 10^{-11}$ m^2/s and $K_d = 8.8$ L/Kg or $D_e = 10^{-10}$ m^2/s and $K_d = 35.4$ L/Kg.

A fully 3-D finite element model which accounts for the anisotropic behavior of diffusion and imposes no restrictions for diffusion across the bedding was built up to simulate the DI-B in situ experiment. Calculations were performed with the code $CORE^{3D}$ (Yang et al., 2003). Model parameters were calibrated by a trial-and-error method by fitting model results to measured data in the borehole and along profiles. After, a sensitivity analysis was performed to evaluate model uncertainties. These tasks were reported in Samper et al. (2006) and Soler et al. (2008), and those performed by the author of this dissertation are included in Appendixes 3 and 4.

2.6. DI-A2 experiment

The DI-A2 experiment focuses in the diffusion of sorbing tracers (Wersin et al., 2008). The experiment was performed in a borehole drilled in the DI niche of the URL (shaly facies). In this location, bedding dipped at about 30º.

The set up of the test was similar to that of the previous DI-A experiment. However, the injection interval was equipped with a porous Teflon screen, instead of the stainless-steel one of the DI-A experiment, to minimize retention of sorbing tracers in it. A tracer cocktail containing HTO, I^-, Br^-, $^{85}Sr^{2+}$, Cs^+ and $^{60}Co^{2+}$ was injected in April 2004 and circulated over 1 year along the system. Tracer dilution in the circuit was monitored by taking aliquots from the circuit. In addition, an in situ high-resolution □-spectrometer was used for on-line counting of $^{85}Sr^{2+}$ and $^{60}Co^{2+}$ in the field for the first time. The count rates obtained were converted into activity concentrations via water samples analysis using precisely calibrated high-resolution □-spectrometers. The relative decrease was the lowest for Br^- and I^-, followed by HTO. Cations showed a more rapid decrease relative to HTO, even faster for Cs^+ and $^{60}Co^{2+}$ than for $^{85}Sr^{2+}$. The agreement between on-line and sampled $^{60}Co^{2+}$ and $^{85}Sr^{2+}$ was very good.

During the test, a variable amount of colloidal particles in the circulation system was noted. At the beginning some reddish-yellowish colloids were observed, possibly because of pyrite oxidation that resulted from the ingress of O_2 during drilling. However, the amount of brownish colour colloids visibly increased after. They were particles from the clay formation generated because of the design of the Teflon screen which forced the circulation of water between the screen and the borehole wall instead of the circulation within the filters. Some erosion at the borehole wall took place which may have partly affected the edges of the tracer profiles.

After 1 year, the experiment was finalized and dismantled and the borehole section was successfully overcored. Six subcores at various locations were drilled from the overcore and cut with a band saw in slices of 1 cm. The concentrations measured on the samples illustrated the movement of each tracer. The HTO, I^- and Br^- diffused about 15 cm from the borehole. HTO overcoring data at different depths suggests that transport distances for HTO were large enough to start noticing the effect of clay anisotropy. Overcoring data of I^- and Br^- showed considerable scatter possibly due to large analytical uncertainties resulting of the low ratio between tracer and background concentrations. The cationic tracers ($^{85}Sr^{2+}$, Cs^+ and $^{60}Co^{2+}$) showed significantly slower migration rates relative to HTO. Their behavior can be explained by sorption effects.

Alternatively, 6 subcores were taken in order to obtain accurate resolution of tracer distribution around the injection borehole. They were embedded in epoxy resin and cut in 1 mm thick slices with a diamond wire saw. $^{60}Co^{2+}$ was analyzed on these additional samples via high sensitivity non-destructive ?-spectrometry and total Cesium was investigated by energy-dispersive X-ray fluorescence (XFR) analysis. A significant variation in the profiles of both tracers was found. This spreading may arise from: 1) small-scale mineralogical heterogeneity in the rock; 2) the mechanical disturbance around the borehole induced by drilling; and 3) the limited resolution of the profile with the slicing method applied.

Dilution and overcoring data were numerically interpreted by means of a 2D model similar to that of DI-A experiment (Wersin et al., 2008). Calculations were performed with CRUNCH code. Linear sorption was assumed for $^{85}Sr^{2+}$ and $^{60}Co^{2+}$ injected at very low total concentrations, whereas a Freundlich isotherm model was assumed for Cs^+ injected at moderately high concentrations. Radioactive decay for HTO, $^{85}Sr^{2+}$ and $^{60}Co^{2+}$ was considered in the calculations by correcting the measured activities for decay.

The values of the diffusion and sorption parameters corresponding to the best fit of the model to the experimental data are listed in Table 2. In general, results are consistent with other values from laboratory and previous field experiments. $^{85}Sr^{2+}$ and Cs^+ showed a slightly higher $D_{e//}$ relative to HTO and a small sorption capacity relative to the batch sorption experiments. This is in

agreement with previous experiments and other studies (Melkior et al., 2005) and could be due to an additional driving force for diffusion in the diffuse double layer.

Later, a more complex geochemical model was presented by Appelo (2008c) accounting with accessible porosities, exchange parameters, fraction of dead-end pores and tortuosity. The filter and the gap between the filter and the borehole wall were also taken into account. Results suggested the existence of advective flux through the filter.

Table 2 Derived values of the effective diffusion coefficient, D_e, parallel (//) to the bedding, accessible porosity, Φ_{acc}, and sorption parameters from numerical interpretation of field DI-A2 experiment data (Wersin et al., 2008).

Tracer	D_e // (m^2/s)	Φ_{acc}	Sorption
HTO	6×10^{-11}	0.15	-
I^-	3×10^{-11}	0.08	-
Br^-	3×10^{-11}	0.10	-
$^{85}Sr^{2+}$	7×10^{-11}	0.15	K_d= 1 L/Kg
Cs^+	2×10^{-10}	0.15	$S=0.186 \cdot C^{0.53}$
$^{60}Co^{2+}$	6×10^{-11}	0.15	K_d= 90 L/Kg

2.7. DR experiment

The concept for the DR experiment (Wersin and van Dorp, 2005; Fierz, 2006; Leupin et al., 2010) was optimized to determine in situ the diffusion anisotropy. The length of the injection intervals was shorter (15 cm) than that of previous experiments (1 m). The duration of the experiment, between 3 and 4 years, was such that the transport distance of conservative tracers is larger than the length of the injection interval to allow the estimation of the diffusion anisotropy.

The experiment was performed in a borehole drilled in the DR niche at the Mont Terri URL. The borehole was drilled at an angle of 45º with respect to the tunnel bottom, so it is normal to the bedding (Figure 5). Three borehole intervals were isolated by packers. The interval at the bottom served as an auxiliary interval for the observation of the hydraulic pressure during the experiment. Tracer cocktails were injected into the upper two intervals. Each injection interval was connected to surface equipment which included a reservoir tank of approximately 20 L. It also incorporated a circulation fluid flow meter and an electrode module in which pH, Eh and conductivity could be continuously measured. To avoid a pressure drop within the intervals, the circuits are connected to a reservoir tank pressurized by Helium. In or out-flow of the interval was measured by weighting the reservoir tanks. The design of the completion was focused on minimizing sorption of reactive tracers on the equipment surfaces. Therefore equipment parts in contact with the sorbing tracers were made of inert materials such as PEEK or Teflon.

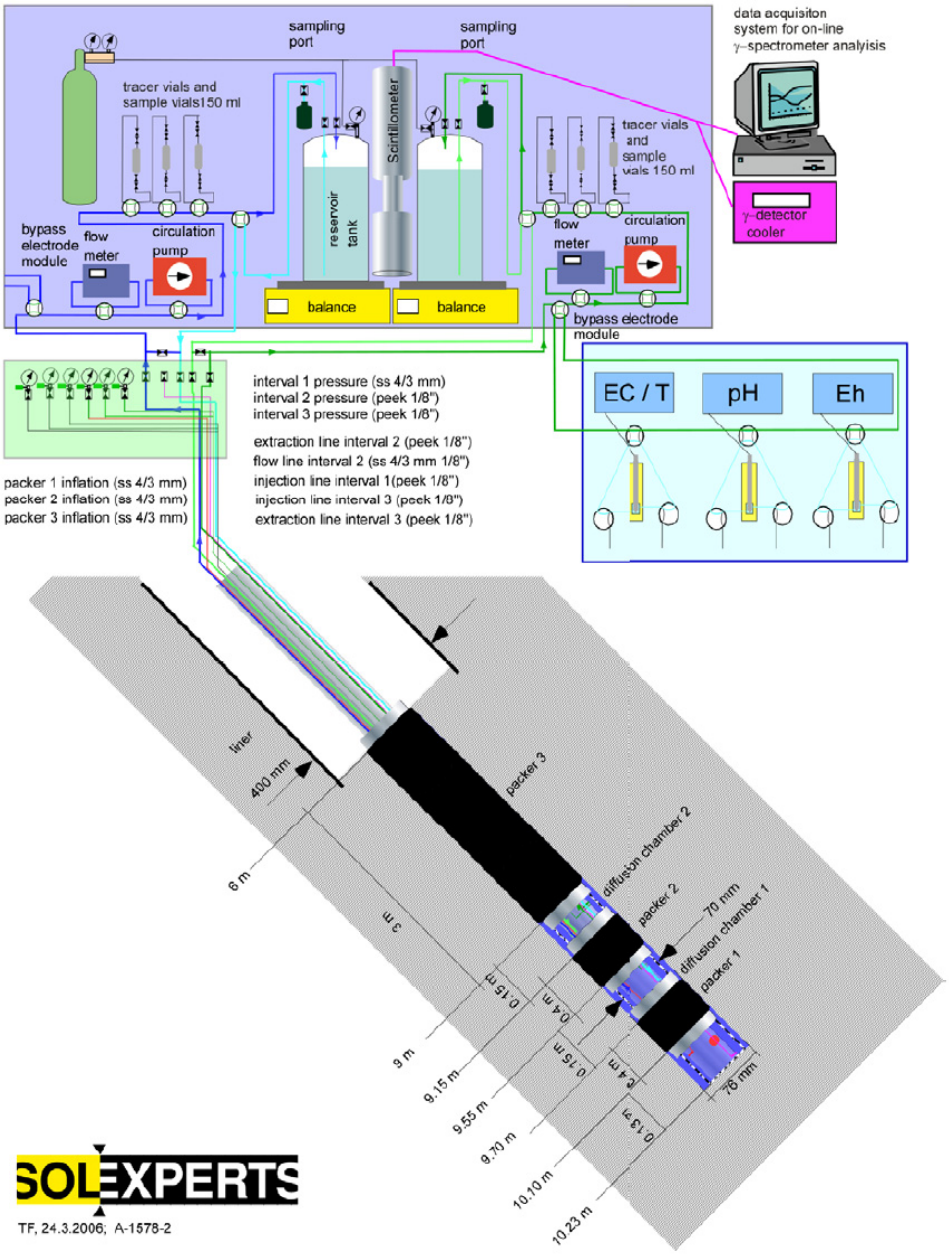

Figure 5 Schematic drawing of the entire test setup of the DR experiment (Fierz, 2006).

Once the equipment was installed, it is filled with artificial porewater and the fluid was circulated continuously. The selected tracers for the upper borehole interval include: HDO, $^{60}Co^{2+}$, $^{137}Cs^{+}$, $^{133}Ba^{2+}$ and $^{152}Eu^{3+}$. The selected tracer tracers for the lower borehole interval include: HTO, I^{-} (stable), Br^{-} (stable), $^{22}Na^{+}$, $^{85}Sr^{2+}$, ^{18}O (water) and $^{75}Se^{4+}$. The tracer cocktails were injected into the two circuits in April 2006, but $^{152}Eu^{+3}$ that was injected in February 2007 and ^{18}O and $^{75}Se^{4+}$ that were injected later.

The decrease of tracer concentrations and activities in the water of the circulation system were monitored by taking water samples at regular intervals in sampling vials. In addition, □-emitter tracers (all radioactive tracers but HTO) were monitored on line in both circuits with an online □-counting technique which was successfully tested in the DI-A experiment.

During the experiment the water chemistry in the upper loop was significantly affected by microbial-mediated sulphate reduction (Leupin et al., 2010). This was explained by leaching of glycerol which was a component of the pH electrode used. The lower loop, where such component was not present, did not show any signs of sulphate reduction.

At the end of the experiment (January 2010) the rock around the injection interval was overcored (Th. Gimmi and O.X. Leupin, personal communication). Samples were taken from the overcore at both injection interval positions. Measured tracer distribution revealed interesting insights into the 3D distribution of the radionuclides throughout the rock and the rock heterogeneities. Additionally, several subcores parallel to bedding were embedded in epoxy resin and cut in thin slices (1-3 mm) to measure strongly sorbing tracers around the injection borehole with high precision.

The DR experiment was accompanied from the beginning with several modeling studies, which helped to design the setup of the experiment and will allow its interpretation.

In a first stage, four different modeling groups using different reactive transport codes (Flotran at PSI, Crunch at IDAEA-CSIC, CORE^{2D} at UDC, and r3t at GRS) modeled the experiment for a set of pre-defined parameters (Soler, 2005; 2007; Gimmi, 2007; Yang and Samper, 2007). The results of all the teams were consistent.

Currently, sensitivity and identifiability analyses and finally dilution and overcoring data interpretation are being performed by three modeling groups, using different tools and approaches: a semi-analytical solution in the Laplace domain at PSI, Crunch at IDAEA-CSIC and CORE^{2D} at UDC. This work is still ongoing at present and only a few results have been published (Samper et al., 2008a; Gimmi et al., 2010; Soler et al., 2010). Results of several of the DR modeling tasks performed by the author of this PhD dissertation are included in Appendixes 6, 7 and 8.

2.8. DR-A experiment

The DR-A experiment (Disturbances, Diffusion and Retention experiment) is an in-situ diffusion test that is currently being performed in a borehole in the DR-A niche (shaly facies) (Soler, 2010). In previous experiments, the behavior of different tracers was studied using tracers in synthetic porewater at equilibrium with the host rock. On the contrary, the behavior of tracers will be studied in the DR-A experiment using solutions out of equilibrium with the host rock. Mineral reactions will be induced in the rock and tracers will respond to different solution chemistries and altered clay mineralogies, allowing the assessment of the capabilities and processes included in reactive transport models.

Scoping calculations have been performed to explore different possible types of alterations and expected responses, helping with final experiment design. The configuration will induce an

alteration by a high-pH solution (pH = 13.4) during 6 months. Tracer tests are possible before, during and after circulation of the high-pH solution. Different tracer responses will be correlated to the different solution chemistries, occupancies on the cation exchange sites and mineralogies.

3. IN SITU DIFFUSION EXPERIMENTS AT THE MEUSE/HAUTE-MARNE URL

The French National Agency for radioactive waste management (ANDRA) has undertaken an extensive characterization program of the Callovo-Oxfordian Clay at the Bure site in order to assess the feasibility of a deep geological disposal of high-level radioactive wastes in that formation (ANDRA, 2005; Delay et al., 2007a). In August 1999, the French government authorized ANDRA to build a scientific underground research laboratory (URL) on the border between Meuse and Haute-Marne in northeast of France. The URL includes surface facilities (administrative offices, laboratories and a public reception building) and two vertical shafts which connect the surface to underground facilities. The underground engineered structure is installed in the Callovo-Oxfordian layer. It consists of an experimental drift located at a depth of 445 m and a large network of drifts at a depth of 490 m (Figure 6).

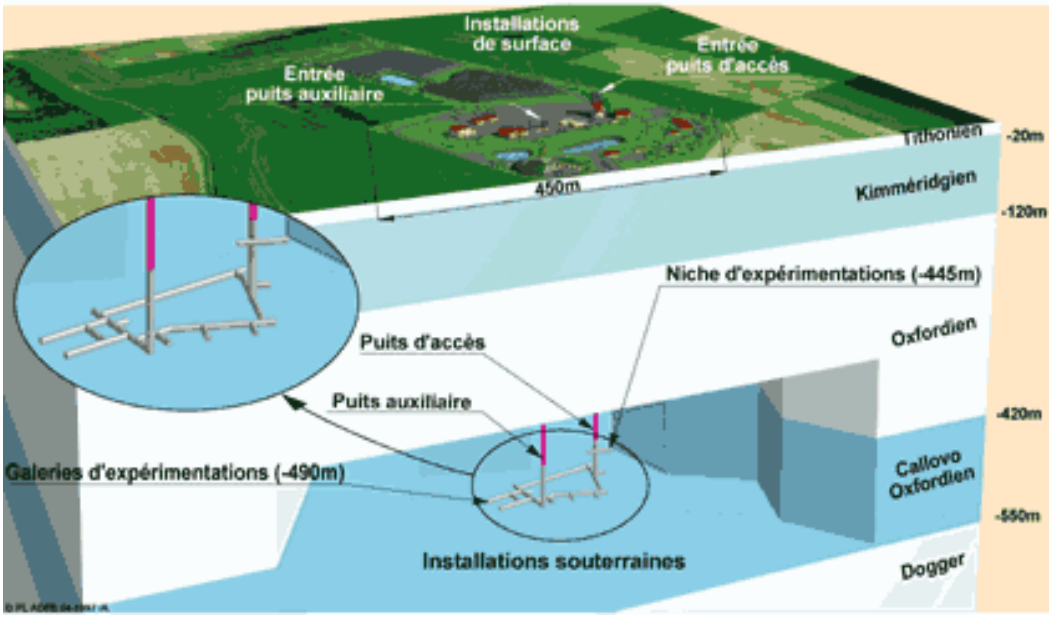

Figure 6 Layout of the Bure underground laboratory (www.andra.fr).

The laboratory enables the in situ study of the rock that is a suitable host formation for a repository. Callovo-Oxfordian (C-Ox) Clay, which is a 150-million-year-old formation, has a considerable thickness (about 150 m). It is made up, on average, of 40 to 45% clay minerals and 50 to 55% quartz and carbonates. The presence of clay minerals is favorable for the retention of radionuclides and its carbon and quartz content have good mechanical properties. The layer shows the following zones with distinct mineralogical and sedimentary characteristics:

- From C-Ox top (~417 m) to ~456 m, where illite and smectite content is small and calcite and dolomite are the dominant mineral phases.
- From ~456 m to ~490 m, where illite and smectite content is larger and calcite and dolomite content is smaller than in the above layer.

From ~490 m to the bottom of C-Ox clay formation (~555 m), where Illite/smectite are the dominant minerals.

The low porosity (between 10-20%) and low permeability (from 10^{-13} to 10^{-14} m/s) of the formation significantly restrict water flow and therefore favor radionuclide confinement. No significant convective flux has been detected in the field experiments. Therefore, diffusion is the main solute transport mechanism.

Diffusion of inert and reactive tracers (DIR) is the experimental program which aims at characterizing diffusion and retention of radionuclides in the C-Ox Clay. The main purpose of DIR in situ diffusion experiments is to analyze the predictive capabilities of the current diffusion-retention models and study scale effects by comparing results obtained at laboratory experiments with field scale data (ANDRA, 2000).

Seven in situ diffusion experiments were performed in vertical boreholes in the Bure URL to derive diffusion and retention parameters of selected tracers. Experiments DIR2001, DIR2002 and DIR2003 have been carried out in boreholes drilled from the experimental gallery located at a depth of ~445 m (Figure 7). Experiments DIR1001, DIR1002 and DIR1003 have been carried out in boreholes from a gallery located at ~490 m depth corresponding to the main level of the laboratory. Last, the EST208 experiment is taking place in a 542.5 m depth borehole drilled from the ground surface.

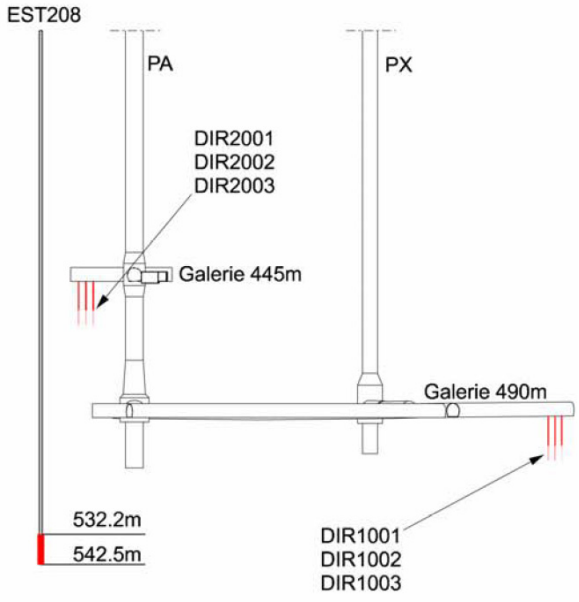

Figure 7 Location of the DIR and EST208 in situ diffusion experiments (ANDRA, 2005).

The DIR in situ diffusion experiments were performed as single point dilution tests by injecting tracers into a 1 m long packed-off section of the boreholes (ANDRA, 2007). The experiment design is similar to those performed previously at Mont Terri URL (Palut, 2001; 2003). The required downhole instrumentation consists of a pneumatic packer system with a porous screen made of sintered stainless steel mounted just below the packer at the bottom of the borehole. The isolated borehole interval is connected with a stainless steel circuit located in the surface that allows for injection and sampling of tracers. The surface instrumentation also includes: a stainless steel tank with a security mechanism that avoids pressure gradients between the system and the formation; by-passes that allow tracer injection and sampling and a set of electrodes (pH, Eh, O_2, pCO_2, electric conductivity) to measure on line chemical parameters. For DIR1002 and DIR1003 experiments, the surface circuit was also connected to a □-detector which allows the on line monitoring of the decrease of tracer activity in the system.

The volume of synthetic water (Pearson, 2006) in the circulation system is about 10 L for all the DIR experiments and it is continuously circulating. Its composition is similar to that expected in the formation (Altmann and Jacquot, 2004; Descostes et al., 2005). Once the chemical equilibrium between the synthetic water and porewater has been reached, the following tracers were injected (Table 3): tritium (HTO), chloride ($^{36}Cl^-$), iodide ($^{125}I^-$), sodium ($^{22}Na^+$), strontium ($^{85}Sr^+$), selenium ($^{75}Se^{2+}$) and cesium ($^{134}Cs^+$). Chloride and iodide are subject to anion exclusion while sodium, strontium, selenium and cesium undergo sorption. Tracers were injected in March 2005 for DIR2001 and DIR2002 experiments and in July 2005 for DIR2003 experiment. The diffusion experiments at the lower gallery started nearly one year after. Tracer injection took place in February 2006 for DIR1002 and DIR1003 experiments and in March 2006 for DIR1001 experiment.

Table 3 Tracers injected in the DIR and EST208 in situ diffusion experiments.

Experiment	Injected tracers
DIR1001	HTO
DIR1002	HTO, $^{22}Na^+$, $^{85}Sr^+$ and $^{134}Cs^+$
DIR1003	$^{125}I^-$ and $^{75}Se^{2+}$
DIR2001	HTO, $^{36}Cl^-$ and $^{125}I^-$
DIR2002	HTO, $^{22}Na^+$ and $^{134}Cs^+$
DIR2003	HTO, $^{36}Cl^-$, $^{22}Na^+$ and $^{134}Cs^+$
EST208	HTO, $^{36}Cl^-$ and $^{134}Cs^+$

The decrease of tracer concentrations in the system was monitored for about 1 year by taking aliquots from the circuit. Then, the instrumentation was dismantled and the boreholes were arranged for overcoring. The overcoring of the DIR2002 was performed in February 2006. The removal of the core was unsuccessful and just a piece of about 60 cm could be used to sample. Consequently, the overcoring of the DIR2001 experiment was postponed. The DIR2003 experiment

was dismantled in August 2008 and the DIR2002 and DIR 2003 tests were successfully overcored in January 2009.

The design of the EST208 experiment differs from that of the DIR experiments because EST208 is being performed in a 542.5 m deep borehole drilled from ground surface (Delay et al., 2007b). The set up of the experiment has been adapted for this kind of borehole. Downhole instrumentation consists of a 10 m long packed diffusion interval with a stainless steel porous filter and two hydraulic lines for flux circulation. One allows the circulation from the diffusion chamber (at the bottom of the borehole) to the ground surface. The other ensures the water flow along the surface equipment used for monitoring the geochemical parameters and the extraction of water samples during the experiment. The system was filled with ~192 L synthetic porewater that had been circulated for several months reaching chemical equilibrium with the formation. Then, HTO, $^{36}Cl^-$ and $^{134}Cs^+$ were injected as tracers in April 2005. Samples are regularly taken from then to follow the evolution of the tracers in the circulating fluid over time. Due to the design of the experiment, the overcoring of the rock around the injection interval is not feasible.

Dilution and overcoring data of these diffusion experiments were presented in some international conferences (Dewonck et al., 2009; 2010). Two effects have been clearly observed in the dilution data: 1) The effect of ionic exclusion for anionic tracers which diffusion in the rock is slowed down respect to the HTO and 2) The effect of sorption of the cationic species trapped in the rock which concentration in the circulating fluid drops faster than that of the HTO. On the other hand, $^{134}Cs^+$ is too strongly sorbed to migrate beyond the zone disturbed by the drilling (2–3 cm) and it is not possible to determine the diffusion parameters in the undisturbed rock for this element.

The modeling groups from CEA (France) and the University of La Coruña developed numerical models of the experiments using different tools and approaches (Dewonck et al., 2009). They performed sensitive and identifiability analyses and estimated diffusion and sorption parameters from dilution data, before the overcoring of the boreholes. Results showed that a 1D axisymmetric model can be used to simulate the DIR in situ diffusion experiments and the necessity to take into account a zone around the injection borehole disturbed by drilling (EdZ). Therefore, 5 diffusion parameters are required to fit the data: the D_e and the α in the EdZ, the D_e and the α in the pristine rock and the thickness of the EdZ. Despite some uncertainties (model not enough constraint), but using assumptions, the estimates are consistent with parameters measured on samples at the laboratory.

Once the dilution and overcoring data were available, CEA and Subatech modeling groups interpreted numerically the experiments by inverse modeling. The interpretation of the experiments

from dilution data or from dilution and overcoring data were presented by Dewonck et al. (2010) and Filippi et al. (2010).

Some of the modeling tasks performed by the UDC, which do not include real data, have been already published (Samper et al., 2007, 2008; Naves et al., 2010) and those performed by the author of this PhD dissertation are included in Appendixes 5 and 9.

4. REFERENCES

Altmann, S., Jacquot, E., 2004. La chimie des eaux interstitielles dans la couche du Callovo-Oxfordien à l'état initial (Site Meuse/Haute-Marne). *ANDRA Technnical Report* C.NT.ASTR.03.023.

ANDRA, 2000. Cahier des charges de réalisation du programme expérimental DIR. *ANDRA Technnical Report* D.CC.AHYG.00.020.

ANDRA, 2005. Dossier 2005 Argile –Synthèse: Evaluation de la faisabilité du stockage géologique en formation argileuse.

ANDRA, 2007. Experimentation DIR. Synthese des resultants obtenus au 01/03/07. Laboratoire de recheche souterrain de Meuse/Haute-Marne. *ANDRA Technnical Report* D.RP.ALS.07.0044.

Appelo, C.A.J., 2005. Modeling of HTO-, Na-, Cs-data from a Mont Terri diffusion experiment (DI-A1) with account of heterogeneity of the Opalinus Clay formation and geochemical reactions. Technnical report for Nagra. November 2005.

Appelo, C.A.J., Wersin, P, 2007. Multicomponent diffusion modeling in clay systems with application to diffusion of tritium, iodide and sodium in Opalinus Clay. *Enviromental Science and Technology*, 41, 50002-5007.

Appelo, C.A.J., 2008a. Modeling of Cs-data from diffusion experiments in the laboratory and in-situ DI-A experiments (phase 12) in Opalinus Clay. Part 1: Modeling laboratory data. Technnical report for Nagra. March 2008.

Appelo, C.A.J., 2008b. Modeling of Cs-data from diffusion experiments in the laboratory and in-situ DI-A experiments (phase 12) in Opalinus Clay. Part 2: Modeling DI-A1 experiment. Technnical report for Nagra. May 2008.

Appelo, C.A.J., 2008c. Modeling of Cs-data from diffusion experiments in the laboratory and in-situ DI-A experiments (phase 12) in Opalinus Clay. Part 3: Modeling DI-A2 experiment. Technnical report for Nagra. July 2008.

Bath, A., Gautschi, A., Gimmi, T., Pearson, F.J., Rübel, A., 2003. Geochemical evolution. In: *Mont Terri Project, Geochemistry Synthesis*.

Benet, L.V., Mouche, E., 2000. Evaluation du code numérique CASTEM 2000 sur les castests de migration de radio-éléments dans le site Est. *CEA technical report*. DMTSEMT/MTMS/RT/00-18/A.

Bossart, P., 2000. DI (diffusion experiment). Overcoring of borehole BD-1. Lessons learned and recommendations. *Mont Terri Project Technical Note* TN 2000-30.

Degueldre, C., Scholtis, A., Laubea, A., Turrero, M.J., Thomas, B., 2003. Study of the pore water chemistry through an argillaceous formation: a paleohydrochemical approach. *Applied Geochemistry* 18, 55–73.

Delay, J. Vinsot, A., Krieguer, J.M., Rebours, H., Armand, G., 2007a. Making of the underground scientific experimental programme at the Meuse/Haute-Marne underground research laboratory, North Eastern France. *Physics and Chemistry of the Earth* 32, 2–18

Delay, J., Distinguin, M., Dewonck, S., 2007b. Characterization of a clay-rich rock through development and installation of specific hydrogeological and diffusion test equipment in deep boreholes. *Physics and Chemistry of the Earth* 32, 393–407.

Descostes, M., Beaucaire, C., Blin, V, 2005. Rapprot de fin de phase d'équilibration – Expérimentation DIR. *ANDRA Technnical Report* D.RP.17CEA.05.016.A.

Dewonck, S., Blin, V., Radwan, J., Naves, A., Samper, J., Landesman, C., 2009. Long term in situ tracer diffusion tests in the Callovo-Oxfordian clay: Results and modeling. In: MIGRATION Conference in Kennewick (Washington, USA) in September 2009.

Dewonck, S., Blin, V., Radwan, J., Filippi, M., Landesman, C., Ribet, S., 2010. Long term in situ tracer diffusion tests in the Callovo-Oxfordian clay: Results and modeling. In: *Clays In Natural & Engineered Barriers for Radioactive Waste Confinement 4th International Meeting* in March 2010, Nantes, France.

Fierz, T., 2000a. DI Experiment: Field Activities, tracer injection, sampling, maintenance of the test equipment. *Mont Terri Project Technical Note,* TN 99-39.

Fierz, T., 2000b. DI Experiment: Overcoring operation - Suggestions for equipment improvements and optimization of test procedures. *Mont Terri Project Technical Note* TN 2000-16.

Fierz, T., 2000c. FM-C Experiment: Pilot ^{3}He and ^{4}He in-Situ diffusion tests in WS-A4. *Mont Terri Project Technical Note* TN 99-65.

Fierz, T., 2001a. FM-C Experiment: Phases 5 and 6 Helium-diffusion tests in BFM-C2 y BFM-C3. *Mont Terri Project Technical Note* TN 2000-35.

Fierz, T., 2001b. FM-C Experiment: Tritium/Iodine diffusion experiment in BFMC-3. *Mont Terri Project Technical Note* TN 2001-18.

Fierz, T., 2006. Diffusion and retention (DR) experiment. Field activities phase 11: instrumentation and tracer injection. *Mont Terri Project Technical Note* TN 2006-18.

Filippi, M., Armand, G., Blin, V., Dewonck, S., Martínez, J.M., Radwan, J., 2010. Determination of Callovo-Oxfordian argillite diffusion and thermal characteristics by inverse method: TER and DIR experiments. In: *Clays In Natural & Engineered Barriers for Radioactive Waste Confinement 4th International Meeting* in March 2010, Nantes, France.

Gimmi, Th., 2007. DR experiment Mont Terri: Scoping calculations for water tracers (HTO, HDO), iodide, sodium, strontium, barium, caesium and cobalt. *Unpublished Funmig Project Internal Report* PID 3-3-1.

Gimmi, Th., Soler, J.M., Samper, J., Naves, A., Yi, S., Leupin, O.X., Wersin, P. Van Loon, L.R. , Eikenberg, J., Dewonck, S., Wittebroodt, Ch., 2010. Insights from modelling the Diffusion and Retention experiment at the Mont Terri URL. In: *Clays In Natural & Engineered Barriers for Radioactive Waste Confinement 4th International Meeting* in March 2010, Nantes, France.

Glaus, M.A., Baeyens, B., Bradbury, M., Jakob, A., Van Loon, L.R., Yaroshchuk, A., 2007. Diffusion of ^{22}Na and ^{85}Sr in montmorillonite: Evidence of interlayer diffusion being the dominant pathway at high compaction. *Enviromental Science and Technology* 41, 478-485.

Gómez, J.J., 2000. FM-C Experiment: Part A) Effective diffusivity and accessible porosity derived from in-situ ^{4}He tests. Part B) Prediction of ^{3}He concentration in a cross-hole experiment. *Mont Terri Project Technical Note* TN 2000-40.

Gómez, J.J., Hendricks, H.J., 2000. FM-C Experiment: Scoping calculations. *Mont Terri Project Technical Note* TN 99-75.

Gómez, J.J., Cassiraga, E., Guardiola, C., 2004. FM-C Experiment: Modeling ^{3}He concentration in a cross-hole experiment. *Mont Terri Project Technical Note* TN 2000-41.

Jury, W.A., Roth, K., 1990. Transfer functions and solute movement through soil. Theory and applications. *Birkhäuser,* Basel, Switzerland.

Lauber, M., Baeyens, B., Bradbury, M.H., 2000. Physico-chemical characterisation and sorption measurements of Cs, Sr, Ni, Eu, Th, Sn and Se on Opalinus Clay from Mont Terri. *PSI Technical Report* Nr. 00-10, Paul Scherrer Institut, Villigen, Switzerland.

Leupin, O.X., Wersin, P., Gimmi, Th., Soler,J. M., Dewonck, S., Wittebroodt, C, Van Loon, L., Eikenberg, J., Baeyens, B., Samper, J., Yi, S., Naves, A., 2010. Diffusion and retention experiment at the Mont Terri underground rock laboratory in St. Ursanne. In: *Clays In Natural & Engineered Barriers for Radioactive Waste Confinement 4th International Meeting* in March 2010, Nantes, France.

Melkior, T., Yahiaoui, S., Motellier, S., Thoby, D., Tevissen, E., 2005. Cesium sorption and diffusion in Bure mudrock samples. *Applied Clay Science* 29, 172–186

Molinero, J., Samper, J., 2001. Modelización numérica preliminar del ensayo de difusión in situ (DI-B). Mont Terri. Proyecto Arcillas. Informe de progreso de la subtarea 3.1. Grupo de Hidrología subterránea, E.T.S. Caminos, Canales y Puertos. Universidade da Coruña.

Molinero, J., Samper, J., 2002. Actualización de los cálculos previos del experimento de difusión DI-B (Mont Terri). Informe de progreso. Grupo de Hidrología subterránea, E.T.S. Caminos, Canales y Puertos. Universidade da Coruña.

Montarnal, P., Lamoreux, M., 2000. DI Experiment: Numerical modeling of the experiment. *CEA technical report.* DMT SEMT/MTMS/PU/00-031.

Montarnal, P., Lamoreux, M., 2001. DI Experiment: Numerical modeling of the experiment II. *CEA technical report*. DM2S SFME/MTMS/RT/01-018.

Naves, A., Dewonck, S., Samper, J., 2010. In situ diffusion experiments: Effect of water sampling on tracer concentrations and parameters. *Physics and Chemistry of the Earth* 35, 242-247.

Nussbaum, C., Möri, A., Eikenberg, J., Rüthi, M., Aubry, C., Brisset, N., Mazurek, M., Waber, H.N., Steiger, H., Bossart, P., Drouiller, Y., 2001. FM-C Experiment: Sampling documentation and rock-water analyses of BFM-C3 overcoring borehole. *Mont Terri Project Technical* Note 2001-07.

Palut, J.M., 2001. Spécifications générales – Expérimentation DIR – Essai de Diffusion de Traceurs Inertes et Réactifs. *ANDRA Technnical Report* D.SP.ADPE.01-097.

Palut, J.M., Fierz, T., Eikenberg, J., Van Dorp, F., Mori, A., Bossart, P., Aubry, C., Garcia-Gutierrez, M., Drouiller, Y., 2002. In situ diffusion experiment DI: Field activity and data report. *Mont Terri Project Technical Note* TR 2000-03.

Palut, J.M., Montarnal, Ph., Gautschi, A., Tevissen, E., Mouche, E., 2003. Characterisation of HTO diffusion properties by an in situ tracer experiment in Opalinus Clay at Mont Terri. *Journal of Contaminant Hydrology* 61, 203-218.

Pearson, F.J., 1998. Artificial waters for use in laboratory and field experiments: status 1998. *Paul Scherrer Institute Technnical Report* TM 44-98-08.

Pearson, F.J., 2006. Diffusion and retention (DR) experiment: experimental water chemistry. *Mont Terri Technical Note* TN 2006-26.

Pocachart, J., 1997. Coefficients de diffusion et de perméabilité d'eau tritiee et d'iode à travers des échantillons du Mont Terri. ANDRA technical report D RP 3 CEA 97-006.

Rübel, A., Lippmann, J., Sonntag, C., 1999. Noble gases and isotopes from porewaters and rocks. In: *Mont Terri Rock Laboratory-Results of the Hydrogeological, Geochemical and Geotechnical Experiments Performed in 1996 and 1997* (eds. M. Thury and P. Bossart), pp. 148–151. Geological Reports Swiss National Hydrological and Geological Survey 23.

Rübel, A., Sonntag, C., Lippmann, J., Pearson, J.P., Gautschi, A., 2002. Solute transport in formations of very low permeability: Profiles of stable isotope and dissolved noble gas contents of pore water in the Opalinus Clay, Mont Terri, Switzerland. *Geochimica et Cosmochimica Acta* 66, 1311–1321.

Samper, J., Molinero, J., Yang, C., Naves, A., Yllera, A., Soler, J., Hernán, P., Mayor, J.C., Astudillo, J., 2004. . Modelización numérica tridimensional de difusión anisotrópica en rocas arcillosas consolidadas: el ensayo DI-B en el laboratorio subterráneo de Mont Terri (Suiza). *Hidropress* 45, 18-22.

Samper, J., Yang, C., Montenegro, L., 2003. Users Manual of CORE^{2D} version 4: A COde for groundwater Reactive solute transport. *UDC Technical report*, 83 pp.

Samper, J., Yang, C., Naves, A., Yllera, A., Hernández, A., Molinero, J., Soler, J.M., Hernán, P., Mayor, J.C., Astudillo, J., 2006. A fully 3-D anisotropic numerical model of the DI-B in situ diffusion experiment in the Opalinus Clay formation. *Physics and Chemistry of the Earth* 31, 531-540.

Samper, J., Yang, Q., 2007. Scoping numerical calculation for the design of the in situ diffusion and retention (DR) experiment. In: *2nd Annual Workshop Proceedings of IP FUNMIG 6th EC FP, SKB Technical report* TR-07-05, 337-343.

Samper, J., Dewonck, S., Zheng, L., Yang, Q., Naves, A., 2007. Numerical interpretation of in situ DIR diffusion experiments on C-Ox clay at Bure site. In: *Clays In Natural & Engineered Barriers for Radioactive Waste Confinement 4th International Meeting* in September 2007, Lille, France.

Samper, J., Dewock, S., Zheng, L., Yang, Q., Naves, A., 2008. Normalized sensitivities and parameter identifiability of in situ diffusion experiments on Callovo- Oxfordian clay at Bure site. *Physics and Chemistry of the Earth* 33, 1000-1008.

Soler, J.M., 2005. DR (diffusion and retention) experiment: 3D scoping calculations for water (HTO/D_2O), Iodide (I^-), Sodium ($^{22}Na^+$) and Strontium ($^{85}Sr^{2+}$). *Mont Terri Technical Note* TN 2005-24.

Soler, J.M., 2007. Diffusion and retention (DR) experiment: scoping calculations and comparison with initial tracer monitoring data. *Mont Terri Technical Note* TN 2007-01.

Soler, J.M., Samper, J., Yllera, A., Hernández, A., Quejido, A., Fernández, M., Yang, C., Naves, A., Hernán, P., Wersin, P., 2008. The DI-B in situ diffusion experiment at Mont Terri: Results and modeling. *Physics and chemistry of the Earth* 33, S196-S207.

Soler, J.M., Leupin, O.X., Gimmi, Th., Hirschorn, S., 2010. A test case for reactive transport modeling. In: 2010 *EGU General Assembly 2010, Geophysical Research Abstracts* Vol. 12, EGU2010-2071-2.

Soler, J.M., 2010. DR-A (disturbances, diffusion and retention) experiment: Reactive transport scoping calculations. *Mont Terri Technical Note* TN 2010-09.

Steefel, C.I., 2001. GIMRT, Version 1.2: software for modeling multicomponent, multidimensional reactive transport. User's Guide. Lawrence Berkeley National Laboratory, USA.

Steefel, C.I., 2006. CrunchFlow, Software for Modeling Multicomponent Reactive Flow and Transport. User's Manual. Lawrence Berkeley National Laboratory, USA.

Swisstopo, 2008. International Research Project in the Mont Terri Rock Laboratory for the Hydrogeological, Geochemical and Geotechnical Characterization of an Argillaceous Formation (Opalinus Clay). Programme Overview and Work Programme of Phase 14 (July 2008 – June 2009). Federal Office for Topography, Swisstopo. Geotechnical Institute Ltd, Switzerland

Tevissen, E., Soler, J.M., 2003. In situ diffusion experiment (DI): Synthesis Report. *Mont Terri Project Technical Note* TN 2001-05.

Thury, M., Bossart, P., 1999. The Mont Terri rock laboratory, a new international research Project in a Mesozoic shale formation, in Switzerland. *Engineering Geology* 52, 347-359.

Van Loon, L., Soler, J.M., Bradbury, M., 2003a. Diffusion of HTO, $^{36}Cl^-$ and $^{125}I^-$ in Opalinus Clay samples from Mont Terri effect of confining pressure. *Journal of Contaminant Hydrology* 61, 73– 83.

Van Loon, L., Soler, J.M., Jakob, A., Bradbury, M.H., 2003b. Effect of confining pressure on the diffusion of HTO, $^{36}Cl^-$ and $^{125}I^-$ in a layered argillaceous rock (Opalinus Clay): perpendicular to the fabric. *Applied Geochemistry* 18, 1653-1662.

Van Loon, L.R., Wersin, P., Soler, J.M., Eikenberg, J., Gimmi, Th., Hernán, P., Dewonck, S., Matray, J.M., 2004a. In-situ diffusion of HTO, $^{22}Na^+$, Cs^+ and I^- in Opalinus Clay at the Mont Terri underground laboratory. *Radiochimica Acta* 92, 757-763.

Van Loon, L., Soler, J.M., Müller, W., Bradbury, M., 2004b. Anisotropy diffusion in layered argillaceous rocks: a case of study with Opalinus Clay. *Enviromental Science and Technology* 38, 5721-2728.

Verpeaux, P., Charras, T., Millard, A., 1998. CASTEM2000, une approche modern du calcul des strcutures. IN : Fouet, J.M., Ladevevèze, P., Ohayon, R. (Eds.), *Calcul des structures et intelligence artificielle,* vol. 2, Pluralis Publishers, París, pp. 261-271.

Vitart, X., Calmels, P., 1997. Flow mechanisms FM-C: laboratory feasibility studies interim report. *Mont Terri Project Technical Note* 96-13.

Wersin, P., Van Loon, L.R., Soler, J.M., Yllera, A., Eikenberg, J., Gimmi, Th., Hernán, P., Boisson, J.-Y., 2004. Long-term diffusion experiment at Mont Terri: first results from field and laboratory data. *Applied Clay Science* 26, 123-135.

Wersin, P., van Dorp, F., 2005. Diffusion and retention (DR) experiment in borehole BDR-1 Phase 11 (1 July 2005-30 June 2006): radiation protection and working plan. *Mont Terri Project Technical Note* 2005-47.

Wersin, P., Baeyens, B., Bossart, P., Cartalade, A., Dewonck, S., Eikenberg, J., Fierz, T., Fisch, H.R., Gimmi, T., Grolimund, D., Hernán, P., Möri, A., Savoye, S., Soler, J.M., van Dorp, F., Van Loon, L., 2006. Long-term diffusion experiment (DI-A): Diffusion of HTO, I^-, $^{22}Na^+$ and Cs^+. Field activities, data and modeling. *Mont Terri Technical Report* TR 2003-06.

Wersin, P., Soler, J.M., Van Loon, L., Eikenberg, J., Baeyens, B., Grolimund, D., Gimmi, Th., Dewonck, S., 2008. Diffusion of HTO, Br^-, I^-, Cs^+, $^{85}Sr^{2+}$ and $^{60}Co^{2+}$ in a clay formation: results and modeling from an in situ experiment in Opalinus Clay. *Applied Geochemistry* 23, 678-691.

Yang, C., Juanes, R., Samper, J., Molinero, Montenegro, L., 2003. User's Manual of CORE3D. *Technical Report*, University of La Coruña, Spain.

Yang, Q., Samper, J., 2007. Numerical model of a long-term in situ diffusion and retention (DR) experiment in Opalinus Clay. In: *3rd Annual Workshop Proceedings 6th EC FP - FUNMIG IP,* November 2007, Edinburgh (Scotland).

Yllera, A., Fernández, A.M., Hernández, A.I., 2002. DI-B Experiment: Hydrogeochemistry and transport mechanisms in the Opalinus Clay formation. Test Plan. *Ciemat Technical Report* CIEMAT/DIAE/54470/8/01.

Yllera, A., Hernández, A., Mingarro, M., Quejido, A., Sedano, L.A., Soler, J.M., Samper, J., Molinero, J., Barcala, J.M., Martín, P.L., Fernández, M., Wersin, P., Rivas, P., Hernán, P., 2004. DI-B experiment: planning, design and performance of an in situ diffusion experiment in the Opalinus Clay formation. *Applied Clay Science* 26, 181-196.

APPENDIX 3

A FULLY ANISOTROPIC NUMERICAL MODEL OF THE DI-B IN SITU DIFFUSION EXPERIMENT IN OPALINUS CLAY

This appendix presents the paper "A fully anisotropic numerical model of DI-B experiment in the Opalinus Clay formation" which was presented in the international conference MIGRATION05 which took place in Avignon (France) in August 2005 and also published by Physics and Chemistry of the Earth in 2006

This paper is the result of a joint research work including the contributions from other researchers. My main contribution includes the predictive calculations, the sensitivity runs and the parameter calibration for HDO and I^-.

Available online at www.sciencedirect.com
SCIENCE DIRECT
Physics and Chemistry of the Earth 31 (2006) 531–540
PHYSICS and CHEMISTRY of the EARTH
www.elsevier.com/locate/pce

A fully 3-D anisotropic numerical model of the DI-B in situ diffusion experiment in the Opalinus clay formation

J. Samper [a,*], C. Yang [a], A. Naves [a], A. Yllera [b], A. Hernández [b], J. Molinero [c], J.M. Soler [d], P. Hernán [e], J.C. Mayor [e], J. Astudillo [e]

[a] *Escuela Técnica Superior de Ingenieros de Caminos, Canales y Puertos, Campus de Elviña s/n, 15192 LA Coruña, Spain*
[b] *Dpto. de Medio Ambiente, Unidad Barreras de Ingeniería y Geológica, CIEMAT, Edificio 20-A, Avda. Complutense, 22, 28040 Madrid, Spain*
[c] *Escola Politécnica Superior, Universidad de Santiago de Compostela, 27002 Lugo, Spain*
[d] *CSIC-ICTJA, Lluís Solé i Sabarís s/n, 08028 Barcelona, Spain*
[e] *ENRESA, Emilio Vargas 7, 28043 Madrid, Spain*

Received 12 August 2005; received in revised form 28 January 2006
Available online 27 June 2006

Abstract

In situ diffusion experiments have been performed at underground research laboratories in clay formations to overcome the limitations of laboratory diffusion experiments and investigate possible scale effects. The DI-B experiment is a long-term, natural-scale, in situ diffusion experiment performed in a packed section in a borehole drilled vertically into the anisotropic Opalinus clay formation at Mont Terri in Switzerland. A cocktail of non-radioactive tracers was used. Tracers were monitored for one year at the test interval and measured at samples taken from an overcored interval. Contrary to the methods used so far for the interpretation of in situ experiments which rely on 2-D models and disregard diffusion across bedding, here we present a fully 3-D anisotropic finite element model of the DI-B experiment. The numerical model has been calibrated with iodide and deuterium data. The fully anisotropic 3-D model provides reliable estimates of effective diffusion coefficients and accessible porosities for deuterium and iodide which are within the range of published values. We show that a simple 2-D model can be safely used to interpret data along central profiles although it may lead to biased estimates when applied to profiles located near the edges of the test interval. Computed concentrations in the borehole are much less sensitive to changes in model parameters than concentrations along profiles. Computed concentrations close to the borehole are most sensitive to the accessible porosity while concentrations at distances greater than 0.085 m are most sensitive to the diffusion coefficient parallel to the bedding. Computed concentrations along some profiles are sensitive to the effective diffusion perpendicular to bedding.

Keywords: Anisotropic diffusion; DI-B in situ experiment; 3-D numerical model; Deuterium; Iodide; Opalinus clay

1. Introduction

Safety assessment of nuclear waste disposal in a deep geological repository requires understanding and quantifying radionuclide transport through the hosting geological formation. Clay media usually exhibit extremely low hydraulic conductivities and therefore molecular diffusion becomes the most relevant transport process.

Diffusion and sorption laboratory experiments have enlarged our understanding of these processes and provided a wealth of data on diffusion and sorption parameters (Horseman et al., 1996). These experiments are often performed on small samples up to 1 cm which may have suffered alterations during their preparation. To prevent the limitations of lab experiments and investigate possible scale effects, various in situ diffusion experiments have been performed at underground research laboratories such as that of Mont Terri in Switzerland (Palut et al., 2003; Tevissen et al., 2004; Wersin et al., 2004; Van Loon et al., 2004b; Yllera et al., 2004). In situ experiments typically involve a

* Corresponding author. Tel.: +34 981 16 70 00x1433; fax: +34 981 16 71 70.
E-mail address: jsamper@udc.es (J. Samper).

1474-7065/$ - see front matter © 2006 Elsevier Ltd. All rights reserved.
doi:10.1016/j.pce.2006.04.017

mass of rock having a length at least an order magnitude larger than that of lab experiments.

The DI-B experiment is a long-term, natural-scale, in situ diffusion experiment performed in a packed section into a borehole drilled vertically in the Opalinus clay formation at Mont Terri. The following non-radioactive tracers were used: $^{6}Li^{+}$, $^{87}Rb^{+}$, D_2O and I^{-}. Tracers were monitored for one year at the test interval. In addition, clay samples were taken from the overcored interval. Hydrogeochemical modeling confirmed the stability of all tracers. Supporting batch sorption experiments showed no sorption for ^{6}Li, D_2O and I (conservative tracers), whereas ^{87}Rb was near 100% sorbed (Yllera et al., 2004). Laboratory diffusion experiments were carried out both parallel and perpendicular to the bedding to provide diffusion coefficients for modeling purposes. Predictive numerical models were used for the design of the in situ experiment. Based on lab diffusion experiments performed parallel and perpendicular to the bedding, Van Loon et al. (2004a) reported that the effective diffusion coefficient of the Opalinus clay parallel to bedding is 4 times greater than the diffusion perpendicular to bedding at Mont Terri. They also found that sorption coefficients and accessible porosities of tritium, $^{36}Cl^{-}$ and $^{22}Na^{+}$ were the same in both types of experiments. Wersin et al. (2004) reported the results of theDI-A in situ diffusion experiment. They interpreted concentration profiles from overcoring by using a 1-D axial symmetric model. Such a model which assumes that diffusion takes place only along bedding planes is valid if the length of the testing interval is much larger than the penetration of the tracer into the rock. Since the length of the testing interval of the DI-B experiment is shorter than that of DI-A, the assumption of negligible diffusion perpendicular to bedding may not be acceptable. Here we present a fully 3-D finite element model which accounts for the anisotropic behavior of diffusion and imposes no restrictions for diffusion across the bedding. The numerical model has been calibrated with iodide and deuterium data. It is planned to model also in the future the diffusion of $^{6}Li^{+}$ and $^{87}Rb^{+}$.

The paper starts by describing the DI-B in situ diffusion experiment. Then, available tracer data for iodide and deuterium at the testing interval and along profiles from overcoring are presented. After that, we present a fully 3-D anisotropic numerical model of the experiment. Sensitivity analyses of concentrations to changes in key transport parameters are used to evaluate parameter uncertainties, quantify model errors and calibrate accessible porosity and effective diffusion coefficients.

2. In situ DI-B diffusion experiment

The diffusion experiment was carried out at the BDI-B3 borehole located at the entrance of the DI niche in the New Gallery of the Mont Terri underground laboratory in Switzerland. This zone of the Mont Terri tunnel corresponds to the shaly facies of the Opalinus clay, a few meters away from the underlying formation (Jurensis Marl, Toarcian). The in situ diffusion experiment was performed as a single point dilution test by injecting stable tracers into a packed-off section at the bottom of a vertical borehole 7.7 m deep. The bedding planes of the rock dip in the NW–SE direction, at an angle of 58° with respect to the vertical borehole which has a radius of 0.038 m. The length of the borehole where tracers were injected is 0.6 m. The experiment included downhole and surface instrumentation. Downhole instrumentation consisted of a pneumatic single-packer system with a porous screen made of sintered stainless steel mounted just below the packer at the bottom of the borehole. Surface instrumentation included a closed 316-l stainless steel circuit intended to circulate the water containing the following tracers: ^{6}Li, ^{87}Rb, D_2O and I (as I^{-}) (Yllera et al., 2004). Injection and sampling of tracers was done from the main tank through a valve system.

3. Borehole and overcoring data

3.1. Borehole data

Tracers in the borehole were monitored during the experiment at increasing times starting from hours at the beginning to several days at the end of the experiment. Deuterium was measured with mass spectrometry (MS) and iodide with an ion selective electrode (ISE) technique (Yllera et al., 2004).

Deuterium and iodide data in the borehole are plotted in Figs. 3(A) and 5(A), respectively. Concentrations of both tracers in the borehole show slow overall decreasing trends with time from an initial relative concentration (C/C_0) of 1 to 0.91 for iodide and to 0.87 for deuterium. In addition to the gentle decreasing trends, both tracers show fluctuations which are especially noticeable during the first 150 days for deuterium. These fluctuations caused by pressure oscillations in the injection system and sporadic clogging of the filters of the circulation system, however, did not affect the overall performance of the experiment.

3.2. Overcoring data

Tracer distribution in the surrounding host rock was obtained by overcoring of the DI-B test interval. The removal of the overcore in the test interval was completed successfully with no core losses (see Fig. 1(A)). Several sandy layers and a small tectonic fracture were observed in the overcore at the upper part of the interval (Inderbitzin et al., 2004). Such sandy layers, which are common in the shaly facies of the Opalinus clay, have transport parameters different than those of the bulk claystone. Samples were taken from the overcore to obtain concentration profiles of D_2O and I^{-} in different directions from the pilot borehole (Inderbitzin et al., 2004).

Fig. 1(A) shows a view image of the overcore of BDI-B3. Fig. 1(B) illustrates the location of the 12 profiles which were sampled from the overcore while Fig. 1(C) shows also the bedding. The drilling core in each profile was sliced into

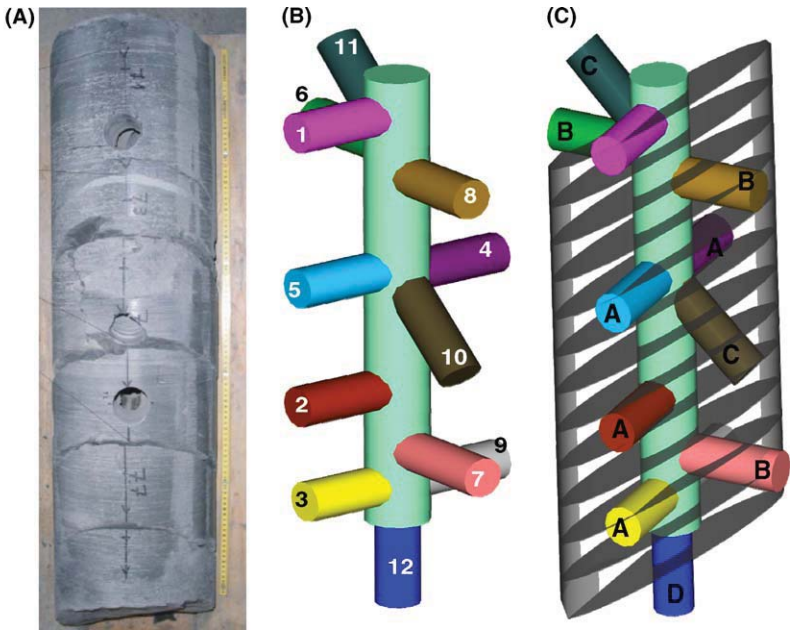

Fig. 1. (A) View of overcore of BDI-B3, (B) schematic location of the 12 sampling profiles and (C) types of profiles depending on their orientation with respect to the bedding.

a number of samples ranging from 9 to 12, each one having a thickness of 1 cm. Profiles 1–5 and 9 are horizontal and parallel to bedding, profiles 6, 7 and 8 are also horizontal but perpendicular to profiles 1–5, profiles 10 and 11 are quasi perpendicular to the bedding and profile 12 is vertical from the bottom of the borehole.

Deuterium and iodide profile data are shown in Figs. 3 and 5 where radial distances are measured to the center of the borehole. Concentration data along overcore profiles show less noise than data in the borehole.

Concentrations of deuterium along profile 5 are greater than those along profile 10 for the same distance to the center of the borehole. Relative concentrations of deuterium along profiles 5 and 10 are shown in Fig. 3(B). Profile 5 is parallel to the bedding while profile 10 intersects the bedding at an angle of 74° (Fig. 1(B) and (C)). It can be seen that the smaller the angle between the profile and the bedding, the larger the penetration of deuterium into the rock. Deuterium diffusion is fastest along planes parallel to bedding while the slowest diffusion occurs along the direction perpendicular to bedding. This confirms that the anisotropy in diffusion for Opalinus clay identified previously in laboratory experiments (Van Loon et al., 2004a) is observed also in the in situ experiment. In addition, the ratio of diffusion coefficient parallel to bedding to that perpendicular to bedding of around 4 serves also to model the DI-B experiment.

Fig. 5(C) illustrates the relative concentrations of iodide along profiles 2, 3 and 9. Profile 9 is located on the opposite side of profiles 2 and 3. Tracer concentrations are the same along these three profiles. This confirms that tracer concentrations are radially symmetric along horizontal lines parallel to the bedding. Such symmetry is lost at other horizontal directions. It is worth noting that the relative concentrations of iodide near to the borehole along the profiles are smaller than that in the borehole because the relative concentrations along the profiles are the product of concentrations computed in the numerical model and the ratio between accessible porosity and total porosity.

Although the tracer plume in the clay is not axysymmetric, it is symmetric with respect to a vertical plane which passes through the axis of the borehole and is perpendicular to the direction of the stratification.

It should be noticed, however, that contrary to what was expected, iodide concentrations at symmetric profiles 4 and 5 (not shown here) are not identical. Differences in concentrations among the two profiles could be caused by local rock heterogeneities.

Figs. 3(D) and 5(D) show the relative concentrations of deuterium and iodide along profile 7, respectively.

4. Numerical model

4.1. Solute transport equation

The transport equation for a tracer which diffuses into a very low permeability medium is given by Bear (1972)

$$\phi_a R \frac{\partial C}{\partial t} = \nabla \cdot (\overline{D}_e \cdot \nabla C) \quad (1)$$

where C is tracer concentration, t is time, ϕ_a is accessible porosity which accounts for anion exclusion and R is retardation factor. R is equal to 1 and ϕ_a is equal to the total porosity if the tracer is not affected by anion exclusion or by adsorption. $\overline{D}_e$ is the effective diffusion tensor given by

$$\overline{D}_e = \begin{pmatrix} D_{xx} & D_{xy} & D_{xz} \\ D_{yx} & D_{yy} & D_{yz} \\ D_{zx} & D_{zy} & D_{zz} \end{pmatrix} \quad (2)$$

which can be diagonalized as

$$\overline{D}'_e = \begin{pmatrix} D_{\xi\xi} & 0 & 0 \\ 0 & D_{\eta\eta} & 0 \\ 0 & 0 & D_{\zeta\zeta} \end{pmatrix} \quad (3)$$

where $D_{\xi\xi}$, $D_{\eta\eta}$ and $D_{\zeta\zeta}$ are the principal components of the tensor. The components of the effective diffusion tensor in (2) can be calculated from the main components in (3) using equations similar to those of the permeability tensor (Bear, 1972). In this study, $D_{\xi\xi}$ and $D_{\eta\eta}$ are equal to the diffusion coefficient parallel to the bedding while $D_{\zeta\zeta}$ is equal to the diffusion coefficient perpendicular to the bedding.

4.2. Model domain and spatial discretization

Tracer diffusion plumes are symmetric with respect to a vertical plane perpendicular to bedding which divides vertically the borehole into two equal parts. Therefore, only half of the system needs to be modeled. A domain of $2\,m \times 1\,m \times 2.6\,m$ has been taken into consideration for the numerical model (Fig. 2(A)).

The model domain was discretized using hexahedral finite elements which are small near the borehole and increase their size far away from the borehole. The mesh of the model has 16321 nodes and 14923 elements (Fig. 2(B)).

4.3. Material zones and boundary conditions

The numerical model considers three material zones: (1) the packed-off section of the borehole where tracers are injected; (2) the steel plate at the bottom of the borehole with a thickness of 1 cm and (3) the Opalinus clay. In the model the borehole has a porosity equal to 1 and a sufficiently large diffusion coefficient to ensure a homogenous tracer distribution within the borehole. Small values of porosity (10^{-5}) and an extremely small effective diffusion coefficient ($\sim 10^{-21}$ m^2/s) are adopted for the steel plate at the bottom of the borehole. Parameters of the Opalinus clay are tracer-dependent and are discussed in Section 5. The numerical model considers the angle between bedding and the x–y horizontal plane to be 32° (Inderbitzin et al., 2004). Background tracer concentrations are much smaller than measured concentrations along profiles. According to Yllera et al. (2004) the background concentration of iodide is less than 1 mg/L while concentrations measured along profiles range from 180 to 700 mg/L. Therefore, it can be assumed that initial tracer concentrations in the clay are equal to zero. Tracers diffuse from the borehole into the Opalinus clay. All external boundaries of the model are no-flow boundaries.

4.4. Numerical code

CORE^{3D} (Yang et al., 2003) has been used to simulate the DI-B in situ experiment. CORE^{3D} is a fully 3-D computer code for modeling saturated water flow, heat transport and multi-component reactive solute transport under both local chemical equilibrium and kinetic conditions. The capability of CORE^{3D} to simulate anisotropic diffusion has been verified with analytical solutions for 3-D configurations (Yang et al., 2003).

5. Results for deuterium

Deuterium diffuses into the clay as a conservative tracer. Model results depend on effective diffusion coefficient and

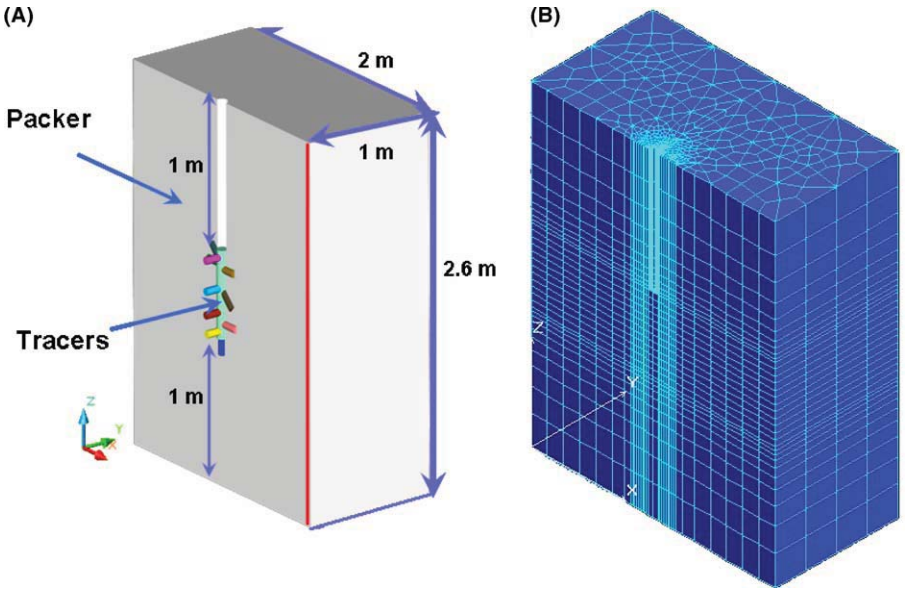

Fig. 2. (A) Domain of the numerical model and (B) finite element mesh used in the numerical model.

total porosity. Available values of the total porosity of Opalinus clay include: 0.12–0.18 (Thury, 2002) and 0.1 (Wersin et al., 2004). Wersin et al. (2004) adopted a value of 10^{-11} m^2/s for the effective diffusion coefficient of deuterium parallel to bedding in the numerical simulation of DI-A and DI-B in situ experiments. Van Loon et al. (2004a) reported values of porosity and effective diffusion coefficients for tritium. Van Der Kamp and Van Stempvoort (2001) reported that the effective diffusion coefficient of D_2O ranges from 5.1×10^{-11} to 10.0×10^{-11} m^2/s and porosity from 0.17 to 0.25. Reported values of transport parameters of D_2O in Opalinus clay are listed in Table 1.

Model parameters were calibrated by a trial-and-error method fitting model results to measured data in the borehole and along profiles starting with an effective diffusion coefficient parallel to the bedding of 10^{-11} m^2/s, an

Table 1
Summary of reported values of transport parameters for deuterium and iodide in Opalinus clay

TRACER	D_e parallel (m^2/s)	D_e perpendicular (m^2/s)	ϕ (%)	References
D_2O	–	–	12–17	Thury (2002)
	–	$(3.5\pm1.3)\times10^{-11}$		Rübel et al. (2002)
	–	$(5.2\pm1.6)\times10^{-11}$		Degueldre et al. (2002)
	$(5.1, 10.0)\times10^{-11}$	–	17–25	Van Der Kamp and Van Stempvoort (2001)
I	14×10^{-12}	3.2×10^{-12}	12	Pocachart (1997)
	7.1×10^{-12}	$(2.3–3.0)\times10^{-12}$	12–17	Yllera et al. (2001, 2004)
	$7.14\pm0.46\times10^{-12}$	–	–	Tevissen et al. (2004)
	–	$(3.2\pm0.2)\times10^{-12}$	6–8	Van Loon et al. (2004a,b)
	–	4.1×10^{-12}	9	Jefferies and Myatt (2000)
	–	$(2.4–3.3)\times10^{-12}$	7	Maes et al. (2000) and Van Loon et al. (2001)
	25×10^{-12}	–	5	Gómez-Hernández and Guardiola-Albert (2004)
	15×10^{-12}	–	13	Tevissen et al. (2004)
	16×10^{-12}		8.5	Wersin et al. (2004)
	10×10^{-12}	–	9	Van Loon et al. (2004a,b)

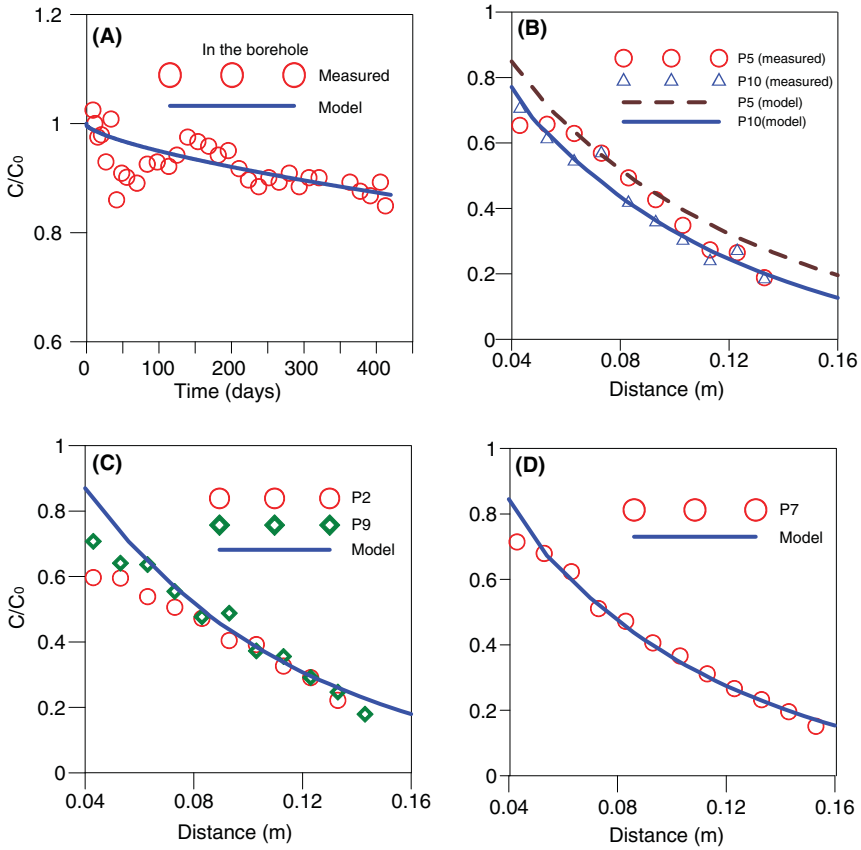

Fig. 3. Measured and computed relative concentrations of D_2O in: (A) borehole, (B) profiles 5 and 10, (C) profiles 2 and 9, and (D) profile 7.

anisotropy ratio of 4 and a total porosity of 0.2. Calibrated values are 4×10^{-11} and 10^{-11} m^2/s for the effective diffusion coefficients parallel and perpendicular to bedding, respectively and 0.15 for total porosity.

Calibration results are shown in Fig. 3. A comparison of computed and measured concentrations in the borehole is shown in Fig. 3(A). One can see that the numerical model reproduces the overall trend of measured data in the borehole. Model results fit also measured data along profiles 10 (Fig. 3(B)), 2 and 9 (Fig. 3(C)), and 7 (Fig. 3(D)). However, data along profile 5 (Fig. 3(B)) are slightly overestimated probably due to the local heterogeneities of the rock.

Computed concentrations near the borehole overestimate measured values along profiles 2, 7 and 9 (Fig. 3). This could be caused by a disturbed zone (DZ) around the borehole. Experimental evidence from boreholes drilled in the Callovo-Oxfordian clay at Bure site (Dewonck, 2005) indicate that DZ around boreholes have a porosity double of that of the formation and a thickness of around 2–3 cm. Their effect on in situ diffusion experiments include: (1) a relatively rapid initial decrease of concentrations in the borehole fluid, and (2) a flattening of concentration profiles in the formation close to the borehole. Interpretation methods failing to account for a DZ underestimate the formation diffusion coefficient. Deuterium data from DI-B experiment do not allow drawing clear conclusions about the relevance of a DZ because: (1) only some profiles show the flattening of concentrations near the borehole, (2) data measured in the borehole fluid show fluctuations which preclude a clear analysis of a possible change in the slope of the curve, and (3) the size of clay samples (1 cm) is not small enough to characterize properly the DZ. A sensitivity analysis was performed by accounting for a DZ of 2 cm thickness with a porosity twice that of the formation. Such analysis indicates that the DZ has a much larger effect on deuterium than on iodide concentrations. DZ affects mostly the concentrations in the portion of the rock located in the vicinity (5 cm) of the DZ.

A model always entails simplifications of the real system. Model results depend on parameters that may contain uncertainties. A sensitivity analysis was performed to evaluate model uncertainties. Taking the calibrated model as the base run, several sensitivity runs were performed by changing one-at-a-time porosity and effective diffusion coefficients parallel and perpendicular to bedding.

Fig. 4(A) shows the sensitivity of the concentration in the borehole to changes in effective diffusion coefficient parallel to bedding. Fig. 4(B) and (C) shows the sensitivities of computed concentrations along profile 7 to the effective diffusion coefficient parallel to bedding and the porosity of the clay, respectively. The larger the porosity and the effective diffusion coefficient parallel to bedding, the larger the

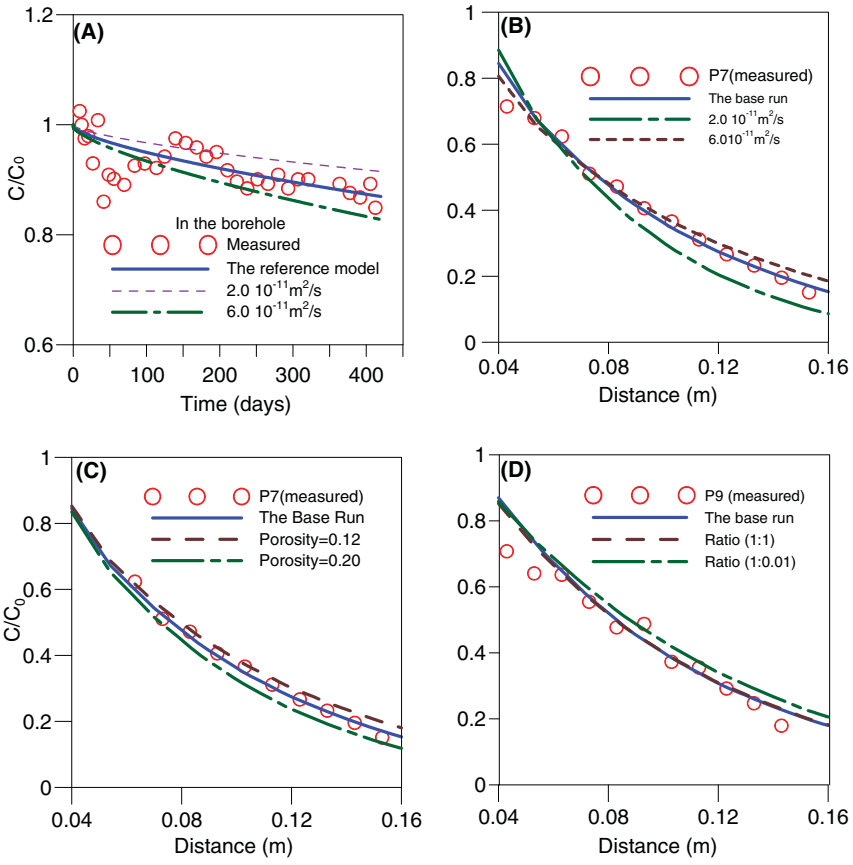

Fig. 4. Sensitivity of relative concentrations of D_2O in: (A) borehole to effective diffusion coefficient parallel to bedding, (B) profile 7 to effective diffusion coefficient parallel to bedding, (C) profile 7 to porosity and (D) profile 9 to diffusion anisotropy ratio (horizontal to perpendicular to bedding).

concentrations at the tails of the profiles. Fig. 4(D) illustrates the sensitivity of the computed concentrations along profile 9 to the effective diffusion coefficient perpendicular to bedding. In the base run, the ratio of the effective diffusion coefficient parallel to bedding to that perpendicular to bedding is 1:0.25. The sensitivity run with a ratio of 1:0.01 corresponds to quasi 2-D diffusion through planes parallel to bedding. The sensitivity run with a ratio of 1:1 corresponds to the isotropic diffusion case.

The results of sensitivity runs are evaluated by means of relative or normalized sensitivities which are summarized in Table 2. Computed concentrations along profiles are much more sensitive to changes in parameters than computed concentrations in the borehole. Computed concentrations in the borehole are most sensitive to the effective diffusion coefficient parallel to bedding. Computed concentrations for radial distances smaller than 0.085 m are most sensitive to the porosity while for $r > 0.085$ m computed concentrations are most sensitive to the effective diffusion coefficient parallel to bedding. Computed concentrations of deuterium along profiles show some sensitivity to the effective diffusion coefficient perpendicular to bedding (Fig. 4(D)).

The estimation error of a parameter is inversely proportional to the sensitivity of concentration to such parameter. Therefore, from the results of Table 2 it can be concluded

Table 2
Summary of the sensitivity analysis of deuterium concentrations[a]

Parameter		Concentration sensitivities					
Name	Relative change (%)	In the borehole		<0.085 m		>0.085 m	
		Relative change (%)	Relative sensitivity	Relative change (%)	Relative sensitivity	Relative change (%)	Relative sensitivity
Total porosity	33.3	1.1	0.033	4.1	0.123	13	0.39
De parallel to bedding	50	5	0.1	1.4	0.028	70	1.4
De perpendicular to bedding	300	1.7	0.00567	0.3	0.001	4.728	0.0158

[a] Relative changes of parameters (CP) are defined as $\frac{|\Delta P|}{P_b} \times 100$, and relative changes in concentrations (AS) as $\frac{|\Delta C|}{C_b} \times 100$, where ΔP is the parameter change with respect to its calibrated base value, P_b, and ΔC is the change in concentration compared to the concentration in the base run C_b. Relative sensitivity is defined as $\frac{AS}{CP}$.

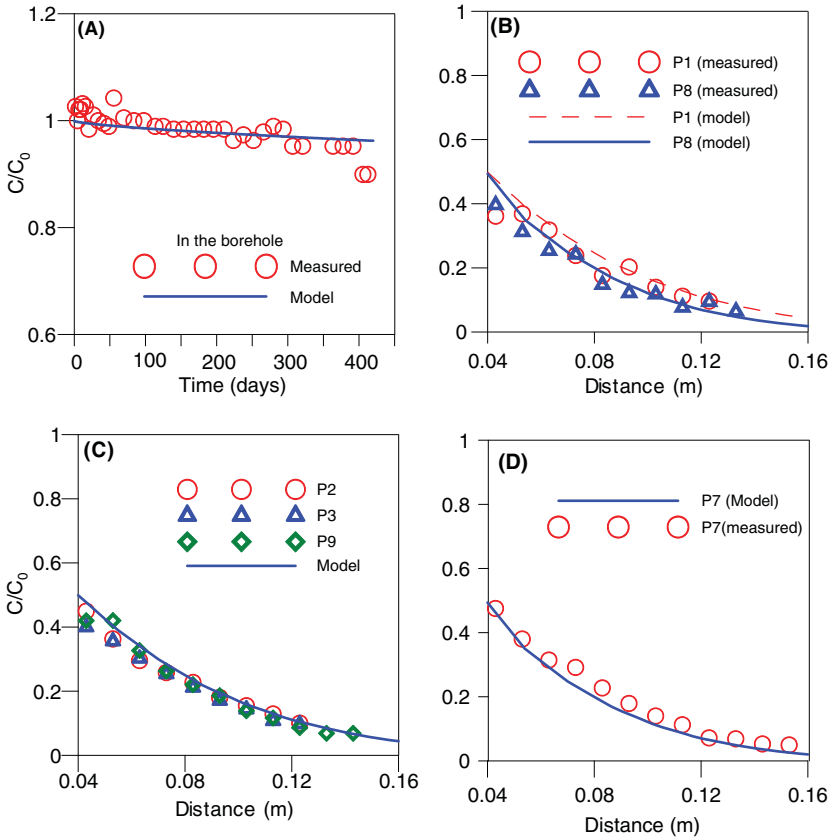

Fig. 5. Measured and computed relative concentrations of iodide in: (A) borehole, (B) profiles 1 and 8, (C) profiles 2, 3 and 9, and (D) profile 7.

that the relative estimation error of the effective diffusion parallel to bedding is 3 times smaller than that of porosity and 10 times smaller than that of the effective diffusion perpendicular to bedding when one uses concentration data measured at $r > 0.085$ m. It should be noticed that the estimation error for porosity is smaller than that of effective diffusion parallel to bedding when one uses concentration data measured at $r > 0.085$ m.

6. Results for iodide

Laboratory experiments provide estimates of iodide transport parameters in Opalinus clay. Yllera et al. (2001, 2004) obtained an effective diffusion coefficient parallel to bedding of $(1.38 \pm 0.49) \times 10^{-11}$ m^2/s, with an anisotropy ratio of 5.1. Tevissen et al. (2004) reported an effective diffusion coefficient of 7.1×10^{-12} m^2/s. Pocachart (1997) obtained an effective diffusion coefficient parallel to bedding of 1.4×10^{-11} m^2/s and an anisotropy ratio of 4.3. Wersin et al. (2004) presented a numerical model to interpret the DI-A diffusion experiment and obtained a value of 1.6×10^{-11} m^2/s for the effective diffusion coefficient parallel to bedding. They fitted data with an accessible porosity of 0.085. Van Loon et al. (2004a) in their review of available values of parameters for several tracers provided a value of 10^{-11} m^2/s for the effective diffusion coefficient parallel to bedding and a value of 0.09 for accessible porosity for iodide. Reported values of transport parameters for iodide in Opalinus clay are summarized in Table 1.

Calibrated values are 0.08 for porosity and 8.27×10^{-12} m^2/s for the effective diffusion coefficient parallel to bedding with an anisotropy ratio of 4. Calibrated results are shown in Fig. 5. The numerical model reproduces the overall trend of the time evolution of iodide in the borehole (Fig. 5(A)). Fig. 5(B)–(D) shows the comparison of computed concentrations and measured data along several profiles. One can see that numerical results agree well with data along profiles 1 (Fig. 3(B)), 2, 3 and 9 (Fig. 3(C)) and 7 (Fig. 3(D)). The numerical model overestimates slightly the data along profile 8 (Fig. 5(B)) probably due to the local heterogeneities of the rock in the upper part of the testing interval where sandy layers were observed.

Sensitivity runs were performed for accessible porosity and diffusion coefficients parallel and perpendicular to bedding (Fig. 6). Fig. 6(A) shows the sensitivity of computed concentration in the borehole to changes in accessible porosity. It can be seen that computed concentrations are not sensitive to accessible porosity. Fig. 6(B) and (C) illustrates the sensitivity of computed concentrations along

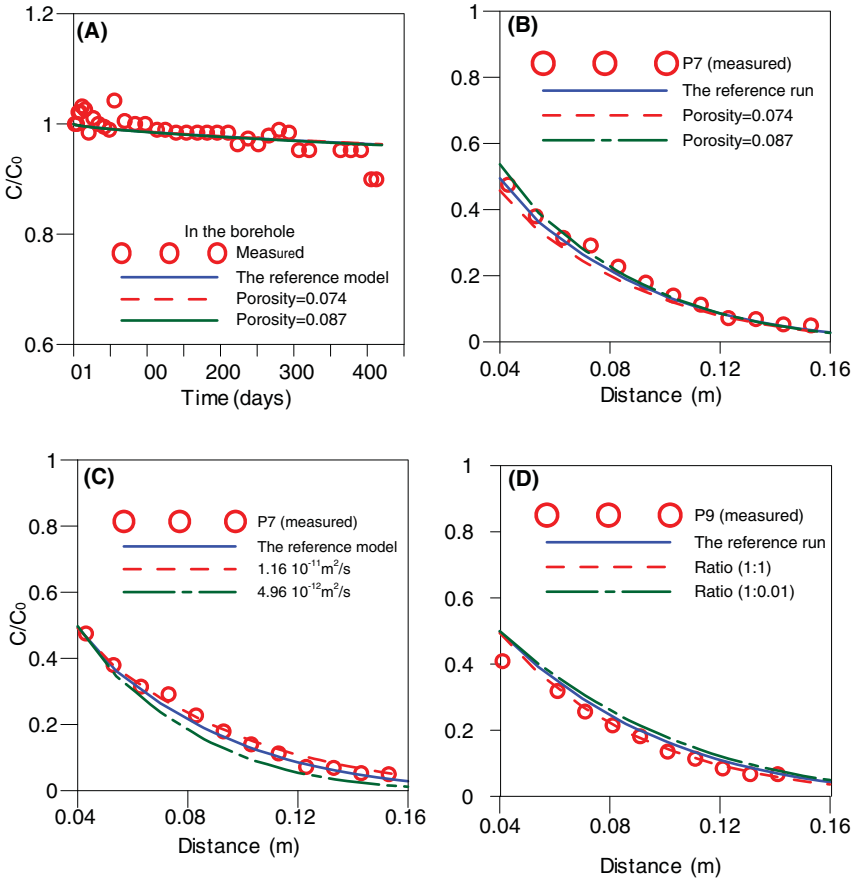

Fig. 6. Sensitivity of relative concentrations of iodide in: (A) the borehole to porosity, (B) profile 7 to porosity, (C) profile 7 to effective diffusion coefficient parallel to bedding and (D) profile 9 to diffusion anisotropy ratio.

Table 3
Summary of the sensitivity analysis performed of iodide concentrations[a]

Parameter		Concentration sensitivities					
Name	Relative change (%)	In the borehole		<0.085 m		>0.085 m	
		Relative change (%)	Relative sensitivity	Relative change (%)	Relative sensitivity	Relative change (%)	Relative sensitivity
Accessible porosity	8.7	0.01	0.00115	7.29	0.833	3.3	0.377
De parallel to bedding	40	0.9	0.02	4.2	0.105	21.4	0.53
De perpendicular to bedding	300	0.42	0.0014	5.9	0.02	19.4	0.065

[a] See Table 2 for definitions of relative changes and sensitivities.

profile 7 to accessible porosity and effective diffusion coefficient parallel to bedding, respectively. It can be seen that the larger the accessible porosity, the larger the concentrations near the borehole (Fig. 6(B)). Similarly, the larger the effective diffusion coefficient, the larger the concentrations in the tails of the curves (Fig. 6(C)). Computed concentrations along profile 9 show some sensitivity to changes in the effective diffusion coefficient perpendicular to bedding (Fig. 6(D)).

The results of sensitivity runs are evaluated by means of relative or normalized sensitivities which are summarized in Table 3. Similar to deuterium, computed concentrations in the borehole are less sensitive to changes in parameters than concentrations computed along profiles. Moreover, computed concentrations in the borehole are most sensitive to the diffusion coefficient parallel to bedding. Computed concentrations at radial distances less than 0.085 m are most sensitive to accessible porosity while for distances greater than 0.085 m, concentrations are most sensitive to effective diffusion coefficient parallel to bedding.

7. Conclusions

Tracer data measured along the profiles of the overcore of the DI-B in situ experiment confirm the anisotropy of diffusion through Opalinus clay. A fully 3-D finite element model accounting for anisotropic diffusion has been used to interpret concentration data in the borehole and along profiles of the overcore and to derive in situ transport parameters for deuterium and iodide. Model results match concentrations measured in the borehole and along profiles of the overcore and capture the anisotropy of tracer plumes. The best fit for deuterium is achieved with a porosity of 0.15, an effective diffusion coefficient parallel to bedding equal to 4×10^{-11} m^2/s and an anisotropy ratio of 4. For iodide the best fit is obtained with an accessible porosity of 0.08, an effective diffusion coefficient parallel to bedding of 8.27×10^{-12} m^2/s and an anisotropy ratio equal to 4. These values fall within the range of reported transport parameters for deuterium and iodide in Opalinus clay.

A suite of sensitivity runs have been performed to evaluate parameter uncertainties. Computed concentrations in the borehole are much less sensitive to changes in model parameters than concentrations along profiles. Computed concentrations close to the borehole are most sensitive to the accessible porosity while concentrations at distances greater than 0.085 m are most sensitive to the diffusion coefficient parallel to the bedding. The least sensitivity of computed concentrations corresponds to the effective diffusion perpendicular to bedding. However, concentrations along some profiles show some sensitivity to this parameter.

It can be argued that a simple 2-D anisotropic model which disregards diffusion across bedding could provide similar results to those obtained here with a fully 3-D anisotropic model. However, a fully 3-D model is needed to evaluate the uncertainties of the simpler 2-D model. On the other hand, the 3-D model is the most appropriate way to test the role of anisotropy at in situ conditions without resorting to unnecessary simplifying conditions. It has been shown here that the 3-D model allows the simultaneous interpretation of the concentrations measured along all profiles. The comparison of the fully 3-D anisotropic model with a 2-D anisotropic model indicates that both give similar results along profiles located at the center of the interval. Concentrations along profiles located near the edges of the interval computed with 2-D and 3-D models show some noticeable differences. From a practical point of view, a simple 2-D model can be safely used to interpret data along central profiles. However, it may lead to biased estimates (up to 50% error in effective diffusion) when applied to profiles located near the edges of the interval.

Acknowledgments

This work was supported by the Spanish Nuclear Waste Company (ENRESA) within the framework of Contract 0770125 signed with Universidad de La Coruña. We thank the two anonymous reviewers for their thoughtful comments and suggestions.

References

Bear, J., 1972. Dynamics of Fluids in Porous Media. Elsevier, New York.
Degueldre, C., Scholtis, A., Laube, A., Turrero, M.J., Thomas, B., 2002. Study of the pore water chemistry through an argillaceous formation: a hydropaleochemical approach. Appl. Geochem. 18, 55–73.
Dewonck, S., 2005. Expérimentation DIR-Synthèse des résultats obtenus sur les forages EST208, DIR2001, DIR2002 et DIR2003 au 30/09/05.

Technical Report, D RP ADPE 05-0719, Laboratoire de Recherche Souterrain de Meuse/Haute-Marne, France (in French).

Gómez-Hernández, J.J., Guardiola-Albert, C., 2004. FM-C Experiment: three-dimensional model predictions of tracer evolution of HTO and iodine in the main fault. Mont Terri Project, Technical Note, TN 00-42, Switzerland.

Horseman, S.T., Higgo, J.J.W., Alexander, J., Harrington, F.F., 1996. Water, gas, and solute movement through argillaceous media, NEW-OECD Report CC-96, Nuclear Energy Agency, Organisation for Economic Co-Operation and Development, Paris, France.

Inderbitzin, L., Möri, A., Nussbaum, C., Yllera, A., Brisset, N., Steiger, Y., Bossart, P., 2004. Long term diffusion (DI-B) experiment: sampling documentation of BDI-B3 OC borehole. Mont Terri Project Technical Note, TN04-69, Switzerland.

Jefferies, N.L., Myatt, B.J., 2000. DI Experiment: laboratory experiment on an Opalinus clay sample. Mont Terri Project Technical Note, TN 99-61, Switzerland.

Maes, N., Aertsens, M., De Cannière, P., Put, M., 2000. DI Experiment: results of the trough diffusion experiments performed at SCK-CEN. Mont Terri Project Technical Note, TN 99-59, Switzerland.

Palut, J.M., Montarnal, P., Gautschi, A., Tevissen, E., Mouche, E., 2003. Characterisation of HTO diffusion properties by an in situ tracer experiment in Opalinus clay at Mont Terri. J. Contam. Hydrol. 61 (1), 203–218.

Pocachart, J., 1997. Coefficients de diffusion et de permeabilité d'eau tritiée et d'iode à travers des echantillons du Mont Terri. Technical Report ANDRA D RP 3 CEA 97-006 (in French).

Rübel, A., Sonntag, C., Lippmann, J., Pearson, F.J., Gautschi, A., 2002. Solute transport in formations of very low permeability: profiles of stable isotope and dissolved noble gas contents of pore water in the Opalinus clay, Mont Terri, Switzerland. Geochim. Cosmochim. Acta 66 (8), 1311–1321.

Tevissen, E., Soler, J.M., Montarnal, P., Gautschi, A., Van Loon, L.R., 2004. Comparison between in situ and laboratory diffusion studies of HTO and halides in Opalinus clay from the Mont Terri. Radiochim. Acta 92, 781–786.

Thury, M., 2002. The characteristics of the Opalinus clay investigated in the Mont Terri underground rock laboratory in Switzerland. CR Phys. 3, 923–933.

Van Der Kamp, G., Van Stempvoort, D.R., 2001. WS-B Experiment: laboratory measurement of porosity, pore water isotopic composition and effective diffusivities of Opalinus clay core samples. Mont Terri Project, Technical Note, TN98-38, Switzerland.

Van Loon, L.R., Soler, J., Bradbury, M.H., 2001. DI Experiment: a laboratory comparison exercise (SCK.SCN/AEA/CIEMAT). Mont Terri Project Technical Note, TN00-02, Switzerland.

Van Loon, L.R., Soler, J., Müller, W., Bradbury, L., 2004a. Anisotropic diffusion in layered argillaceous rocks: a case study with Opalinus clay. Environ. Sci. Technol. 38, 5721–5728.

Van Loon, L.R., Wersin, P., Soler, J.M., Eikenberg, J., Gimmi, Th., Hernán, P., Dewonck, S., Savoye, S., 2004b. In situ diffusion of HTO, $^{22}Na^{+}$, Cs^{+} and I^{-} in Opalinus clay at the Mont Terri underground rock laboratory. Radiochim. Acta 92, 757–763.

Wersin, P., Van Loon, L.R., Soler, J., Yllera, A., Eikenberg, J., Gimmi, T., Hernan, P., Boisson, J.-Y., 2004. Long-term diffusion experiment at Mont Terri: first results from field and laboratory data. Appl. Clay Sci. 26, 123–135.

Yang, C., Juanes, R., Samper, J., Molinero, J., Montenegro, L., 2003. Users manual of CORE^{3D}, Technical Report, Universidad de La Coruña, Spain.

Yllera, A., Mingarro, M., García-Guiérrez, M., 2001. Tritium and iodide diffusion through Opalinus clay. Mater. Res. Soc. Symp. Proc. 663, 1179–1185.

Yllera, A., Hernández, A., Mingarro, M., Quejido, A., Sedano, L.A., Soler, J.M., Samper, J., Molinero, J., Barcala, J.M., Martín, P.L., Fernández, M., Wersin, P., Rivas, P., Hernán, P., 2004. DI-B experiment: planning, design and performance of an in situ diffusion experiment in the Opalinus clay formation. Appl. Clay Sci. 26, 181–196.

APPENDIX 4

THE DI-B IN SITU DIFFUSION EXPERIMENT AT MONT TERRI: RESULTS AND MODELING

This appendix contains the paper "The DI-B in situ diffusion experiment at Mont Terri: Results and modeling" which was presented in the international conference *Clays in Natural & Engineered Barriers for Radioactive Waste Confinement* which took place in Lille (France) in September 2007 and also published by Physics and Chemistry of the Earth in 2008.

This paper is the result of a joint research work including the contributions from other researchers. My main contribution included the sensitivity runs and the calibration of the three-dimensional model performed with CORE^{3D} for all the tracers.

Physics and Chemistry of the Earth 33 (2008) S196–S207

Contents lists available at ScienceDirect

Physics and Chemistry of the Earth

journal homepage: www.elsevier.com/locate/pce

The DI-B in situ diffusion experiment at Mont Terri: Results and modeling

J.M. Soler [a,f,*], J. Samper [b], A. Yllera [c], A. Hernández [c], A. Quejido [c], M. Fernández [c], C. Yang [b], A. Naves [b], P. Hernán [d], P. Wersin [e]

[a] Institut de Ciències de la Terra "Jaume Almera" (CSIC), Lluís Solé i Sabarís s/n, 08028 Barcelona, Spain
[b] Universidade da Coruña, Campus de Elviña, 15192 A Coruña, Spain
[c] CIEMAT, Avda. Complutense 22, 28040 Madrid, Spain
[d] ENRESA, Emilio Vargas 7, 28043 Madrid, Spain
[e] NAGRA, Hardstrasse 73, CH-5430 Wettingen, Switzerland
[f] IDAEA (CSIC), Jordi Giroma 18, 08034 Barcelona, Spain

ARTICLE INFO

Article history:
Available online 11 October 2008

Keywords:
Diffusion
Sorption
Clay
Moldeling

ABSTRACT

The diffusion experiment "DI-B" aimed at studying the transport and retention properties of selected non radioactive tracers in the Opalinus Clay (shaly facies) at the Mont Terri URL. Selected tracers were: ^{2}H (water), I^- (anionic species), $^{6}Li^+$ (non- or weakly-sorbing cation) and $^{87}Rb^+$ (strongly-sorbing cation). The experiment was performed as a single point dilution test by injecting tracers into a packed-off section at the bottom of a vertical borehole. The experiment, which lasted slightly over one year, was designed so that the length of the injection interval (0.6 m) was larger than tracer transport distances. A rock overcoring around the injection interval after the experiment allowed the measurement of tracer distribution profiles.

Two and three-dimensional modeling has been performed using the CRUNCH and CORE^{3D} reactive transport codes, respectively. The experimental setup favored, in principle, a 2D interpretation of the results, since diffusion occurs mainly along bedding planes. Conservative tracers from 2D modeling gave: $De_{||} = 5.0 \times 10^{-11}$ m^2/s, $\varphi = 0.16$ (HDO) and $De_{||} = 1.2 \times 10^{-11}$ m^2/s, $\varphi = 0.09$ (I^-). Results from 3D modeling are: $De_{||} = 4.0 \times 10^{-11}$ m^2/s, $De_{||}/De_{\perp} = 4$, $\varphi = 0.15$ (HDO) and $De_{||} = 8.3 \times 10^{-12}$ m^2/s, $De_{||}/De_{\perp} = 4$, $\varphi = 0.08$ (I^-). Differences in the results may be due to the two geometries (3D / 2D), to various aspects of the calculations or to comparison methods between model and experimental data. A previous sensitivity analysis performed with the 3D model had shown that the effect of considering only diffusion along the bedding planes ($De_{||}/De_{\perp} = 100$) was relatively minor, causing only a significant effect on tracer distribution in the rock near the top and bottom edges of the injection interval. The differences between the two sets of results are small and confirm the smaller effective diffusion coefficient and accessible porosity of I^- with respect to HDO. The results corresponding to $^{6}Li^+$ and $^{87}Rb^+$ have also been modeled using both 2D and 3D approaches. For $^{6}Li^+$ ($C_0 = 3 \times 10^{-5}$ mol/l), the best fit for both models was achieved with $De_{||} \approx 7 \times 10^{-11}$ m^2/s, Kd ≈ 0.2 l/kg and $\varphi = 0.15$–0.16. The De and Kd values are very similar to those obtained previously for Na^+ at Mont Terri. This Kd value is certainly larger than what was initially expected. Regarding $^{87}Rb^+$ ($C_0 = 3 \times 10^{-7}$ mol/l), only three profiles were finally measured, and they showed significant variability. This variability has also been observed for other strongly sorbing tracers (Cs^+, Co^{2+}) in the DI-A and DI-A2 in situ experiments at Mont Terri. It has not been possible to obtain unique values for $De_{||}$ and Kd for $^{87}Rb^+$, although strong sorption has been confirmed.

1. Introduction

Argillaceous formations are being considered as potential host rocks for the deep geological disposal of radioactive waste, mainly due to their low permeability and good sorption properties. In this type of rocks, water and solute transport is dominated by diffusion.

Within the framework of the Mont Terri Project, the study of the transport and retention properties of the Opalinus Clay Formation has been the focus of a major experimental effort. Chemical profiles of chloride, bromide, sodium, helium, deuterium and ^{18}O in the Opalinus Clay porewater at Mont Terri are consistent with slow diffusion from the saline Opalinus Clay porewater to the young groundwaters of the adjacent limestone formation (Degueldre et al., 2003; Rübel et al., 2002). The results obtained from a first

* Corresponding author. Address: Institut de Ciències de la Terra "Jaume Almera" (CSIC), Lluís Solé i Sabarís s/n, 08028 Barcelona, Spain. Fax: +34 934110012.
E-mail addresses: jsoler@ija.csic.es (J.M. Soler), jsamper@udc.es (J. Samper), abel.yllera@ciemat.es (A. Yllera), pher@enresa.es (P. Hernán), paul.wersin@nagra.ch (P. Wersin).

1474-7065/$ - see front matter © 2008 Elsevier Ltd. All rights reserved.
doi:10.1016/j.pce.2008.10.010

in situ diffusion experiment with conservative tracers (DI Experiment) showed that the transport properties for tritium (HTO) were consistent with through-diffusion measurements obtained on small-sized Opalinus Clay samples (Palut et al., 2003; Tevissen et al., 2004). The DI-A experiment made use of both conservative (HTO, I^-) and sorbing tracers ($^{22}Na^+$, Cs^+). The results (Wersin et al., 2004; Van Loon et al., 2004b; Wersin et al., 2006) showed a good agreement between laboratory and field results and confirmed the effect of anion exclusion on the transport properties of I^- (reduced effective diffusion coefficient and accessible porosity).

After the start of the DI-A experiment, the DI-B project was designed. The DI-B experiment was a Spanish Project led by Enresa and financed by Enresa and Nagra. One of its main objectives was to study the transport and retention properties of selected tracers in the Opalinus Clay, but using only non radioactive species. The selected tracers (Yllera et al., 2004) were deuterated water (HDO), I^- (anionic species), $^6Li^+$ (non- or weakly-sorbing cation) and $^{87}Rb^+$ (strongly-sorbing cation).

2. Experimental concept

The diffusion experiment was carried out in the BDI-B3 borehole located at the entrance of the DI niche in the Gallery 98 of the Mont Terri Underground Rock Laboratory. This zone corresponds to the shaly facies of the Opalinus Clay, a few meters away from the underlying formation (Jurensis Marl, Toarcian). The in situ diffusion experiment was performed as a single point dilution test by injecting stable tracers into a packed-off section at the bottom of a vertical borehole 7.7 m deep (Fig. 1). At this location, bedding dips 32° to the SE. The length of the borehole interval where tracers were injected was 0.6 m, with a 0.038 m radius.

Downhole instrumentation consisted of a pneumatic single packer system with a porous screen made of sintered stainless steel mounted just below the packer at the bottom of the borehole. Surface instrumentation included a closed 316-l stainless steel circuit intended to circulate the synthetic porewater containing the tracers. To ensure that solution chemistry and pressure were in equilibrium with the rock, synthetic Opalinus Clay porewater (Yllera et al., 2004) without any added tracers was circulated during approximately 5 months prior to tracer injection. Injection and monitoring of tracers were done from the main tank through a valve system. The total volume of solution in the circulation system was about 30 l. Further details regarding the experimental setup are reported by Yllera et al. (2004).

A volume of rock around the injection interval was overcored after the end of the experiment, allowing the measurement of tracer distribution profiles. The experiment lasted slightly over one year (417 days; September 6th 2002–October 28th 2003). The overcore removal in the test interval was completed successfully with no core losses (Fig. 2A). Several sandy layers and a small tectonic fracture were observed in the overcore at the upper part of the interval. Such sandy layers, which are common in the shaly facies of the Opalinus Clay, are probably characterized by transport parameters different than those of the bulk claystone. Several subcores were taken from the overcore in order to obtain tracer concentration profiles along different directions from the pilot borehole (Fig. 2B). Each subcore was sliced into a number of samples (1 cm thick) ranging from 9 to 12. Profiles 1–5 and 9 are horizontal and parallel to bedding (Fig. 2C); profiles 6–8 are also horizontal but perpendicular to profiles 1–5 (32° angle with respect to bedding); profiles 10 and 11 are at an angle of 74° with respect to bedding; profile 12 is vertical (Fig. 2C).

Every sliced sample was weighed and placed into pre-weighed plastic (polyethylene) bottles containing 40 ml of deionized water. The bottles were closed and, previously to the chemical and isotopic analyses, shaken for two months in an orbital shaker at 4 °C, until total disintegration of the solid. Then, the samples were centrifuged (26,300 g) and the liquid fractions separated from the solid phase for tracer analyses. The remaining solid fraction was kept for gravimetric determination of the moisture content by heating at 105 °C until constant weight. The average moisture content for the samples was 6.77 ± 0.71%.

The analyses of the aqueous extracts obtained from the solid (overcore) and liquid samples (monitoring from circulation tank) were performed as follows:

Deuterated water: Analyses of the samples highly enriched in deuterium give rise to some difficulties. Common isotope ratio mass spectrometers are not designed to analyze waters with such peculiar isotope compositions. In order to avoid possible analytical inaccuracies from the mass spectrometer (mainly produced by poor linearity) or from the preparative method, and to make adequate corrections and normalization, four standards were prepared from commercial deuterium oxide enriched to 99.9% in deuterium (Cambridge Isotope Laboratories, Inc). The selected dilutions for the standards were 1:50 (1.998% D), 1:200 (0.4995% D, 1:500 (0.1998% D) and 1:1000 (0.0999% D). A considerable number of standards were processed together with the samples and their results were employed to correct the isotope composition of the water samples by linear correlation. The standard deviation in the δD determination is 1‰.

The hydrogen for the isotope ratio analysis was extracted from the water by reduction with zinc (provided by Indiana University). In this process, 8 μl of water are added to "Ace Glass" stopcocks containing 0.5 g of Zn. The mixture is frozen at liquid nitrogen temperature and a vacuum is applied through a diffusion pump. Then, the stopcocks are heated in an aluminum furnace during 90 min at 475 °C. After cooling, the stopcock is connected to the manifold of a dual inlet "VG Prism II" Isotope Ratio Mass Spectrometer.

Iodide was determined by using two analytical techniques; the potentiometric method (also called Ion Selective Electrode) and ion chromatography. In the first method, an Orion Model 94–53 iodide electrode, together with a simple-junction Orion 90-01 reference electrode and an Orion Model 901 microprocessor ion analyzer, were used. The electrode potential of standard solutions was measured to determine the calibration curve in two concentration intervals. The direct measurement procedure was used in all linear regions. The detection limit was 10 μg l^{-1}. Iodide was also quantified by the ion chromatography technique using a Dionex 4500i ion chromatograph. The analytical columns included a guard column Dionex AG9 and a separator column Dionex AS9. Detection was achieved with a conductivity detector. A Dionex Anion Micromembrane Suppressor AMMS-II was used in order to suppress the conductivity of the eluent. The calibration standard was prepared daily by dilution of a 1000 mg l^{-1} stock solution (1.18 g reagent-grade NaI in a 1 l volumetric flask). The detection limit for a 25 μl injection volume was 0.11 mg l^{-1} (calibration curve in the range 1–25 mg l^{-1}) and for a 100 μl injection volume was 10 μg l^{-1} (calibration curve in the range 25–1000 μg l^{-1}).

Lithium and rubidium: Total Li was analyzed by flame photometry using a Perkin Elmer 2280 atomic absorption spectrophotometer, measuring the lithium emission at 670.6 nm. Due to the low Li concentrations observed in the pore water samples, calibration standards ranging from 0.01 to 1.0 mg l^{-1} of Li were prepared. The quantification limit, according to Eurachem recommendations, was 0.01 mg l^{-1}. Reproducibility was close to 5% at concentrations close to the quantification limit and below 1% at concentrations above 0.1 mg l^{-1}. The method was validated against a water sample containing 0.02738 mg l^{-1} of Li prepared by the US Geological Survey and the National Institute for Science and Technology and certified by the JRC-IRMM during the IMEP-9 programme.

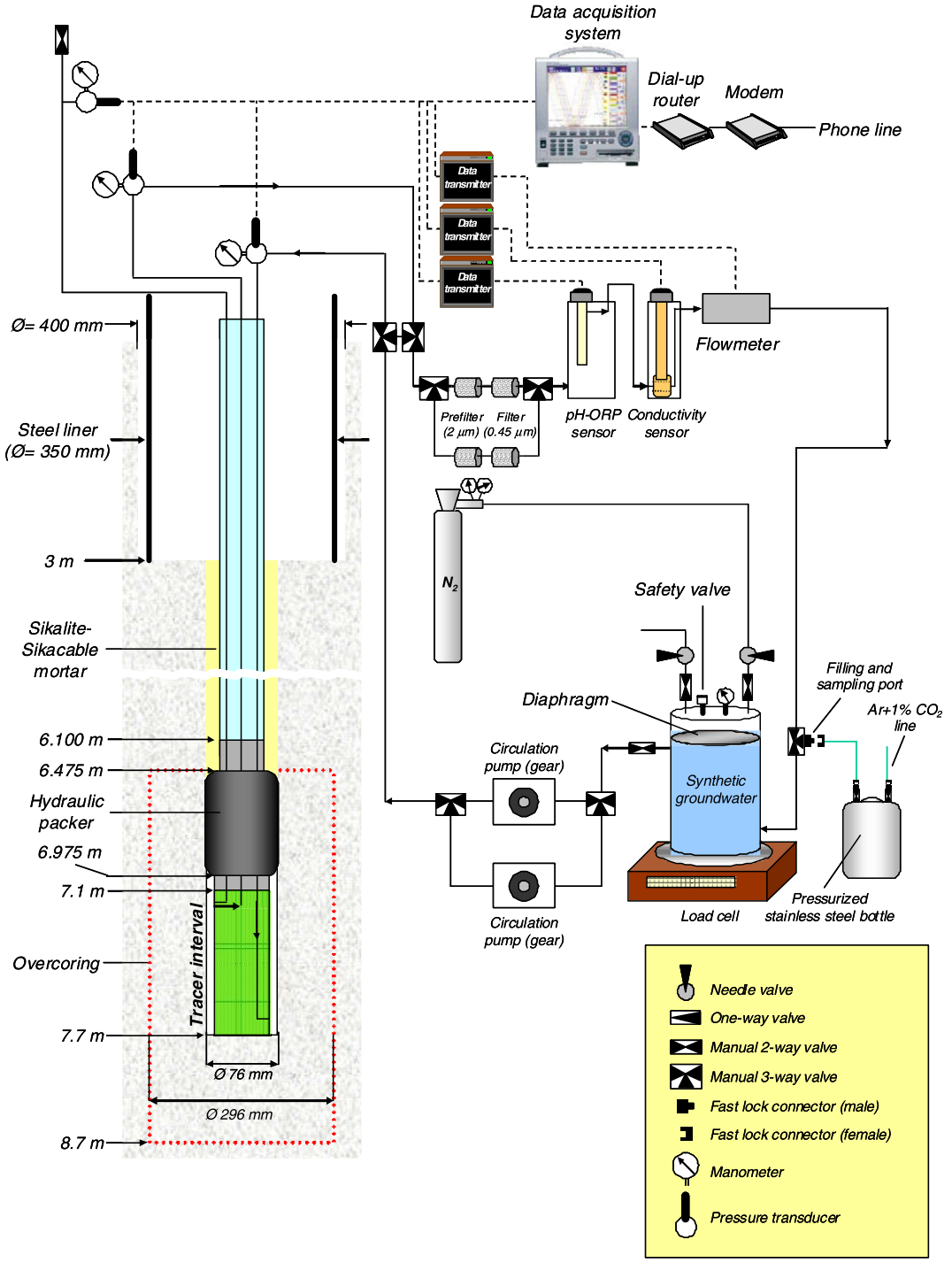

Fig. 1. Experimental setup of the DI-B in situ diffusion experiment. Downhole (left) and surface (right) instrumentation. After Yllera et al. (2004).

The total Rb content was determined by inductively coupled plasma mass spectrometry (ICP-MS), using a Finnigan MAT SOLA instrument equipped with a quadrupole analyzer and both Faraday cup and continuous dynode electron multiplier. The measurements were performed using external calibration and Ga as internal standard. Final concentration was calculated taking into account the $^{85}Rb/^{87}Rb$ isotopic ratio for each sample. Detection limit was below 0.2 µg l^{-1} and reproducibility was close to 2%.

The isotopic analysis of Li and Rb was performed in two steps: (i) purification and separation of Li and Rb from the sample matrix using a cation exchange resin, and (ii) measurement of $^{6}Li/^{7}Li$ and $^{85}Rb/^{87}Rb$ isotopic ratio by thermal ionization mass spectrometry (TIMS). The whole procedure is summarized in the flow chart given in the Fig. 3 and the experimental details are given below.

Ion exchange chromatography: The purification and separation procedure developed in this study is an optimized combination of several chromatographic methods used for the separation of Li and Rb from geological samples (Sanz and Wasserburg, 1969; You and Chan, 1996; Moriguti and Nakamura, 1998). PTFE columns with a PTFE mesh plug as support of the resin bed were filled up with Dowex resin (50W-X8, 200–400 mesh). Then, the resin was cleaned with H_2O and 6 M HCl and finally conditioned with

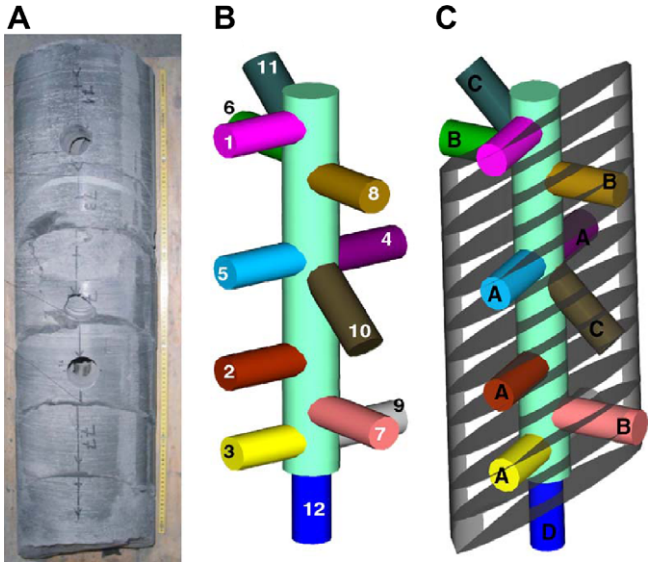

Fig. 2. (A) View of overcore of BDI-B3, (B) schematic location of the 12 sampling profiles and (C) types of profiles depending on their orientation with respect to bedding. After Samper et al. (2006).

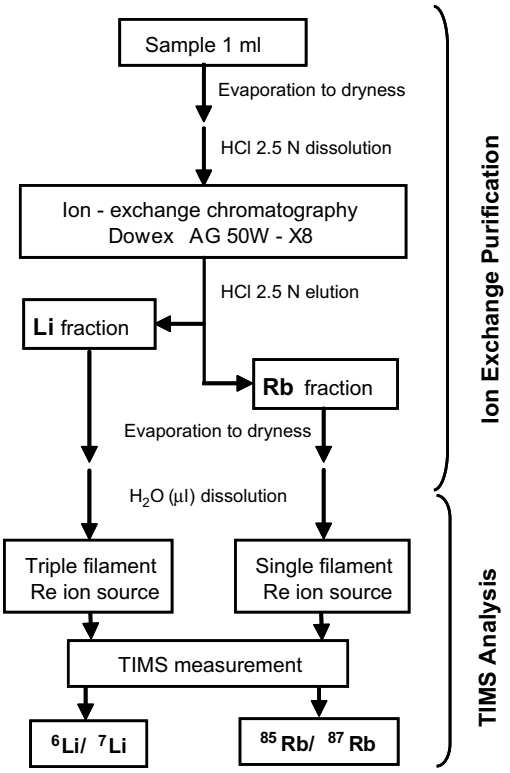

Fig. 3. Protocol for the purification and isotopic analysis of the Li and Rb tracers.

2.5 M HCl. The whole separation process was performed using 2.5 M HCl as eluent. 1 ml of the aqueous sample was evaporated to dryness and the residue was dissolved in 2 ml of 2.5 M HCl. This solution was loaded onto the resin bed, which was then rinsed with 5 ml of the eluent. The Li fraction was subsequently eluted with 4 ml of the 2.5 M HCl. After that, 13 ml of 2.5 M HCl were passed through the column to eliminate Na, prior to the Rb collection with 7 ml of the acid eluent. The separated Li and Rb fractions were then evaporated to dryness under infrared light. The residues were finally dissolved with the appropriate H_2O volume, according to the element concentration previously determined.

Mass spectrometry: The samples were analyzed in a 60° magnetic sector NIST mass spectrometer, fitted with a Faraday collector. The source and the collector slit openings were 0.007 and 0.04 inches, respectively, for both elements. The accelerating voltage was set at 9780 V. The source configuration was triple rhenium filament for Li and single rhenium filament with the silica gel technique for Rb. The measurements were performed using a program developed in the laboratory based on LabView 7.0 software. When the isotope ratios were calculated, a linear interpolation was applied in order to correct for possible variations in signal intensity during the measurement. The instrumental mass discrimination factors were checked against the standards SRM-987 and IRMM-016a for Rb and Li, respectively. The typical internal reproducibility was below 0.5% (average of 10 ratios) for both elements and is expressed as 1 standard deviation.

3. Results and interpretation

The results of the diffusion experiment included the evolution of tracer concentrations in the injection system and tracer distribution profiles in the rock. Two and three-dimensional modeling of the results has been performed using the CRUNCH (Steefel, 2006) and CORE^{3D} (Yang et al., 2003) reactive transport codes, respectively.

3.1. Modeling with CRUNCH

The results from the field experiment have been interpreted by means of two-dimensional transport calculations including diffusion and sorption. The experiment was designed so the length of the injection interval was larger than tracer transport distances. This experimental setup favors, in principle, a simple 2D interpretation of the results, since diffusion occurs mainly along bedding planes.

The finite difference reactive transport code CRUNCH has been used for the simulations. CRUNCH is the latest evolution of the GIMRT/OS3D software package (Steefel, 2001; Steefel and Yabusaki, 1996).

The equation of conservation of mass for a given tracer can be written as

$$\frac{\partial c_{tot}}{\partial t} = \nabla \cdot (D_e \nabla_c) \quad (1)$$

where c is concentration in solution [moles per volume of solution], t is time [s], D_e is the effective diffusion coefficient [m^2 s^{-1}], φ is the accessible porosity for the tracer and c_{tot} is the total concentration of tracer [moles per bulk volume], which is given by

$$c_{tot} = \phi c + \rho_d s \quad (2)$$

where ρ_d is the bulk dry density [kg m^{-3}] and s is the concentration of tracer sorbed on the solids [moles per mass of solid].

Linear sorption ($s = K_d c$) has been assumed for the sorbing tracers. With the inclusion of linear sorption, the total concentration c_{tot} can also be expressed as the product of a rock capacity factor α and the concentration in solution c ($c_{tot} = \alpha\varpi$ $c = (\varphi + \rho_d K_d)$ c).

The geometry of the problem is schematically shown in Fig. 4. The calculation domain corresponds to a bedding plane. The fact that the bedding is at an angle (58°) with respect to the borehole is taken into account by the elliptical shape of the borehole (intersection of bedding and borehole). The dip of bedding is 32°. All the boundaries of the domain are no-flux boundaries. The initial conditions are

$$\text{Borehole}: \quad c(x,y,t=0) = c_{tot}(x,y,t=0) = c_0$$
$$\text{Rock}: \quad c_{tot}(x,y,t=0) = c_{back}$$

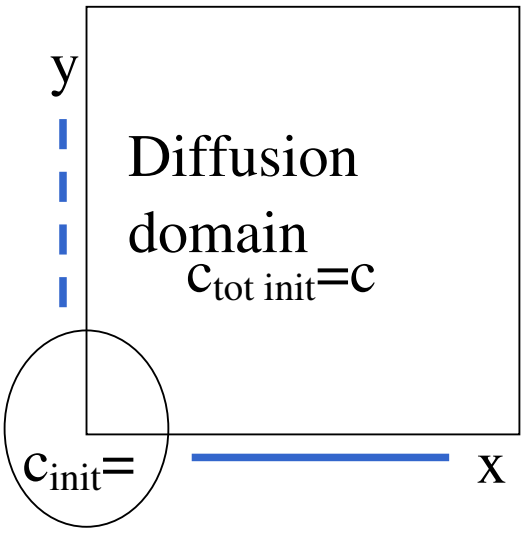

Fig. 4. Schematic representation of the geometry of the model. The calculation domain corresponds to a bedding plane and the borehole (area enclosed by the square). The trace of the borehole is not cylindrical due to the 58° angle between bedding and borehole. The solid and dashed lines parallel to the x and y axes make reference to the orientations of the calculated tracer profiles shown in Figures that follow.

where c_0 is the initial concentration in the injection system and c_{back} is the background concentration of the tracer in the Opalinus Clay. Only a quarter of the two-dimensional system is taken into account in the calculations due to symmetry considerations (diffusion is assumed to be homogeneous and isotropic along the plane). A large value of D_e is assumed in the borehole, in order to maintain a homogeneous concentration (well mixed conditions in the injection system). The total volume of solution in the injection system (about 30 l) is also taken into account.

The results of model calculations are compared with the evolution of tracer concentrations in the injection system and the measured tracer profiles in the rock around the borehole. In the case of the tracer profiles not measured along a bedding plane it has been necessary to project those profiles onto the bedding plane, in order to be able to compare them with the results of the 2D model calculations. Profile 12, at the bottom of the borehole, was not included in any of the results for the 2D calculations. Fitting tracer concentrations in (a) the injection system and (b) in the rock profiles provides a unique set of effective diffusion coefficients (D_e) and porosity/sorption values (rock capacity factors in the case of linear sorption).

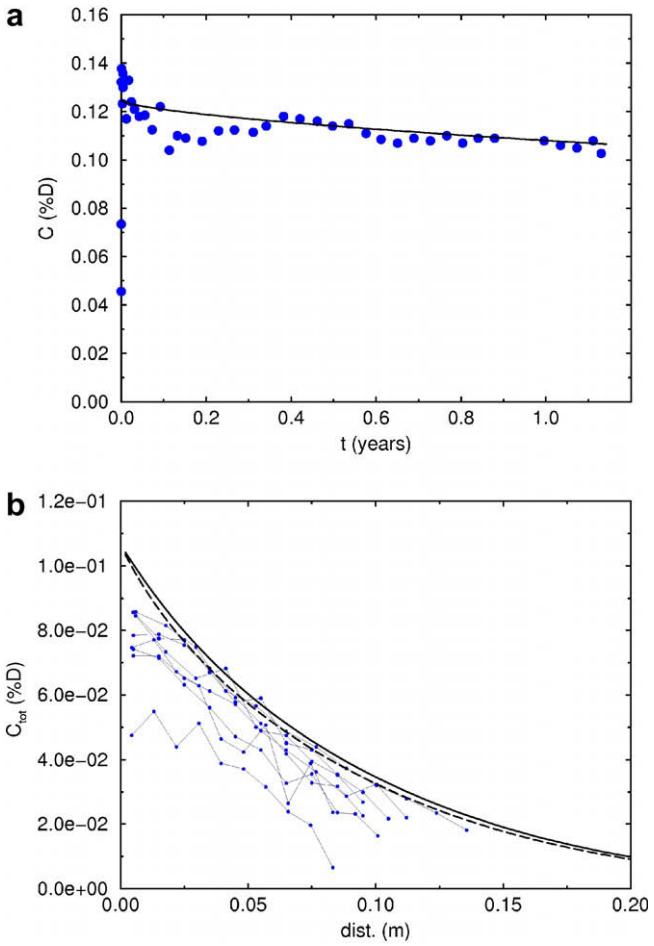

Fig. 5. Results for HDO. Model parameters: $D_e = 5.0 \times 10^{-11}$ m^2/s, $\varphi = 0.16$. (a) Concentration in the injection system vs. time. The dots are experimental data; the line represents model calculations. (b) Tracer profiles in the rock (total concentration vs. distance from borehole wall). Thick lines correspond to model results; thin lines correspond to experimental data. All concentrations are in units of atom% of deuterium in the water.

HDO is a non-sorbing tracer and is used to measure the transport properties of water. The best agreement between model calculations and experimental results was obtained using $D_e = 5.0 \times 10^{-11}$ m^2/s and $\varphi = 0.16$ (Fig. 5). The obtained value of porosity is identical to the measured average water content poros-

Table 1
Effective diffusion coefficients (D_e, parallel to bedding), porosities (φ) and distribution coefficients (K_d) from this study (DI-B), other in situ diffusion experiments at Mont Terri (DI-A1, DI-A2), and small-scale laboratory through-diffusion experiments.

Tracer	Parameter D_e (m^2/s) φ K_d (l/kg)	In situ test DI-B CRUNCH (2D)	In situ test DI-B CORE^{3D}	In situ test DI-A1[a] CRUNCH (2D)	In situ test DI-A2[b] CRUNCH (2D)	Lab data diffusion || bedding
HDO	D_e ($\times 10^{-11}$)	5.0	4.0	5.4	6.0	5.4 (HTO)[c], 4.0 (HTO)[d]
	φ	0.16	0.15	0.18	0.15	0.15-0.17 (HTO)[c]
I^-	D_e ($\times 10^{-11}$)	1.2	0.83	1.3	3.0	1.4 (I^-)[d],[e], 1.6 (Cl^-)[c], 1.5 (Br^-) [e]
	φ	0.09	0.08	0.09	0.08	0.12 (I^-)[e], 0.08 (Cl^-)[c], 0.09 (Br^-)[e]
$^6Li^+$	D_e ($\times 10^{-11}$)	7.0	7.1	7.2 (Na^+)		7.2 (Na^+)[c]
	φ	0.16	0.15	0.18 (Na^+)		0.15–0.17 (HTO)[c]
	K_d	0.24	0.20	0.20 (Na^+)		0.20 (Na^+)[c]
$^{87}Rb^+$	D_e ($\times 10^{-11}$)	5–10	14.1			
	φ	0.16	0.15			
	K_d	9–36	10			

[a] Van Loon et al. (2004b)-Wersin et al. (2006).
[b] Wersin et al. (2008).
[c] Van Loon et al. (2004a).
[d] Yllera et al. (2004).
[e] Unpublished results from Paul Scherer Institute.

ity. These values are similar to the parameters obtained from laboratory through-diffusion experiments parallel to bedding at 23 °C and also to the results of the DI-A in situ diffusion experiment (Table 1). Notice that at very early times, concentrations in the circulation tank show a very large dispersion of values possibly due to incomplete mixing of the tracer at the time of the sampling. Also, this fit was obtained using a value of the initial concentration c_0 equal to 0.125 (12.5% deuterium), instead of the theoretical value of 0.132, which was based on the volume of synthetic solution in the circulation system and the mass of tracer added to the system. Background concentration in the rock porewater was assumed to be equal to 10^{-4} (0.01% deuterium), based on the natural abundance of deuterium.

Regarding the tracer profiles in the rock, one of the profiles (profile 11) shows distinctively lower concentrations than the rest of the profiles. This effect may be due to the fact that profile 11 is in the uppermost part of the overcore and pointing upwards (Fig. 2). This profile may capture the curvature of the tracer plume near this end of the interval, which cannot be reproduced by the 2D model. However, the effect of the natural heterogeneity of the rock cannot be ruled out, as discussed below.

The error in the fitting procedure for HDO has been estimated to be about 40% for D_e and 20% for φ, based on the sensitivity of model results to changes in the values of the parameters.

Iodide was assumed to be non-sorbing. The best agreement between model calculations and experimental results was obtained using $D_e = 1.2 \times 10^{-11}$ m^2/s and $\varphi = 0.09$ (Fig. 6). These values are in good agreement with the results for Cl^-, Br^- and I^- from through-diffusion experiments at 23 °C (Table 1). Comparison with the results from the DI-A in situ diffusion coefficient shows also similar values. Notice that at very early times, concentrations in the circulation tank show a very large dispersion of values possibly due to incomplete mixing of the tracer at the time of the sampling. Also, this fit was obtained using a value of the initial concentration c_0 equal to 1.52×10^{-2} mol/l, instead of the theoretical value of 1.58×10^{-2} mol/l, which was based on the volume of synthetic solution in the circulation system and the mass of tracer added to the system. Background concentration in the rock was assumed to be equal to 10^{-5} mol/l, based on the composition of porewaters sampled in the vicinity of the test borehole (Pearson et al., 2003).

Two different sets of iodide profiles can be observed in Fig. 6b. First, iodide concentrations in the pore water are calculated from the experimental data using the measured water content, i.e., the total water-filled porosity. The average water content porosity of the analyzed samples is 0.164 (standard deviation = 0.02). Dividing the tracer concentrations in the profiles by a factor of 0.53, a good agreement between model and experimental results is achieved. This factor of 0.53 is equivalent to assuming that only 53% of the

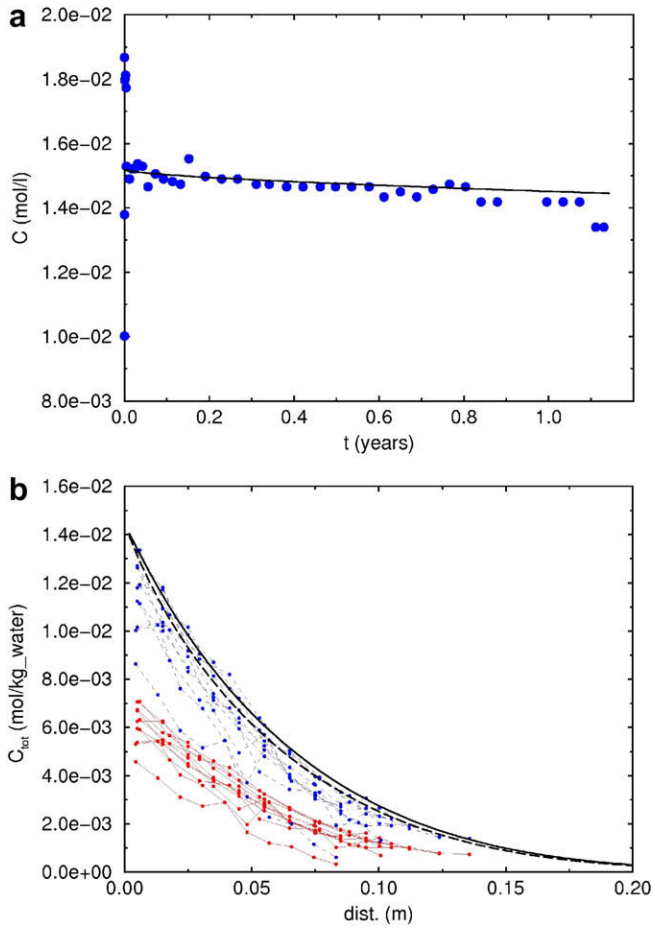

Fig. 6. Results for I^-. Model parameters: $D_e = 1.2 \times 10^{-11}$ m^2/s, $\varphi = 0.09$. (a) Concentration in the injection system vs. time. The dots are experimental data; the line represents model calculations. (b) Tracer profiles in the rock (total concentration vs. distance from borehole wall). Thick lines correspond to model results; thin lines correspond to experimental data. Two sets of profiles, calculated with different water contents, are shown (see text for explanation).

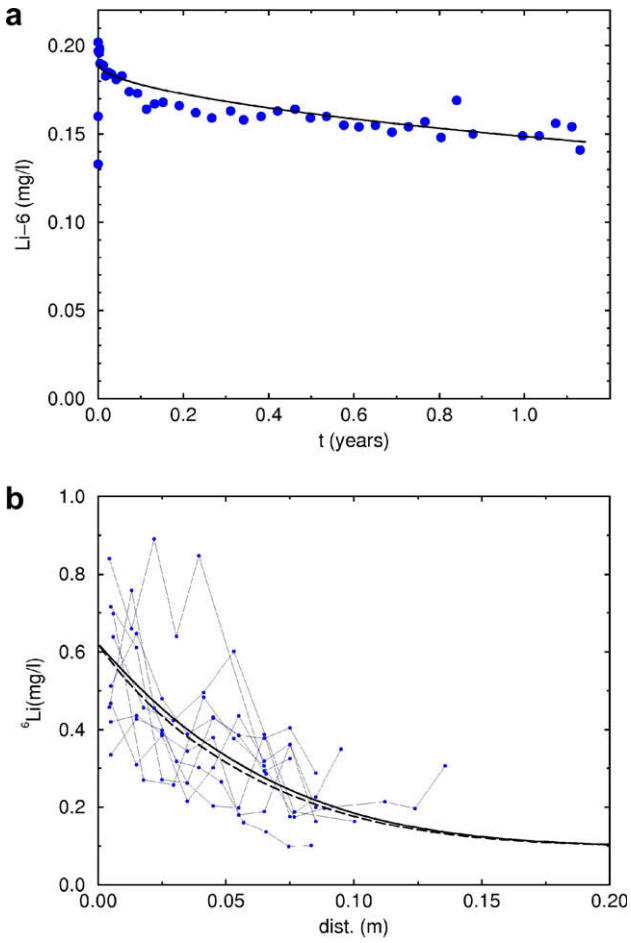

Fig. 7. Results for $^6Li^+$. Model parameters: $D_e = 7.0 \times 10^{-11}$ m^2/s, $\alpha = 0.70$ ($\varphi = 0.164$, $K_d = 0.24$ l/kg). (a) Concentration in the injection system vs. time. The dots are experimental data; the line represents model calculations. (b) Tracer profiles in the rock (total concentration vs. distance from borehole wall). Thick lines correspond to model results; thin lines correspond to experimental data. Notice that in the rock profiles, concentrations correspond to the sum of sorbed concentrations and concentrations in solution.

water content porosity is accessible to iodide, i.e., the average accessible porosity for iodide is 0.09. This is the value used in the model calculations.

Regarding the tracer profiles in the rock, one of the profiles (profile 11, same as for HDO) shows distinctively lower concentrations than the rest of the profiles. This effect may be due to the fact that profile 11 is in the uppermost part of the overcore and pointing upwards (Fig. 2). This profile may capture the curvature of the tracer plume near this end of the interval, which cannot be reproduced by the 2D model. However, the effect of the natural heterogeneity of the rock cannot be ruled out, as discussed below.

The error in the fitting procedure for I^- has been estimated to be about 20% for both D_e and φ, based on the sensitivity of model results to changes in the values of the parameters.

$^6Li^+$ was used as a stable isotope tracer. In principle, it was assumed that it should behave as a conservative or very weakly-sorbing tracer. The best agreement between model calculations and experimental results was obtained using $D_e = 7 \times 10^{-11}$ m^2/s and a rock capacity factor $\alpha = 0.70$ ($\varphi = 0.164$, $K_d = 0.24$ l/kg, Fig. 7). These values are similar to the parameters obtained from laboratory through-diffusion experiments parallel to bedding at 23 °C for Na^+ ($D_e = 7.2 \pm 0.5 \times 10^{-11}$ m^2/s, $\alpha = 0.62 \pm 0.05$, Van Loon et al., 2004a). Clearly, $^6Li^+$ did not behave as a conservative tracer. As it occurred with the other tracers, concentrations in the circulation tank at very early times show a very large dispersion of values possibly due to incomplete mixing of the tracer at the time of the sampling. Also, this fit was obtained using a value of the initial concentration c_0 equal to 0.19 mg/l (3.16×10^{-5} mol/l) instead of the theoretical value of 0.202 mg/l (3.36×10^{-5} mol/l), which was based on the volume of synthetic solution in the circulation system and the mass of tracer added to the system. Total (sorbed + solution) background concentration in the rock was assumed to be equal to 0.1 mg/l (0.023 mg/l in the porewater), based on the composition of porewaters sampled in the vicinity of the test borehole (Pearson et al., 2003), the natural abundance of ^6Li relative to total Li ($^6Li/(^6Li + ^7Li) = 0.075$), and the value of K_d used in the calculation.

Regarding the tracer profiles in the rock, one of the profiles (profile 11) shows distinctively higher concentrations than the rest of the profiles. This effect cannot only be due to the fact that profile 11 is in the uppermost part of the overcore and pointing upwards (Fig. 2). It is probable that profile 11 also reflects the natural heterogeneity of the rock.

The error in the fitting procedure for $^6Li^+$ has been estimated to be about 30% for both D_e and α, based on the sensitivity of model results to changes in the values of the parameters.

$^{87}Rb^+$ was used as a stable isotope tracer subject to relatively strong sorption. Due to the variability displayed between the different measured profiles in the rock it has not been possible to assign a unique value of D_e and α to this tracer. Fig. 8 shows two sets of results corresponding to two possible average sets of values for the diffusion and sorption parameters. In one case (Fig. 8a and b) the values of the effective diffusion coefficient and rock capacity factor are $D_e = 5 \times 10^{-11}$ m^2/s and $\alpha = 20$ ($\varphi = 0.164$, $K_d = 8.8$ l/kg),

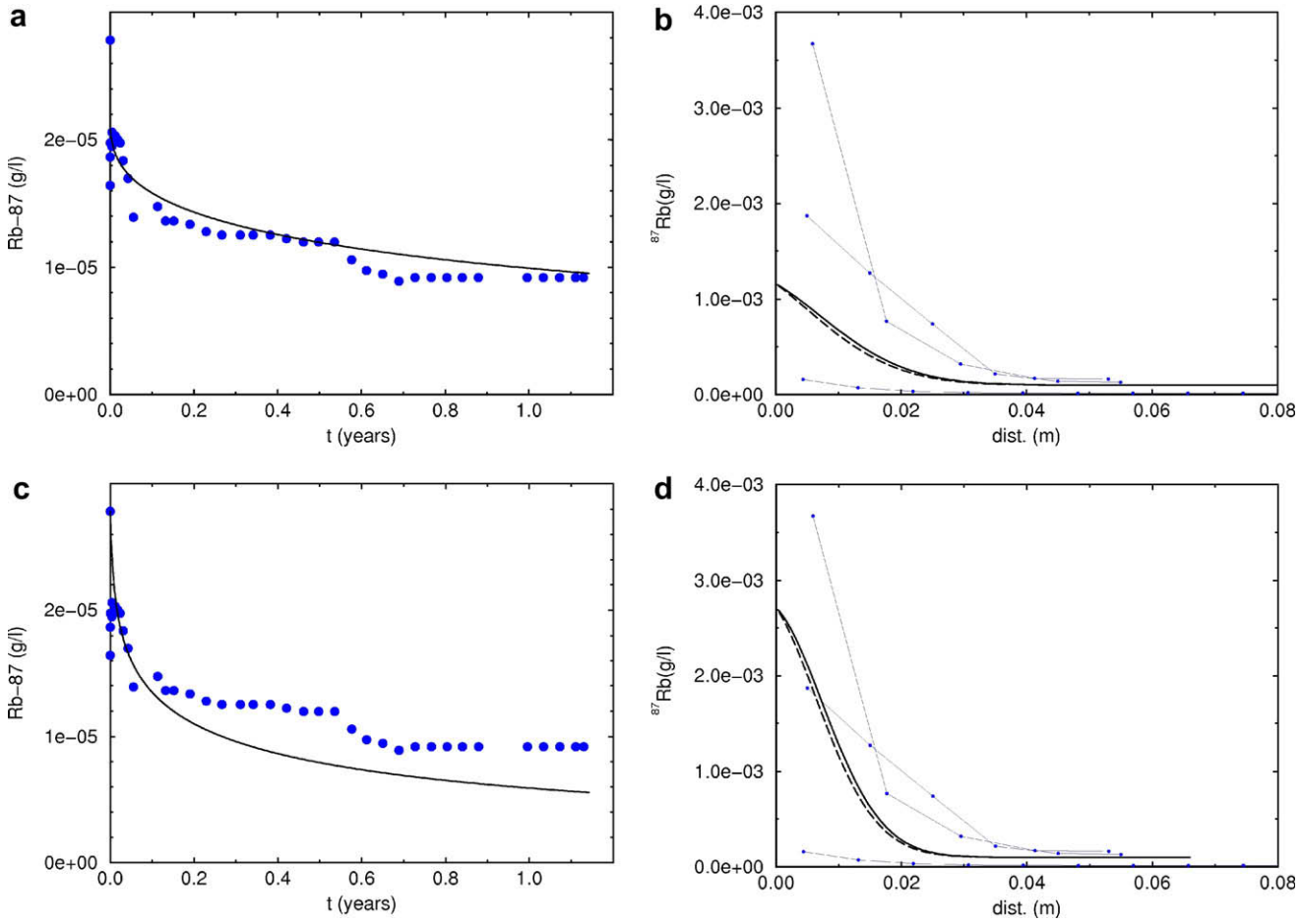

Fig. 8. Results for $^{87}Rb^+$. Model parameters (a and b): $D_e = 5.0 \times 10^{-11}$ m^2/s, $\alpha = 20$ ($\varphi = 0.164$, $K_d = 8.8$ l/kg). Model parameters (c and d): $D_e = 10^{-10}$ m^2/s, $\alpha = 80$ ($\varphi = 0.164$, $K_d = 35.4$ l/kg). (a and c) Concentration in the injection system vs. time. The dots are experimental data; the line represents model calculations. (b and d) Tracer profiles in the rock (total concentration vs. distance from borehole wall). Thick lines correspond to model results; thin lines correspond to experimental data. Notice that in the rock profiles, concentrations correspond to the sum of sorbed concentrations and concentrations in solution.

and an initial concentration c_0 equal to 2.1×10^{-5} g/l (2.4×10^{-7} mol/l) was used instead of the theoretical value of 2.783×10^{-5} g/l (3.2×10^{-7} mol/l), which was based on the volume of synthetic solution in the circulation system and the mass of tracer added to the system. In the other case (Fig. 8c and d) the values of the effective diffusion coefficient and rock capacity

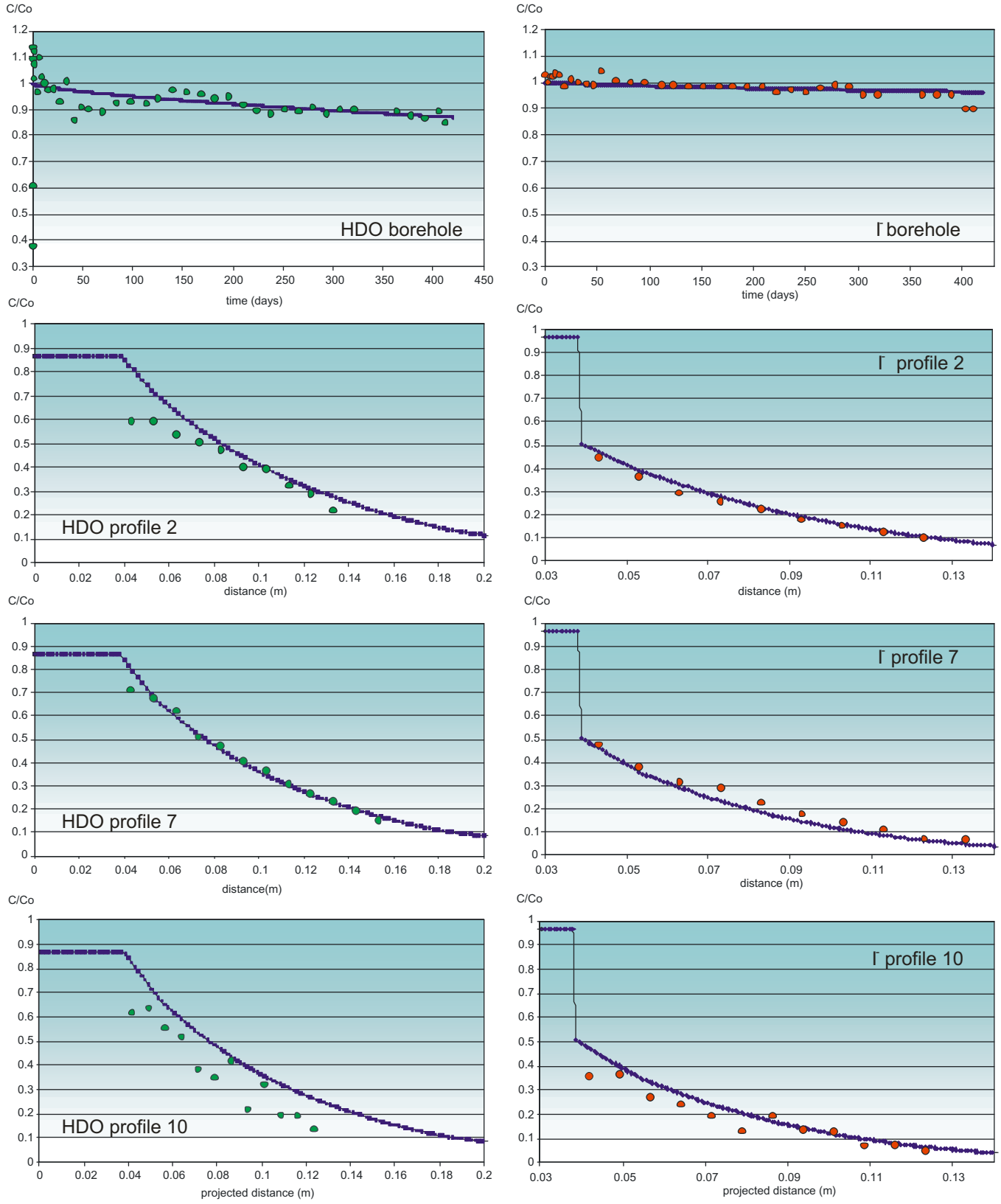

Fig. 9. Fit of HDO and iodide computed concentrations to measured data in the borehole and along different profiles of at the end of the experiment. All concentrations are relative concentrations in solution (C/C_0). Distance is with respect to borehole axis (borehole radius = 0.038 m). The sudden drop of I^- concentrations in the profiles at the borehole wall reflects the correction applied to the calculated values to account for anion exclusion.

factor are $D_e = 10^{-10}$ m^2/s and $\alpha = 80$ ($\varphi = 0.164$, $K_d = 35.4$ l/kg), and the theoretical concentration c_0 equal to 2.783×10^{-5} g/l (3.2×10^{-7} mol/l) was used. The large variability in the profiles for strongly sorbing tracers has also been observed for Cs^+ and Co^{2+} in the DI-A and DI-A2 experiments at Mont Terri (Van Loon et al., 2004b; Wersin et al., 2006, 2008). This variability seems to reflect the natural small-scale heterogeneity of the Opalinus Clay regarding sorption properties.

3.2. Modeling with CORE^{3D}

A fully 3D anisotropic finite element model of the DI-B experiment has been used for the interpretation of in situ experiments. Tracer diffusion plumes are symmetric with respect to a vertical plane perpendicular to bedding which divides vertically the borehole into two equal parts. Therefore, only half of the system needs to be modeled. The model domain was discretized using hexahedral finite elements which are small near the borehole and increase their size far away from the borehole.

The numerical model considers three material zones: (1) the packed-off section of the borehole where tracers are injected; (2) the steel plate at the bottom of the borehole with a thickness of 1 cm and (3) the Opalinus clay. In the model the borehole has a porosity equal to 1 and a sufficiently large diffusion coefficient to ensure a homogenous tracer distribution within the borehole. Small values of porosity and an extremely small effective diffusion coefficient are adopted for the steel plate at the bottom of the borehole. Parameters of the Opalinus Clay are tracer-dependent. The numerical model considers the angle between bedding and the x–y horizontal plane to be 32°. Background tracer concentrations are much smaller than measured concentrations along profiles. Therefore, it can be assumed that initial tracer concentrations in the clay are equal to zero. Tracers diffuse from the borehole into the Opalinus Clay. All external boundaries of the model are no-flow boundaries.

The transport equation for a tracer which diffuses into a very low permeability medium is given by (Bear, 1972)

$$\phi R \frac{\partial c}{\partial t} = \nabla \cdot (\bar{D}_e \nabla c) \tag{3}$$

where c is tracer concentration, t is time, φ is accessible porosity, which accounts also for anion exclusion, and R is the retardation factor ($R = 1 + \rho_d K_d/\varphi$). For a conservative tracer, R is equal to 1 and φ is equal to the total porosity if the tracer is not affected by anion exclusion. $\bar{D}_e$ is the effective diffusion tensor given by

$$\bar{D}_e = \begin{pmatrix} D_{xx} & D_{xy} & D_{xz} \\ D_{yx} & D_{yy} & D_{yz} \\ D_{zx} & D_{zy} & D_{zz} \end{pmatrix} \tag{4}$$

which can be diagonalized as

$$\bar{D}_e = \begin{pmatrix} D_{\zeta\zeta} & 0 & 0 \\ 0 & D_{\eta\eta} & 0 \\ 0 & 0 & D_{\zeta\zeta} \end{pmatrix} \tag{5}$$

where $D_{\zeta\zeta}$, $D_{\eta\eta}$ and $D_{\zeta\zeta}$ are the principal components of the diffusion tensor. The components of the effective diffusion tensor in (4) can be calculated from the main components in (5) using equations similar to those of the permeability tensor (Bear, 1972).

CORE^{3D} (Yang et al., 2003) has been used to simulate the DI-B in situ experiment. CORE^{3D} is a fully three-dimensional computer code for modeling saturated water flow, heat transport and multi-component reactive solute transport under both local chemical equilibrium and kinetic conditions and its capability to simulate 3D anisotropic diffusion has been verified with analytical solutions.

HDO and iodide: Model parameters were calibrated with deuterium and iodide measured concentrations in the borehole and along profiles (Fig. 9). Calibrated values for deuterium diffusion parameters are 4×10^{-11} m/s^2 and 10^{-11} m/s^2 for the effective diffusion coefficients parallel ($De_{||}$) and perpendicular ($De_{\perp}$) to bedding, respectively, and 0.15 for total porosity. In the case of iodide, the calibrated effective diffusion coefficient parallel to bedding is 8.3×10^{-12} m/s^2 with an anisotropy ratio of 4, and the calibrated value for porosity is 0.08. For both tracers, the value of the anisotropy ratio $De_{||}/De_{\perp} = 4$ is based on the results of small-scale laboratory experiments (Van Loon et al., 2004a).

Comparison of computed and measured concentrations for HDO and I^- has been already presented in Samper et al. (2006, 2007). The numerical model reproduces the overall trend for measured data in the borehole and along profiles. However, computed profiles 10 and 11 slightly overestimate measured data. Sensitivity analysis performed to evaluate uncertainties (Samper et al., 2006, 2007) show that is not possible to improve fit of profiles 10 and

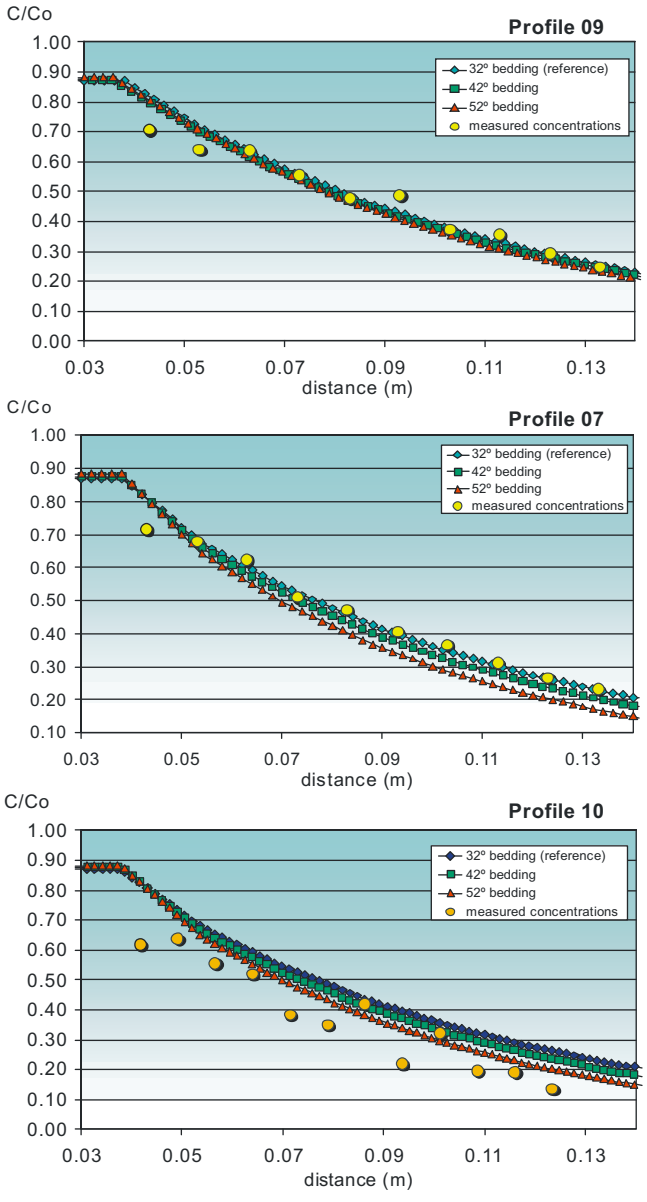

Fig. 10. Sensitivity analysis of HDO computed concentrations to variation of bedding angle. Relative concentrations are presented against horizontally projected distance to borehole axis.

11 by varying diffusion parameter values without spoiling fit of the other computed profiles to measured data. Variation of anisotropy ratio in the range of values obtained in the laboratory does not imply significant variations in computed profiles and therefore, does not improve the fit of profiles 10 and 11 to experimental data. On the other hand, influence of anisotropy ratio variation increases proportional to angle between bedding plane and profile. Experimental errors during measurement or variation of bedding angle with depth might lead to error in the value of this angle. Thus, a sensitivity analysis to bedding angle and to angle between profiles and bedding has been performed for both tracers in order to achieve a simultaneous fit of all the profiles (Fig. 10).

Sensitivity of dilution inside borehole to a variation of bedding angle that can be caused by experimental errors is negligible. Com-

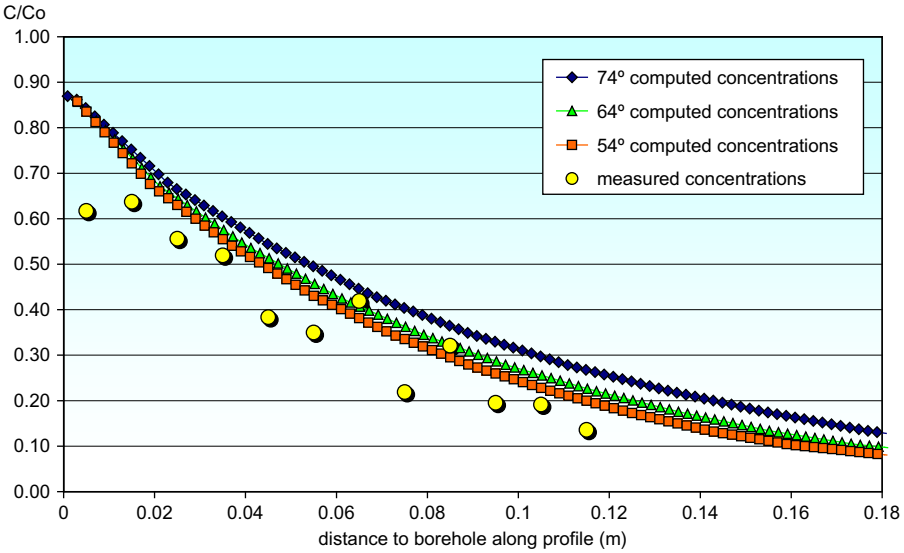

Fig. 11. Fit of HDO computed concentrations to measured data for profile 10, considering different values of the angle between profile direction and bedding plane.

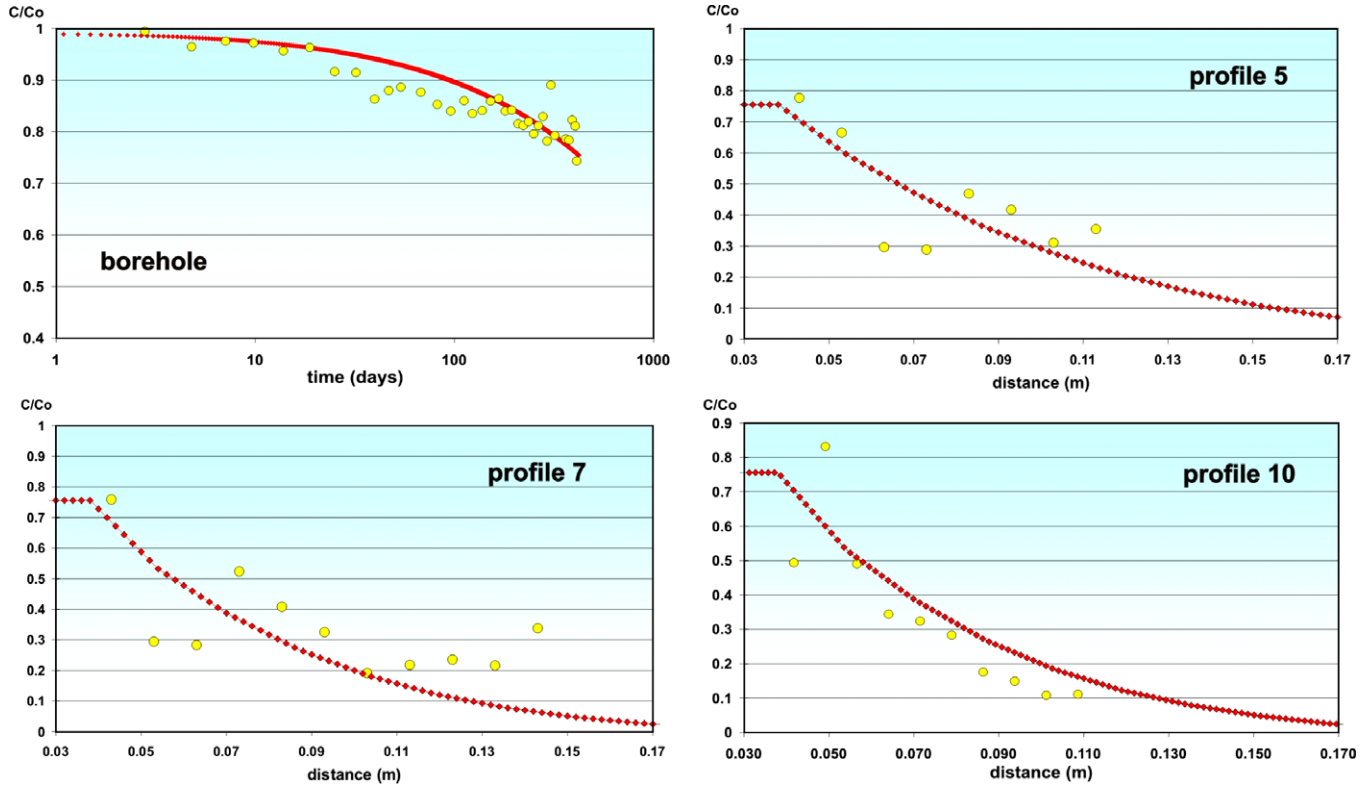

Fig. 12. Fit of $^{6}Li^{+}$ computed concentrations to measured data into the borehole and along profiles in different directions at the end of the experiment. All concentrations are relative concentrations in solution (C/C_0). Distance is with respect to borehole axis (borehole radius = 0.038 m).

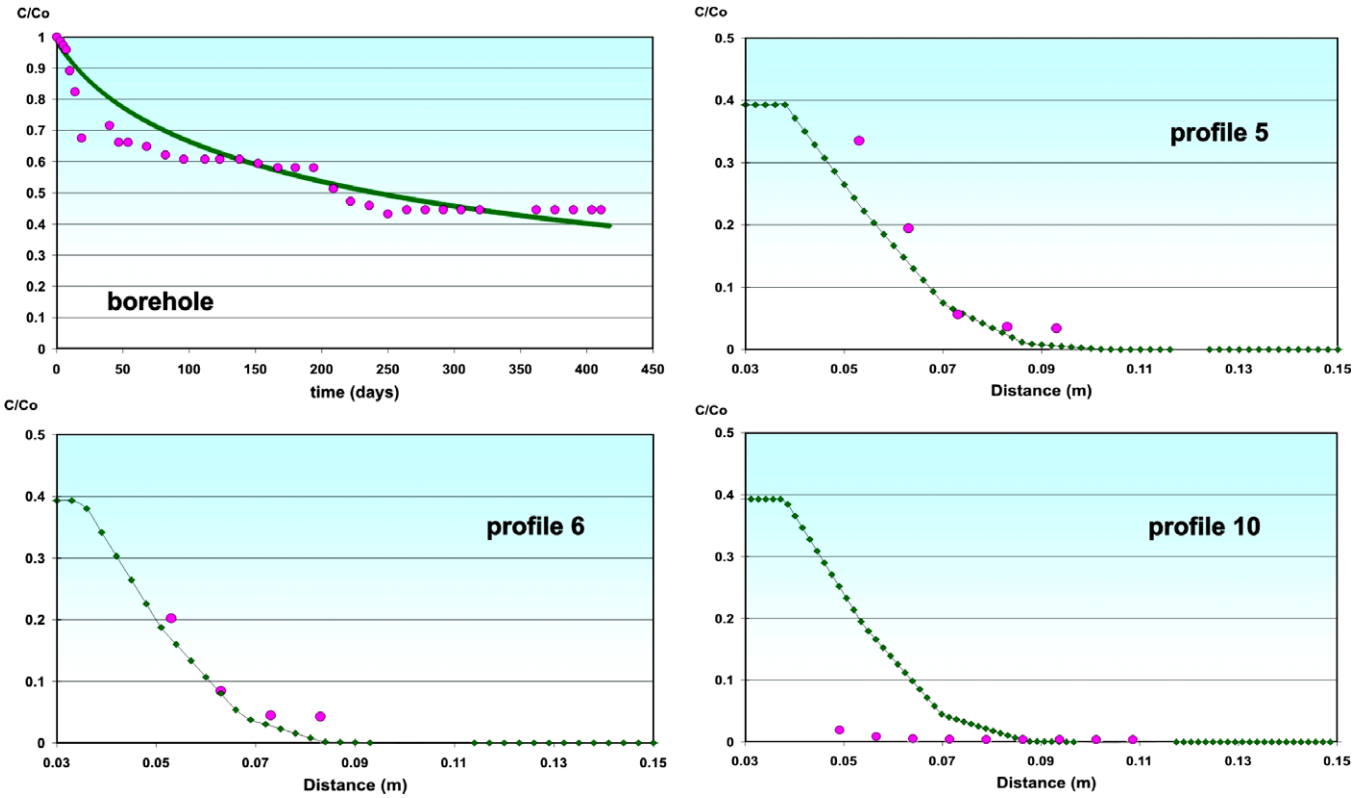

Fig. 13. Fit of $^{87}Rb^{+}$ computed concentrations to measured data into the borehole and along profiles of different directions at the end of the experiment. All concentrations are relative concentrations in solution (C/C_0). Distance is with respect to borehole axis (borehole radius = 0.038 m).

puted profiles sensitivity depends on profile direction and increases with distance to axis. Profiles parallel to bedding are not sensitive to bedding angle variation but the rest of profiles are. Increase of bedding angle leads to a better fit of profiles 10 and 11 but implies underestimation of profiles 6–8.

Fixing the bedding angle value, uncertainty in the measured orientation of profiles 10 and 11 has been evaluated by means of a sensitivity analysis of computed concentrations to variation of angle between profile direction and bedding plane (Fig. 11). Reference value of angle is 74° for both profiles. The fit of computed profiles to measured data improves when the angle decreases. An angle of 54°, which would be equivalent to a 20° experimental error, leads to an excellent fit of profile 10 for both tracers. In the case of profile 11, computed profiles overestimate measured data for any feasible angle value. This is probably due to the existence of heterogeneities in the rock.

$^{6}Li^{+}$ and $^{87}Rb^{+}$ measured concentrations along profiles present strong fluctuations (Figs. 12 and 13). Thus, calibration of diffusion parameters has been performed from available dilution data (tracer concentrations in the circulation system). Accessible porosity and anisotropy ratio were fixed and assumed to be equal to those of HDO. The best fit of computed dilution curve to measured data for $^{6}Li^{+}$ was achieved for $D_e = 7.07 \times 10^{-11}$ m^2/s and $K_d = 0.2$ l/kg. In the case of $^{87}Rb^{+}$, the best fit was achieved for $D_e = 1.41 \times 10^{-10}$ m^2/s and $K_d = 10$ l/kg, although subject to a very significant uncertainty.

3.3. Comparison of the results

Table 1 shows a summary of the results from this study (interpretation of the experimental data using CRUNCH and CORE^{3D}), and a comparison with results from other in situ and small-scale laboratory experiments.

Inspection of the results reveals that the parameters obtained for HDO and iodide agree well with the results from the other experiments and their range of variability. Anion exclusion clearly affects iodide, which displays effective diffusion coefficients and accessible porosities smaller than those for water (HDO, HTO).

Regarding $^{6}Li^{+}$, it had been expected that it would behave in a conservative or very weakly-sorbing manner. However, the parameters obtained for this tracer agree well with those obtained for Na^{+} in other studies. Na^{+} behaves in the Opalinus Clay as a weakly-sorbing element. Na^{+} is the major cation in the Opalinus clay porewater, with a porewater concentration of about 0.25 mol/kg_H_2O in the vicinity of the DI niche (Pearson et al., 2003), where the different in situ experiments have been performed.

The measured $^{87}Rb^{+}$ profiles show a large variability. Also, the shape of the tracer evolution curve in the circulation system is rather irregular (Figs. 8 and 13). These experimental results do not allow the determination of a unique set of transport (D_e) and sorption (K_d) parameters. However, strong sorption of $^{87}Rb^{+}$ has been confirmed. The large variability of tracer profiles in the rock has also been observed for other strongly sorbing tracers (Cs^{+}, Co^{2+}) in the DI-A1 and DI-A2 in situ diffusion experiments (Van Loon et al., 2004b; Wersin et al., 2006, 2008). This variability suggests that the small-scale heterogeneity associated with the mineralogy of the rock plays an important role in the distribution of tracers with strong affinities for mineral surfaces.

4. Conclusions

The DI-B experiment has contributed to study the transport and retention properties of selected non radioactive tracers in the Opalinus Clay: ^{2}H (water), I^{-} (anionic species), $^{6}Li^{+}$

(non- or weakly-sorbing cation) and $^{87}Rb^{+}$ (strongly-sorbing cation).

The experimental results were modeled using two different reactive transport codes and spatial geometries (CRUNCH (2D) and CORE^{3D}). The results for HDO and iodide from both approaches showed good consistency and compare well with the results from other in situ tests and small-scale laboratory experiments. The effect of anion exclusion on the behavior of iodide has been confirmed. $^{6}Li^{+}$ has been shown to behave as a weakly-sorbing tracer, with effective diffusion coefficients (D_e) and sorption parameters (K_d) very similar to those of Na^{+}. Tracer profiles for $^{87}Rb^{+}$ showed a large degree of variability and it was not possible to assign unique values of D_e and K_d. This variability has also been observed for other strongly sorbing tracers in the DI-A1 and DI-A2 in situ diffusion tests, and it may be related to the small-scale mineralogical heterogeneity of the rock.

A larger scale heterogeneity has also been observed. One of the measured tracer profiles (profile 11) displays anomalous tracer concentrations when compared with the other measured profiles. A sensitivity analysis concerning geometrical aspects has confirmed that this anomalous profile is the result of a natural heterogeneity of the rock.

Acknowledgements

The assistance from the site support group under the lead of Andreas Möri and funding from Enresa and Nagra are gratefully acknowledged.

References

Bear, J., 1972. Dynamics of Fluids in Porous Media. Elsevier.

Degueldre, C., Scholtis, A., Laube, A., Turrero, M.J., Thomas, B., 2003. Study of pore water chemistry through an argillaceous formation: a paleohydrochemical approach. Appl. Geochem. 18 (1), 55–73.

Moriguti, T., Nakamura, E., 1998. High-yield lithium separation and the precise isotopic analysis for natural rock and aqueous samples. Chem. Geol. 145, 91–104.

Palut, J.-M., Montarnal, P., Gautschi, A., Tevissen, E., Mouche, E., 2003. Characterisation of HTO diffusion properties by an in situ tracer experiment in Opalinus clay at Mont Terri. J. Contam. Hydrol. 61, 203–218.

Pearson, F.J., Arcos, D., Bath, A., Boisson, J.-Y., Fernández, A. M., Gäbler, H.-E., Gaucher, E., Gautschi A., Griffault L., Hernán P., Waber H.N., 2003 Mont Terri Project – Geochemistry of Water in the Opalinus Clay Formation at the Mont Terri Rock Laboratory. Reports of the FOWG (Federal Office of Water and Geology), Geology Series, No. 5. Bern, Switzerland.

Rübel, A.P., Sonntag, C., Lippmann, J., Pearson, F.J., Gautschi, A., 2002. Solute transport in formations of very low permeability: profiles of stable isotope and dissolved gas contents of pore water in the Opalinus clay, Mont Terri, Switzerland. Geochim. Cosmochim. Acta 66, 1311–1321.

Samper, J., Yang, C., Naves, A., Yllera, A., Hernández, A., Molinero, J., Soler, J.M., Hernán, P., Mayor, J.C., Astudillo, J., 2006. A fully 3-D anisotropic numerical model of the DI-B in situ diffusion experiment in the Opalinus clay formation. Phys. Chem. Earth 31, 531–540.

Samper, J., Yang, C., Naves, A., Molinero, J., 2007. Modelización del Ensayo de Difusión In Situ DI-B Realizado en la Formación Opalinus clay en el Laboratorio de Mont Terri (Suiza). Universidade da Coruña, Final Report.

Sanz, H., Wasserburg, G.J., 1969. Determination of an internal 87Rb/87Sr isochrone for the Olivenza chondrite. Earth Planet. Sci. Lett. 6, 335–345.

Steefel, C.I., 2001. GIMRT, Version 1.2: Software for Modeling Multicomponent, Multidimensional Reactive Transport. User's Guide, UCRL-MA-143182. Livermore, California: Lawrence Livermore National Laboratory.

Steefel, C.I., 2006. CrunchFlow, Software for Modeling Multicomponent Reactive Flow and Transport. User's Manual. Lawrence Berkeley National Laboratory, USA.

Steefel, C.I., Yabusaki, S.B., 1996. OS3D/GIMRT, Software for Multicomponent-Multidimensional Reactive Transport: User's Manual and Programmer's Guide, PNL-11166, Pacific Northwest National Laboratory, Richland, Washington.

Tevissen, E., Soler, J.M., Montarnal, P., Gautschi, A., Van loon, L., 2004. Comparison between in situ and laboratory diffusion studies of HTO and halides in Opalinus clay from the Mont Terri. Radiochim. Acta 92, 781–786.

Van Loon, L.R., Soler, J.M., Müller, W., Bradbury, M.H., 2004a. Anisotropic diffusion in layered argillaceous formations: a case study with Opalinus clay. Environ. Sci. Technol. 38, 5721–5728.

Van Loon, L.R., Wersin, P., Soler, J.M., Eikenberg, J., Gimmi, Th., Hernán, P., Dewonck, S., Savoye, S., 2004b. In-situ diffusion of HTO, $^{22}Na^{+}$, Cs^{+} and I^{-} in Opalinus clay at the Mont Terri underground rock laboratory. Radiochim. Acta 92, 757–763.

Wersin, P., Van Loon, L.R., Soler, J.M., Yllera, A., Eikenberg, J., Gimmi, Th., Hernán, P., Boisson, J.Y., 2004. Long-term diffusion experiment at Mont Terri: first results from field and laboratory data. Appl. Clay Sci. 26, 123–135.

Wersin, P., Baeyens, B., Bossart, P., Cartalade, A., Dewonck, S., Eikenberg, J., Fierz,T., Fisch, H.R., Gimmi, T., Grolimund, D., Hernán, P., Möri, A., Savoye, S., Soler, J., van Dorp, F., Van Loon, L. 2006. Long-Term Diffusion Experiment (DI-A): Diffusion of HTO, I^{-}, $^{22}Na^{+}$ and Cs^{+}. Field Activities, Data and Modelling. Mont Terri Technical Report 2003–06.

Wersin, P., Soler, J.M., Van Loon, L., Eikenberg, J., Baeyens, B., Grolimund, D., Gimmi, T., Dewonck, 2008. Diffusion of HTO, I^{-}, Cs^{+}, $^{85}Sr^{2+}$ and $^{60}Co^{2+}$ in a clay formation: results and modelling from an in situ experiment in Opalinus clay. Applied Geochemistry 23, 678–691.

Yang, C., Juanes, R., Samper, J., Molinero, Montenegro, L., 2003. User's Manual of CORE^{3D}. Technical Report, University of La Coruña, Spain.

Yllera, A., Hernández, A., Mingarro, M., Quejido, A., Sedano, L.A., Soler, J.M., Samper, J., Molinero, J., Barcala, J.M., Martín, P.L., Fernández, M., Wersin, P., Rivas, P., Hernán, P., 2004. DI-B experiment: planning, design and performance of an in situ diffusion experiment in the Opalinus clay formation. Appl. Clay Sci. 26, 181–196.

You, C.-F., Chan, L.-H., 1996. Precise determination of lithium isotopic composition in low concentration natural samples. Geochim. Cosmochim. Acta 60, 909–915.

APPENDIX 5

NORMALIZED SENSITIVITIES AND PARAMETER IDENTIFIABILITY OF IN SITU DIFFUSION EXPERIMENTS ON CALLOVO-OXFORDIAN CLAY AT BURE SITE

This appendix presents a paper presented in the international conference MIGRATION07 which took place in Munich (Germany) in August 2007 and was published in Physics and Chemistry of the Earth in 2008.

This paper is the result of a joint research work including the contributions from other researchers. My main contribution includes the development of the 2D and 1D forward models, the sensitivity analyses to changes in model parameters and the evaluation of the non-ideal effects in the tracer concentrations and the estimation errors.

Physics and Chemistry of the Earth 33 (2008) 1000–1008

Contents lists available at ScienceDirect

Physics and Chemistry of the Earth

journal homepage: www.elsevier.com/locate/pce

Normalized sensitivities and parameter identifiability of *in situ* diffusion experiments on Callovo–Oxfordian clay at Bure site

J. Samper [a,*], S. Dewonck [b], L. Zheng [a], Q. Yang [a], A. Naves [a]

[a] *Universidad de A Coruña. E-15192 A Coruña, Spain*
[b] *ANDRA, F-55290 Bure, France*

ARTICLE INFO

Article history:
Available online 10 June 2008

Keywords:
Diffusion
Retention
Numerical model
Sensitivity analysis
Identifiability analysis
CORE

ABSTRACT

Diffusion of inert and reactive tracers (DIR) is an experimental program performed by ANDRA at Bure underground research laboratory in Meuse/Haute Marne (France) to characterize diffusion and retention of radionuclides in Callovo–Oxfordian (C–Ox) argillite. *In situ* diffusion experiments were performed in vertical boreholes to determine diffusion and retention parameters of selected radionuclides. C–Ox clay exhibits a mild diffusion anisotropy due to stratification. Interpretation of *in situ* diffusion experiments is complicated by several non-ideal effects caused by the presence of a sintered filter, a gap between the filter and borehole wall and an excavation disturbed zone (EdZ). The relevance of such non-ideal effects and their impact on estimated clay parameters have been evaluated with numerical sensitivity analyses and synthetic experiments having similar parameters and geometric characteristics as real DIR experiments. Normalized dimensionless sensitivities of tracer concentrations at the test interval have been computed numerically. Tracer concentrations are found to be sensitive to all key parameters. Sensitivities are tracer dependent and vary with time. These sensitivities are useful to identify which are the parameters that can be estimated with less uncertainty and find the times at which tracer concentrations begin to be sensitive to each parameter. Synthetic experiments generated with prescribed known parameters have been interpreted automatically with INVERSE-CORE^{2D} and used to evaluate the relevance of non-ideal effects and ascertain parameter identifiability in the presence of random measurement errors. Identifiability analysis of synthetic experiments reveals that data noise makes difficult the estimation of clay parameters. Parameters of clay and EdZ cannot be estimated simultaneously from noisy data. Models without an EdZ fail to reproduce synthetic data. Proper interpretation of *in situ* diffusion experiments requires accounting for filter, gap and EdZ. Estimates of the effective diffusion coefficient and the porosity of clay are highly correlated, indicating that these parameters cannot be estimated simultaneously. Accurate estimation of D_e and porosities of clay and EdZ is only possible when the standard deviation of random noise is less than 0.01. Small errors in the volume of the circulation system do not affect clay parameter estimates. Normalized sensitivities as well as the identifiability analysis of synthetic experiments provide additional insight on inverse estimation of *in situ* diffusion experiments and will be of great benefit for the interpretation of real DIR *in situ* diffusion experiments.

1. Introduction

In situ diffusion experiments have been performed at underground research laboratories in clay formations to overcome the limitations of laboratory diffusion experiments and to investigate possible scale effects. Such experiments have been performed in Opalinus clay in Switzerland (Palut et al., 2003; Tevissen et al., 2004; Wersin et al., 2004; Van Loon et al., 2004; Yllera et al., 2004; Samper et al., 2006a) and Callovo–Oxfordian clay at Bure in France (Dewonck, 2007; Descostes et al., 2007; Radwan et al., 2005).

ANDRA has undertaken an extensive characterization program at the Bure site to assess the feasibility of a deep high level radioactive waste (HLW) repository in the Callovo–Oxfordian (C–Ox) clay. Diffusion of inert and reactive tracers (DIR) is one of such experimental programs which aims at characterizing diffusion and retention of radionuclides in the clay rock. Various *in situ* diffusion experiments were performed in vertical boreholes to determine diffusion and retention parameters of selected radionuclides (Dewonck, 2007; Radwan et al., 2005; Descostes et al., 2007). C–Ox clay exhibits a mild diffusion anisotropy due to stratification. Interpretation of *in situ* diffusion experiments is complicated by several non-ideal effects caused by the presence of a sintered filter, a gap between the filter and the borehole wall and an excavation disturbed zone (EdZ) (see Fig. 1).

* Corresponding author. Tel.: +34 981 16 70 00; fax: +34 981 16 71 70.
E-mail address: jsamper@udc.es (J. Samper).

1474-7065/$ - see front matter © 2008 Elsevier Ltd. All rights reserved.
doi:10.1016/j.pce.2008.05.017

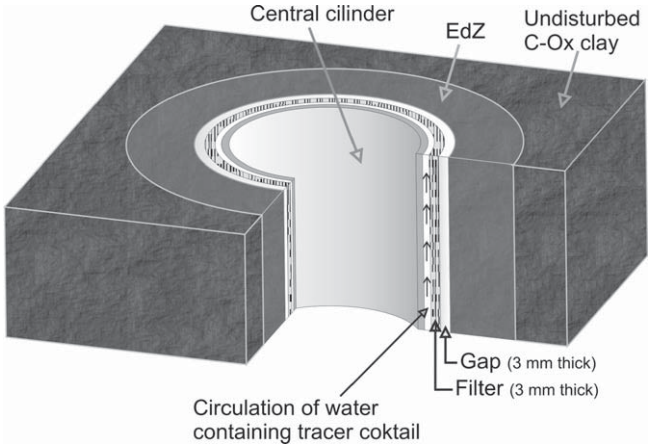

Fig. 1. Sketch of borehole geometry for DIR experiments.

In this paper we evaluate the relevance of such non-ideal effects and their impact on estimated clay parameters by numerical sensitivity analyses and synthetic experiments having similar parameters and geometric characteristics as real DIR *in situ* diffusion experiments. The paper starts by describing DIR *in situ* diffusion experiments. Then, numerical methods for their interpretation are presented. A systematic sensitivity analysis performed in terms of normalized sensitivities is also presented after that. Then, the identifiability analysis of tritium and chloride diffusion parameters based on synthetic diffusion experiments is explained. Finally, main conclusions and their relevance for the interpretation of real DIR *in situ* diffusion experiments are presented.

2. DIR *in situ* diffusion experiments at Bure site

Several vertical boreholes were drilled in which *in situ* diffusion experiments were performed to determine radionuclide diffusion and retention parameters of radioactive tracers. The DIR2001 and DIR2002 experiments were carried out in boreholes drilled from a gallery located at 445 m depth in the Meuse/Haute–Marne underground laboratory. *In situ* diffusion experiments were performed as single-point dilution tests by injecting tracers into a 1 m long packed-off section into the boreholes. The required equipment included downhole and surface instrumentation (Palut, 2001). Downhole instrumentation consisted of a pneumatic packer system with a porous screen made of sintered stainless steel mounted just below the packer at the bottom of the borehole. Surface instrumentation included a stainless steel circuit to circulate the water containing the tracers and to allow for injection and sampling of tracers. Tracer activities at the injection section were monitored from 15th March of 2005 to 30th January of 2006. Tritium (HTO), chloride ($^{36}Cl^-$) and iodide ($^{125}I^-$) were employed as tracers in DIR 2001, while tritium (HTO), sodium ($^{22}Na^+$) and cesium ($^{134}Cs^+$) were used in DIR 2002. Chloride and iodide are subject to anion exclusion while sodium and cesium undergo sorption. The design of the EST208 experiment differs from that of the DIR 2001 and 2002 experiments because EST208 was performed in a deep borehole drilled from ground surface to a depth of −542.5 m. Downhole instrumentation consists of a 10 m long packed diffusion interval with a steel porous filter and two hydraulic lines for flux recirculation. The test equipment includes two circulation systems. One allows circulation from the diffusion chamber to ground surface and the other ensures flow along surface equipment and allows monitoring of geochemical parameters and the extraction of water samples during the experiment. The following tracers were injected in this borehole: tritium (HTO), chloride ($^{36}Cl^-$) and cesium ($^{134}Cs^+$).

Diffusion in Bure clay exhibits a mild anisotropy due to stratification. Effective diffusion coefficients along horizontal planes are from 1.5 to 2 times larger than vertical effective diffusion coefficients (Dewonck, 2007).

3. Numerical interpretation of DIR *in situ* diffusion experiments

Attempts were made to interpret diffusion experiments using the analytical solution of Cooper et al. (1967) based on the analogy between *in situ* diffusion experiments and pulse tests (Samper et al., 2007). It was not possible to obtain clay parameters because measured tracer data are affected by a number of factors which are not taken into account by the analytical solution such as the presence of a sintered filter, a gap between the casing and the borehole wall and the excavation disturbed zone (Samper et al., 2007). Given the limitations of the analytical methods, *in situ* diffusion experiments were interpreted using inverse numerical models.

3.1. Solute transport equation

The transport equation for a tracer which diffuses through a low permeability medium is given by (Bear, 1972):

$$\phi_a R \frac{\partial C}{\partial t} = \nabla \cdot (\bar{D}_e \cdot \nabla C) \tag{1}$$

where C is the tracer concentration, t is time, ϕ_a is the accessible porosity which accounts for anion exclusion and R is the retardation coefficient defined as

$$R = 1 + \frac{\rho K_d}{\phi_a} \tag{2}$$

R is equal to 1 and ϕ_a is equal to the total porosity if the tracer is not affected by anion exclusion or by adsorption. $\bar{D}_e$ is the effective diffusion tensor given by

$$\bar{D}_e = \begin{pmatrix} D_{xx} & D_{xy} & D_{xz} \\ D_{yx} & D_{yy} & D_{yz} \\ D_{zx} & D_{zy} & D_{zz} \end{pmatrix} \tag{3}$$

which can be diagonalized as

$$\bar{D}'_e = \begin{pmatrix} D_{\xi\xi} & 0 & 0 \\ 0 & D_{\eta\eta} & 0 \\ 0 & 0 & D_{\zeta\zeta} \end{pmatrix} \tag{4}$$

where $D_{\xi\xi}$, $D_{\eta\eta}$ and $D_{\zeta\zeta}$ are the principal components of the tensor. Components of the effective diffusion tensor in (3) can be calculated from the main components in (4) using equations similar to those of the permeability tensor. Here $D_{\xi\xi}$ and $D_{\eta\eta}$ are horizontal diffusion coefficients parallel to bedding while $D_{\zeta\zeta}$ is the vertical diffusion coefficient.

3.2. Inverse problem of solute transport and sorption

The essence of the inverse problem lies on deriving optimum parameter estimates from known concentration data. The optimum parameters are those which minimize an objective function measuring the difference between measured and computed concentrations. Our formulation of the inverse problem is based on a generalized least squares criterion (Sun, 1994; Dai and Samper, 2004). Let $p = (p_1, p_2, p_3, \ldots, p_M)$ be the vector of M unknown parameters. The objective function, $E(p)$, can be expressed as:

$$E(p) = \sum_{i=1}^{NE} W_i E_i(p) \tag{5}$$

where $i = 1, \ldots, N_E$ denotes different types of data, $i = 1$ for the water head; $i = 2$ for dissolved concentrations; $i = 3$ for the total

concentration; $i = 4$ for the water fluxes; $i = 5$ for the water contents in unsaturated media; $i = 6$ for the temperature; and $i = 7$ for prior information on model parameters. W_i is the weighting coefficient of the ith generalized least-squares criterion, $E_i(p)$, which is defined as

$$E_i(p) = \sum_{l=1}^{L_i} w_{li}^2 r_{li}^2(p) \quad (6)$$

$$r_{li} = u_l^i(p) - F_l^i \quad (7)$$

where $u_l^i(p)$ is the computed value of the ith variable at the observation point; the F_l^i are measured values; L_i is the number of observations, either in space or in time for the ith type data; and r_{li} is the residual or difference weighting coefficient for the lth measurement of the ith type of data. Its value depends on the accuracy of the observations. If some data are judged to be unreliable, they should be assigned very small weights w_{li} in order to prevent their pernicious effect on the optimization process. Weights for different types of data W_i in (5) are updated automatically during the iterative optimization process as indicated by Carrera and Neuman (1986) and Dai and Samper (2004). The Gauss–Newton–Levenberg–Marquardt method has been used to minimize the objective function in (5) using the inverse code INVERSE-CORE^{2D} (Dai and Samper, 1999, 2004). This code can estimate flow and transport parameters and provides statistical measures of goodness-of-fit as well as parameter uncertainties by computing the covariance and correlation matrices, the eigenvalues and approximate confidence intervals (García-Gutiérrez et al., 2001; Dai and Samper, 2004, 2006; Dai et al., 2006; Samper et al., 2006b).

3.3. Numerical models

Numerical interpretation of DIR experiments requires the use of 3D models due to diffusion anisotropy. However, symmetry with respect to the borehole axis allows the use of 2D axi-symmetric models. The relevance of diffusion anisotropy on tracer evolution at the test interval depends on the ratio between borehole length and tracer penetration. Anisotropy is especially relevant when the length of the testing interval is not much larger than the tracer penetration. Since tracer penetration is clearly much smaller than the tracer diffusion interval for the EST208 experiment, this experiment can be safely interpreted with a 1D axisymmetric model. The relevance of anisotropy for the DIR 2001 and DIR 2002 experiments was unknown *a priori* and had to be ascertained with a 2D axisymmetric anisotropic numerical model. Thus, 2D finite element models were performed. They account for four material zones: (1) borehole with tracer circulation system, (2) excavation disturbed zone (EdZ), (3) undisturbed clay, and (4) steel plate at the bottom of the borehole. Tracer diffusion parameters for the undisturbed clay and the EdZ were derived from available data from laboratory experiments (Dewonck, 2007; Radwan et al., 2005; Descostes et al., 2007). The results of experiment simulations show that penetration of all tracers is much smaller than the length of the tracer interval. Concentrations at the testing interval computed with 1D and 2D models are completely similar and are not sensitive to the anisotropy of the effective diffusion coefficient. Therefore, a 1D axisymmetric model was used to simulate the DIR *in situ* diffusion experiments.

The injection section is composed of an empty central steel cylinder and a 3 mm thick steel filter between which the fluid containing the tracer cocktail circulates. There is a gap of 3 mm between the filter and the borehole wall. This gap is initially filled with artificial water injected during the hydraulic equilibration period. Later on, water in contact with argillite forms possibly a viscous mud. The gap and the filter were taken into account in the model. Therefore five material zones were considered: the injection zone, the filter, the gap, a 2 cm thick EdZ and the undisturbed C–Ox clay.

Models of *in situ* diffusion experiments usually consider the borehole, the geological formation and, sometimes, an EdZ. They rarely take into account filters and gaps. Previous studies indicate that tracer dilution curves of *in situ* DIR experiments cannot be reproduced unless an EdZ is considered (Radwan et al., 2005; Descostes et al., 2007; Samper et al., 2007). The effect of a sintered filter and a gap has been analyzed here by comparing concentrations computed with a detailed model which accounts for filter and gap with those computed with a simplified model which has only three material zones: the borehole, the EdZ and the undisturbed clay. Although patterns of time evolution of the tracer concentration in the tracer interval, the EdZ and the undisturbed clay are similar for both models, there are some differences which are small for HTO and noticeable for tracers that are subject to anion exclusion or sorption (see Fig. 2). The simplified model overestimates chloride and iodide concentrations in the tracer interval. However, for cesium the tracer concentrations in the tracer interval are underestimated during the first 4 days and then they are overestimated (see Fig. 2). In summary, failing to account for the filter and the gap may result in significant errors in tracer concentrations and in turn may lead to biased estimates of tracer parameters.

Values of the effective diffusion coefficient, the accessible porosity and the distribution coefficient of each tracer in C–Ox clay were derived from available through-diffusion laboratory experiments (see Table 1). An anisotropy ratio of 1.56 was considered. The distribution coefficient, K_d, for $^{22}Na^+$ in C–Ox clay is assumed to be equal to 0.74 ml/g (Radwan et al., 2005). For $^{134}Cs^+$ a K_d of

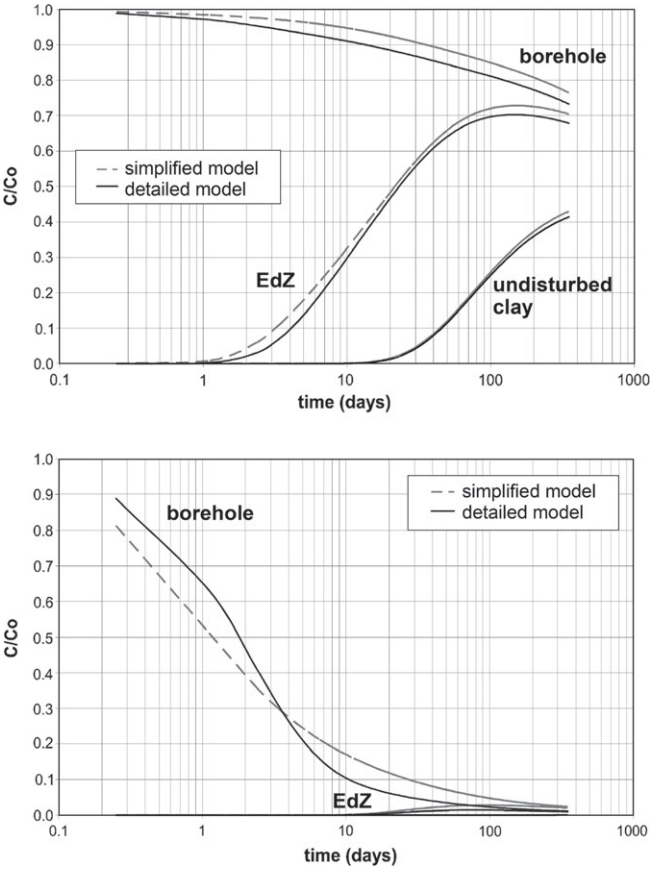

Fig. 2. Time evolution of $^{36}Cl^-$ (top) and $^{134}Cs^+$ (bottom) concentrations in borehole, EdZ and undisturbed clay for the DIR2001 experiment computed with detailed (solid lines) and simplified (dashed lines) models.

Table 1
Reference values of diffusion and sorption parameters in different materials for all the tracers

		HTO	$^{36}Cl^-$	$^{125}I^-$	$^{22}Na^+$	$^{134}Cs^+$
Clay	D_e (m^2/s)	4.1×10^{-11}	9.1×10^{-12}	4.4×10^{-12}	6.7×10^{-11}	3.6×10^{-10}
	Φ_{acc}	0.18	0.09	0.13	0.18	0.18
	K_d (ml/g)	–	–	–	0.74	50
EdZ	D_e (m^2/s)	10^{-10}	2.3×10^{-11}	1.1×10^{-11}	1.7×10^{-10}	9×10^{-10}
	Φ_{acc}	0.36	0.18	0.26	0.36	0.36
	K_d (ml/g)	–	–	–	0.74	50
Gap	D_e (m^2/s)	2×10^{-10}	1.1×10^{-10}	3.4×10^{-11}	3.3×10^{-10}	1.8×10^{-9}
	Φ_{acc}	0.6	0.6	0.6	0.6	0.6
	K_d (ml/g)	–	–	–	0.74	50
Filter	D_e (m^2/s)	8×10^{-11}	4.5×10^{-11}	1.3×10^{-11}	1.3×10^{-10}	7.1×10^{-11}
	Φ_{acc}	0.3	0.3	0.3	0.3	0.3

D_e is the horizontal effective diffusion coefficient, Φ_{acc} is the accessible porosity and K_d is the distribution coefficient.

50 ml/g was used. Effective diffusion coefficients for other materials were derived from those of undisturbed clay by adopting an Archie's law with an exponent equal to 4/3. The filter porosity was 0.3 (Dewonck, 2007). On the other hand, porosities of EdZ and gap are unknown. As an educated guess, the porosity of the EdZ was assumed to be twice that of clay while the porosity of the gap was assumed to be 0.6. The undisturbed clay and the EdZ were assumed to have the same distribution coefficient.

4. Sensitivity analysis

A model always entails simplifications of the real system. Model results depend on parameters that may contain uncertainties. Since parameter estimation errors are related to sensitivities of concentrations to changes in parameters, a detailed sensitivity analysis was performed to evaluate parameter uncertainties. For each tracer, its dilution curve was computed first for a set of tracer reference parameters. With these reference parameters, sensitivity runs were performed by changing relevant parameters one-at-a-time within prescribed ranges. Such sensitivities were evaluated for all tracers and the following parameters: (1) effective diffusion coefficient of the filter, (2) porosity of the gap, (3) effective diffusion coefficient and accessible porosity of the EdZ, (4) effective diffusion coefficient and accessible porosity of undisturbed clay, (5) distribution coefficient, (6) thickness of EdZ and (7) volume of the injection system.

Since model parameters have different units and vary over different ranges of values, their sensitivities cannot be compared directly. In order to compare sensitivities of concentrations to changes in different parameters, relative sensitivities, *RS*, have been used. Such sensitivities are defined as the ratio between relative changes in concentrations and relative changes in parameters, ΔP, which are defined as parameter changes with respect to reference values, P_b:

$$\Delta P(\%) = \frac{|P_s - P_b|}{P_b} \times 100 \tag{8}$$

where | | denotes the absolute value and P_s is the parameter value chosen for the sensitivity analysis. Relative sensitivity is computed as the ratio between the relative change in concentration and the relative change in parameter:

$$\Delta C(\%) = \frac{|C_s - C_b|}{C_b} \times 100 \tag{9}$$

where C_b and C_s are computed concentrations for base and sensitivity runs, respectively.

$$RS = \frac{\Delta C}{\Delta P} \tag{10}$$

Calculated *RS* for each tracer are listed in Table 2. It should be noticed that relative sensitivities are dimensionless and therefore relative sensitivities corresponding to different parameters can be compared directly.

Largest relative sensitivities correspond to a decrease in the volume of the circulation system. Such sensitivities range from 0.45 for HTO to 1.09 for $^{134}Cs^+$ in the DIR2002 experiment. Therefore, the volume of the circulation system is a key parameter affecting the tracer dilution in the testing interval.

Variations in EdZ thickness affect significantly all tracers. It should be noticed that the tracer concentrations are more sensitive to a decrease (from 2 to 0 cm) than to an increase (from 2 to 4 cm) of the EdZ thickness. This is especially true for sorbing tracers.

Sensitivities to diffusion and sorption parameters are different for different tracers. HTO is more sensitive to the EdZ porosity and the D_e of clay and EdZ. Iodide, however, is more sensitive to EdZ parameters. The influence of EdZ parameters is largest for chloride concentrations which are also sensitive to the gap porosity.

Table 2
Computed relative sensitivities, *RS*, of tracer dilution curves to changes in parameters

		HTO	$^{36}Cl^-$	$^{125}I^-$	$^{22}Na^+$	$^{134}Cs^+$	
		DIR2001	DIR2001	DIR2001	DIR2002	DIR2002	EST208
Total volume	$\Delta V = -10\%$	*0.462*	*0.221*	*0.194*	*0.77*	*1.09*	*1.11*
EdZ thickness	$\Delta e = -2$ cm	*0.124*	*0.072*	*0.055*	*0.21*	*0.387*	*0.344*
	$\Delta e = +2$ cm	0.074	0.038	0.012	0.082	0.018	0.016
Filter D_e	$\Delta D_e > 0$	0.014	0.018	0.012	0.033	0.053	0.049
	$\Delta D_e < 0$	0.051	0.024	0.038	*0.125*	*0.258*	*0.24*
Gap D_e	$\Delta D_e > 0$	0.014	0.014	0.003	0.011	0.026	0.025
	$\Delta D_e < 0$	0.018	0.022	0.011	0.045	0.11	0.106
Gap Φ_{acc}	$\Delta\Phi_{acc} > 0$	0.061	*0.051*	0.02	0.03	0.063	0.071
	$\Delta\Phi_{acc} < 0$	0.071	*0.062*	0.033	0.031	0.071	0.076
EdZ D_e	$\Delta D_e > 0$	0.034	0.016	0.022	0.089	*0.22*	*0.334*
	$\Delta D_e < 0$	*0.113*	*0.047*	*0.054*	*0.316*	*0.726*	*1.388*
EdZ Φ_{acc}	$\Delta\Phi_{acc} > 0$	*0.084*	*0.053*	*0.043*	0.039	*0.22*	*1.289*
	$\Delta\Phi_{acc} < 0$	*0.171*	*0.074*	*0.057*	0.033	*0.186*	*0.198*
Clay D_e	$\Delta D_e > 0$	*0.082*	0.02	0.006	*0.1*	0.018	0.016
	$\Delta D_e < 0$	*0.143*	0.031	0.010	*0.197*	0.033	0.03
Clay Φ_{acc}	$\Delta\Phi_{acc} > 0$	0.06	0.016	0.006	0.012	0.005	0.005
	$\Delta\Phi_{acc} < 0$	0.072	0.022	0.007	0.011	0.005	0.005
K_d	$\Delta K_d > 0$	–	–	–	*0.163*	*0.245*	*0.263*
	$\Delta K_d < 0$	–	–	–	*0.32*	*0.689*	*0.76*

Cesium results are shown for two experiments in order to compare the variation of *RS* with the experimental design.

Relative sensitivities for $^{36}Cl^-$ and $^{125}I^-$ are similar. They are generally smaller than those of other tracers. Therefore, it can be concluded that $^{36}Cl^-$ and $^{125}I^-$ parameters are the most difficult ones to estimate.

Relative sensitivities of $^{22}Na^+$ attain values which are between those of HTO and $^{134}Cs^+$. Sodium is the most sensitive tracer to changes in K_d and D_e of EdZ. This tracer is also sensitive to the D_e of clay and filter.

Cesium concentrations are very sensitive to changes in the D_e of the filter, the K_d and parameters of the EdZ. On the other hand, sodium and cesium lack sensitivity to clay porosity.

Relative sensitivities of a given tracer such as $^{134}Cs^+$ are similar in all experiments in which such a tracer is used (see Table 2).

Sensitivities of tracer concentrations to changes in parameters vary with time. Changes in D_e of undisturbed clay affect tracer dilution curves after some time (Fig. 3). Early time concentrations are not affected by changes in D_e. Times at which curves are sensitive to changes in D_e depend on the tracer. For instance, HTO data begin to be sensitive to D_e after 20 days while those of sodium are sensitive after 45 days. $^{125}I^-$ concentrations start to be sensitive to D_e after more than 100 days. These times at which tracer concentrations start to be sensitive to D_e are inversely proportional to tracer penetration depths. This depth is largest for HTO and smallest for $^{134}Cs^+$. Sorption of $^{134}Cs^+$ is so strong that its concentration in the tracer interval is not sensitive to changes in D_e by a factor of 0.5 and 2 (Fig. 3).

Sensitivities of tracer dilution curves to changes in clay accessible porosity are qualitatively similar to those of clay D_e (not shown here). Both early and late time tracer data lack sensitivity to clay porosity. Only tracer data at intermediate times are sensitive to porosity.

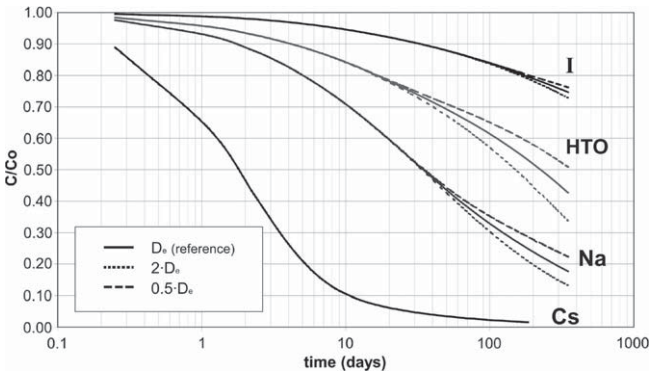

Fig. 3. Sensitivity of tracer concentrations in the injection zone to changes in D_e of clay.

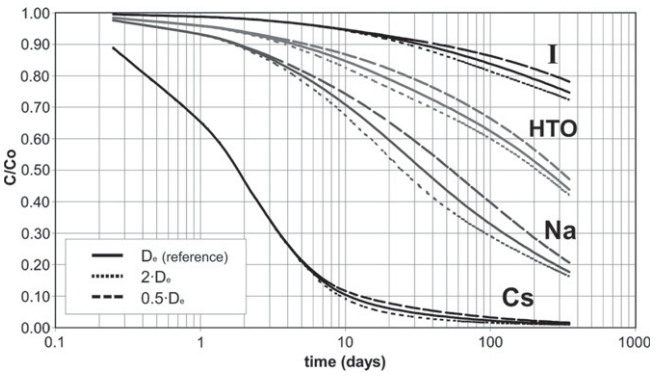

Fig. 4. Sensitivity of tracer concentrations in the injection zone to changes in D_e of EdZ.

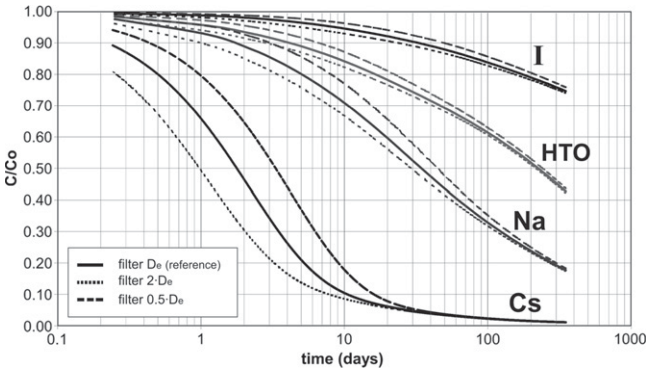

Fig. 5. Sensitivity of concentrations in the injection zone to changes in D_e of filter.

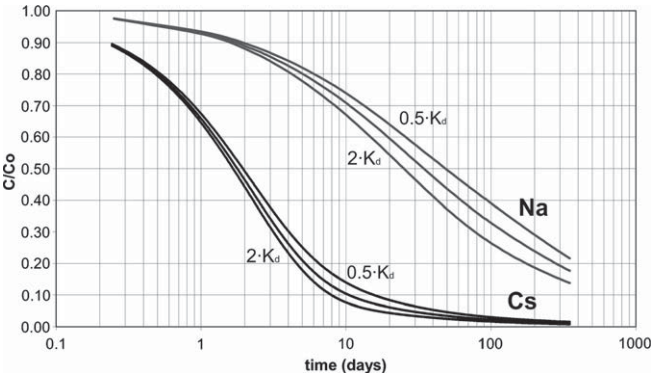

Fig. 6. Sensitivity of concentrations in the injection zone to changes in K_d of clay.

The sensitivity of tracer dilution curves to changes in D_e of the EdZ depends also on time (Fig. 4). Times at which curves are sensitive to changes in D_e of the EdZ are smaller than those corresponding to the D_e of clay (compare Figs. 3 and 4). Concentrations are sensitive to changes in D_e of EdZ after 3 days for HTO and $^{22}Na^+$ and after 20 days for $^{125}I^-$. These times coincide approximately with the times needed for tracers to diffuse through filter and gap.

All dilution curves are sensitive to changes in D_e of gap and filter. Changes in any of these parameters affect sorbing tracers more strongly than conservative tracers. Dilution curves are sensitive to such changes from the beginning of the experiment (Fig. 5).

Sensitivities of $^{22}Na^+$ and $^{134}Cs^+$ concentrations to changes in K_d by factors of 0.5 and 2 are remarkable (Fig. 6). Tracer concentrations at the injection zone begin to be sensitive after approx 1 day. The largest sensitivity is achieved from 20 to 100 days for $^{22}Na^+$ and from 3 to 20 days for $^{134}Cs^+$. For a reliable estimation of K_d, the tracer sampling frequency should be intensified during time periods at which tracer concentrations are most sensitive to K_d.

5. Identifiability analysis

5.1. Methodology

Synthetic data have been generated in order to provide insight on inverse estimation of diffusion and sorption experiments and to study parameter identifiably. Synthetic diffusion experiments having the same geometric properties as real experiments have been simulated numerically for reference values of diffusion and sorption parameters. Synthetic concentration data have then been used

to estimate parameters. Since true values are known, one can clearly identify which parameters can be estimated and how reliable these estimates really are. The difference between the estimation of real and synthetic experiments is that in real experiments true parameters are unknown while in synthetic experiments they are known.

Synthetic experiments are often used to study parameter identifiability and parameter uncertainties (Carrera et al., 1989). The procedure for performing the identifiably study with synthetic data involves the following steps: (1) Generating synthetic data from a forward run of the numerical model; (2) Adding multiplicative random noise to synthetic data with increasing standard deviations ranging from 0 to 0.05, a value similar to that of noise of actual data from the DIR experiments (Samper et al., 2007); (3) Estimating key diffusion parameters from noisy synthetic data in several stages, starting first with the estimation of D_e and accessible porosity, Φ_{acc}, of clay, followed by the estimation of the EdZ parameters and ending with estimating of all four parameters simultaneously; (4) Evaluating uncertainties caused by uncertainties in EdZ existence and thickness, the values of the volume of water in the injection system, the effective diffusion coefficient of the filter and of the porosity of the gap.

5.2. Results for HTO

Table 3 summarizes results of the identifiability analysis for HTO. Estimation runs have been performed considering different initial starting values of parameters and standard deviations of synthetic data.

When only the diffusion coefficient of clay is estimated, estimated values are close to the true value (4.05×10^{-11} m^2/s) even for a standard deviation of noise of 0.1. It can be seen that noise in the HTO data introduces a bias in D_e estimates which for a standard deviation of 5% is smaller than 5% and for a standard deviation of 10% is about 10%.

On the other hand, poor estimates of D_e and Φ_{acc} are obtained for noisy data when they are estimated simultaneously. Since clay D_e and Φ_{acc} are highly correlated ($\rho = -0.99$), they cannot be estimated simultaneously when the data have noise.

When D_e and Φ_{acc} of the EdZ are estimated, it is found that they are strongly correlated (-0.91) and therefore cannot be estimated properly when the data have noise.

Joint estimation of effective diffusion coefficients of clay and EdZ as well as porosities of clay and EdZ is only possible when the data have no noise. Parameter estimates are strongly correlated. Their correlation coefficients are close to either +1 or -1. Estimates are close to true values when the standard deviation of noise is 0 or 0.01. However, when the standard deviation of noise is 0.05, the parameter estimates depend on initial values.

It is well known that prior information on parameters can greatly improve the estimation process (Carrera and Neuman, 1986; Dai and Samper, 2004). The role of prior information on parameter estimation of DIR experiments has been evaluated with a set on runs in which D_e and Φ_{acc} in clay were estimated. Prior information for each parameter was set equal to its true value. Different weights were tested for prior information. For large weights of prior information, estimates are close to prior information, and consequently, a small value of the objective function is obtained. It should be noticed, however, that the objective function reaches nearly a constant value for weights larger than 1.5 (Fig. 7).

Poor estimates are obtained when all four parameters are estimated simultaneously when data have noise, even if parameter prior information for the clay formation is available.

A set of runs has been performed assuming no EdZ (see Table 4). Since D_e and Φ_{acc} of the EdZ are larger than those of undisturbed clay, estimated values of D_e and Φ_{acc} are larger than reference values when the thickness of the EdZ is 0. Acceptable estimates are obtained when D_e and Φ_{acc} are estimated separately by starting with large initial values. However, the inverse algorithm stops at local minima with suboptimal parameter estimates when the initial values are smaller than the reference values. Clearly, synthetic data cannot be fit with a model without EdZ.

Uncertainties caused by possible errors in the volume of water in the injection system have been evaluated by estimating clay diffusion parameter for volumes from 5 to 10% smaller than the true value. Errors of 5–10% in the volume of water of the system do not have a large effect on the clay D_e, but introduce a marked bias in the clay porosity (see Table 4).

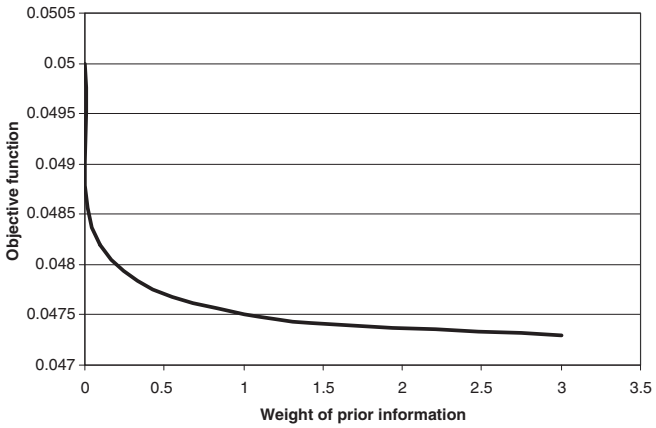

Fig. 7. Variation of objective function with the weight given to prior information.

Table 3
Summary of inverse runs in which effective diffusion coefficients, D_e, and accessible porosities, Φ_{acc}, of the undisturbed clay and of the EdZ are estimated for HTO

Standard dev σ	Clay D_e (m^2/s)		Clay Φ_{acc}		EdZ D_e (m^2/s)		EdZ Φ_{acc}	
	Initial	Estimated	Initial	Estimated	Initial	Estimated	Initial	Estimated
0.01	8.2×10^{-11}	3.6×10^{-11}	–	–	–	–	–	–
0.05	8.2×10^{-11}	2.1×10^{-11}	0.36	0.36	–	–	–	–
0.01	–	–	–	–	5.1×10^{-11}	2×10^{-10}	0.18	0.18
0.01	2.1×10^{-11}	3×10^{-11}	0.09	0.28	5.1×10^{-11}	1.4×10^{-10}	0.54	0.29
0.01	8.1×10^{-11}	4.1×10^{-11}	0.36	0.13	2.1×10^{-10}	1.1×10^{-10}	0.54	0.35
0.05	2.1×10^{-11}	2.1×10^{-11}	0.09	0.36	5.1×10^{-11}	7.9×10^{-10}	0.54	0.18
0.05	8.1×10^{-11}	3.2×10^{-11}	0.36	0.15	2.1×10^{-10}	1.7×10^{-10}	0.54	0.32
0.05	8.1×10^{-11}	[a] 3.7×10^{-11}	0.25	[a] 0.24	–	–	–	–
0.05	8.1×10^{-11}	[a] 3.4×10^{-11}	0.25	[a] 0.21	2×10^{-10}	9.8×10^{-11}	0.56	0.55
True value		4.1×10^{-11}		0.18		10^{-10}		0.36

[a] With the following prior information estimates for intact clay: effective diffusion = 4.1×10^{-11} m^2/day and porosity = 0.18. Weight given to prior information equal to 1.

Table 4
Summary of inverse runs in which effective diffusion coefficient, D_e, and accessible porosity, $\Phi_{acc,}$ of the undisturbed clay and of the EdZ are estimated for HTO in order to study the relevance of uncertainties in the thickness of the EdZ, the volume of the water in the injection system, the porosity of the gap and the diffusion coefficient of the filter

Hypothesis	Clay D_e (m^2/s)		Clay Φ_{acc}		EdZ D_e (m^2/s)		EdZ Φ_{acc}		σ
	Initial	Estimated	Initial	Estimated	Initial	Estimated	Initial	Estimated	
No EdZ	8.1×10^{-11}	8.1×10^{-11}	0.25	0.24	–	–	–	–	0
	2.1×10^{-11}	5×10^{-11}	0.09	0.1	–	–	–	–	0
5% smaller water volume	8.1×10^{-11}	5×10^{-11}	0.25	0.09	–	–	–	–	0
	8.1×10^{-11}	4.4×10^{-11}	0.25	0.1	–	–	–	–	0.05
Porosity of gap equal 1	4.1×10^{-11}	3.9×10^{-11}	0.18	0.23	10^{-10}	7.4×10^{-11}	0.36	0.36	0
	2.1×10^{-11}	3.1×10^{-11}	0.09	0.35	5.1×10^{-11}	1.4×10^{-10}	0.18	0.18	0
	8.1×10^{-11}	3×10^{-11}	0.36	0.36	2.1×10^{-11}	1.2×10^{-11}	0.56	0.25	0
D_e of filter = two times reference value	4.1×10^{-11}	3.9×10^{-11}	0.18	0.23	10^{-10}	7.4×10^{-11}	0.36	0.37	0
	2.1×10^{-11}	2.9×10^{-11}	0.09	0.29	5.1×10^{-11}	1.4×10^{-10}	0.18	0.18	0
	8.1×10^{-11}	3×10^{-11}	0.36	0.36	2.1×10^{-11}	1.2×10^{-11}	0.56	0.25	0
True value		4.1×10^{-11}		0.18		10^{-10}		0.36	

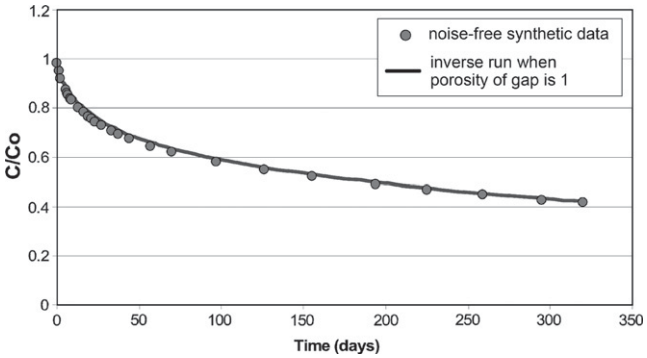

Fig. 8. Best fit to HTO noise-free synthetic data when the porosity of the gap is fixed equal to 1.

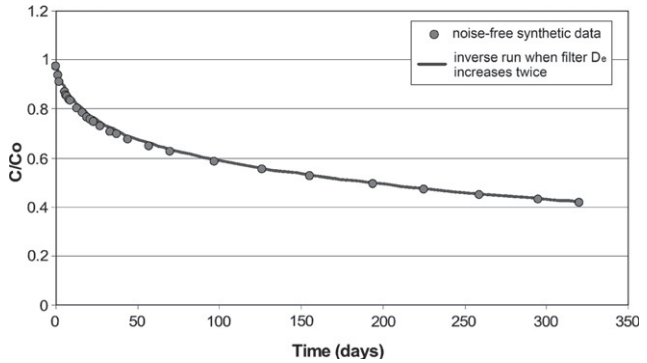

Fig. 9. Best fit to HTO noise-free synthetic data when the D_e of the filter is twice its reference value.

An increase of the gap porosity from 0.6 (reference value) to 1 causes a small, but noticeable deviation from the synthetic data (Fig. 8). In order to compensate for the change in the gap porosity, diffusion coefficients and porosities of clay and EdZ have to change. The optimum fit is achieved with clay porosities larger than the reference values and with effective diffusion coefficients slightly smaller than the reference values. The inverse algorithm converges to local minima when the estimation starts at values either larger or smaller than the reference values (see Table 4). This means that errors in the porosity of the gap lead to errors in the estimation of tracer diffusion parameters.

If the D_e of the filter is taken to be twice its reference value, an optimum fit is achieved with porosities larger and effective diffusion coefficients slightly smaller than the reference values (Fig. 9). The smallest value of the objective function is obtained when estimation starts at reference values. The inverse algorithm converges to local minima when the estimation starts at values either larger or smaller than the reference values. Therefore, the D_e value of the filter is a key parameter for estimating tracer diffusion parameters too.

5.3. Results for chloride

Identifiability analysis for chloride has been performed similar to that of HTO. Estimates of effective diffusion coefficients and accessible porosities in clay and EdZ are summarized in Table 5. D_e and Φ_{acc} of $^{36}Cl^-$ in clay can be estimated accurately when the data are free of noise ($\sigma = 0$). When data include noise, the estimated Φ_{acc} reaches either its lower or upper bound no matter what the initial guess was. Therefore, it can be concluded that these two parameters cannot be estimated at the same time because they are strongly correlated ($\rho = -0.99$). Estimates of EdZ parameters are excellent if $\sigma = 0$ and are acceptable for $\sigma = 0.02$ and 0.05. A similar conclusion is reached when the D_e value of clay and EdZ are estimated simultaneously. These two parameters can be properly estimated simultaneously, because their correlation coefficient is not large ($\rho = -0.76$). Results of runs in which accessible porosities of clay and EdZ are estimated show that estimated values coincide with true values for $\sigma = 0$ and are close to true values for noisy data

Table 5
Summary of inverse runs in which effective diffusion, D_e, and accessible porosity, Φ_{acc}, of the undisturbed clay and of the EdZ are estimated for $^{36}Cl^-$

Standard dev σ	Clay D_e (m^2/s)		Clay Φ_{acc}		EdZ D_e (m^2/s)		EdZ Φ_{acc}	
	Initial	Estimated	Initial	Estimated	Initial	Estimated	Initial	Estimated
0.02	1.9×10^{-11}	1.6×10^{-12}	0.15	0.04	–	–	–	–
0.02	–	–	–	–	4.5×10^{-11}	2.3×10^{-11}	0.36	0.19
0.02	1.9×10^{-11}	1×10^{-11}	–	–	4.5×10^{-11}	2.3×10^{-11}	–	–
0.02	–	–	0.05	0.11	–	–	0.12	0.18
0.02	4.5×10^{-12}	1.3×10^{-10}	0.05	0.04	1.1×10^{-11}	1.5×10^{-9}	0.09	0.27
0.02	1.9×10^{-11}	1.3×10^{-10}	0.12	0.04	4.5×10^{-11}	7.9×10^{-12}	0.26	0.56
True value		9.1×10^{-12}		0.09		2.3×10^{-11}		0.18

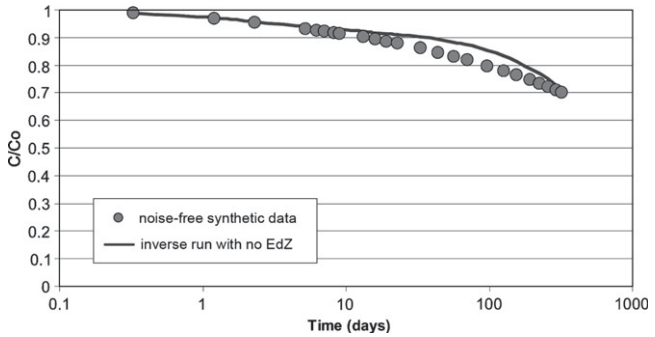

Fig. 10. Model fit to $^{36}Cl^-$ noise-free synthetic data for EdZ thickness equal to zero.

Table 6
Summary of inverse runs in which effective diffusion coefficient, D_e, and accessible porosity, Φ_{acc}, of undisturbed clay and EdZ are estimated for $^{36}Cl^-$ in order to study the relevance of uncertainties related to the thickness of the EdZ, the volume of the water in the injection system, the porosity of the gap and the diffusion coefficient of the filter

Hypothesis	Clay D_e (m^2/s)		Clay Φ_{acc}		
	Initial	Estimated	Initial	Estimated	σ
No EdZ	4.5×10^{-12}	10^{-10}	0.05	0.36	0
	1.9×10^{-11}	10^{-10}	0.18	0.36	0
Total volume 5% smaller	4.5×10^{-12}	9.1×10^{-12}	0.05	0.089	0
	4.5×10^{-12}	9.8×10^{-12}	0.05	0.12	0.02
	1.9×10^{-11}	1.3×10^{-11}	0.15	0.06	0.02
Porosity of gap equal 1	4.5×10^{-12}	3.9×10^{-12}	0.05	0.17	0
	1.9×10^{-11}	7.9×10^{-12}	0.18	0.05	0
D_e of filter two times reference one	4.5×10^{-12}	2.8×10^{-12}	0.05	0.38	0
	1.9×10^{-11}	1.4×10^{-11}	0.18	0.05	0
True value		9.1×10^{-12}		0.09	

even though the correlation between these two parameters is significant ($\rho = -0.86$).

When four parameters are estimated at the same time, estimates coincide with true values for $\sigma = 0$. However, for $\sigma = 0.02$ parameter estimates are poor and depend on the initial values.

D_e and Φ_{acc} of clay cannot be estimated simultaneously when it is assumed that there is no EdZ (Fig. 10). Estimated values are out of the parameter range regardless the initial guess (Table 6). Both parameters have been estimated in the case when the volume of water in the circulation system is 5% smaller than the true value. There are no differences between estimated and true values for $\sigma = 0$. However, estimates for data having noise ($\sigma = 0.02$) depend on initial values.

Clay diffusion parameters were estimated for a gap porosity of 1. In general, parameter estimates are not close to true values. When initial values are larger than true values, the estimated effective diffusion coefficient is acceptable. However, the estimated accessible porosity then reaches a local minimum. Therefore, uncertainties in the porosity of the gap affect strongly the estimation of the clay porosity and to a less extent the diffusion coefficient of the clay.

Identifiability runs performed using a D_e value of the filter of twice its true value show that parameter estimates deviate from true values even though the fit to synthetic data is good. Estimates of D_e are similar in all cases regardless the initial parameter values or data noise and estimates of the clay porosity reach always lower or upper bounds. Therefore, it can be concluded that uncertainties in the D_e values of filter affect strongly the estimation of the clay porosity and to a less extent the diffusion coefficient of clay for $^{36}Cl^-$.

6. Conclusions and relevance for real diffusion experiments

Interpretation of the DIR *in situ* diffusion experiments performed at Bure site on C–Ox clay is complicated by several non-ideal effects caused by the presence of a sintered filter, a gap between the filter and the borehole wall and an excavation disturbed zone (EdZ). The relevance of such non-ideal effects and their impact on estimated clay parameters have been evaluated with numerical sensitivity analyses and synthetic experiments.

Model results indicate that DIR *in situ* diffusion experiments can be safely interpreted with a simple 1D axisymmetric model because tracer dilution curves are not sensitive to diffusion anisotropy.

The effect of filter and gap has been analyzed by comparing tracer dilution curves with detailed and simplified models. Model results indicate that failing to account for filter and gap may result in significant errors in tracer concentrations.

Normalized dimensionless sensitivities of tracer concentrations at the test interval have been computed numerically. Tracer concentrations are sensitive to all key parameters. Their sensitivities are tracer dependent and vary with time. Sensitivities have been used to identify parameters that can be estimated with less uncertainty. Times at which tracer concentrations begin to be sensitive to each parameter have been identified.

Synthetic experiments generated with predefined parameters have been interpreted automatically with INVERSE-CORE^{2D} and then used to evaluate the relevance of non-ideal effects and to ascertain parameter identifiability for HTO and $^{36}Cl^-$ in the presence of random measurement errors. Identifiability analysis of synthetic experiments reveals that data noise makes the estimation of clay parameters difficult. Parameters of clay and EdZ cannot be estimated simultaneously when the data contain noise. Models without an EdZ fail to reproduce synthetic data. Proper interpretation of *in situ* diffusion experiments requires accounting for filter, gap and EdZ. Estimates of the effective diffusion coefficient and of the porosity of clay are highly correlated, indicating that these parameters cannot be estimated simultaneously. Accurate estimation of D_e values and porosities of clay and EdZ is only possible when the standard deviation of random noise is less than 0.01. Small errors in volume of the circulation system do not affect clay parameter estimates.

Normalized sensitivities, transient tracer sensitivities to parameters as well as conclusions of identifiability analysis will be most useful for calibration and interpretation of real DIR *in situ* diffusion experiments (see Samper et al., 2007).

References

Bear, J., 1972. Dynamics of fluids in porous media. Elsevier, New York.
Carrera, J., Neuman, S.P., 1986. Estimation of aquifer parameters under steady-state and transient conditions: background and statistical framework. Water Resour. Res. 22 (2), 199–210.
Carrera, J., Samper, J., Vives, L., Kulhman, U., 1989. Automatic inverse methods for the analysis of four pulse tests at the Leuggern borehole. NAGRA NTB, 34–88.
Cooper, H.H., Bredehoeft, J.D., Papadopoulus, I.S., 1967. Response of a finite diameter well to an instantaneous charge of water. Water Resour. Res. 3 (1), 263–269.
Dai, Z., Samper, J., 1999. INVERSE-CORE^{2D}: a code for the inverse problem of water flow and reactive solute transport, Users Manual, Version 0. University of La Coruña.
Dai, Z., Samper, J., 2004. Inverse problem of multicomponent reactive chemical transport in porous media: formulation and applications. Water Resour. Res. 40, W07407. doi:10.1029/2004WR00324.
Dai, Z., Samper, J., 2006. Inverse modeling of water flow and multicomponent reactive transport in coastal aquifer systems. J. Hydrol. 327 (3–4), 447–461.
Dai, Z., Samper, J., Ritzi, R., 2006. Identifying geochemical processes by inverse modeling of multicomponent reactive transport in Aquia aquifer. Geosphere 4 (4), 210–219.
Descostes M., Radwan J., Blin V., Tevissen E., 2007. Rapport de suivi scientifique II – Expérience DIR – Analyses en actif et conception associée. ANDRA report D.RP.17CEA06-014.

Dewonck, S., 2007. Expérimentation DIR. Synthese des résultats obtenus au 01/03/07. Laboratoire de recherche souterrain de Meuse/Haute-Marne. ANDRA report D.RP.ALS.07-0044.

García-Gutiérrez, M., Missana, T., Mingarro, M., Samper, J., Dai, Z., Molinero, J., 2001. Solute transport properties of compacted Ca-bentonite used in FEBEX project. J. Cont. Hydrol. 47 (2–4), 127–137.

Palut, J.M., 2001. Spécifications générales – Expérimentation DIR – Essai de Diffusion de Traceurs Inertes et Réactifs. Rapport Andra D.SP.ADPE.01.097.

Palut, J.M., Montarnal, P., Gautschi, A., Tevissen, E., Mouche, E., 2003. Characterisation of HTO diffusion properties by an *in situ* tracer experiment in Opalinus clay at Mont Terri. J. Cont. Hydrol. 61 (1), 203–218.

Radwan, J., Tevissen, E., Descostes, M., Blin, V., 2005. Premiers éléments d'interprétation et de modélisation des expériences de diffusion de traceurs inertes et réactifs en laboratoire souterrain de Meuse/Haute-Marne. Note technique CEA NTDPC/SECR 05-046/A.

Samper, J., Yang, C., Naves, A., Yllera, A., Hernández, A., Molinero, J., Soler, J.M., Hernán, P., Mayor, J.C., Astudillo, J., 2006a. A fully 3-D anisotropic model of DI-B *in situ* diffusion experiment in the Opalinus clay formation. Phys. Chem. Earth 31, 531–540.

Samper, J., Dai, Z., Molinero, J., García-Gutiérrez, M., Missana, T., Mingarro, M., 2006b. Interpretation of solute transport experiments in compacted Ca-bentonites using inverse modelling. Phys. Chem. Earth 31, 640–648.

Samper, F.J., Zheng, L., Yang, Q., Naves, A., Yang, C., 2007. Modeling and numerical interpretation of *in situ* DIR diffusion experiments on C–Ox Clay at Bure site (Phase 1). Final Report. Universidad de La Coruña, Spain.

Sun, N.Z., 1994. Inverse Problems in Groundwater Modeling. Kluwer Academic Publishers, Netherlands. pp. 364.

Tevissen, E., Soler, J.M., Montarnal, P., Gautschi, A., Van Loon, L.R., 2004. Comparison between *in situ* and laboratory diffusion studies of HTO and halides in Opalinus clay from the Mont Terri, Radiochim. Acta 92, 781–786.

Van Loon, L.R., Wersin, P., Soler, J.M., Eikenberg, J., Gimmi, Th., Hernán, P., Dewonck, S., Savoye, S., 2004. *In-situ* diffusion of HTO, $^{22}Na^{+}$, Cs^{+} and I^{-} in Opalinus clay at the Mont Terri underground rock laboratory, Radiochim. Acta 92, 757–763.

Wersin, P., Van Loon, L.R., Soler, J., Yllera, A., Eikenberg, J., Gimmi, T., Hernan, P., Boisson, J.-Y., 2004. Long-term diffusion experiment at mont terri: first results from field and laboratory data. Appl. Clay Sci. 26, 123–135.

Yllera, A., Hernández, A., Mingarro, M., Quejido, A., Sedano, L.A., Soler, J.M., Samper, J., Molinero, J., Barcala, J.M., Martín, P.L., Fernández, M., Wersin, P., Rivas, P., Hernán, P., 2004. DI-B experiment: planning, design and performance of an *in situ* diffusion experiment in the Opalinus clay formation. Appl. Clay Sci. 26, 181–196.

APPENDIX 6

ANALYSIS OF PARAMETER IDENTIFIABILITY OF THE IN SITU DIFFUSION AND RETENTION DR EXPERIMENT

This appendix presents a paper which was presented in the international conference MIGRATION09 which took place in Keneewick (Washington, USA) in September 2009 and was also published in Physics and Chemistry of the Earth in 2010.

This paper is the result of a joint research work including the contributions from other researchers. My main contribution includes the development of the numerical model and the sensitivity analyses for the strongly-sorbing tracers.

Physics and Chemistry of the Earth 35 (2010) 207–216

Contents lists available at ScienceDirect

Physics and Chemistry of the Earth

journal homepage: www.elsevier.com/locate/pce

Analysis of the parameter identifiability of the *in situ* diffusion and retention (DR) experiments

Javier Samper *, Shuping Yi, Acacia Naves

ETS Ingenieros de Caminos, Canales y Puertos, Universidad de La Coruña, Campus de Elviña s/n, ES-15192 La Coruña, Spain

ARTICLE INFO

Article history:
Received 26 October 2009
Received in revised form 11 March 2010
Accepted 10 April 2010
Available online 18 April 2010

Keywords:
Diffusion
Sorption
Numerical model
Dimensionless sensitivity
Identifiability analysis
DR experiments

ABSTRACT

In situ diffusion experiments are performed at underground research laboratories to overcome the limitations of laboratory diffusion experiments. The diffusion and retention (DR) experiments are long-term, natural-scale, *in situ* experiments performed in the anisotropic Opalinus Clay Formation at Mont Terri, Switzerland. Dilution data are monitored at the injection interval and overcoring data will be measured at samples around the injection interval at the end of the experiment during overcoring. Interpretation of DR experiments is complicated by the non-ideal effects caused by the sintered filter, the gap between the filter and the borehole wall and the excavation disturbed zone (EdZ). Their impact on parameter estimates has been evaluated with numerical sensitivity analyses and synthetic experiments having the same geometry and parameters as the real DR experiments. Dimensionless sensitivities of tracer concentrations in the injection interval and along the overcoring profiles have been computed numerically. They have been used to identify the tracer parameters that can be estimated with the least uncertainty from tracer dilution and overcoring data. Sensitivities of tracer dilution data change with time and those of overcoring concentrations along the bedding are different from those along profiles normal to the bedding. Concentrations along overcoring profiles are sensitive to the effective diffusion normal to the bedding. Synthetic experiments generated with prescribed known parameters have been interpreted automatically with INVERSE-CORE^{2D} and used to evaluate the relevance of non-ideal effects and determine parameter identifiability in the presence of random errors for HTO and $^{22}Na^{+}$. Model results show that it is difficult to estimate the parameters of the undisturbed clay when the tracer dilution data contain noise. The convergence of the estimation algorithm improves when the starting values are smaller than the true parameters. Although the parameters of the undisturbed clay and the EdZ cannot be estimated using tracer dilution data, their joint estimation from overcoring noisy data is possible for standard deviations of the noise up to 0.05. Large estimation errors in the parameters of the undisturbed clay and poor fits are obtained when the assumption about the existence of EdZ is incorrect. The effective diffusion of the filter is a key parameter for the interpretation of the experiments. Small errors in the volume of the circulation system do not affect the estimates of the component of the effective diffusion of undisturbed clay parallel to bedding. The results of the identifiability analysis clearly shows that: (1) The proper interpretation of *in situ* DR experiments requires accounting for the filter and the EdZ and (2) Overcoring data allow a more accurate estimation of the parameters of the undisturbed clay than the tracer dilution data.

1. Introduction

In situ diffusion experiments are performed at underground research laboratories (URL) in clay formations to overcome the limitations of laboratory diffusion experiments and to investigate possible scale effects. Such experiments have been performed in Opalinus Clay in Switzerland (Palut et al., 2003; Tevissen et al., 2004; Wersin et al., 2004; van Loon et al., 2004; Yllera et al., 2004; Samper et al., 2006a; Soler et al., 2008) and Callovo-Oxfordian clay, C-Ox, at Bure in France (Dewonck, 2007; Samper et al., 2008a; Naves et al., 2010).

The experimental program at the Mont Terri URL (Switzerland) aims at investigating the hydrogeological, geochemical and rock mechanical properties of the Opalinus Clay. The ongoing *in situ* diffusion and retention (DR) experiment are designed to study the transport and retention properties of the Opalinus Clay Formation. Opalinus Clay exhibits significant diffusion anisotropy due to stratification. The interpretation of *in situ* diffusion experiments is complicated by several non-ideal effects caused by the presence of the sintered filter, the gap between the filter and the borehole wall and the excavation disturbed zone, EdZ. Samper et al. (2008a)

* Corresponding author.
E-mail address: jsamper@udc.es (J. Samper).

1474-7065/$ - see front matter © 2010 Elsevier Ltd. All rights reserved.
doi:10.1016/j.pce.2010.04.012

evaluated the relevance of such non-ideal effects and their impact on estimated clay parameters with numerical sensitivity analyses and synthetic experiments for DIR diffusion experiments at the Bure URL on C-Ox clay. They found that DIR experiments can be interpreted with a simple 1D axisymmetric model because tracer dilution curves are not sensitive to diffusion anisotropy. They computed normalized sensitivities of tracer concentrations at the injection interval for several tracers using a time average sensitivity. They found tracer concentrations to be sensitive to all key parameters. Sensitivities were tracer dependent. They analyzed the identifiability of the parameters for HTO and ^{36}Cl from tracer dilution data and found that data noise makes difficult the estimation of clay parameters. Parameters of clay and EdZ cannot be estimated simultaneously when the data contain noise. Models without an EdZ fail to reproduce synthetic data. The proper interpretation of *in situ* diffusion experiments requires accounting for filter, gap and EdZ. Estimates of the effective diffusion and of the porosity of the clay are highly correlated, showing that these parameters cannot be estimated simultaneously. The accurate estimation of D_e values and porosities of clay and EdZ is only possible when the standard deviation of random noise is less than 0.01. Small errors in the volume of the circulation system do not affect the estimates of the clay parameters.

Here we present a thoroughfull sensitivity analysis for the DR diffusion experiments performed on Opalinus Clay which exhibits a diffusion anisotropy larger than that of C-Ox clay. Our analysis includes not only the sensitivities of tracer dilution data but also the sensitivities of tracer concentrations along overcoring profiles. We extend the analysis of Samper et al. (2008a) by performing the identifiability analysis for HTO and $^{22}Na^{+}$ by using tracer dilution and overcoring data. We also address the estimation of the two main components of the effective diffusion parallel and normal to the bedding.

The paper starts by describing the DR experiments. Then, numerical methods for their interpretation are presented. A systematic sensitivity analysis performed in terms of dimensionless sensitivities is also described. Then, the identifiability analysis of HTO and $^{22}Na^{+}$ diffusion and sorption parameters from synthetic diffusion experiments is presented. Finally, the paper ends with the main conclusions.

2. DR experiments at Mont Terri

DR experiments are similar to previous *in situ* diffusion experiments such as the DI-A (Wersin et al., 2004; van Loon et al., 2004) and DI-B (Yllera et al., 2004; Samper et al., 2006a; Soler et al., 2008) in the Opalinus Clay and DIR experiments in Callovo-Oxfordian clay (Dewonck, 2007; Samper et al., 2008a). The concept, however, has been optimized to determine *in situ* the diffusion anisotropy. The length of the injection intervals is shorter than that of previous experiments. The duration of the experimental is such that the transport distance of conservative tracers is larger than the length of the injection interval to allow the estimation of the diffusion anisotropy.

The experiments are performed in a borehole of the DR niche at the Mont Terri URL. The borehole was drilled at an angle of 45° with respect to the tunnel bottom so that it is normal to the bedding. Three test intervals were isolated by packers. The interval at the bottom serves as an auxiliary interval for the observation of the hydraulic pressure during the experiment. Tracer cocktails were injected into the upper two intervals. Each injection interval is connected to the surface equipment which includes a reservoir tank of 20 L. The fluid circulates continuously to ensure that the tank water and the downhole water are well mixed.

The following tracers were added at the upper interval: $^{60}Co^{+2}$, $^{137}Cs^{+}$, $^{133}Ba^{+2}$, $^{152}Eu^{+3}$, Eu^{+3} and HDO. The tracers injected in the lower interval are: HTO, $^{22}Na^{+}$, $^{85}Sr^{+2}$, I^{-} (stable), Br^{-} (stable), $^{75}Se^{+6}$, Cs^{+} and ^{18}O. Tracer concentrations and activities in the water of the circulation system were monitored by taking water samples at regular intervals in sampling vials. In addition, γ-emitter tracers (all radioactive tracers but HTO) were monitored on line in both circuits with an online γ-counting technique which was successfully tested in the DI-A experiment. At the end of the experiment the rock around the injection intervals was overcored and tracer distribution profiles measured. The time evolution of the tracer concentrations in the two injection systems denoted here as "tracer dilution data" and the tracer profiles in the rock after overcoring ("overcoring data") will be used to derive tracer diffusion and retention parameters.

3. Numerical interpretation

3.1. Solute transport equation

The transport equation for a tracer which diffuses through a low permeability medium is given by (Bear, 1972):

$$\nabla \cdot (\bar{D}_e \cdot \nabla c) = \alpha \frac{\partial c}{\partial t} \tag{1}$$

where c is the tracer concentration, t is time, and α is the capacity factor which is given by:

$$\alpha = \phi_{acc} + \rho K_d \tag{2}$$

where ϕ_{acc} is the accessible porosity which is equal to the total porosity if the tracer is not affected by anion exclusion, K_d is the distribution coefficient, and ρ is the bulk density. $\bar{D}_e$ is the effective diffusion tensor which, in a coordinate system defined along the bedding planes, is given by:

$$\bar{D}_e = \begin{pmatrix} D_{e//} & 0 & 0 \\ 0 & D_{e//} & 0 \\ 0 & 0 & D_{e^{\perp}} \end{pmatrix} \tag{3}$$

where $D_{e//}$ and $D_{e^{\perp}}$ are the components of the effective diffusion tensor parallel and normal to the bedding, respectively.

3.2. Numerical models

The numerical interpretation of the DR experiments requires the use of 3D models due to the diffusion anisotropy. However, symmetry with respect to the borehole axis allows the use of 2D axi-symmetric models. The left-hand-side boundary of the domain corresponds to the borehole axis. All outer boundaries of the model domain are no-flux boundaries. The following five material zones are considered for modelling the DR experiment: the injection interval, the 3 mm thick Teflon filter, the 2 mm gap, the EdZ which has a thickness of 20 mm and the undisturbed Opalinus Clay.

Prior estimates of the effective diffusion, the distribution coefficient and the accessible porosity for the undisturbed Opalinus Clay were derived from available laboratory experiments results or field experiments (Table 1). An anisotropy ratio of 4.0 was considered (van Loon et al., 2004). The effective diffusion and the capacity factor, α, of different tracers in porous Teflon filters were measured by van Loon and Glauss (2008) using a through-diffusion method. They found that the effective diffusion in the filter is about 10% of the diffusion coefficient in free water. Effective diffusions for other materials were derived from those of undisturbed clay by using Archie's law with an exponent equal to 4/3. The filter porosity is 0.3 (Fierz, 2006; Dewonck, 2007). On the other hand, the porosities of the EdZ and the gap are unknown. As an educated guess, the porosity of the EdZ was assumed to be twice that of the undisturbed clay while the porosity of the gap was assumed

Table 1
Reference values of diffusion and sorption parameters in different materials for all the tracers. $D_{e//}$ is the effective diffusion parallel to the bedding. The component normal to the bedding is four times smaller than $D_{e//}$. Φ_{acc} is the accessible porosity and K_d is the distribution coefficient.

		HTO, HDO	Br^-, I^-	$^{22}Na^+$	$^{133}Ba^{2+}$, $^{85}Sr^{2+}$	$^{137}Cs^+$, Cs^+, $^{60}Co^{2+}$
Filter	D_e (10^{-11} m^2/s)	6.27	2.00	8.79	8.79	14
	Φ_{acc}	0.30				
Gap	D_e (10^{-11} m^2/s)	31.7	10.1	44.5	44.5	190
	Φ_{acc}	0.60				
EdZ	$D_{e//}$ (10^{-11} m^2/s)	12.6	9.3	17.6	17.6	75.6
	Φ_{acc}	0.30				
	Thickness (cm)	3.0				
	K_d (10^{-4} m^3/kg)	0	0	2.048	13	5500
Undisturbed clay	$D_{e//}$ (10^{-11} m^2/s)	5.0	1.6	7.0	7.0	30
	Φ_{acc}	0.15	0.08	0.15	0.15	0.15
	K_d (10^{-4} m^3/kg)	0	0	2.048	13	5500

to be 0.6. The undisturbed clay and the EdZ are assumed to have the same distribution coefficient. No sorption takes place in the filter and the gap.

Diffusion experiments have been interpreted automatically with the inverse code INVERSE-CORE^{2D} (Dai and Samper, 2004) and by minimizing the least-squares objective function with the Gauss–Newton–Levenberg–Marquardt method. This code can estimate flow and transport parameters and provides statistical measures of goodness-of-fit as well as parameter uncertainties by computing the covariance and correlation matrices as well as approximate confidence intervals for the estimated parameters (García-Gutiérrez et al., 2001; Dai and Samper, 2004, 2006; Dai et al., 2006; Samper et al., 2006b). Details of the application of INVERSE-CORE^{2D} to the estimation of parameters in diffusion experiments can be found in Samper et al. (2008a,b).

4. Sensitivity analysis

4.1. Sensitivity runs

A model always entails simplifications of the real system. Model results depend on parameters that may contain uncertainties. A detailed sensitivity analysis was performed to identify the key parameters. Sensitivities for a given tracer were computed for the dilution data at the injection interval and overcoring data in two profiles parallel to the bedding and along four profiles normal to the bedding (Fig. 1). Sensitivity runs were performed by changing one-at-a-time within prescribed ranges the following parameters: (1) The effective diffusion of the filter and the gap; (2) the components of the effective diffusion parallel and perpendicular to the bedding, $D_{e//}$ and $D_{e\perp}$, for the EdZ and the undisturbed clay formation; (3) the accessible porosity of the gap, the EdZ and the undisturbed clay; (4) the distribution coefficient, (5) the thickness of the EdZ, and (6) the volume of water in the circulation system.

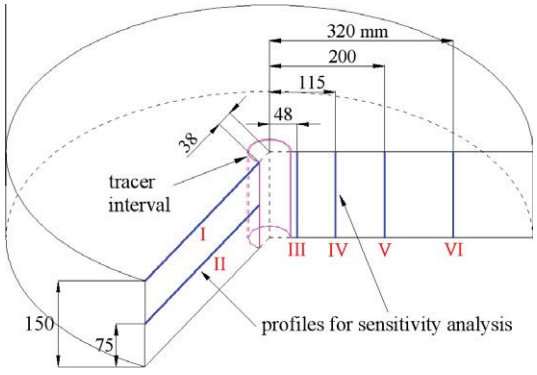

Fig. 1. Location of the six profiles along which the sensitivities of overcoring data are calculated.

4.2. Definition of relative sensitivities

Tracer concentrations, c, are normalized to their initial values, c_0. Relative concentrations, C, are defined as $C = c/c_0$.

Since model parameters have different units and vary over different ranges of values, their sensitivities cannot be compared directly. To compare sensitivities of concentrations to changes in different parameters, relative sensitivities, RS, have been computed according to:

$$RS = \frac{\Delta C}{\Delta P} \tag{4}$$

where ΔC is the average change in concentrations produced by the change in the parameter, and ΔP is the relative change in the parameter,

$$\Delta P(\%) = \frac{|P_S - P_b|}{P_b} \times 100 \tag{5}$$

where P_b is the value of the parameter in the base run and P_s is the value in the sensitivity run.

Relative sensitivities change with time in the injection interval and vary over space for the overcoring data. The average relative sensitivity, $\overline{RS}$, is computed from the average change in concentration $\overline{\Delta C}$ according to

$$\overline{RS} = \frac{\overline{\Delta C}}{\Delta P} \tag{6}$$

The average change in the concentration at the injection interval, $\overline{\Delta C}_d$, is calculated from:

$$\overline{\Delta C}_d = \frac{1}{T}\int_0^T |C_b - C_s| dt \tag{7}$$

where T is the time period over which sensitivities are calculated, C_b and C_s are computed concentrations in the base and sensitivity runs, respectively and $|\ |$ denotes the absolute value. This method to compute sensitivities is more systematic than that used by Samper et al. (2008a) for the sensitivities of the DIR experiments who simply computed the arithmetic average of sensitivities at arbitrary times.

Average changes in computed concentrations of overcoring data along profiles normal and parallel to the bedding, $\overline{\Delta C}_n$ and $\overline{\Delta C}_p$ are calculated according to:

$$\overline{\Delta C}_n = \frac{1}{V_n}\int_0^{V_n} |C_b - C_s| dV = \frac{1}{L}\int_0^{L} |C_b - C_s| dz \tag{8}$$

$$\overline{\Delta C}_p = \frac{1}{V_p}\int_0^{V_p} |C_b - C_s| dV = \frac{2}{\left(R_o^2 - R_i^2\right)}\int_{R_i}^{R_o} |C_b - C_s| r dr \quad (9)$$

For the profile normal to the bedding, z is the coordinate along the profile, and L is the total length of the profile which is defined as the interval in which computed concentrations are above a threshold of 0.01% of the maximum concentration in such profile. For the profile parallel to the bedding, r is the radial coordinate along the profile, and R_i and R_o are the inner and outer radii. The outer radius, R_o, is the radial distance beyond which the concentration is below a prescribed threshold of 0.01% the maximum concentration along such profile.

It should be noticed that the average relative sensitivities are dimensionless. Therefore, the relative sensitivities of different parameters can be compared directly for dilution and overcoring data.

4.3. Results

Relative sensitivities for dilution data at the injection interval after 3.6 years are listed in Table 2. Sensitivities for overcoring data along profile II are listed in Table 3 while those of overcoring data along profile III are shown in Table 4.

Changes in the thickness of the EdZ and the volume of the circulation system, V, affect significantly tracer concentrations at the injection interval and in most of the studied overcoring profiles. Therefore, both parameters are key factors for tracer diffusion and sorption in the DR experiments.

Sensitivities to diffusion and sorption parameters are tracer dependent. Conservative tracers are more sensitive to $D_{e//}$ and Φ_{acc} of the undisturbed clay and the EdZ. Weakly-sorbing tracers, however, are more sensitive to the $D_{e//}$ of the filter and the EdZ, and the K_d and the $D_{e//}$ of the undisturbed clay. Stongly-sorbing tracers are most sensitive to the D_e of the filter, the K_d and the $D_{e//}$ of the EdZ. Strongly-sorbing tracers lack sensitivities to changes in the parameters of the undisturbed clay.

Changes in the parameters of the gap do not affect tracer concentrations neither at the injection interval nor in overcoring profiles for all the tracers. Therefore, uncertainties in the parameters of the gap do not affect significantly the interpretation of the DR experiments.

Relative sensitivities of dilution data for Br^- and I^- are generally smaller than those of other tracers, showing that the parameters of Br^- and I^- are the most difficult to estimate from dilution data. Something similar happens for the relative sensitivities of strongly-sorbing tracers along overcoring profiles. Therefore, it can be concluded that it may be difficult to estimate the parameters of strongly-sorbing tracers from overcoring data.

Fig. 2 shows that the concentrations of $^{22}Na^+$ at the injection interval at early times are very sensitive to the changes in the D_e of the filter and less sensitive to the $D_{e//}$ of the EdZ and the undisturbed clay. Tracer concentrations start to be sensitive to the $D_{e//}$ of the EdZ after 1 day. Finally, the concentrations of $^{22}Na^+$ are sensitive to changes of the $D_{e//}$ of the undisturbed clay after 50 days. This conclusion is similar to the sensitivities found by Samper et al. (2008a) for the DIR experiments.

Sensitivities of the tracer concentrations to the changes in the parameters vary with time. Fig. 3 shows the time evolution of the relative sensitivities for HTO. Clearly, HTO concentrations are most sensitive to changes in the D_e of the filter, the $D_{e//}$ and the Φ_{acc} of the EdZ during the first 100 days. After 100 days, concentrations are most sensitive to changes in $D_{e//}$ of the undisturbed clay and the EdZ. $^{22}Na^+$ concentrations, however, are most sensitive to changes in the D_e of the filter and the D_{eh} of the EdZ during the first 100 days. Between 100 and 400 days, sensitivities to changes in the K_d and the D_{eh} of the undisturbed clay become relevant and concentrations are most sensitive to the D_{eh} of the undisturbed clay after 400 days (Fig. 4). The time evolution of the relative sensitivities for strongly-sorbing tracers is shown in Fig. 5. Undoubtedly,

Table 2
Average relative sensitivities, $\overline{RS}$, (defined in Eq. (6)) of dilution data at the injection interval at 3.6 years to changes in the parameters. $D_{e//}$ and $D_{e\perp}$ are the effective diffusion components parallel and normal to the bedding, Φ_{acc} is the accessible porosity and K_d is the distribution coefficient. The largest sensitivities are marked in boldface.

		HTO	HDO	Br^-/I^-	$^{22}Na^+$	$^{133}Ba^{2+}$	$^{85}Sr^{2+}$	Cs^+
Clay $D_{e//}$	$\Delta D_e < 0$	***0.0644***	***0.0635***	***0.0235***	***0.0782***	***0.0667***	***0.0596***	<0.0001
	$\Delta D_e > 0$	***0.0422***	***0.0417***	***0.0160***	***0.0465***	***0.0367***	***0.0323***	<0.0001
Clay $D_{e\perp}$	$\Delta D_e < 0$	0.0070	0.0069	0.0022	0.0050	0.0017	0.0015	<0.0001
	$\Delta D_e > 0$	0.0053	0.0053	0.0017	0.0041	0.0015	0.0013	<0.0001
Clay Φ_{acc}	$\Delta\Phi_a < 0$	***0.0140***	***0.0138***	0.0097	0.0048	0.0011	0.0010	<0.0001
	$\Delta\Phi_a > 0$	0.0056	0.0056	0.0036	0.0023	0.0005	0.0005	<0.0001
EdZ $D_{e//}$	$\Delta D_e < 0$	***0.0296***	***0.0292***	***0.0152***	***0.0473***	***0.0818***	***0.0743***	***0.0417***
	$\Delta D_e > 0$	0.0092	0.0090	0.0050	***0.0146***	***0.0266***	***0.0240***	***0.0153***
EdZ $D_{e\perp}$	$\Delta D_e < 0$	***0.0101***	0.0099	0.0044	***0.0118***	0.0105	0.0092	0.0002
	$\Delta D_e > 0$	0.0077	0.0075	0.0033	0.0088	0.0077	0.0067	0.0002
EdZ Φ_{acc}	$\Delta\Phi_a < 0$	0.0096	0.0095	***0.0109***	0.0065	0.0039	0.0035	<0.0001
	$\Delta\Phi_a > 0$	0.0093	0.0092	***0.0104***	0.0063	0.0038	0.0035	<0.0001
EdZ thickness	Δthick = −1 cm	***0.0227***	***0.0224***	***0.0105***	***0.0341***	***0.0515***	***0.0465***	***0.0134***
	Δthick = 1 cm	0.0092	0.0091	0.0040	***0.0136***	0.0180	0.0161	<0.0001
Gap D_e	$\Delta D_e < 0$	0.0028	0.0013	0.0016	0.0044	0.0079	0.0072	0.0099
	$\Delta D_e > 0$	0.0008	0.0008	0.0004	0.0013	0.0023	0.0021	0.0014
Gap Φ_{acc}	$\Delta\Phi_a < 0$	0.0010	0.0010	0.0012	0.0007	0.0005	0.0005	<0.0001
	$\Delta\Phi_a > 0$	0.0005	0.0005	0.0006	0.0004	0.0002	0.0002	<0.0001
Filter D_e	$\Delta D_e < 0$	0.0063	0.0070	0.0020	***0.0325***	***0.0567***	***0.0772***	***0.2069***
	$\Delta D_e > 0$	0.0019	0.0019	0.0005	0.0096	***0.0168***	***0.0242***	***0.0554***
Volume of the circulation system	ΔV = −10%	***0.0133***	***0.0131***	0.0064	***0.0186***	***0.0234***	***0.0228***	***0.1642***
K_d	$\Delta K_d < 0$	–	–	–	***0.0354***	***0.0802***	***0.0728***	***0.0652***
	$\Delta K_d > 0$	–	–	–	***0.0253***	***0.0489***	***0.0437***	***0.0144***

Table 3
Average relative sensitivities, $\overline{RS}$, (defined in Eq. (6)) of overcoring data along profile II after 3.6 years to changes in the parameters. $D_{e//}$ and $D_{e^\perp}$ are the effective diffusion components parallel and normal to the bedding, Φ_{acc} is the accessible porosity and K_d is the distribution coefficient. The largest sensitivities are marked in boldface.

		HDO	$^{133}Ba^{2+}$	HTO	$^{22}Na^{+}$	$^{85}Sr^{2+}$	Br/I^-	Cs^+/Co^{2+}
Clay $D_{e//}$	$\Delta D_e < 0$	***0.1052***	***0.1130***	***0.1056***	***0.1024***	***0.1097***	***0.1017***	0.0004
	$\Delta D_e > 0$	***0.0485***	***0.0388***	***0.0487***	***0.0388***	***0.0374***	***0.0427***	0.0008
Clay $D_{e^\perp}$	$\Delta D_e < 0$	***0.0291***	0.0028	***0.0297***	***0.0198***	0.0022	***0.0179***	<0.0001
	$\Delta D_e > 0$	***0.0157***	0.0036	***0.0159***	***0.0146***	0.0032	***0.0110***	<0.0001
Clay Φ_{acc}	$\Delta\Phi_a < 0$	***0.0833***	0.0037	***0.0832***	***0.0139***	0.0037	***0.1129***	<0.0001
	$\Delta\Phi_a > 0$	***0.0497***	0.0036	***0.0496***	***0.0168***	0.0036	***0.0558***	<0.0001
EdZ $D_{e//}$	$\Delta D_e < 0$	***0.0176***	***0.0313***	***0.0176***	***0.0251***	***0.0301***	***0.0329***	0.0068
	$\Delta D_e > 0$	0.0056	0.0087	0.0056	0.0069	0.0084	0.0061	0.0073
EdZ $D_{e^\perp}$	$\Delta D_e < 0$	0.0021	0.0036	0.0017	0.0026	0.0032	0.0011	<0.0001
	$\Delta D_e > 0$	0.0013	0.0029	0.0013	0.0023	0.0027	0.0007	<0.0001
EdZ Φ_{acc}	$\Delta\Phi_a < 0$	0.0021	0.0011	0.0022	0.0017	0.0011	0.0026	<0.0001
	$\Delta\Phi_a > 0$	0.0021	0.0011	0.0055	0.0010	0.0032	0.0076	<0.0001
EdZ thickness	Δthick = −1 cm	***0.0132***	***0.0219***	***0.0131***	***0.0143***	***0.0211***	***0.0125***	0.0066
	Δthick = 1 cm	***0.0112***	***0.0206***	***0.0111***	***0.0141***	***0.0198***	***0.0115***	0.0011
Gap D_e	$\Delta D_e < 0$	0.0014	0.0014	0.0012	0.0014	0.0013	0.0014	<0.0001
	$\Delta D_e > 0$	0.0004	0.0003	0.0004	0.0003	0.0003	0.0004	<0.0001
Gap Φ_{acc}	$\Delta\Phi_a < 0$	0.0002	0.0002	0.0002	0.0002	0.0002	0.0002	<0.0001
	$\Delta\Phi_a > 0$	0.0002	0.0002	0.0002	0.0002	0.0002	0.0002	<0.0001
Filter D_e	$\Delta D_e < 0$	0.0037	***0.0132***	0.0030	***0.0114***	***0.0195***	0.0017	0.0020
	$\Delta D_e > 0$	0.0009	0.0031	0.0009	0.0033	0.0051	0.0005	0.0014
Volume of the circulation system	ΔV = −10%	***0.0211***	***0.0598***	***0.0215***	***0.0436***	***0.0560***	0.0078	***0.0147***
K_d	$\Delta K_d < 0$	–	***0.0796***	–	***0.0355***	***0.0598***	–	***0.0252***
	$\Delta K_d > 0$	–	***0.0491***	–	***0.0405***	***0.0481***	–	0.0086

Table 4
Average relative sensitivities, $\overline{RS}$, (defined in Eq. (6)) of overcoring data along profile IV after 3.6 years to changes in the parameters. $D_{e//}$ and $D_{e^\perp}$ are the effective diffusion components parallel and normal to the bedding, Φ_{acc} is the accessible porosity and K_d is the distribution coefficient (see Fig. 1 for the location of profile IV). The largest sensitivities are marked in boldface.

		HDO	$^{133}Ba^{2+}$	HTO	$^{22}Na^{+}$	$^{85}Sr^{2+}$	Br/I^-
$D_{eh\text{-clay}}$	$\Delta D_e < 0$	***0.0249***	***0.0541***	***0.0278***	***0.0177***	***0.0493***	***0.0310***
	$\Delta D_e > 0$	***0.0195***	***0.0105***	***0.0226***	***0.0165***	0.0095	***0.0105***
$D_{ev\text{-clay}}$	$\Delta D_e < 0$	***0.0443***	0.0092	***0.0461***	***0.0310***	0.0090	***0.0446***
	$\Delta D_e > 0$	***0.0256***	0.0065	***0.0253***	***0.0187***	0.0060	***0.0270***
$\Phi_{a\text{-clay}}$	$\Delta\Phi_a < 0$	***0.0503***	0.0031	***0.0492***	***0.0133***	0.0029	***0.0979***
	$\Delta\Phi_a > 0$	***0.0401***	0.0031	***0.0391***	***0.0123***	0.0029	***0.0694***
$D_{eh\text{-EdZ}}$	$\Delta D_e < 0$	***0.0298***	***0.0228***	***0.0288***	***0.0244***	***0.0203***	***0.0443***
	$\Delta D_e > 0$	0.0074	0.0068	0.0079	0.0069	0.0061	***0.0136***
$D_{ev\text{-EdZ}}$	$\Delta D_e < 0$	***0.0133***	0.0055	0.0131	0.0109	0.0052	***0.0164***
	$\Delta D_e > 0$	***0.0104***	0.0040	0.0103	0.0085	0.0037	***0.0124***
$\Phi_{a\text{-EdZ}}$	$\Delta\Phi_a < 0$	0.0036	0.0010	0.0038	0.0021	0.0009	0.0091
	$\Delta\Phi_a > 0$	0.0041	0.0009	0.0040	0.0021	0.0009	0.0093
EdZ thickness	Δthick = −1 cm	***0.0248***	***0.0164***	***0.0240***	***0.0194***	***0.0146***	***0.0352***
	Δthick = 1 cm	***0.0177***	***0.0151***	***0.0189***	***0.0161***	***0.0135***	***0.0300***
$D_{e\text{-gap}}$	$\Delta D_e < 0$	0.0027	0.0018	0.0026	0.0021	0.0016	0.0041
	$\Delta D_e > 0$	0.0007	0.0005	0.0007	0.0007	0.0005	0.0011
$\Phi_{a\text{-gap}}$	$\Delta\Phi_a < 0$	0.0003	0.0001	0.0003	0.0002	0.0001	0.0004
	$\Delta\Phi_a > 0$	0.0003	0.0001	0.0003	0.0002	0.0001	0.0004
$D_{e\text{-filter}}$	$\Delta D_e < 0$	0.0066	***0.0128***	0.0055	***0.0153***	***0.0171***	0.0049
	$\Delta D_e > 0$	0.0018	0.0036	0.0017	0.0043	0.0051	0.0013
Volume of the circulation system	ΔV = −10%	***0.0367***	***0.0248***	***0.0361***	***0.0405***	***0.0213***	***0.0172***
K_d	$\Delta K_d < 0$	–	***0.1033***	–	***0.0495***	***0.0803***	–
	$\Delta K_d > 0$	–	***0.0435***	–	***0.0323***	***0.0402***	–

the concentrations of Cs^+ are most sensitive to changes in the D_e of the filter and the volume of the circulation system. Relative sensitivities to changes in the K_d and the D_{eh} of the EdZ increase before 700 days and then decrease slightly with time.

The sensitivities of overcoring data along profiles contain information which is complementary to that provided by dilution data at the injection interval. For instance, overcoring data are sensitive to changes in the $D_{e^\perp}$ of the undisturbed clay for HTO and Br in all the profiles (Figs. 6 and 7). The concentrations of the sorbing tracers along profile I are slightly sensitive to changes in the $D_{e^\perp}$ of the EdZ. However, tracer dilution data lack sensitivity to the $D_{e^\perp}$ of the undisturbed clay.

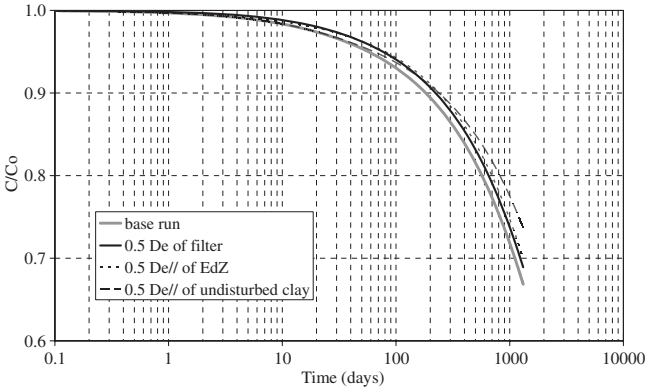

Fig. 2. Sensitivity of the concentrations of $^{22}Na^{+}$ at the injection interval to changes in the D_e of the filter, the $D_{e//}$ of the EdZ and the undisturbed clay. The times at which tracer concentrations start to be sensitive are different for each parameter.

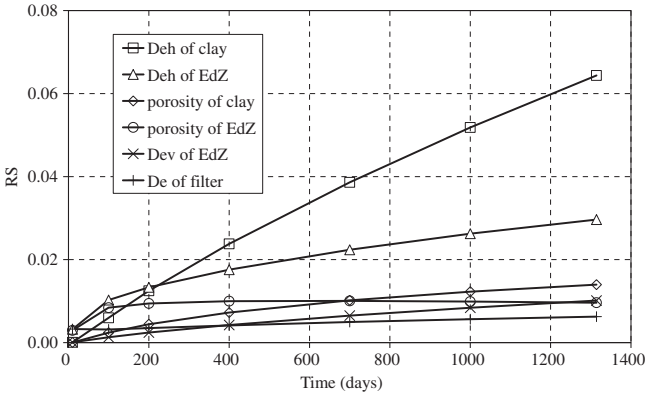

Fig. 3. Time evolution of the relative sensitivities at the injection interval for HTO. Curves are shown only for the most sensitive parameters.

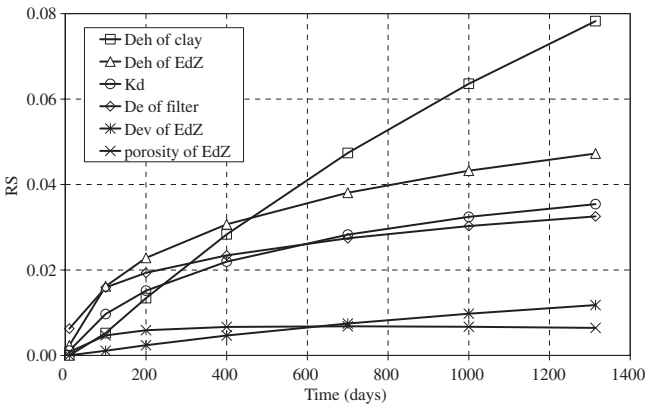

Fig. 4. Time evolution of the relative sensitivities at the injection interval for $^{22}Na^{+}$. Curves are shown only for the most sensitive parameters.

Relative sensitivities along overcoring profiles are also tracer dependent and vary between different profiles (see Tables 3 and 4). The largest sensitivities occur along the radial profiles I and II and the vertical profiles located closer to the injection interval (profiles III and IV). Sensitivities for conservative tracers are larger than those of sorbing tracers because the former penetrate more into the clay formation.

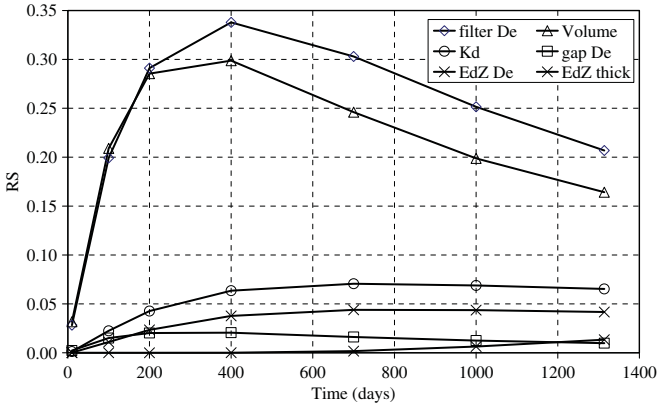

Fig. 5. Time evolution of the relative sensitivities at the injection interval for Cs^{+}. Curves are shown only for the most sensitive parameters.

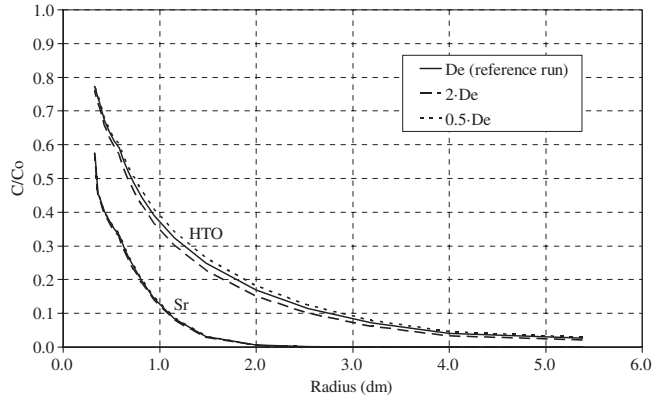

Fig. 6. Sensitivity of the concentrations along profile I to changes in the $D_{e^{\perp}}$ of the undisturbed clay (see Fig. 1 for the location of profile I).

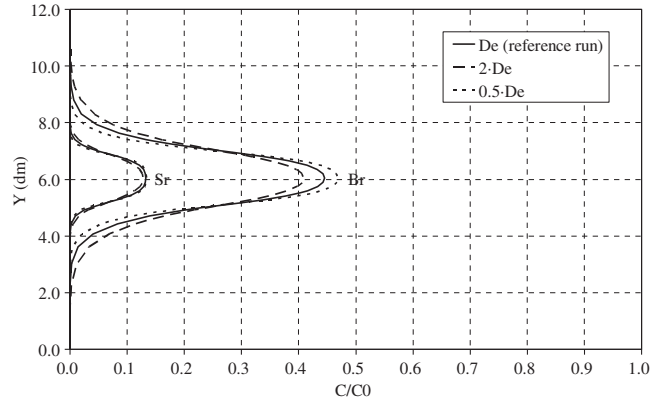

Fig. 7. Sensitivity of the concentrations along profile IV to changes in the $D_{e^{\perp}}$ of the undisturbed clay (see Fig. 1 for the location of profile IV).

5. Identifiability analysis

5.1. Methodology

Synthetic experiments are often used to study parameter identifiability and parameter uncertainties. Synthetic diffusion experiments having the same geometric properties as the real experiments have been simulated numerically for reference values

of diffusion and sorption parameters. Synthetic concentration data have then been used to estimate such parameters. Since true values are known, one can clearly identify which parameters can be estimated and how reliable these estimates really are.

The method for performing the identifiably study with synthetic data involves the following steps: (1) Generating synthetic data from a forward run of the numerical model; (2) adding multiplicative random noise to the synthetic data with a standard deviation, σ, which ranges from 0 to 0.1 to include the values of σ of the measured data in the DR experiments; (3) estimating key diffusion parameters from noisy synthetic data in several stages, starting first with the estimation of $D_{e//}$, the accessible porosity or the K_d of the undisturbed clay, followed by the estimation of the EdZ parameters and ending with the joint estimation of all parameters; (4) evaluating the effect of the uncertainties in the EdZ, the volume of water in the injection system, V, and the D_e of the filter. There is no need to evaluate the uncertainties in the parameters of the gap because the sensitivity analysis shows that gap parameters do not play a major role on the DR experiments.

Parameter identifiability analyses have been performed with synthetic dilution and overcoring data. Nineteen synthetic dilution data are generated at the same times as the real experiments. Synthetic overcoring data are generated for two assumptions: (1) 10 data along profile II (one datum per cm) and (2) 42 data along profiles I and II.

5.2. Results for HTO

Table 5 summarizes the results of the identifiability analysis for HTO. Estimation runs have been performed considering different initial starting values of the parameters and increasing values of σ.

The estimates of the $D_{e//}$ of the clay are close to its true value (5.0×10^{-11} m^2/s) even for $\sigma = 0.05$ when only this parameter is estimated. Clearly, the noise in the HTO data introduces bias in the estimate of $D_{e//}$ which for $\sigma = 0.05$ is 17.8% for the inverse run performed with dilution data and 6.4% for that performed with overcoring data in profile II.

On the other hand, poor estimates of $D_{e//}$ and Φ_{acc} of the undisturbed clay are obtained for noisy dilution data when they are estimated simultaneously because $D_{e//}$ and Φ_{acc} are highly correlated ($\rho = -0.99$). However, acceptable estimates of $D_{e//}$ and Φ_{acc} are obtained simultaneously from noisy overcoring data along profile II even for $\sigma = 0.05$. Since tracer concentrations along overcoring profiles are more sensitive to changes in Φ_{acc} than to dilution data, Φ_{acc} of HTO can be estimated with overcoring data better than with dilution data. Similar conclusions can be drawn when the $D_{e//}$ and $D_{e^\perp}$ of the undisturbed clay are estimated simultaneously. These parameters cannot be estimated simultaneously with noisy dilution data. However, their estimation errors are small when they are estimated from noisy overcoring data along profile II even for $\sigma = 0.05$.

Table 5
Summary of the inverse runs for synthetic experiments of HTO. The following parameters are estimated: $D_{e//}$, $D_{e^\perp}$ and porosity of the undisturbed clay and $D_{e//}$ of the EdZ. σ is the standard deviation of the noise (see Fig. 1 for the location of profile II).

Parameter		Clay $D_{e//}$ (m^2/s)		Clay Φ_{acc}		Clay $D_{e^\perp}$ (m^2/s)		EdZ $D_{e//}$ (m^2/s)	
True value		5.0×10^{-11}		0.15		1.25×10^{-11}		1.26×10^{-10}	
Data	σ	Initial	Estimated	Initial	Estimated	Initial	Estimated	Initial	Estimated
Dilution	0.05	2.5×10^{-11}	5.89×10^{-11}	–	–	–	–	–	–
	0.05	2.5×10^{-11}	6.79×10^{-11}	0.20	0.087	–	–	–	–
	0.02	2.5×10^{-11}	3.75×10^{-11}	–	–	6.3×10^{-12}	7.50×10^{-11}	–	–
	0.01	2.5×10^{-11}	5.14×10^{-11}	0.10	0.223	–	–	6.31×10^{-11}	1.04×10^{-10}
	0.02	2.5×10^{-11}	6.55×10^{-11}	0.10	0.11	–	–	6.31×10^{-11}	1.02×10^{-10}
	0.02	1.0×10^{-10}	6.22×10^{-11}	0.20	0.091	–	–	2.52×10^{-10}	1.28×10^{-10}
Profile II	0.05	2.5×10^{-11}	4.68×10^{-11}	–	–	–	–	–	–
	0.05	2.5×10^{-11}	4.75×10^{-11}	0.10	0.135	–	–	–	–
	0.02	2.5×10^{-11}	5.01×10^{-11}	–	–	6.3×10^{-12}	1.18×10^{-11}	–	–
	0.02	2.5×10^{-11}	4.91×10^{-11}	0.10	0.154	6.3×10^{-12}	1.13×10^{-11}	–	–
	0.02	2.5×10^{-11}	4.92×10^{-11}	0.10	0.153	6.3×10^{-12}	1.16×10^{-11}	6.31×10^{-11}	1.29×10^{-10}
	0.05	1.0×10^{-10}	4.81×10^{-11}	0.20	0.159	6.3×10^{-12}	1.02×10^{-11}	6.31×10^{-10}	1.33×10^{-10}

Table 6
Summary of the inverse runs for synthetic experiments of HTO to evaluate the effect of the uncertainties in the thickness of the EdZ, the volume of water in the circulation system and the D_e of the filter. σ is the standard deviation of the noise (see Fig. 1 for the location of profile II).

Parameter		Clay $D_{e//}$ (m^2/s)		Clay Φ_{acc}		Clay $D_{e^\perp}$ (m^2/s)		
True value		5.00×10^{-11}		0.15		1.25×10^{-11}		
Hypothesis	Data	Initial	Estimated	Initial	Estimated	Initial	Estimated	σ
No EdZ	Dilution	2.5×10^{-11}	8.74×10^{-11}	–	–	–	–	0
	Profile II	2.5×10^{-11}	5.00×10^{-10}	0.10	0.08	6.25×10^{-12}	1.25×10^{-12}	0
	Dilution	2.5×10^{-11}	9.49×10^{-11}	–	–	–	–	0.05
	Profile II	2.5×10^{-11}	5.00×10^{-10}	0.10	0.08	6.25×10^{-12}	1.25×10^{-12}	0.05
10% smaller volume of circulation system	Dilution	2.5×10^{-11}	4.69×10^{-11}	0.10	0.08	–	–	0
	Profile II	2.5×10^{-11}	4.48×10^{-11}	0.10	0.141	6.25×10^{-12}	1.26×10^{-11}	0
	Dilution	2.5×10^{-11}	4.78×10^{-11}	0.10	0.14	–	–	0.05
	Profile II	2.5×10^{-11}	4.29×10^{-11}	0.10	0.139	6.25×10^{-12}	9.81×10^{-12}	0.05
D_e of filter = twice its true value	Dilution	2.5×10^{-11}	5.17×10^{-11}	0.10	0.12	–	–	0
	Profile II	2.5×10^{-11}	5.04×10^{-11}	0.10	0.152	6.25×10^{-12}	1.29×10^{-11}	0
	Dilution	2.5×10^{-11}	6.79×10^{-11}	0.10	0.08	–	–	0.05
	Profile II	2.5×10^{-11}	4.83×10^{-11}	0.10	0.164	6.25×10^{-12}	9.90×10^{-12}	0.05

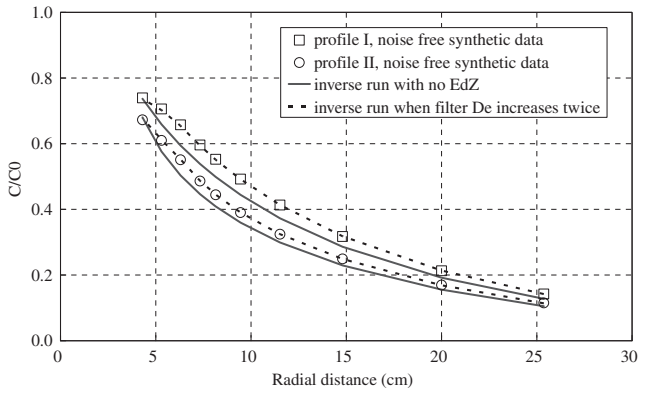

Fig. 8. Best fit to HTO noise-free synthetic overcoring data for the inverse runs: (1) with a D_e of the filter twice its true value and (2) no EdZ.

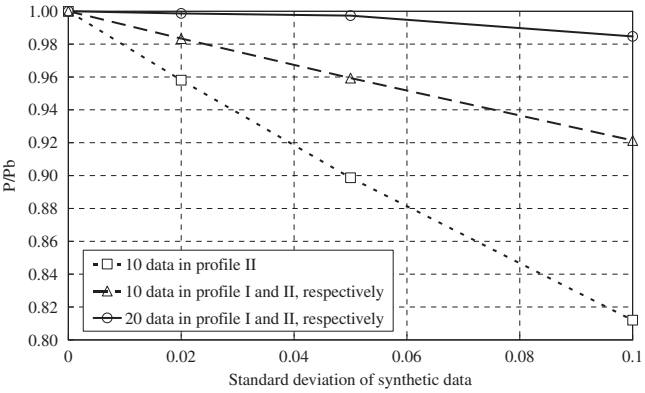

Fig. 9. Estimation errors of Φ_{acc} for HTO versus the standard deviation of the synthetic data when the $D_{e//}$ and Φ_{acc} of the undisturbed clay are estimated simultaneously. P is the estimated value of the parameter and P_b is the true value of the parameter.

$D_{e//}$, $D_{e^\perp}$ and Φ_{acc} of the undisturbed clay and the $D_{e//}$ of the EdZ can be estimated simultaneously from noisy overcoring data along profile II even for $\sigma = 0.05$. However, parameter estimates depend on the initial starting values. The joint estimation of these parameters from dilution data is only possible with noise-free data.

Several runs were performed by assuming no EdZ (see Table 6). No acceptable estimates are obtained in this case. Since the $D_{e//}$ of the EdZ is larger than that of the undisturbed clay, the estimated values of the $D_{e//}$ of the clay are larger than the reference values when the thickness of the EdZ is 0. Clearly, synthetic data cannot be fit with a model which disregards the EdZ for inverse runs with either dilution or overcoring data (Fig. 8).

Uncertainties caused by possible errors in the volume of water in the injection system, V, have been evaluated by estimating clay diffusion parameter with a value 10% smaller than the true value of V. The error in V does not have a large effect on the estimate of the $D_{e//}$ of the undisturbed clay but introduces a marked bias in the estimate of the clay porosity, especially in the inverse runs performed with dilution data (see Table 6). Clearly, the effect of the uncertainties in V on parameter estimates from dilution data is larger than from the overcoring data.

If the D_e of the filter is taken to be twice its reference value, an optimum fit is achieved with a clay porosity slightly smaller than the true value and a $D_{e//}$ of the undisturbed clay slightly larger than the reference value when these parameters are estimated from dilution data. Acceptable estimates of the parameters of the undisturbed clay are obtained from overcoring data even for $\sigma = 0.05$. The best fit here is shown in Fig. 8.

The number of synthetic data has a significant effect on the estimates of the parameters of the undisturbed clay. Such an effect has been evaluated by estimating the parameters of the undisturbed clay for the following three cases: (1) 10 data along profile II, (2) 10 data along profiles I and II, respectively and (3) 20 data along profiles I and II, respectively. Model results show that the estimation errors are smallest for case 3. Fig. 9 shows the comparison of the estimation errors of the clay porosity for the three cases. The estimation errors of Φ_{acc} in cases 1 and 2 for $\sigma = 0.1$ are 12.3 and 5.1 times larger than that in case 3.

5.3. Results for $^{22}Na^+$

The identifiability analysis for $^{22}Na^+$ has been performed in a manner similar to that of HTO. Parameter estimation results are summarized in Table 7. The $D_{e//}$ and K_d of $^{22}Na^+$ in the undisturbed clay can be estimated properly even for $\sigma = 0.1$ when the rest of the parameters are perfectly known. Parameter estimation errors from overcoring synthetic data are smaller than those from dilution synthetic data (Fig. 10). The estimates of the $D_{e//}$ and the K_d of the undisturbed clay from dilution data depend on the initial values.

Table 7
Summary of the inverse runs for synthetic experiments of $^{22}Na^+$. The following parameters are estimated: $D_{e//}$, $D_{e^\perp}$ and K_d of the undisturbed clay and $D_{e//}$ of the EdZ. σ is the standard deviation of the noise (see Fig. 1 for the location of profiles I and II).

Parameter True value		Clay $D_{e//}$ (m^2/s) 7.00×10^{-11}		K_d (m^3/kg) 2.048×10^{-4}		Clay $D_{e^\perp}$ (m^2/s) 1.75×10^{-11}		EdZ $D_{e//}$ (m^2/s) 1.76×10^{-10}	
Data	σ	Initial	Estimated	Initial	Estimated	Initial	Estimated	Initial	Estimated
Dilution	0.05	3.5×10^{-11}	7.86×10^{-11}	–	–	–	–	–	–
	0.1	–	–	4.096×10^{-4}	2.902×10^{-4}	–	–	–	–
	0.02	3.5×10^{-11}	8.28×10^{-11}	1.024×10^{-4}	1.574×10^{-5}	–	–	–	–
	0.02	1.4×10^{-10}	8.55×10^{-11}	4.096×10^{-4}	1.479×10^{-4}	–	–	–	–
	0.05	3.5×10^{-11}	6.55×10^{-11}	–	–	8.74×10^{-12}	1.39×10^{-10}	–	–
	0.01	1.4×10^{-10}	8.21×10^{-11}	4.096×10^{-4}	1.831×10^{-4}	3.50×10^{-11}	2.34×10^{-12}	–	–
	0.01	3.5×10^{-11}	7.20×10^{-11}	1.024×10^{-4}	1.701×10^{-4}	–	–	8.80×10^{-11}	2.11×10^{-10}
	0.01	1.4×10^{-11}	7.79×10^{-11}	4.096×10^{-4}	1.826×10^{-4}	–	–	3.52×10^{-10}	1.64×10^{-10}
Profiles I and II	0.05	3.5×10^{-11}	6.99×10^{-11}	–	–	–	–	–	–
	0.1	–	–	1.024×10^{-4}	2.054×10^{-4}	–	–	–	–
	0.02	3.5×10^{-11}	6.99×10^{-11}	1.024×10^{-4}	2.045×10^{-4}				
	0.05	3.5×10^{-11}	7.02×10^{-11}	1.024×10^{-4}	2.056×10^{-4}	8.74×10^{-12}	1.70×10^{-11}	–	–
	0.1	3.5×10^{-11}	7.04×10^{-11}	1.024×10^{-4}	2.070×10^{-4}	8.74×10^{-12}	1.54×10^{-11}	–	–
	0.02	3.5×10^{-11}	7.02×10^{-11}	1.024×10^{-4}	2.055×10^{-4}	8.74×10^{-12}	1.83×10^{-11}	8.80×10^{-11}	1.85×10^{-10}
	0.05	3.5×10^{-11}	6.84×10^{-11}	1.024×10^{-4}	2.090×10^{-4}	8.74×10^{-12}	2.09×10^{-11}	8.80×10^{-11}	2.00×10^{-10}

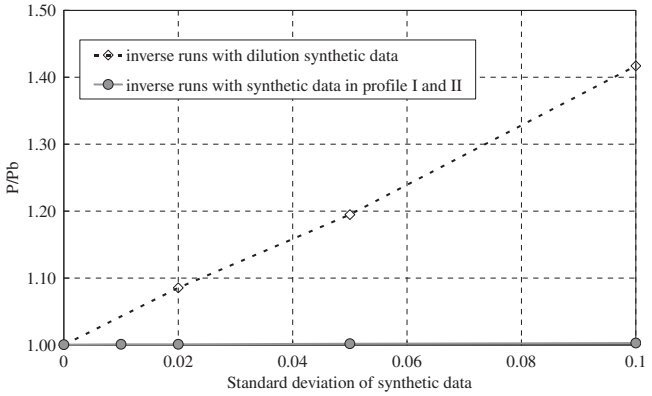

Fig. 10. Estimation errors of K_d for $^{22}Na^+$ versus the standard deviation of the synthetic data when only K_d is estimated. P is the estimated value of the parameter and P_b is the true value of the parameter.

They can be estimated only for $\sigma < 0.02$ because they are strongly correlated ($\rho = -0.95$). The $D_{e//}$ and K_d of the undisturbed clay can be estimated from noisy overcoring data even for $\sigma = 0.05$ when their correlation coefficient is equal to 0.57.

The joint estimation of the $D_{e//}$, $D_{e^\perp}$ and K_d of the undisturbed clay is only possible when dilution data are free of noise. However, they can be estimated simultaneously from noisy overcoring data even for $\sigma = 0.1$. Data noise affects the estimate of the $D_{e^\perp}$ more strongly than the estimates of $D_{e//}$ and K_d of the undisturbed clay.

When the $D_{e//}$ of undisturbed clay, the $D_{e//}$ of the EdZ and the K_d are estimated simultaneously from dilution data, parameter estimates are poor and depend on the initial values. Acceptable estimates are obtained for $\sigma \leqslant 0.01$ with initial values smaller than the true values even though the $D_{e//}$ of the undisturbed clay and the EdZ are highly correlated ($\rho = -0.96$). In the inverse runs performed with overcoring data, however, the $D_{e//}$ and the $D_{e^\perp}$ of the undisturbed clay, the $D_{e//}$ of the EdZ and the K_d can be estimated simultaneously even for $\sigma = 0.1$. Therefore, the effect of data noise on parameter estimates is much stronger on dilution data than on overcoring data.

The parameters of the undisturbed clay ($D_{e//}$, $D_{e^\perp}$ and K_d) cannot be estimated simultaneously when the EdZ is disregarded. Poor estimates are obtained (see Table 8). The fit to the data is poor (Fig. 12). Therefore, the uncertainty in the existence of the EdZ has a large effect on the estimates of the parameters of the undisturbed clay.

A decrease of 10% in V leads to estimation errors for $\sigma = 0$. The best fit to the dilution data is shown in Fig. 11. Uncertainties in V affect the estimate of K_d more strongly than the estimates of the $D_{e//}$ and the $D_{e^\perp}$ of the undisturbed clay. Parameter estimates obtained from overcoring data contain less error than those obtained from dilution data. Estimation errors from overcoring data are 13.4% for K_d, 10.4% for $D_{e//}$ of the clay and 4.0% for the $D_{e^\perp}$ of the clay.

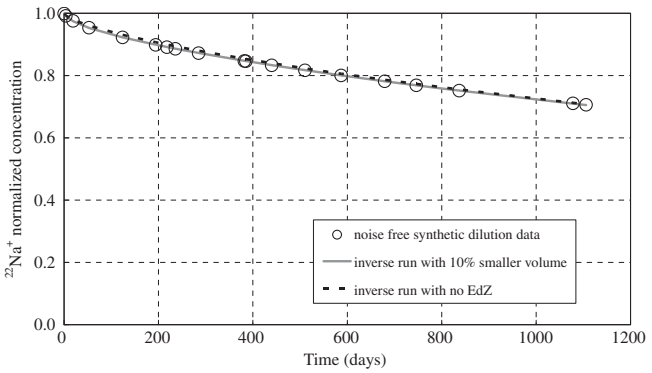

Fig. 11. Best fit to $^{22}Na^+$ noise-free synthetic dilution data for the inverse runs: (1) with D_e of the filter twice its true values and (2) 10% smaller volume of water in the circulation system.

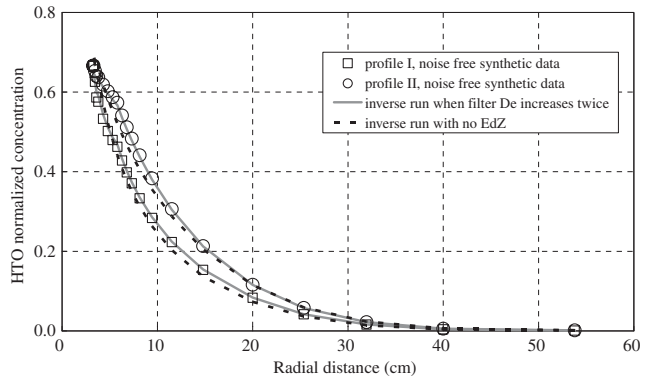

Fig. 12. Best fit to $^{22}Na^+$ noise-free synthetic overcoring data for the inverse runs: (1) with D_e of the filter twice its true values and (2) no EdZ.

Table 8
Summary of the inverse runs for synthetic experiments of $^{22}Na^+$ to evaluate the effect of the uncertainties in the thickness of the EdZ, the volume of water in the circulation system and the D_e of the filter. The following parameters are estimated: $D_{e//}$, $D_{e^\perp}$ and K_d of the undisturbed clay.

Parameter True value		Clay $D_{e//}$ (m^2/s) 7.00×10^{-11}		K_d (m^3/kg) 2.048×10^{-4}		Clay $D_{e^\perp}$ (m^2/s) 1.75×10^{-11}		
Hypothesis	Data	Initial	Estimated	Initial	Estimated	Initial	Estimated	σ
No EdZ	Dilution	1.4×10^{-10}	7.29×10^{-11}	4.096×10^{-4}	6.550×10^{-4}	–	–	0
	Profile II	3.5×10^{-11}	8.36×10^{-11}	1.024×10^{-4}	2.429×10^{-4}	8.74×10^{-12}	4.10×10^{-12}	0
	Dilution	3.5×10^{-11}	1.35×10^{-10}	1.024×10^{-4}	1.133×10^{-4}	–	–	0.05
	Profile II	3.5×10^{-11}	9.34×10^{-10}	1.024×10^{-4}	2.807×10^{-4}	8.74×10^{-12}	1.76×10^{-12}	0.05
10% smaller volume of circulation system	Dilution	1.4×10^{-10}	6.33×10^{-11}	4.096×10^{-4}	1.377×10^{-4}	–	–	0
	Profile II	3.5×10^{-11}	6.27×10^{-11}	1.024×10^{-4}	1.774×10^{-4}	8.74×10^{-12}	1.82×10^{-11}	0
	Dilution	3.5×10^{-11}	1.02×10^{-10}	1.024×10^{-4}	2.982×10^{-5}	–	–	0.05
	Profile II	3.5×10^{-11}	6.23×10^{-11}	1.024×10^{-4}	1.752×10^{-4}	8.74×10^{-12}	1.78×10^{-11}	0.05
D_e of filter = twice its true value	Dilution	1.4×10^{-10}	1.03×10^{-10}	4.096×10^{-4}	6.550×10^{-4}	–	–	0
	Profile II	3.5×10^{-11}	7.27×10^{-11}	1.024×10^{-4}	2.173×10^{-4}	8.74×10^{-12}	1.92×10^{-11}	0
	Dilution	3.5×10^{-11}	1.08×10^{-10}	1.024×10^{-4}	1.133×10^{-4}	–	–	0.05
	Profile II	3.5×10^{-11}	7.33×10^{-11}	1.024×10^{-4}	2.205×10^{-4}	8.74×10^{-12}	1.79×10^{-11}	0.05

Identifiability runs performed with a D_e of the filter twice its true value show that parameter estimates deviate from their true values in the inverse runs using dilution data even though the fit to synthetic data is good. Acceptable estimates and good fits to data (see Fig. 12) are obtained in the inverse runs performed with overcoring data (see Table 8). Therefore, it can be concluded that uncertainties in the D_e of the filter affect strongly the estimates of the parameters of the undisturbed clay when they are derived from dilution data. Such effect is negligible when overcoring data are used.

6. Conclusions

The interpretation of the DR diffusion and retention experiments performed at the Mont Terri on Opalinus Clay is complicated by several non-ideal effects caused by the sinter filter, the gap between the filter and the borehole wall and the EdZ. The relevance of such non-ideal effects and their impact on clay parameter estimates have been evaluated with numerical sensitivity analyses and synthetic experiments.

Dimensionless sensitivities of tracer concentrations at the injection interval and 6 profiles in the rock have been computed numerically. Computed concentrations are tracer dependent, vary with time and are different among different profiles. Contrary to the dilution data, concentrations along overcoring profiles are sensitive to the effective diffusion normal to the bedding. Sensitivities have been used to identify which parameters can be estimated with less uncertainty.

Synthetic experiments generated with known parameters have been interpreted automatically with INVERSE-CORE^{2D} and then used to evaluate the relevance of non-ideal effects and to determine parameter identifiability for HTO and $^{22}Na^+$ in the presence of random measurement errors. The identifiability analysis of synthetic experiments reveals that data noise makes difficult the estimation of undisturbed clay parameters. The joint estimation of undisturbed clay and EdZ parameters with dilution data is only possible when $\sigma < 0.01$. However, excellent parameter estimates are obtained simultaneously with the inverse runs performed with overcoring data. The diffusion anisotropy can be estimated from overcoring data but cannot be estimated from dilution data. A model which neglects the EdZ fails to reproduce the synthetic data. The proper interpretation of the *in situ* DR experiments requires accounting for filter and EdZ. Small errors in the volume of the circulation system do not affect significantly the estimates of the clay parameters. Parameter estimates derived from overcoring data contain fewer errors than those obtained from dilution data.

Dimensionless sensitivities for tracer dilution and overcoring data and the conclusions of the identifiability analysis will be most useful for the calibration and interpretation of the real DR experiments.

Our analysis of parameter identifiability has been performed with either dilution or overcoring data. At the end of an *in situ* diffusion experiment both types of data are available. Therefore, our analysis could be improved in the future by exploring the parameter identifiability using both types of data simultaneously.

Acknowledgements

This work was supported by the Mont Terri Consortium and the Spanish Ministry of Science and Technology through Project CGL2006-09080 and a research scholarship awarded to the third author. We thank Josep Soler, Thomas Gimmi and Olivier Leupin for fruitful discussions on the DR experiments and their interpretation. We are also grateful to the two anonymous reviewers for their comments which improved the paper.

References

Bear, J., 1972. Dynamics of Fluids in Porous Media. Elsevier, New York.
Dai, Z., Samper, J., 2004. Inverse problem of multicomponent reactive chemical transport in porous media: formulation and applications. Water Resour. Res. 40, W07407. doi:10.1029/2004WR003248.
Dai, Z., Samper, J., 2006. Inverse modeling of water flow and multicomponent reactive transport in coastal aquifer systems. J. Hydrol. 327 (3–4), 447–461.
Dai, Z., Samper, J., Ritzi, R., 2006. Identifying geochemical processes by inverse modeling of multicomponent reactive transport in Aquia aquifer. Geosphere 4 (4), 210–219.
Dewonck, S., 2007. Expérimentation DIR. Synthese des résultats obtenus au 01/03/07. Laboratoire de recherche souterrain de Meuse/Haute-Marne. ANDRA Report D.RP.ALS.07-0044.
Fierz, T., 2006. Diffusion and Retention Experiment Field Activities Phase 11: Instrumentation and Tracer Injection. Mont Terri Project TN 06-18.
García-Gutiérrez, M., Missana, T., Mingarro, M., Samper, J., Dai, Z., Molinero, J., 2001. Solute transport properties of compacted Ca-bentonite used in FEBEX project. J. Cont. Hydrol. 47 (2–4), 127–137.
Naves, A., Dewonck, S., Samper, J., 2010. In situ diffusion experiments: effect of water sampling on tracer concentrations and parameters. Phys. Chem. Earth 35 (6–8), 242–247.
Palut, J.M., Montarnal, P., Gautschi, A., Tevissen, E., Mouche, E., 2003. Characterisation of HTO diffusion properties by an *in situ* tracer experiment in Opalinus clay at Mont Terri. J. Cont. Hydrol. 61 (1), 203–218.
Samper, J., Yang, C., Naves, A., Yllera, A., Hernández, A., Molinero, J., Soler, J.M., Hernán, P., Mayor, J.C., Astudillo, J., 2006a. A fully 3-D anisotropic model of DI-B *in situ* diffusion experiment in the Opalinus clay formation. Phys. Chem. Earth 31, 531–540.
Samper, J., Dai, Z., Molinero, J., García-Gutiérrez, M., Missana, T., Mingarro, M., 2006b. Interpretation of solute transport experiments in compacted Ca-bentonites using inverse modelling. Phys. Chem. Earth 31, 640–648.
Samper, J., Dewonck, S., Zheng, L., Yang, Q., Naves, A., 2008a. Normalized sensitivities and parameter identifiability of *in situ* diffusion experiments on Callovo-Oxfordian clay at Bure site. Phys. Chem. Earth 33, 1000–1008.
Samper, J., Yang, Q., Yi, S., García-Gutiérrez, M., Missana, T., Mingarro, M., Alonso, Ú., Cormenzana, J.L., 2008b. Numerical modelling of large-scale solid-source diffusion experiment in Callovo-Oxfordian clay. Phys. Chem. Earth 33 (Supplement 1), S208–S215.
Soler, J.M., Samper, J., Yllera, A., Hernández, A., Quejido, A., Fernández, M., Yang, C., Naves, A., Hernán, P., Wersin, P., 2008. The DI-B *in situ* diffusion experiment at Mont Terri: results and modelling. Phys. Chem. Earth 33 (Supplement 1), S196–S207.
Tevissen, E., Soler, J.M., Montarnal, P., Gautschi, A., van Loon, L.R., 2004. Comparison between *in situ* and laboratory diffusion studies of HTO and halides in Opalinus clay from the Mont Terri. Radiochim. Acta 92, 781–786.
van Loon, L.R., Wersin, P., Soler, J.M., Eikenberg, J., Gimmi, T., Hernán, P., Dewonck, S., Savoye, S., 2004. *In-situ* diffusion of HTO, $^{22}Na^+$, Cs^+ and I^- in Opalinus clay at the Mont Terri underground rock laboratory. Radiochim. Acta 92, 757–763.
van Loon, L.R., Glauss, M.A., 2008. Effective Diffusion Coefficient of Several Tracers in Teflon Filters. PSI Technical Note, Switzerland.
Wersin, P., van Loon, L.R., Soler, J.M., Yllera, A., Eikenberg, J., Gimmi, T., Hernan, P., Boisson, J.Y., 2004. Long-term diffusion experiment at Mont Terri: first results from field and laboratory data. Appl. Clay Sci. 26, 123–135.
Yllera, A., Hernández, A., Mingarro, M., Quejido, A., Sedano, L.A., Soler, J.M., Samper, J., Molinero, J., Barcala, J.M., Martín, P.L., Fernández, M., Wersin, P., Rivas, P., Hernán, P., 2004. DI-B experiment: planning, design and performance of an *in situ* diffusion experiment in the Opalinus clay formation. Appl. Clay Sci. 26, 181–196.

APPENDIX 7

ANALYSIS OF PARAMETER IDENTIFIABILITY FOR THE STRONGLY-SORBING TRACERS OF THE DR EXPERIMENT

This appendix presents the identifiability analysis of the diffusion and sorption parameters of the strongly-sorbing tracers from dilution and overcoring data of the DR experiment.

Some parts of this appendix were presented in the Mont Terri Technical Note TN2008-71 "DR experiment: modeling and numerical interpretation of in situ diffusion experiment in Opalinus Clay. Final report." (2008). A paper is also being prepared based on this appendix which will be submitted to an international journal in the next months.

All the tasks presented here were performed by the author of this dissertation under the supervision of Javier Samper.

1. INTRODUCTION

In situ diffusion experiments are performed at underground research laboratories (URL) in clay formations to overcome the limitations of laboratory diffusion experiments and to investigate possible scale effects. Such experiments have been performed in Opalinus Clay at Mont Terri URL (Palut, 2001; Palut et al., 2003; Tevissen et al., 2004; Wersin et al., 2004; 2006; 2008; Van Loon et al., 2004; Yllera et al., 2004) and Callovo-Oxfordian Clay at Meuse/Haute Marne URL (Dewonck, 2007). The in situ diffusion and retention (DR) experiment is designed to study the transport and retention properties of the Opalinus Clay Formation.

Numerical models of different complexity have been used to interpret the experimental data obtained in these experiments and derived diffusion and sorption parameters (Van Loon, 2004; Wersin et al., 2004; 2006; 2008; Samper et al., 2007; Soler et al., 2007; Appelo and Wersin, 2007). Model results depend on parameters that may contain uncertainties. Furthermore, the interpretation of diffusion experiments is complicated by disturbing effects caused by the presence of the sintered filter, the gap between the filter and the borehole wall and possibly an excavation disturbed zone, EdZ. Dimensionless sensitivities of tracer concentrations in the injection interval and along the overcoring profiles have been computed numerically (Samper et al., 2007; Samper et al., 2008a; Samper et al., 2010). They have been used to identify the tracer parameters that can be best estimated from tracer dilution and overcoring data. Synthetic experiments generated with prescribed known parameters have been interpreted and used also to ascertain parameter identifiability in the presence of random errors and to evaluate the relevance of the disturbing effects.

Samper et al. (2010) presented a sensitivity analysis for the DR diffusion experiments in terms of dimensionless sensitivities. It includes not only the sensitivities of tracer dilution data but also the sensitivities of tracer concentrations along overcoring profiles. Changes in the thickness of the EdZ and the volume of the water in the circulation system affect significantly tracer concentrations at the injection interval and overcoring profiles. Therefore, both parameters are key factors for tracer diffusion and sorption in the DR experiments. Changes in the parameters of the gap do not affect tracer concentrations neither at the injection interval nor along overcoring profiles for all the tracers. Thus, uncertainties in the parameters of the gap do not affect significantly the interpretation of the DR experiments. Sensitivities to changes in diffusion and sorption parameters are tracer dependent. Strongly-sorbing tracers are most sensitive to the D_e of the filter, the K_d and the $D_{e//}$ of the EdZ. They lack sensitivity to changes in the parameters of the undisturbed clay. Relative sensitivities of strongly-sorbing tracers along overcoring profiles are generally smaller than those of other tracers and those of dilution data. Therefore, it can be concluded that it may be

difficult to estimate the parameters of strongly-sorbing tracers from overcoring data. Samper et al. (2010) performed also the identifiability analysis of HTO and $^{22}Na^{+}$ diffusion and sorption parameters from synthetic diffusion experiments. The results clearly shows that: (1) The proper interpretation of in situ DR experiments requires accounting for the filter and the EdZ; (2) Overcoring data allow a more accurate estimation of the parameters of the undisturbed clay than the tracer dilution data (3) The diffusion anisotropy can be estimated from overcoring data but cannot be estimated from dilution data and (4) Small errors in the volume of the circulation system do not affect significantly the estimates of the clay parameters.

This appendix extends the identifiability analysis of Samper et al. (2010) to strongly-sorbing tracers. It starts by describing the DR experiment. Then, the numerical methods for the interpretation of the experiment are presented. Next, the methodology and the results of the identifiability analysis of diffusion and sorption parameters are described. The appendix ends with the main conclusions.

2. DR EXPERIMENT AT MONT TERRI

The in situ diffusion and retention (DR) is similar to previous in situ diffusion experiments. However, the concept has been optimized to determine in situ diffusion anisotropy. The injection intervals are shorter than those of previous experiments. The duration of the experiment is such that the transport distance of conservative tracers is larger than the length of the injection interval to allow for the estimation of the diffusion anisotropy.

The experiment is performed in a borehole of the DR niche at the Mont Terri URL. The Opalinus Clay exhibits significant diffusion anisotropy due to stratification. The borehole was drilled at an angle of 45º with respect to the tunnel bottom so that it is normal to the bedding. Three test intervals were isolated by packers. The interval at the bottom serves as an auxiliary interval for the observation of the hydraulic pressure during the experiment. Tracer cocktails were injected into the two upper intervals. Each injection interval is connected to the surface equipment which includes a reservoir tank of 20 L. The fluid is circulated continuously to ensure that the tank water and the downhole water are well mixed.

The following tracers were added at the upper interval: $^{60}Co^{2+}$, $^{137}Cs^{+}$, $^{133}Ba^{2+}$, $^{152}Eu^{3+}$, Eu^{3+} and HDO. The tracers injected in the lower interval include: HTO, $^{22}Na^{+}$, $^{85}Sr^{2+}$, I^{-} (stable), Br^{-} (stable), $^{75}Se^{6+}$, Cs^{+} and ^{18}O. Tracer concentrations and activities in the water of the circulation system were monitored by taking water samples at regular intervals in sampling vials. In addition, □-emitter tracers (all radioactive tracers but HTO) were monitored on line in both circuits with an online □-counting technique. The rock around the injection intervals was overcored at the end of the

experiment and tracer distribution profiles were measured. The time evolution of the tracer concentrations in the two injection systems denoted here as ‘‘dilution data’’ and the tracer profiles in the rock after overcoring (‘‘overcoring data’’) can be used to derive tracer diffusion and retention parameters.

3. SOLUTE TRANSPORT EQUATION

The transport equation for a tracer which diffuses through a low permeability medium is given by (Bear, 1972):

$$\nabla \cdot \left(\overline{D_e} \cdot \nabla C \right) = \alpha \frac{\partial C}{\partial t}$$

where C is the tracer concentration, t is time, and α is the capacity factor which is given by:

$$\alpha = \phi_{acc} + \rho K_d$$

where ϕ_{acc} is the accessible porosity which is equal to the total porosity if the tracer is not affected by anion exclusion, K_d is the distribution coefficient, and ρ is the bulk density. $\overline{D_e}$ is the effective diffusion tensor which, in a coordinate system defined along the bedding planes, is given by:

$$\begin{pmatrix} D_{e//} & 0 & 0 \\ 0 & D_{e//} & 0 \\ 0 & 0 & D_{e-\vert} \end{pmatrix}$$

where $D_{e//}$ and $D_{e-|}$ are the components of the effective diffusion tensor parallel and normal to the bedding, respectively.

4. NUMERICAL INTERPRETATION

The numerical interpretation of the DR experiments requires the use of 3D models due to the diffusion anisotropy. However, tracer diffusion exhibits symmetry with respect to the borehole axis. This allows the use of 2D axi-symmetric models. The left-hand-side boundary of the domain corresponds to the borehole axis. All other boundaries of the model domain are no-flux boundaries.

The following five material zones are considered for modeling the DR experiment: the injection interval, the 3 mm thick Teflon filter, the 2 mm gap, the EdZ which has a thickness of 20 mm and the undisturbed Opalinus Clay. Prior estimates of the effective diffusion (D_e= $3 \cdot 10^{-10}$ m^2/s), the distribution coefficient (K_d= 550 L/Kg), and the accessible porosity (Φ_{acc}= 0.15) for the undisturbed Opalinus Clay were derived from available laboratory experiments results or field experiments. An anisotropy ratio of 4.0 was considered (Van Loon et al., 2004). The effective diffusion and the capacity factor, α, of different tracers in porous Teflon filters were measured by Van Loon and Glauss

(2008) using a through-diffusion method. They found that the effective diffusion of the filter (D_e= $1.4 \cdot 10^{-10}$ m^2/s) is approximately equal to 7% of the diffusion coefficient in free water while its porosity is about 0.3. Effective diffusion coefficients for other materials were derived from those of undisturbed clay by using Archie's law with an exponent equal to 4/3. The porosities of the EdZ and the gap are unknown. As an educated guess, the porosity of the EdZ was assumed to be twice that of the undisturbed clay while the porosity of the gap was assumed to be 0.6. The undisturbed clay and the EdZ are assumed to have the same distribution coefficient. No sorption takes place in the filter and the gap.

The relevance of the diffusion anisotropy on tracer evolution at the tracer interval depends on the ratio between the length of the tracer interval and the tracer penetration depth. Anisotropy is not relevant if the interval is much larger than the tracer penetration. The penetration depth for strongly-sorbing tracers is smaller than 3 cm while the injection interval is 15 cm long. Concentrations computed with an anisotropy of 4 have been compared with those obtaining by neglecting the diffusion perpendicular to the bedding (anisotropy factor of 100). Inasmuch as the results of both runs are similar, a 1D axi-symmetric model can be used for simulating tracer dilution in the DR experiment. On the other hand, there are slight differences in the computed concentrations in the rock, indicating that a 2D model is required for interpreting overcoring data.

Diffusion experiments have been interpreted automatically with the inverse code INVERSE-CORE^{2D} (Dai and Samper, 2004) by minimizing the least-squares objective function with the Gauss–Newton–Levenberg–Marquardt method. This code can estimate transport parameters and provides statistical measures of goodness-of-fit as well as parameter uncertainties by computing the covariance and correlation matrices as well as approximate confidence intervals for the estimated parameters. Details of the application of INVERSE-CORE^{2D} to the estimation of diffusion parameters can be found in Samper et al. (2008a; 2008b).

5. IDENTIFIABILITY ANALYSIS

5.1. Methodology

Synthetic experiments are often used to study parameter identifiability and uncertainty. Synthetic diffusion experiments having the same geometric properties as the real experiments have been simulated numerically for reference values of diffusion and sorption parameters. Synthetic concentration data have then been used to estimate such parameters. Since true values are known, one can clearly identify which parameters can be estimated and how reliable these estimates are.

The method for performing the identifiably study with synthetic data involves the following steps: (1) Generating synthetic data from a forward run of the numerical model; (2) Adding multiplicative random noise to the synthetic data with a lognormal distribution having a standard deviation, σ, which ranges from 0 to 0.1 for dilution data and from 0 to 0.2 for overcoring data; (3) Estimating key diffusion parameters from noisy synthetic data in several stages; and (4) Evaluating the effect of the uncertainties in the EdZ, the volume of water in the injection system, V, and the D_e of the filter.

Parameter identifiability analyses have been performed with synthetic dilution and overcoring data. 25 synthetic dilution data have been generated at the times similar to those of the real experiment for $^{137}Cs^{+}$. For $^{60}Co^{2+}$ and Cs^{+}, only 16 dilution data were available. Synthetic overcoring data have been generated along two radial profiles. One is located in the middle of the interval and the other one is at the top of it. The characteristics of synthetic overcoring data were derived on observations from DI-A and DI-B experiments: (1) Concentration data are measured along radial profiles on 1 cm thick samples; (2) Tracer concentration is larger than the detection limit only on the samples closest to the injection interval and (3) Measurement errors of sorbing tracers are larger than those of non-sorbing tracers.

The identifiability analysis of diffusion and sorption parameters is based on the conclusions of the sensitivity analysis of Samper et al. (2010). Strongly-sorbing tracers lack sensitivity to changes in the parameters of the undisturbed clay. Therefore, they cannot be estimated. The largest sensitivities correspond to the K_d and the D_e of the EdZ. First, the parameters of the EdZ are estimated from dilution data. Then, they are estimated from synthetic data along the radial profile located in the middle of the interval. Finally, the identifiability of the anisotropy ratio is evaluated using data from two profiles. Estimation runs have been performed for different initial starting values of the parameters and for increasing values of the standard deviation of the random data noise, σ.

5.2. Results

Table 1 summarizes the results of the identifiability analysis for $^{137}Cs^{+}$. The estimated K_d is equal to its true value when only K_d is estimated from noise-free data. Clearly, the noise in the data introduces a mild bias in the estimate of K_d which for the inverse run performed with dilution data and σ = 0.1 is smaller than 0.8% and for that performed with overcoring data and σ = 0.1 is equal to 3%. The estimates of the D_e of the EdZ are very close to their true values even for σ = 0.1 when only this parameter is estimated. The effect of noise on the estimate of D_e is even smaller than that for K_d. On the other hand, the accesible porosity of the EdZ cannot be properly estimated if data contain noise.

Figure 1 illustrates the values of the objective function as a function of the estimation error in the K_d which is defined as the ratio between the estimated and the true value ($K_{d\text{-}ref}$). The minimum of the objective function occurs at $K_d/K_{d\text{-}ref} = 1$. The objective function versus $K_d/K_{d\text{-}ref}$ is a convex function for all values of σ. A good fit to synthetic data does not guarantee a good parameter estimate. These results are consistent with those obtained by Takeda et al. (2008) in the interpretation of transient concentration data derived from laboratory diffusion experiments.

The estimates of the K_d and the D_e of the EdZ are strongly correlated (ρ = -0.998). Therefore, they cannot be estimated simultaneously. Initial values are crucial for parameter estimation. Initial values of the K_d smaller than its true value facilitates the convergence. Estimates coincide with true values for noise-free dilution and overcoring data. Acceptable estimates are obtained for noisy dilution data with errors of 7.5% in both parameters for σ = 0.02 and 20% for σ = 0.05. However, large estimation errors are found for σ = 0.1. Figure 2 shows the plot of the estimation error versus the standard deviation of the random noise of dilution data. Parameter estimates from overcoring data are much less affected by data noise than estimates from dilution data. Therefore, the estimates are good even when data contain noise. On the other hand, the fit to synthetic data is good even if the parameters contain estimation errors (Figure 3).

Table 1 Summary of inverse runs for synthetic experiments of $^{137}Cs^{+}$. The distribution coefficient (K_d), the effective diffusion coefficient parallel ($D_{e//}$) and perpendicular ($D_{e\text{-}|}$) to the bedding and the accessible porosity of the EdZ are estimated. σ is the standard deviation of the noise.

Parameter		**K_d (L/Kg)**		**EdZ $D_{e//}$ (m^2/s)**		**EdZ $D_{e\text{-}|}$ (m^2/s)**	
True value		550		7.56×10^{-10}		1.89×10^{-10}	
Data	**σ**	Initial	Estimated	Initial	Estimated	Initial	Estimated
Dilution	0.1	100	545.9	-	-	-	-
	0.1	-	-	5.0×10^{-10}	7.55×10^{-10}	-	-
	0.02	100	509.1	5.0×10^{-10}	8.11×10^{-10}	-	-
	0.05	100	441.6	5.0×10^{-10}	9.17×10^{-10}	-	-
Profile	0.1	100	538.9	-	-	-	-
	0.1	-	-	5.0×10^{-10}	7.33×10^{-10}	-	-
	0.05	100	544.3	5.0×10^{-10}	7.49×10^{-10}	-	-
	0.2	100	540.3	5.0×10^{-10}	7.41×10^{-10}	-	-
	0.1	-	-	-	-	1.16×10^{-10}	2.95×10^{-10}

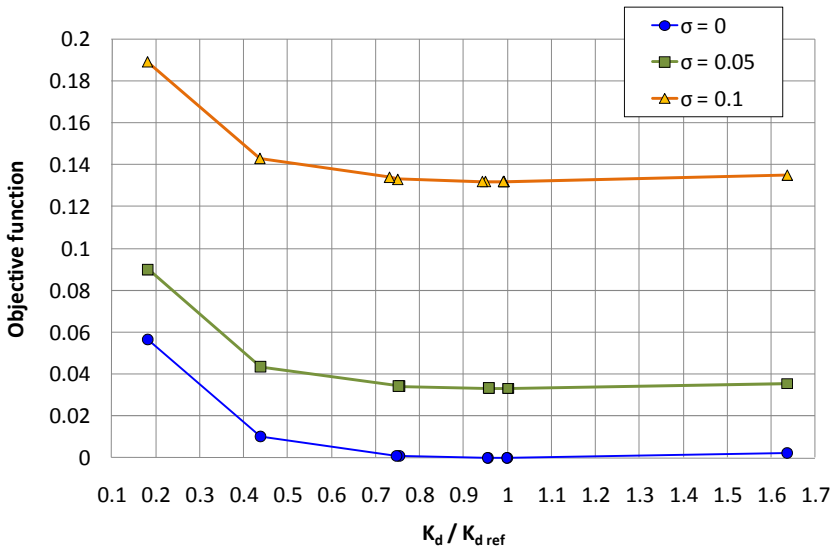

Figure 1 Objective function versus $K_d / K_{d\text{-}ref}$ for several values of the standard deviation of the noise σ.

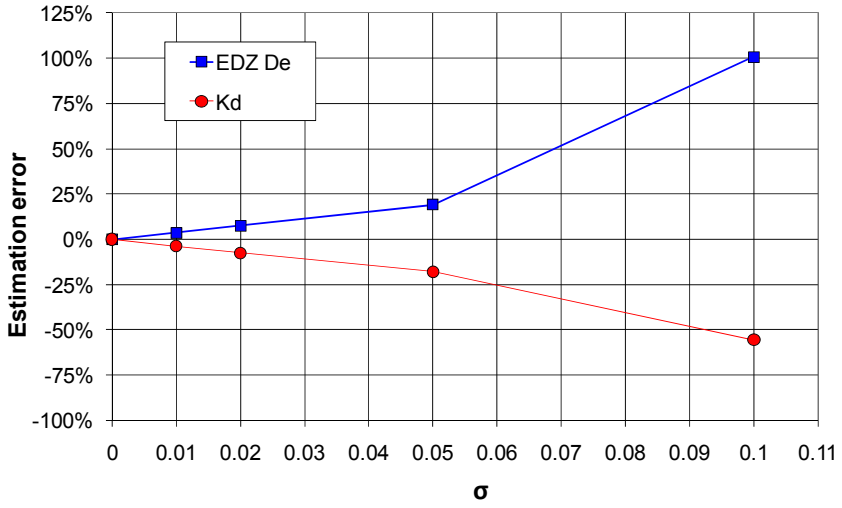

Figure 2 Estimation errors of K_d and D_e of the EdZ for noisy dilution data versus the standard deviation of the noise.

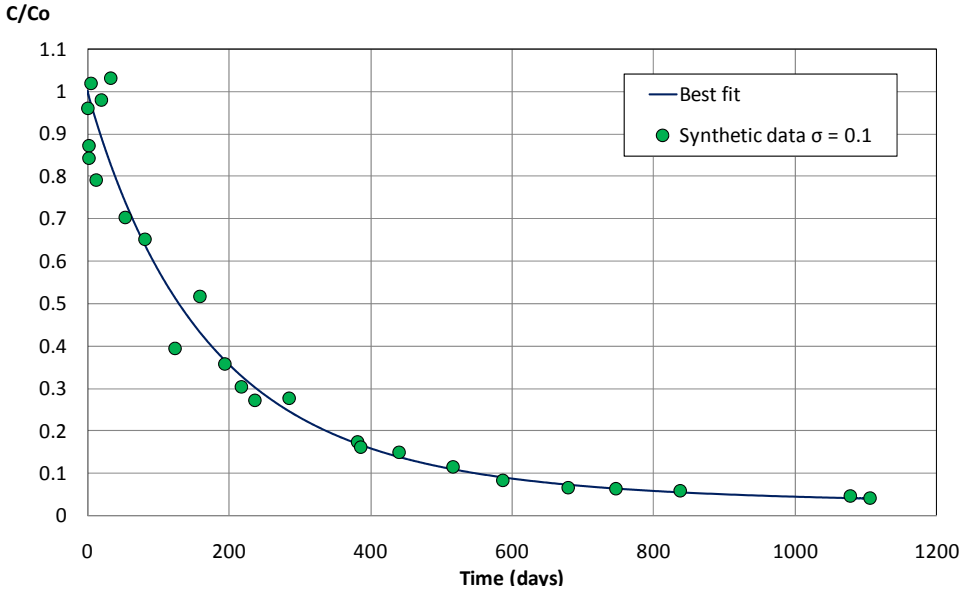

Figure 3 Comparison of computed (line) and measured synthetic dilution data with σ = 0.1 (symbols).

The sensitivity of tracer concentrations to the anisotropy of Opalinus Clay has been analyzed by Samper et al. (2010). Dilution data lack sensitivity to the parameters of the undisturbed clay and the anisotropy ratio of the EdZ. The concentrations along the radial profile located in the middle of the interval are insensitive to changes in the diffusion coefficient perpendicular to the bedding of the EdZ, $D_{e-|}$. However, the concentrations along the radial profiles located at the top or the bottom of the injection interval are sensitive to $D_{e-|}$. Therefore, the $D_{e-|}$ of the EdZ has been estimated from synthetic overcoring data along two radial profiles: one at the middle of the injection interval and another one at the top of it. The $D_{e-|}$ of the EdZ can be properly estimated from noise-free synthetic data. The noise of synthetic data leads to estimation errors. The relative error on the $D_{e-|}$ of the EdZ is of 56% for $\sigma = 0.1$.

There is no evidence of an EdZ in previous diffusion experiments at Mont Terri. The effect of the existence of an EdZ on the identifiability of the K_d and the D_e of the EdZ was analyzed. Dilution and overcoring synthetic data were generated with an EdZ of 2 cm and without EdZ. The two parameters were estimated simultaneously from the two data sets using models with and without EdZ. The estimation results are summarized in Table 2.

Table 2 Results of the inverse runs of $^{137}Cs^{+}$ synthetic experiments in which the effect of the EdZ on parameter estimates has been analyzed. σ is the standard deviation of data noise.

Parameter				**K_d (L/Kg)**		**EdZ or Clay $D_{e//}$ (m^2/s)**	
True value				550		7.56×10^{-10} or 3×10^{-10}	
	Data	**Model**	**σ**	Initial	Estimated	Initial	Estimated
Dilution	With EdZ	With EdZ	0	100	550	5.0×10^{-10}	7.56×10^{-10}
	With EdZ	With EdZ	0.05	100	509.1	5.0×10^{-10}	8.11×10^{-10}
	Without EdZ	With EdZ	0	100	667.1	5.0×10^{-10}	3.0×10^{-10}
	Without EdZ	With EdZ	0.05	100	418.1	5.0×10^{-10}	4.62×10^{-10}
	Without EdZ	Without EdZ	0	100	550	1.7×10^{-10}	3.0×10^{-10}
	Without EdZ	Without EdZ	0.05	100	344.8	1.7×10^{-10}	4.62×10^{-10}
	With EdZ	Without EdZ	0	100	453.7	1.7×10^{-10}	7.56×10^{-10}
	With EdZ	Without EdZ	0.05	100	374.6	1.7×10^{-10}	8.72×10^{-10}
Profile	With EdZ	With EdZ	0	100	550	5.0×10^{-10}	7.56×10^{-10}
	With EdZ	With EdZ	0.1	100	509.1	5.0×10^{-10}	8.11×10^{-10}
	Without EdZ	With EdZ	0	100	667.2	5.0×10^{-10}	3.0×10^{-10}
	Without EdZ	With EdZ	0.1	100	665.9	5.0×10^{-10}	2.95×10^{-10}
	Without EdZ	Without EdZ	0	100	550	1.7×10^{-10}	3.0×10^{-10}
	Without EdZ	Without EdZ	0.1	100	540.7	1.7×10^{-10}	2.95×10^{-10}
	With EdZ	Without EdZ	0	100	453	1.7×10^{-10}	7.40×10^{-10}
	With EdZ	Without EdZ	0.1	100	445.6	1.7×10^{-10}	7.28×10^{-10}

Synthetic dilution and overcoring data generated without EdZ have been interpreted using a model with EdZ. When data are free of noise, the estimate of the D_e of the EdZ is equal to the true value of the D_e of the undisturbed clay while K_d is estimated with an error of 21%. Random noise in dilution synthetic data leads to large estimation errors for the K_d. On the other hand, parameter estimates from overcoring data are much less affected by data errors. Good parameter estimates are derived from synthetic data without EdZ using the model without EdZ. In addition, synthetic dilution and overcoring data generated with EdZ have been interpreted using a model without EdZ. The estimate of the D_e of the undisturbed clay from noise-free synthetic dilution data is equal to the true value of the D_e of the EdZ while estimation error in K_d is 18%. A similar estimate of the K_d is derived from noise-free synthetic overcoring data, but the estimate of the D_e is 2% smaller than the true value D_e of the EdZ. The inverse model is strongly affected by noise when the estimation is performed from dilution data. On the contrary, it is slightly affected when it is done from overcoring data.

The following conclusions can be derived from the analysis of the influence of the EdZ on parameter estimates: 1) The most suitable model is the one with EdZ for synthetic data with EdZ; 2) For synthetic data without EdZ, the most suitable model is the one without EdZ; 3) Models are strongly affected by data noise when the estimation is performed from dilution data. They are slightly affected when the parameters are estimated from overcoring data; 4) The fit is excellent if the model hypothesis about the EdZ is correct; and 5) The fit to synthetic data is good even if the parameter estimates contain errors (Figure 4). According to this, a good fit to synthetic data does not necessarily mean that the selection of the hypothesis about the EdZ is right.

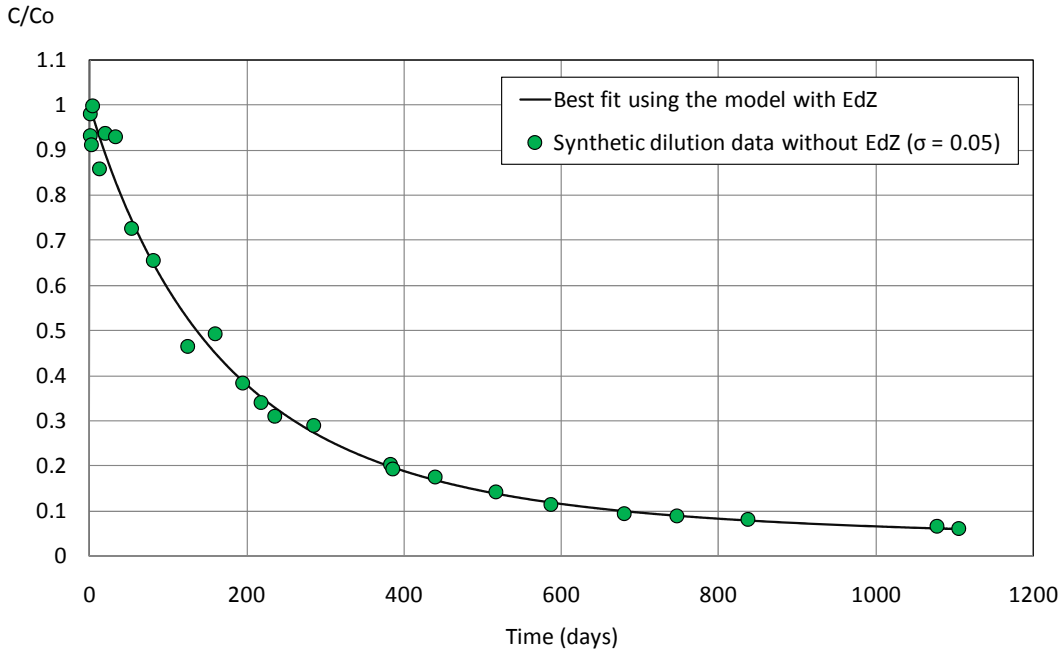

Figure 4 Comparison of synthetic data generated without EdZ and σ = 0.05 with the best fit achieved with a model with EdZ. The relative errors of the estimates of the K_d and the D_e are of 24% and 54%, respectively.

Uncertainties caused by errors in the volume of water in the injection system, V, have been evaluated by estimating the parameters of the EdZ for a volume 5% smaller than the true value. An error of 5% in V does not allow the estimation of the D_e of the EdZ and the K_d simultaneously from synthetic dilution data. Acceptable estimates of both parameters are achieved from synthetic overcoring data with an error of 5% for noise-free data and 7% for σ = 0.1 (see Table 3). Therefore, small errors in V do not affect the parameter estimation from overcoring data, but prevent the simultaneous estimation of the K_d and the D_e of the EdZ from dilution data.

Since the D_e of the filter is a key parameter for strongly-sorbing tracers, the effect of the uncertainty on its value in the identifiability of the diffusion and sorption parameters has been evaluated. The D_e of the EdZ and the K_d are estimated from synthetc dilution data by adopting a D_e of the filter equal to twice its reference value. The estimates of K_d contain large errors. The computed dilution curve with the estimated parameters cannot fit synthetic data (Figure 5). Similar conclusions are obtained if the D_e of the filter is equal to 1.5 times its reference value (Table 3). It can be concluded that the parameters of the EdZ cannot be estimated from synthetic dilution data when the D_e of the filter contains an error larger than 50%. The D_e of the EdZ and the K_d are estimated from synthetic overcoring data by adopting a D_e of the filter equal to twice its reference value. Contrary to what happens with dilution data, it is possible to estimate these parameters from overcoring data with small errors. In fact, the fit to synthetic overcoring data is good even with largely erroneous value of the D_e of the filter.

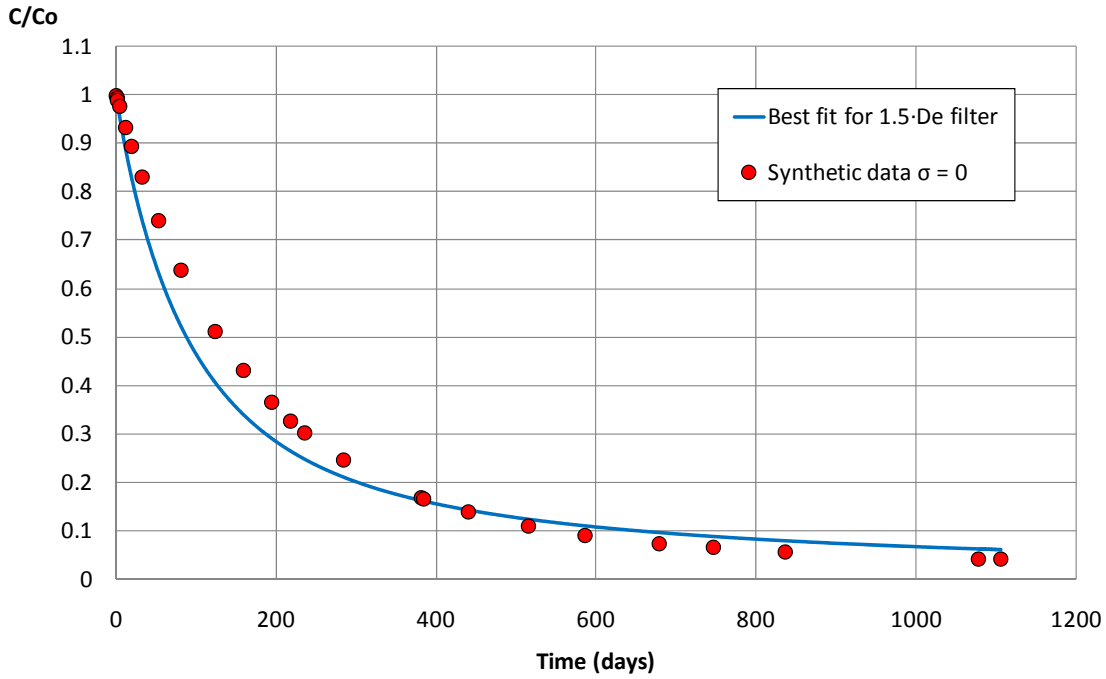

Figure 5 Comparison of synthetic data generated without noise with model results for estimated parameter values fixing the D_e of the filter equal to 1.5 times its true value.

Table 3 Results of the inverse runs of $^{137}Cs^{+}$ synthetic experiments to evaluate the uncertainties in the D_e of the filter and the volume of water of the circulation system.

Parameter			**K_d (L/Kg)**		**EdZ $D_{e//}$ (m^2/s)**	
True value			550		7.56×10^{-10}	
Hypothesis	**Data**	**σ**	Initial	Estimated	Initial	Estimated
V = 0.95 x true value	Overcoring	0	100	520.6	5.0×10^{-10}	7.15×10^{-10}
V = 0.95 x true value	Overcoring	0.1	100	511.3	5.0×10^{-10}	7.05×10^{-10}
D_e of filter = 2 x true value	Dilution	0	100	50	5.0×10^{-10}	7.92×10^{-10}
D_e of filter = 1.5 x true value	Dilution	0	100	100	5.0×10^{-10}	7.89×10^{-10}
D_e of filter = 2 x true value	Overcoring	0	100	551.4	5.0×10^{-10}	7.04×10^{-10}

6. CONCLUSIONS

The interpretation of strongly-sorbing tracer data from the DR experiment is complicated by measurement errors and the disturbing effects caused by the presence of a Teflon filter, the gap between the filter and the borehole wall and possibly an excavation disturbed zone (EdZ). Synthetic experiments having the same geometric properties as the real experiments have been simulated and interpreted automatically with INVERSE-CORE^{2D}. Parameter identifiability in the presence of random measurement errors as well as the uncertainties in the existence of an EdZ, the D_e of the filter and the volume of the system have been evaluated.

Computed concentrations of strongly-sorbing tracers in the injection interval and overcoring profiles are not sensitive to changes in the parameters of the undisturbed clay (Samper et al., 2010). Therefore, only the parameters of the EdZ can be estimated for this kind of tracers. The K_d and the D_e of the EdZ are estimated either separately or simultaneously from synthetic dilution and overcoring data similar to those expected from the real experiment. Estimates of both parameters, when they are estimated separately, are close their true values even for noisy data ($\sigma = 0.1$). Since they are strongly correlated, they cannot be estimated simultaneously. The convergence of the estimation algorithm is facilitated when the initial values of the K_d are lower than their reference values. Clearly, the noise in the data introduces a bias in the estimates. Acceptable estimates are obtained from dilution data for $\sigma \leq 0.05$. Estimates from overcoring are much less affected by data noise than those derived from dilution data. An excellent fit to data is achieved regardless the parameter estimation errors. Therefore, a good fit does not guarantee appropriate parameter estimates. The diffusion anisotropy of the EdZ cannot be estimated from noisy data.

The proper interpretation of the DR experiment requires accounting for the filter. Small uncertainties in the D_e of the filter or in the volume of the circulation system do not allow the

estimation of the parameters of the EdZ from dilution data but they do from overcoring data. The effect of the existence of an EdZ on the joint estimation of the parameters of the EdZ has been analyzed. Data generated with and without EdZ have been interpreted using models with and without EdZ. The most suitable model is that based on the right hypothesis about the EdZ. Models are strongly influenced by noise when the estimation is performed from dilution data. Data errors affect less the estimation from overcoring data. Fit to synthetic data is good in all the cases although in some of them the estimated parameters contain errors. This identifiability analysis could be improved by using dilution and overcoring data simultaneously.

The conclusions of this analysis will be useful for the calibration and interpretation of actual data of the DR experiment.

7. REFERENCES

Appelo, C.A.J., Wersin, P, 2007. Multicomponent diffusion modeling in clay systems with application to diffusion of tritium, iodide and sodium in Opalinus Clay. *Enviromental Science and Technology*, 41, 50002-5007.

Bear, J., 1972. Dynamics of Fluids in Porous Media. Elsevier, New York.

Dai, Z., Samper, J., 2004. Inverse problem of multicomponent reactive chemical transport in porous media: formulation and applications. *Water Resource Reseach* 40,W07407.

Dewonck, S., 2007. Expérimentation DIR. Synthèse des résultats obtenus au 01/03/07. Laboratoire de recherche souterrain de Meuse/Haute-Marne. *ANDRA Technical Report* D.RP.ALS.07-0044.

Palut, J.M., 2001. Spécifications générales – Expérimentation DIR – Essai de Diffusion de Traceurs Inertes et Réactifs. *ANDRA Technnical Report* D.SP.ADPE.01-097.

Palut, J.M., Montarnal, Ph., Gautschi, A., Tevissen, E., Mouche, E., 2003. Characterisation of HTO diffusion properties by an in situ tracer experiment in Opalinus Clay at Mont Terri. Journal of Contaminant Hydrology 61, 203-218.

Samper, J., Yang, C., Naves, A., Yllera, A., Hernández, A., Molinero, J., Soler, J.M., Hernán, P., Mayor, J.C., Astudillo, J., 2006. A fully 3-D anisotropic numerical model of the DI-B in situ diffusion experiment in the Opalinus Clay formation. *Physics and Chemistry of the Earth* 31, 531-540.

Samper, J., Dewonck, S., Zheng, L., Yang, Q., Naves, A., 2008a. Normalized sensitivities and parameter identifiability of in situ diffusion experiments on Callovo-Oxfordian clay at Bure site. *Physics and Chemistry of the Earth* 33, 1000–1008.

Samper, J., Yang, Q., Yi, S., García-Gutiérrez, M., Missana, T., Mingarro, M., Alonso, Ú., Cormenzana, J.L., 2008b. Numerical modelling of large-scale solid-source diffusion experiment in Callovo-Oxfordian clay. *Physics and Chemistry of the Earth* 33 (Supplement 1), S208–S215.

Samper, J., Yi, S., Naves, A., 2010. Analysis of the parameter identifiability of the in situ diffusion and retention (DR) experiment. *Physics and Chemistry of the Earth* 35, 207-216.

Soler, J.M., Samper, J., Yllera, A., Hernández, A., Quejido, A., Fernández, M., Yang, C., Naves, A., Hernán, P., Wersin, P., 2008. The DI_B in situ diffusion experiment at Mont Terri: Results and modeling. *Physics and chemistry of the Earth* 33, S196-S207.

Takeda, M., Nakajima, H., Zhang, M., Hiratsuka, T., 2008. Laboratory longitudinal diffusion tests: 2.Parameter estimation by inverse analysis. *Journal of Contaminant Hydrology* 97, 100-116.

Tevissen, E., Soler, J.M., Montarnal, Ph., Gautschi, A., Van Loon, L.R., 2004. Comparison between in situ laboratory characterization of HTO and halides diffusion in Opalinus Clay at the Mont Terri URL. Radiochimica Acta 92, 781-786.

Van Loon, L.R., Wersin, P., Soler, J.M., Eikenberg, J., Gimmi, T., Hernán, P., Dewonck, S., Savoye, S., 2004. In-situ diffusion of HTO, $^{22}Na^{+}$, Cs^{+} and I^{-} in Opalinus clay at the Mont Terri underground rock laboratory. *Radiochimica Acta* 92, 757–763.

Van Loon, L.R., Glauss, M.A., 2008. Effective Diffusion Coefficient of Several Tracers in Teflon Filters. *PSI Technical Note*, Switzerland.

Wersin, P., Soler, J.M., van Dorp, F., 2002. DI-A Experiment: Methodological basis and test plan for the in situ experiment. Mont Terri Project Technical Note 2002-07.

Wersin, P., Van Loon, L.R., Soler, J.M., Yllera, A., Eikenberg, J., Gimmi, Th., Hernán, P., Boisson, J.-Y., 2004. Long-term diffusion experiment at Mont Terri: first results from field and laboratory data. *Applied Clay Science* 26, 123-135.

Wersin, P., Baeyens, B., Bossart, P., Cartalade, A., Dewonck, S., Eikenberg, J., Fierz, T., Fisch, H.R., Gimmi, T., Grolimund, D., Hernán, P., Möri, A., Savoye, S., Soler, J.M., van Dorp, F., Van Loon, L., 2006. Long-term diffusion experiment (DI-A): Diffusion of HTO, I^{-}, $^{22}Na^{+}$ and Cs^{+}. Field activities, data and modeling. *Mont Terri Technical Report* TR 2003-06.

Wersin, P., Soler, J.M., Van Loon, L., Eikenberg, J., Baeyens, B., Grolimund, D., Gimmi, Th., Dewonck, S., 2008. Diffusion of HTO, Br^{-}, I^{-}, Cs^{+}, $^{85}Sr^{2+}$ and $^{60}Co^{2+}$ in a clay formation: results and modeling from an in situ experiment in Opalinus Clay. *Applied Geochemistry* 23, 678-691.

Yllera, A., Hernández, A., Mingarro, M., Quejido, A., Sedano, L.A., Soler, J.M., Samper, J., Molinero, J., Barcala, J.M., Martín, P.L., Fernández, M., Wersin, P., Rivas, P., Hernán, P., 2004. DI-B experiment: planning, design and performance of an in situ diffusion experiment in the Opalinus Clay formation. *Applied Clay Science* 26, 181-196.

APPENDIX 8

PARAMETER IDENTIFIABILITY OF DR EXPERIMENT FROM DILUTION AND OVERCORING DATA

This appendix presents the identifiability analysis of the diffusion and sorption parameters of HTO and $^{22}Na^{+}$ using simultaneously dilution and overcoring data of the DR experiment.

A paper is being prepared based on this appendix which will be submitted to an international journal in the next months.

All the tasks here presented were performed by the author of this dissertation under the supervision of Javier Samper, her advisor at UDC, and Thomas Gimmi, her co-advisor during her stay at the Paul Scherrer Institute (Switzerland).

1. INTRODUCTION

In situ diffusion experiments are performed at underground research laboratories (URL) in clay formations to overcome the limitations of laboratory diffusion experiments and to investigate possible scale effects. Such experiments have been performed in Boom Clay at HADES URL (De Cannière et al., 1996; Aertsens et al., 2008), Opalinus Clay at Mont Terri URL (Palut et al., 2003; Tevissen et al., 2004; Wersin et al., 2004; 2008; Van Loon et al., 2004; Yllera et al., 2004) and Callovo-Oxfordian Clay at Meuse/Haute Marne URL (Dewonck, 2010). Numerical models have been used to interpret the experimental data obtained in those experiments and derive diffusion and sorption parameters (Van Loon, 2004; Wersin et al., 2006; Samper et al., 2006; Soler et al., 2008; Appelo and Wersin, 2007).

The in situ diffusion and retention (DR) experiment is designed to study the transport and retention properties of the Opalinus Clay Formation. Gimmi et al. (2010) and Samper et al. (2010) presented a dimensionless sensitivity analysis of tracer dilution data and tracer concentration along overcoring profiles for the DR diffusion experiments. Sensitivities to diffusion and sorption parameters are tracer dependent. Dilution data for conservative tracers such as HTO are most sensitive to the effective diffusion parallel to the bedding ($D_{e//}$) and the accessible porosity (ϕ_{acc}) of the undisturbed clay and the excavation disturbed zone (EdZ). Dilution data for weakly-sorbing tracers such as $^{22}Na^{+}$ are most sensitive to the effective diffusion of the filter and the EdZ, the distribution coefficient (K_d) and the $D_{e//}$ of the undisturbed clay. Overcoring data contain information which is complementary to that provided by dilution data. For instance, overcoring data are sensitive to changes in the effective diffusion coefficient of the undisturbed clay perpendicular to the bedding ($D_{e-|}$) for HTO. Changes in the thickness of the EdZ and the volume of the circulation system, V, affect significantly the tracer concentrations at the injection interval and in most of the overcoring profiles.

Samper et al. (2010) presented an identifiability analysis of diffusion and sorption parameters for HTO and $^{22}Na^{+}$ for the DR experiment. It was performed with either dilution or overcoring data. The joint estimation of undisturbed clay and EdZ parameters for HTO is only possible when $\sigma_c < 0.01$ from only dilution data. The K_d and the $D_{e//}$ of the undisturbed clay for $^{22}Na^{+}$ cannot be estimated simultaneously from only noisy dilution data. The diffusion anisotropy cannot be derived from dilution data. However, good estimates are obtained with the inverse runs performed from synthetic overcoring data. Samper et al. (2010) also used synthetic experiments to evaluate the effect of the uncertainties in the volume of water of the injection system, V, the D_e of the filter and the existence of an EdZ on estimates of HTO and $^{22}Na^{+}$diffusion and sorption parameters. Small errors in the volume of the circulation system do not affect significantly the estimates of the clay parameters.

Estimates deviate from their true values in the inverse runs in which a significant error is introduced in the D_e of the filter when they are performed from dilution data, while acceptable estimates are obtained when they are performed from generic overcoring data. The uncertainty in the existence of the EdZ has a large effect on the estimates. The proper interpretation of the experiment requires the right hypothesis about the EdZ. The effect of these uncertainties on the parameter estimates from dilution data is larger than from estimates derived from overcoring data.

Here the identifiability analysis has been improved by using simultaneously both types of data, by accounting for the actual position of the overcoring samples in the rock and by adopting realistic values of the random noise based on real data of previous diffusion experiments. The effect of the uncertainties in V and D_e of the filter on estimates has been analyzed using dilution and overcoring data simultaneously. The contribution of the information given by overcoring data on the reduction of the effect of these uncertainties has been quantified. In addition, the effect on parameter estimates of errors in the location of the sampling profiles and the influence of the sequence of random noise have been evaluated here for the first time.

The paper starts by describing the DR experiment. Then, the formulation of solute diffusion and sorption and the numerical methods for the interpretation of the experiment are presented. Next, the methodology and the results of the identifiability analysis of diffusion and sorption parameters for conservative and weakly-sorbing tracers are described. Then, the improvement of the identifiability of the parameters and the reduction of the estimation errors due to the simultaneous use of dilution and overcoring data are discussed. This appendix ends with the main conclusions.

2. DR EXPERIMENT AT MONT TERRI

The in situ diffusion and retention (DR) is a long-term, natural-scale, in situ experiment designed to study the transport and retention properties of Opalinus Clay (Wersin and Van Dorp, 2005; Fierz, 2006; Leupin et al., 2010). The concept is similar to previous in situ diffusion experiments such as DI-A (Wersin et al., 2004; van Loon et al., 2004) and DI-B (Yllera et al., 2004; Soler et al., 2008), although it has been optimized to determine in situ diffusion anisotropy. The injection intervals are shorter than those of previous experiments. The duration of the experiment is such that the transport distance of conservative tracers is larger than the length of the injection interval to allow the estimation of the diffusion anisotropy.

The experiment is performed in a borehole drilled perpendicular to the bedding at the DR niche of the Mont Terri URL. The Opalinus Clay exhibits diffusion anisotropy due to stratification. Three intervals of the borehole were isolated by packers. The interval at the bottom serves as an auxiliary interval for the observation of the hydraulic pressure during the experiment. Tracer

cocktails were injected into the upper two intervals. The following tracers were added at the upper interval: $^{60}Co^{2+}$, $^{137}Cs^{+}$, $^{133}Ba^{+2}$, $^{152}Eu^{+3}$, Eu^{+3} and HDO. The tracers injected in the lower interval include: HTO, $^{22}Na^{+}$, $^{85}Sr^{2+}$, I^{-} (stable), Br^{-} (stable), $^{75}Se^{6+}$, Cs^{+} and ^{18}O. Injection intervals are connected to the surface equipment which includes reservoir tanks of 20 L. The fluid is circulated continuously to ensure that the tank water and the downhole water are well mixed. Tracer concentrations and activities in the water of the circulation system were monitored by taking water samples at regular intervals in sampling vials. In addition, ɣ-emitter tracers were monitored on line in both circuits with an online ɣ-counting technique.

At the end of the experiment, the rock around the injection intervals was overcored and the tracer distribution within the rock was measured. The removal of the overcore of the host rock surrounding the test intervals was completed successfully in January 2011. HTO and $^{22}Na^{+}$ samples were taken from six discs of rock cut from overcore, having a thickness of 4 cm (Figure 1). They were located below the middle of the lower injection interval. Rock samples were taken out along radial profiles from the discs with a saw. Each profile was sliced into 1 cm thick samples. The surface of the small samples disturbed by drilling and partly desaturated was cut away. 16 samples were taken in each profile, except for one which had only 12 samples. The clay samples were immediately transferred into polyethylene bottles and carried to the laboratory for analysis. The total concentration of the tracers was measured in each sample.

The time evolution of the tracer concentrations in the two injection systems denoted here as ‘‘dilution data’’ and the tracer profiles in the rock after overcoring (‘‘overcoring data’’) will be used to derive tracer diffusion and retention parameters.

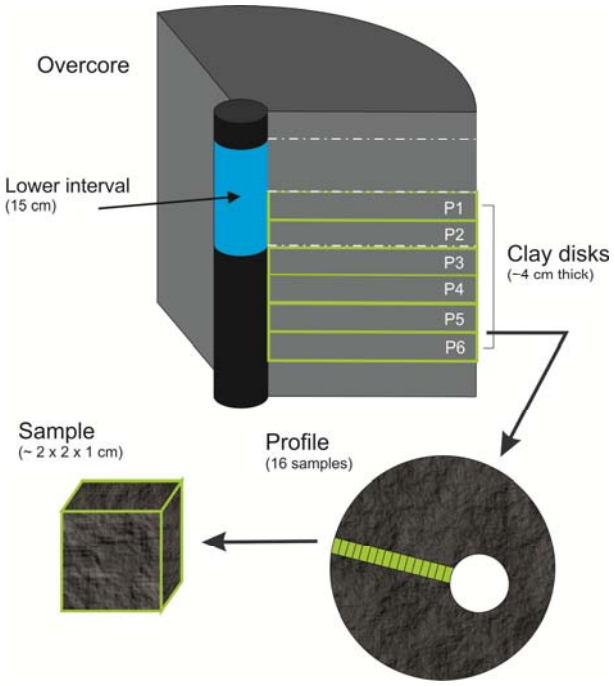

Figure 1 Sketch of overcore sampling at DR experiment for HTO and $^{22}Na^{+}$.

3. SOLUTE TRANSPORT EQUATION

The transport equation for a tracer which diffuses through a low permeability medium is given by (Bear, 1972):

$$\nabla \cdot \left(\overline{D_e} \cdot \nabla C \right) = \alpha \frac{\partial C}{\partial t}$$

where C is the tracer concentration, t is time, and α is the capacity factor which is given by:

$$\alpha = \phi_{acc} + \rho_d K_d$$

where ϕ_{acc} is the accessible porosity which is equal to the total porosity if the tracer is not affected by anion exclusion, K_d is the distribution coefficient, and ρ_d is the bulk density. $\overline{D_e}$ is the effective diffusion tensor which, in a coordinate system defined along the bedding planes, is given by:

$$\begin{pmatrix} D_{e//} & 0 & 0 \\ 0 & D_{e//} & 0 \\ 0 & 0 & D_{e-|} \end{pmatrix}$$

where $D_{e//}$ and $D_{e-|}$ are the components of the effective diffusion tensor parallel and normal to the bedding, respectively.

4. NUMERICAL INTERPRETATION

The numerical interpretation of the DR experiment requires the use of 3D models due to the diffusion anisotropy. However, symmetry with respect to the borehole axis allows the use of 2D axi-symmetric models. The numerical model is solved with a 2D finite element mesh similar to that used by Samper et al. (2010). All the outer boundaries of the domain are no-flux boundaries. Five material zones are considered: the injection interval, the 3 mm thick Teflon filter, the 2 mm gap, the EdZ which has a thickness of 20 mm and the undisturbed Opalinus Clay. Small changes on the finite element mesh have been made to ensure that the nodes of the grid coincide with the center of each sample along the rock profiles.

Prior estimates of the D_e, the K_d and the ϕ_{acc} for HTO and $^{22}Na^+$ in the undisturbed clay were derived from available laboratory experiments (Table 1). An anisotropy ratio of 4 was considered (Van Loon et al., 2003). The D_e and α of these tracers in porous Teflon filters were measured by Van Loon and Glauss (2008) using a through-diffusion method. They found that the D_e of the filter is approximately equal to 7% of the diffusion coefficient while its porosity is about 30%. The effective diffusion for other materials was derived from that of undisturbed clay by using Archie's law with an exponent equal to 4/3. On the other hand, the porosities of the EdZ and the gap are unknown. As an educated guess, the porosity of the EdZ was assumed to be twice that of the undisturbed clay while

the porosity of the gap was assumed to be 0.6. The undisturbed clay and the EdZ are assumed to have the same distribution coefficient. No sorption takes place in the filter and the gap.

Table 1 Reference values of diffusion and sorption parameters in different materials for HTO and $^{22}Na^{+}$. The effective diffusion coefficient parallel to the bedding ($D_{e//}$) is four times larger than the perpendicular to the bedding ($D_{e-|}$). K_d is the distribution and ϕ_{acc} is the accessible porosity.

	Filter		Gap		EdZ			Undisturbed clay		
Tracer	**$D_{e//}$ (m^2/s)**	**Φ_{acc}**	**$D_{e//}$ (m^2/s)**	**Φ_{acc}**	**$D_{e//}$ (m^2/s)**	**Φ_{acc}**	**K_d (L/Kg)**	**$D_{e//}$ (m^2/s)**	**Φ_{acc}**	**K_d (L/Kg)**
HTO	1.9×10^{-10}	0.30	3.17×10^{-10}	0.60	1.26×10^{-10}	0.30	0	5.0×10^{-11}	0.15	0
$^{22}Na^{+}$	7.9×10^{-11}	0.30	4.45×10^{-10}	0.60	1.76×10^{-10}	0.30	0.205	7.0×10^{-11}	0.15	0.205

5. METHODOLOGY

Synthetic experiments having the same geometric properties as the real experiments are often used to study parameter identifiability and model uncertainties. The method for performing the identifiably study with synthetic data involves the following steps: (1) Generating synthetic data from a forward run of the numerical model by assuming reference values of the diffusion and sorption parameters; (2) Adding random noise to the synthetic data; (3) Estimating key diffusion parameters from noisy synthetic data in several stages; and (4) Evaluating the effect of various uncertainties such as the existence of the EdZ and the volume of water in the injection system, V. Since true values are known, one can clearly identify which parameters can be estimated, how reliable parameter estimates really are and the effect of the uncertainties in estimation errors.

5.1. Synthetic data generation

The identifiability analysis of diffusion and sorption parameters for HTO and $^{22}Na^{+}$ accounts for dilution or overcoring synthetic data simultaneously. Synthetic dilution data were generated from a forward run of the numerical model at the same times as those of the real experiment. The 19 available synthetic dilution data coincide with those presented in Samper et al. (2010). Synthetic overcoring data are derived from computed concentrations at the end of the experiment in the same forward run. They account for the real position of the overcoring samples in the rock instead of the "presumed" radial profiles used in the previous analysis of Samper et al. (2010).

For overcoring data generation and interpretation, the average tracer concentration in the sample is assumed to be equal to the concentration at the center of the sample. This hypothesis was tested by comparing the computed tracer concentration at the center of the sample with the average of the computed concentrations at points spaced 1 mm within the sample. Errors are smaller than 0.4% and therefore can be neglected for this experiment design and these tracers.

Tracer concentrations in the rock samples were measured in terms of total concentrations and expressed mass of tracer per unit mass of clay sample. Contrary to Samper et al. (2008a; 2010) who used synthetic overcoring data in terms of porewater concentration, here overcoring data were expressed as total concentration. The total concentration, C_T, and the porewater concentration, C_P, are related through (Samper et al., 2008b):

$$C_T = C_P \frac{\phi_{acc} + \rho_d K_d}{\phi_{acc}\rho_w + \rho_d}$$

where ρ_w is the density of porewater (1000 Kg/m^3), the porosity of the rock, ϕ_{acc}, is 0.17 and its bulk dry density, ρ_d, is equal to 2274 Kg/m^3. The density of porewater is assumed equal to that of pure water, ρ_w =. The distribution coefficient, K_d, is zero for HTO and 0.205 L/Kg for $^{22}Na^+$ (see Table 1).

5.2. Random noise

A multiplicative random noise, ε, was added to the synthetic data: c* = εc, where c* and c are the noisy and true synthetic data, respectively. ε has a lognormal distribution with a standard deviation, σ*. The noise of the experimental data, E, was computed as the difference between the measured data c* and genuine data c calculated by fitting measured data to a polynomial drift. Therefore, E is an additive random noise having a normal distribution with a standard deviation σ_C which is equal to for 0.025 HTO and 0.043 for $^{22}Na^+$.

The relationship between σ* for data generation and the computed σ_C from generated synthetic data has been studied for HTO and $^{22}Na^+$. The values of σ* and σ_C for synthetic dilution data coincide for the range of noise of real data. The followings linear relationships can be established between σ* and σ_C for overcoring synthetic data: $\sigma_C = 0.4\ \sigma^*$ for HTO and $\sigma_C = 0.06\ \sigma^*$ for $^{22}Na^+$ (see Figure 2 for HTO).

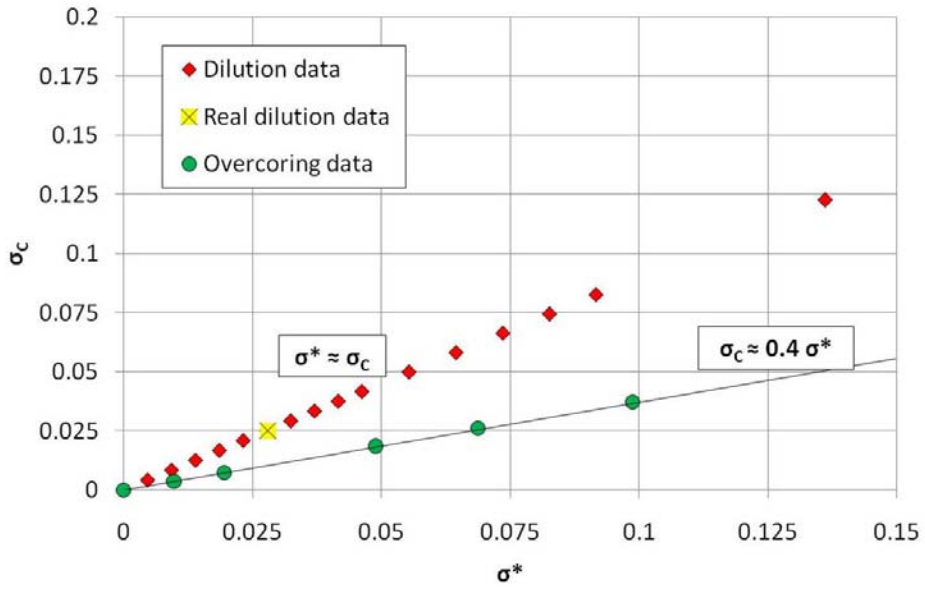

Figure 2 Relation between the standard deviation of the multiplicative noise, σ*, and the standard deviation of additive noise of synthetic data, σ_C, for HTO. The values of σ* and σ_C for real dilution data are also shown.

The σ_C of the synthetic dilution data was taken equal to that of real dilution data for both tracers: $\sigma_C = 0.02$ for HTO and $\sigma_C = 0.05$ for $^{22}Na^+$. The σ_C of the synthetic overcoring data ranges from 0 to 0.05 for HTO and from 0 to 0.025 for $^{22}Na^+$. These values are based on real overcoring data of the DI-A (Wersin et al., 2006) and DI-B experiments (Samper et al., 2006; Soler et al., 2008). Three sets of synthetic overcoring data were generated for each tracer: 1) Noise-free data; 2) Data with the most likely noise $\sigma_C = 0.02$ for HTO and $\sigma_C = 0.015$ for $^{22}Na^+$; and 3) Data with "larger than expected" noise with $\sigma_C = 0.05$ for HTO and $\sigma_C = 0.025$ for $^{22}Na^+$. Parameter estimation was performed for several values of σ_c to evaluate the influence of noise in estimation errors. Figure 3 shows the generated synthetic dilution ($\sigma_C = 0.02$) and overcoring data ($\sigma_C = 0.05$) for HTO.

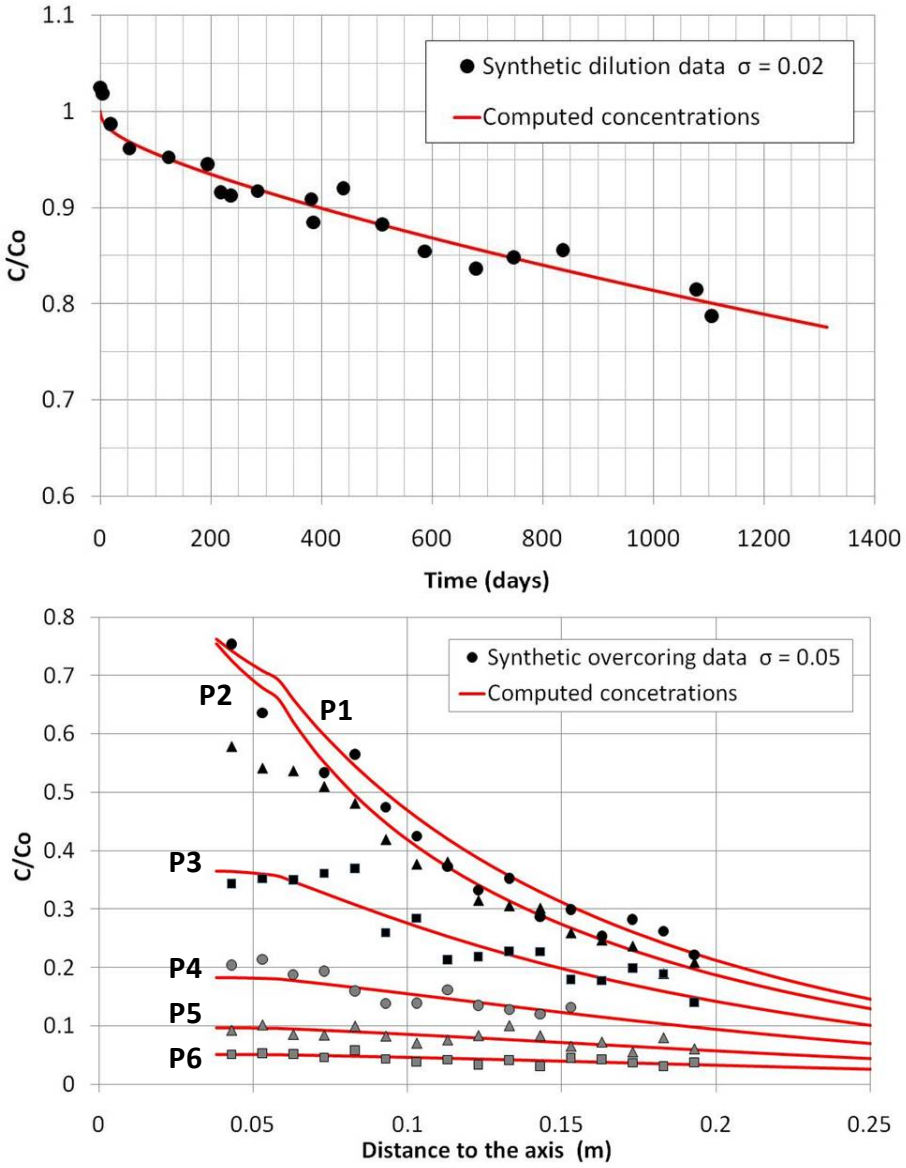

Figure 3 Synthetic dilution ($\sigma_C = 0.02$, top) and overcoring data ($\sigma_C = 0.05$, bottom) for HTO. Different symbols and labels are used for synthetic overcoring data in order to distinguish the different profiles from P1 to P6. Profiles positions are shown in Figure 1.

5.3. Automatic parameter estimation

Synthetic data were interpreted automatically with the INVERSE-CORE^{2D} (Dai and Samper, 2004) by solving the inverse problem. Optimum parameters were derived by minimizing a least-squares objective function with the Gauss–Newton–Levenberg–Marquardt method. Let $\boldsymbol{p} = (p_1, p_2, p_3, ..., p_m)$ be the vector of m unknown parameters. The objective function, E(**p**), is expressed as

$$E(p) = \sum_{i=1}^{NE} W_i E_i(p)$$

where i =1, ..., NE denotes different types of data. There are two types of data, i = 1 for the dilution data in terms of porewater concentrations and i = 2 for the overcoring data in terms of total concentrations. W_i is the weighting coefficient of the ith generalized least-squares criterion, $E_i(\boldsymbol{p})$, which is defined as

$$E_i(p) = \sum_{j=1}^{J_i} w_{ji}^2 r_{ji}^2(p)$$

$$r_{ij} = u_j^i(p) - F_j^i$$

where $u_j^i(p)$ is the computed value of the ith variable at the observation point; the F_j^i are the synthetic measured values; L_i is the number of observations, either in space or in time for the ith type of data; r_{ij} is the residual for the jth measurement of the ith type of data and w_{ji} is its weighting coefficient.

The w_{ji} are taken equal to $1/\sigma_c^i$, where σ_c^i is the standard deviation of the noise of each type of data. The values of W_i are updated automatically during the iterative optimization process as indicated by Dai and Samper (2004). The code provides statistical measures of goodness-of-fit as well as parameter uncertainties by computing the covariance and correlation matrices and approximate confidence intervals.

6. RESULTS

6.1. HTO

Previous sensitivity analyses showed that HTO concentrations are sensitive to changes in the parameters of the undisturbed clay and the EdZ (Samper et al., 2010). Since the accessible porosity for HTO can be deduced from measurements of water content on the rock samples, the identifiability analysis was focused on the identifiability of the $D_{e//}$ and the $D_{e-|}$ of the undisturbed clay and the EdZ. First, the $D_{e//}$ of the undisturbed clay was estimated by fixing the other parameters equal to their true values. Then, several combinations of the parameters were estimated simultaneously to

evaluate the correlation of parameter estimates. Estimation runs were performed with different initial starting values of the parameters and for increasing values of σ_c. The results of the identifiability analysis for HTO is listed Table 2.

Parameter estimates are equal to their true values for noise-free data, regardless the initial values and the number of estimated parameters. The estimated $D_{e//}$ of the undisturbed clay is close to its true value when only this parameter is estimated, even when the data contain noise. Clearly, the noise in the data introduces a mild bias of 6% in the estimate of $D_{e//}$ of the clay for the inverse run performed with noisy dilution and overcoring data having σ_c = 0.02. The estimation error increases to 10% when the noise of overcoring data has σ_c = 0.05.

The $D_{e//}$ of the clay and the EdZ can be estimated simultaneously. The estimation errors are equal to 4% for the $D_{e//}$ of the clay and 8% for the $D_{e//}$ of the EdZ for the inverse run performed with dilution and overcoring data with σ_c = 0.02. The errors in $D_{e//}$ of the clay and the EdZ increase to 10% and 20% when the σ_c of the noise of overcoring data increases to 0.05, respectively.

A similar conclusion was obtained when the $D_{e//}$ and the $D_{e-|}$ of the clay are estimated simultaneously from overcoring data. Their estimation errors for σ_c = 0.02 are 7% and 12%, respectively. Good estimates of these two parameters can be obtained even from overcoring data with σ_c = 0.05.

Table 2 Summary of the inverse runs for the synthetic experiments of HTO. The $D_{e//}$ and $D_{e-|}$of the EdZ and the undisturbed clay are estimated from dilution and overcoring data. σ_c is the standard deviation of the data noise.

Parameter		**Clay $D_{e//}$ (m^2/s)**		**Clay $D_{e-|}$ (m^2/s)**		**EdZ $D_{e//}$ (m^2/s)**		**EdZ $D_{e-|}$ (m^2/s)**	
True value		5.0×10^{-11}		1.25×10^{-11}		1.26×10^{-10}		3.16×10^{-11}	
Dilution σ_c	**Overcoring σ_c**	Initial	Estimated	Initial	Estimated	Initial	Estimated	Initial	Estimated
0	0	2.5×10^{-11}	5.0×10^{-11}	5.8×10^{-12}	1.25×10^{-10}	5.0×10^{-11}	1.26×10^{-10}	1.55×10^{-11}	3.16×10^{-11}
0.02	0.02	2.5×10^{-11}	5.31×10^{-11}	-	-	-	-	-	-
0.02	0.05	2.5×10^{-11}	5.5×10^{-11}	-	-	-	-	-	-
0.02	0.02	2.5×10^{-11}	5.21×10^{-11}	-	-	5.0×10^{-11}	1.16×10^{-10}	-	-
0.02	0.05	2.5×10^{-11}	5.49×10^{-11}	-	-	5.0×10^{-11}	1.01×10^{-10}	-	-
0.02	0.02	2.5×10^{-11}	5.35×10^{-11}	5.8×10^{-12}	1.39×10^{-11}	-	-	-	-
0.02	0.05	2.5×10^{-11}	5.49×10^{-11}	5.8×10^{-12}	1.57×10^{-11}	-	-	-	-
0.02	0.02	2.5×10^{-11}	5.34×10^{-11}	5.8×10^{-12}	1.39×10^{-11}	5.0×10^{-11}	1.24×10^{-10}	-	-
0.02	0.05	2.5×10^{-11}	5.53×10^{-11}	5.8×10^{-12}	1.56×10^{-11}	5.0×10^{-11}	1.05×10^{-10}	-	-
0.02	0.02	2.5×10^{-11}	5.31×10^{-11}	5.8×10^{-12}	1.16×10^{-10}	5.0×10^{-11}	1.05×10^{-10}	1.55×10^{-11}	4.47×10^{-11}

The estimates of the $D_{e//}$ and the $D_{e-|}$ of the clay and the $D_{e//}$ of the EdZ are good when they are estimated simultaneously. These three parameters have been estimated from dilution data with $\sigma_c = 0.02$ and overcoring data with increasing values of σ_c. The estimation errors increase when the σ_c of overcoring data increases (Figure 4). On the contrary, the $D_{e-|}$ of the EdZ cannot be estimated simultaneously with the $D_{e//}$ and $D_{e-|}$ of the clay and the $D_{e//}$ of the EdZ. Actually, this result comes to no surprise given the small sensitivity of the concentrations to changes in the $D_{e-|}$ of the EdZ.

Figure 5 shows the fit of computed concentrations to synthetic data ($\sigma_c = 0.02$) when the $D_{e//}$ and $D_{e-|}$ of the undisturbed clay and the EdZ are estimated simultaneously. The fit is excellent although the estimates contain large estimation errors (see Table 2). In general, good fits to synthetic data are obtained for achieved estimates regardless their errors. Therefore, an excellent fit to data does not ensure necessarily good estimates of diffusion parameters.

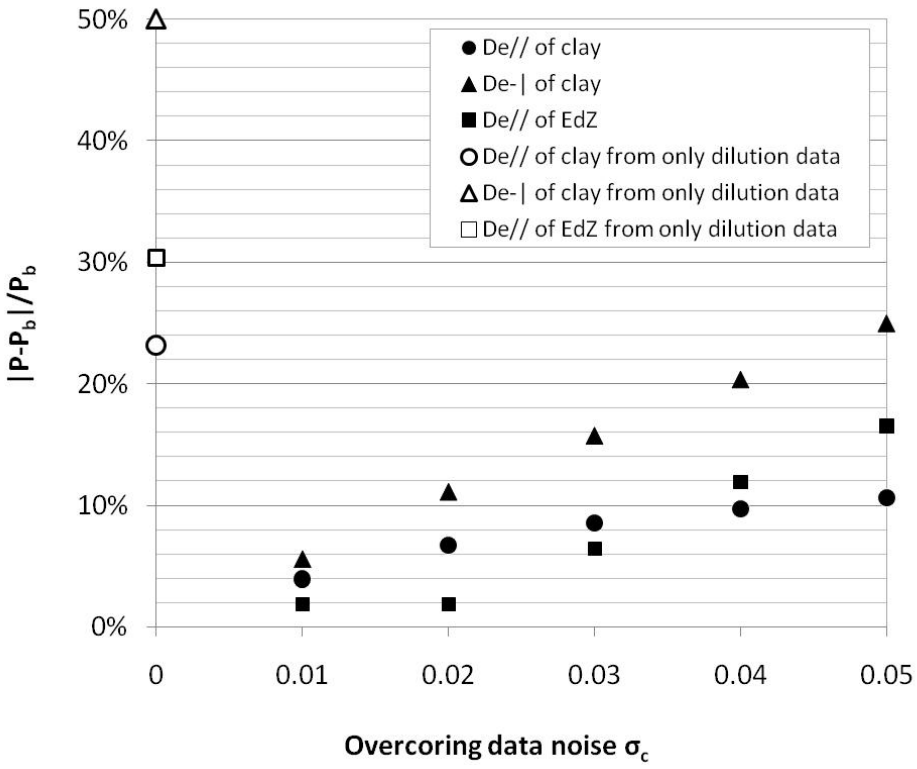

Figure 4 Estimation errors of the $D_{e//}$ and $D_{e-|}$ of the clay and the $D_{e//}$ of the EdZ for HTO versus σ_C of overcoring data. Dilution data has $\sigma_C = 0.02$ and the σ_C of overcoring data with σ_C between 0.01 and 0.05. P is the estimate of the parameter and P_b is its reference value. Estimation errors from only dilution data are shown along the y axis.

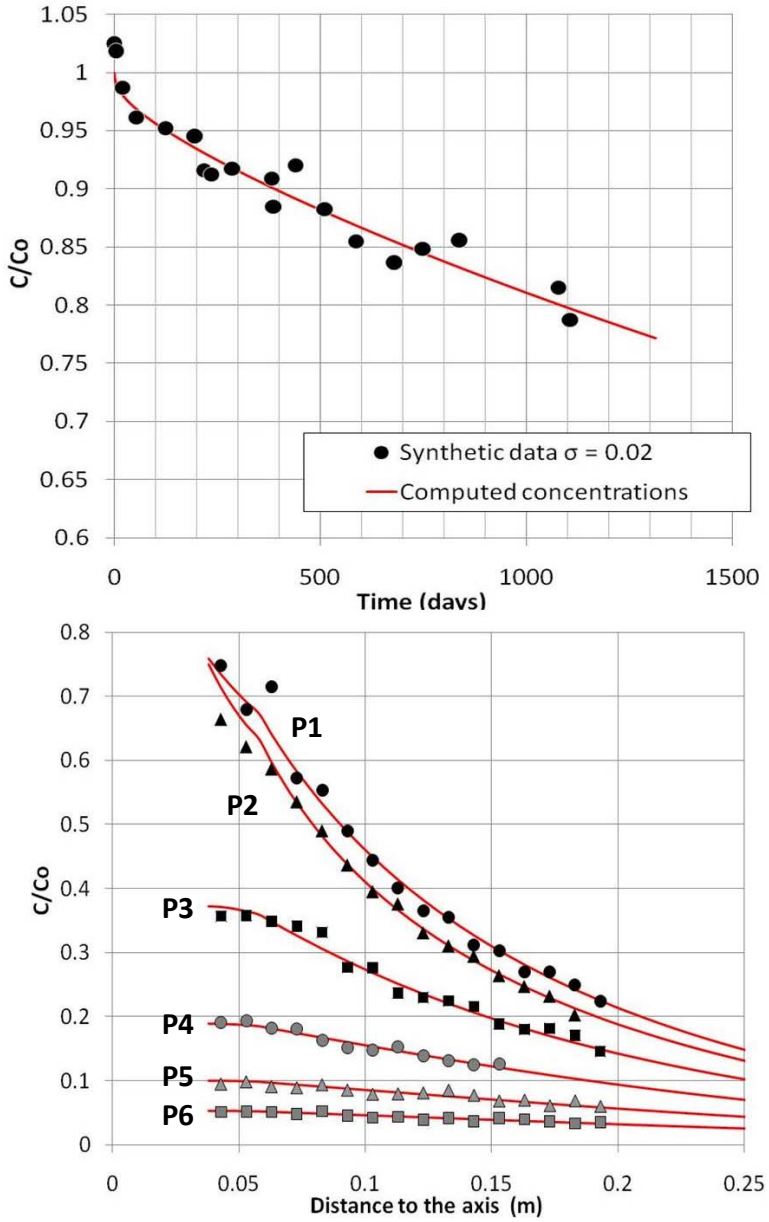

Figure 5 Fit of computed concentrations to synthetic data (σ_c = 0.02) when the De// and De-| of the undisturbed clay and the EdZ are estimated simultaneously. Different symbols and labels are used for synthetic overcoring data in order to distinguish the different profiles from P1 to P6. Profiles positions are shown in Figure 1.

6.2. $^{22}Na^{+}$

The identifiability analysis for a weakly-sorbing tracer such as $^{22}Na^{+}$ is focused on the diffusion and sorption parameters to which computed concentrations are most sensitive: the K_d, the $D_{e//}$ and the $D_{e-|}$ of the undisturbed clay and the $D_{e//}$ of the EdZ. First, the K_d and the $D_{e//}$ of the undisturbed clay were estimated simultaneously. Then, the four parameters were estimated together. Table 3 lists the results of the identifiability analysis for $^{22}Na^{+}$. The estimation runs were performed for different initial starting values of the parameters and several values of σ_c.

Similar to HTO, parameter estimates are equal to their true values for noise-free data, regardless the initial values and the number of estimated parameters. The noise in the data introduces a bias in the parameter estimates. The K_d and the $D_{e//}$ of the undisturbed clay for $^{22}Na^+$ can be estimated simultaneously from dilution data with σ_c = 0.05 and overcoring data with σ_c = 0.015 (similar to that expected for real overcoring data). The estimates of the K_d and the $D_{e//}$ of the undisturbed clay depend on the initial values. However, estimation errors are always smaller than 20%. Estimation errors increase slightly when the σ_c of the overcoring data increases from 0.015 to 0.025. The joint estimation of the K_d, $D_{e//}$ and the $D_{e-|}$ of the undisturbed clay is feasible. Figure 6A shows that the estimation errors of these three parameters increase with the σ_c of overcoring data when they are estimated simultaneously. σ_C of dilution data is fixed equal to 0.05 and σ_C of the overcoring data ranges from 0 to 0.025. Data noise affects more the estimates of $D_{e-|}$ than the estimates of the K_d and the $D_{e//}$.

The $D_{e//}$ and the $D_{e-|}$ of the undisturbed clay, the $D_{e//}$ of the EdZ and the K_d cannot be estimated simultaneously from noisy dilution and overcoring data. The estimation of the $D_{e//}$ of the EdZ leads to large estimation errors of the $D_{e//}$ of the clay and does not allow the estimation of the $D_{e-|}$ of the clay (Figure 6B). The estimates of the $D_{e//}$ of the clay contain estimation errors larger than 40% when the $D_{e//}$ of the clay, the K_d and the $D_{e//}$ of the EdZ are estimated simultaneously from noisy dilution and overcoring data. In summary, good estimates of the $D_{e//}$ of the clay and the EdZ cannot be derived simultaneously when data contain noise. Similar to HTO, an excellent fit to data does not necessarily mean good parameter estimates.

Table 3 Summary of inverse runs for $^{22}Na^+$ synthetic experiments. The K_d, the $D_{e//}$ and $D_{e-|}$of the undisturbed clay and the $D_{e//}$ of the EdZ are estimated from dilution and overcoring data. σ_c is the standard deviation of the noise.

Parameter		**K_d (L/Kg)**		**Clay $D_{e//}$ (m^2/s)**		**Clay $D_{e-|}$ (m^2/s)**		**EdZ $D_{e//}$ (m^2/s)**	
True value		0.205		7×10^{-11}		1.75×10^{-11}		1.76×10^{-10}	
Dilution σ_c	**Overcoring σ_c**	Initial	Estimated	Initial	Estimated	Initial	Estimated	Initial	Estimated
0	0	0.1	0.205	4.63×10^{-11}	7.0×10^{-11}	2.42×10^{-11}	1.75×10^{-11}	0.87×10^{-10}	1.76×10^{-10}
0.05	0.015	0.1	0.171	4.63×10^{-11}	7.78×10^{-11}	-	-	-	-
0.05	0.015	0.4	0.202	1.16×10^{-10}	8.32×10^{-11}	-	-	-	-
0.05	0.025	0.1	0.16	4.63×10^{-11}	7.89×10^{-11}	-	-	-	-
0.05	0.015	0.1	0.172	4.63×10^{-11}	7.5×10^{-11}	2.42×10^{-11}	2.42×10^{-11}	-	-
0.05	0.015	0.1	0.2381	4.63×10^{-11}	9.46×10^{-11}	2.42×10^{-11}	3.56×10^{-11}	0.87×10^{-10}	1.0×10^{-10}
0.05	0.015	0.1	0.212	4.63×10^{-11}	1.0×10^{-10}	-	-	0.87×10^{-10}	1.15×10^{-10}

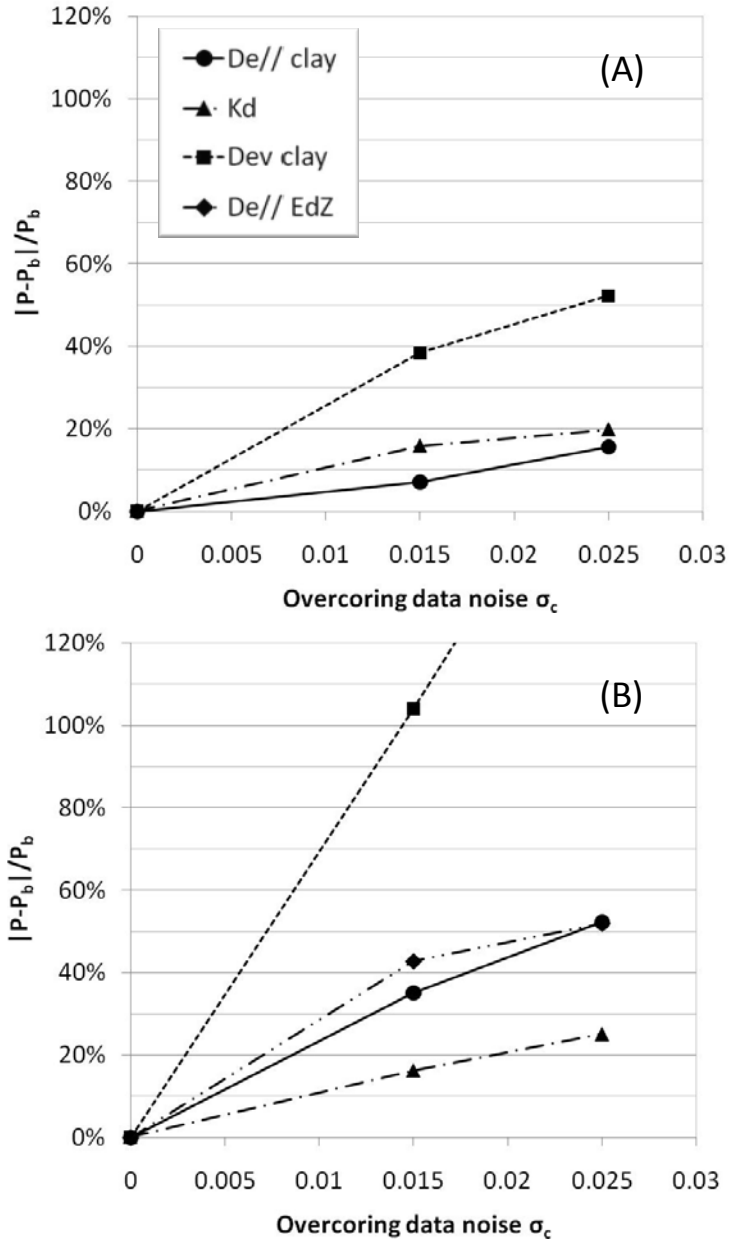

Figure 6 Estimation errors versus σ_C of overcoring data, when (A) the $D_{e//}$ and $D_{e-|}$ of the clay and the K_d are simultaneously estimated and (B) the $D_{e//}$ and $D_{e-|}$ of the clay, the K_d and the $D_{e//}$ of the EdZ are simultaneously estimated from noisy dilution and overcoring data. P is the estimate of the parameter and P_b is its reference value. σ_C of dilution data is equal to 0.05 and σ_C of overcoring data ranges from 0 to 0.025.

6.3. Evaluation of uncertainties

Uncertainties caused by possible errors in the volume of water in the injection system, V, have been evaluated by estimating diffusion and sorption parameters for an imposed value of V 10% smaller than its true value (Table 4). The error in V leads to estimation errors when $\sigma_c = 0$ for HTO and $^{22}Na^{+}$. For both tracers, a decrease of 10% in V does not have a large effect on the parameter estimates from noisy data. It affects the estimate of the K_d more than those of the $D_{e//}$ and the $D_{e-|}$ of the undisturbed clay.

The results of the identifiability runs performed with a D_e of the filter twice its true value show that an error in D_e of the filter has a negligible effect on parameter estimates when overcoring data are also used (Table 4). The estimates of clay parameters are similar when the D_e of the filter is taken equal to its true value or to twice its true value, regardless the noise. In all cases, acceptable estimates are obtained and the estimation errors caused by errors in the parameters of the filter are smaller than 10%.

There is no evidence of an EdZ in previous diffusion experiments at Mont Terri. The effect of an EdZ on the identifiability of the diffusion and sorption parameters was analyzed. Dilution and overcoring data were generated with an EdZ of 2 cm and without EdZ. Parameters were estimated simultaneously from the two sets of data using models with and without EdZ.

Excellent estimates of the $D_{e//}$ and the $D_{e-|}$ of the undisturbed clay and the $D_{e//}$ of the EdZ are derived from synthetic HTO data generated with EdZ using a model with EdZ (Table 2). When these data with EdZ are interpreted using a model without EdZ, the estimates of the $D_{e//}$ and the $D_{e-|}$ of the clay increase to compensate for the lack of EdZ which has a diffusion coefficient larger than that of the undisturbed clay. Estimates are poor. Estimation errors are larger than twice those derived using the model with EdZ.

Excellent estimates are obtained when the $D_{e//}$ and the $D_{e-|}$ of the clay parameter are derived from HTO synthetic dilution and overcoring data generated without EdZ using a model without EdZ. When these data without EdZ are interpreted using a model with EdZ, the estimate of the $D_{e//}$ of the clay is good, but the estimates of the $D_{e-|}$ of clay and the $D_{e//}$ of EdZ are poor.

Table 4 Summary of inverse runs performed to evaluate uncertainties in the volume of water of the circulation system, V, and the D_e of the filter. The $D_{e//}$ and $D_{e-|}$of the undisturbed clay and the $D_{e//}$ of the EdZ are estimated for HTO from dilution and overcoring data. For $^{22}Na^{+}$, the $D_{e//}$ and $D_{e-|}$of the undisturbed clay and the K_d are estimated. σ_c is the standard deviation of the noise.

Hypothesis	Dilution σ_c	Overcoring σ_c	Estimation error for HTO		
			Clay $D_{e//}$ (m^2/s)	Clay $D_{e-|}$ (m^2/s)	EdZ $D_{e//}$ (m^2/s)
No uncertainties	0	0	0 %	0 %	0 %
	0.02	0.02	6.7 %	11.1 %	1.8 %
10 % smaller V	0	0	12 %	12 %	1.8 %
	0.02	0.02	6.3 %	1.9 %	4.6 %
D_e of filter = 2 x true value	0	0	0.7 %	0.9 %	8.6 %
	0.02	0.02	7.4 %	10.2 %	9.6 %
Hypothesis	**Dilution σ_c**	**Overcoring σ_c**	**Estimation error for $^{22}Na^{+}$**		
			Clay $D_{e//}$ (m^2/s)	**Clay $D_{e-|}$ (m^2/s)**	**K_d (L/Kg)**
No uncertainties	0	0	0 %	0 %	0 %
	0.05	0.015	7.1 %	38.4 %	15.9 %
10 % smaller V	0	0	20.7 %	26.5 %	4.9 %
	0.05	0.015	13.2 %	0.7 %	24.6 %
D_e of filter = 2 x true value	0	0	7.4 %	16.6 %	8.5 %
	0.05	0.015	1 %	15.2 %	24 %

The fit of HTO computed concentrations to synthetic data is excellent when the model is based on the right hypothesis about the EdZ. When the hypothesis is wrong, a good fit can be obtained to synthetic data without EdZ and with a model with EdZ, but a poor fit to synthetic data with EdZ with a model without EdZ (Figure 7). According to this, a good fit of the model to the data does not necessarily ensure that the model is right.

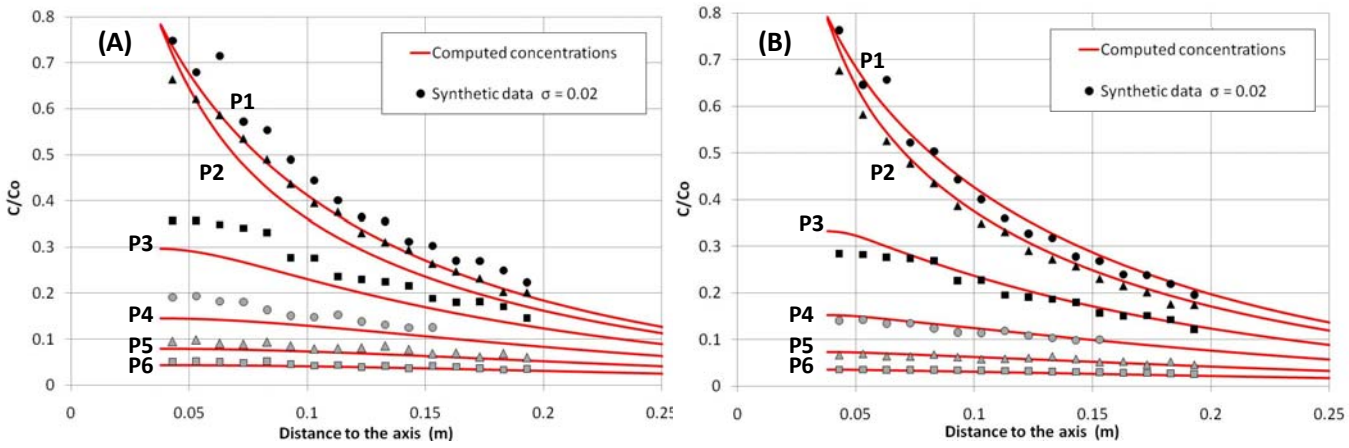

Figure 7 Fit of HTO computed concentrations to synthetic data (σ_c = 0.02) when the hypothesis about the EdZ is wrong. The fit of the model without EdZ to the data with EdZ is poor (A) while the fit of the model with EdZ to the data without EdZ is good (B). Different symbols and labels are used for synthetic overcoring data in order to distinguish the different profiles from P1 to P6. Profiles positions are shown in Figure 1.

Similar conclusions are obtained for $^{22}Na^{+}$. The uncertainty in the existence of the EdZ has a large effect on the estimates of the parameters of the undisturbed clay ($D_{e//}$, $D_{e-|}$ and K_d) which cannot be estimated simultaneously when the EdZ is disregarded.

Uncertainties in the exact location of the sampling profiles and their effect on estimates have been evaluated. The test interval was overcored at the end of the experiment. The entire core was lifted and cut into core sections at the borehole mouth. After removing the overcore, it was reoriented with the help of the bedding planes and the exact depth of the overcore containing the test interval was estimated. 4 cm thick clay disks were cut from the overcore and sampling profiles were taken from them. The depth of the rock samples was assumed equal to the mean depth of the clay disks. Therefore, there are uncertainties in the exact depth of the samples.

Two sets of synthetic data were generated along profiles located 2 cm above and below than that the right depth at which they were assigned for solving the inverse problem (Figure 8). This task was performed for HTO and $^{22}Na^{+}$ and for data without and with noise. Estimation errors are listed in Table 5. A shift of 2 cm in overcoring data introduces large errors on parameter estimates. Therefore, special attention should be paid to minimize the errors in positioning the depth of the samples.

This conclusion holds true for the overcoring samples of the DR experiment and may not apply to other experiments with different designs or different positions of rock samples. Estimation errors are expected to be smaller when the profiles are closest to the middle of the injection interval or in experiments with injection intervals larger than that of the DR experiment.

Table 5 Inverse runs performed to evaluate the influence of the uncertainty in the depth of the overcoring samples. The $D_{e//}$ and $D_{e-|}$ of the undisturbed clay and the $D_{e//}$ of the EdZ are estimated for HTO from dilution and overcoring data. For $^{22}Na^{+}$, the $D_{e//}$ and $D_{e-|}$ of the undisturbed clay and the K_d are estimated. σ_c is the standard deviation of the data noise.

Depth of synthetic concentration profiles	Dilution σ_c	Overcoring σ_c	Estimation error for HTO		
			Clay $D_{e//}$ (m^2/s)	Clay $D_{e-|}$ (m^2/s)	EdZ $D_{e//}$ (m^2/s)
Reference position	0	0	0 %	0 %	0 %
2 cm lower than the reference	0	0	39%	-20%	-50%
2 cm upper than the reference	0	0	34%	29%	83%
Reference position	0.02	0.02	5.1 %	9.3 %	6.2 %
2 cm lower than the reference	0.02	0.02	34 %	29 %	83 %
2 cm upper than the reference	0.02	0.02	29 %	44 %	83 %
Depth of synthetic concentration profiles	**Dilution σ_c**	**Overcoring σ_c**	**Estimation error for $^{22}Na^{+}$**		
			Clay $D_{e//}$ (m^2/s)	Clay $D_{e-|}$ (m^2/s)	K_d (L/Kg)
Reference position	0	0	0 %	0 %	0 %
2 cm lower than the reference	0	0	29 %	67 %	> 200 %
2 cm upper than the reference	0	0	32 %	76 %	47%
Reference position	0.05	0.015	7.1 %	38.4 %	15.9 %
2 cm lower than the reference	0.05	0.015	30 %	49 %	> 200 %
2 cm upper than the reference	0.05	0.015	35 %	70 %	> 200 %

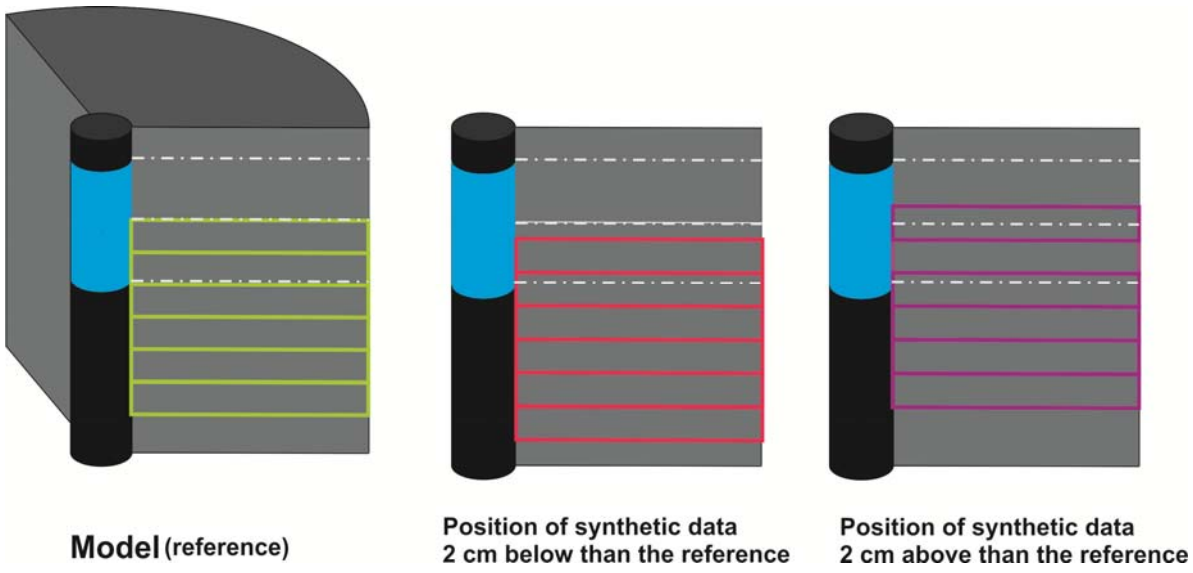

Figure 8 Reference position of the clay disks cut from the overcore assumed for modelling (left) and hypothetical locations of the disks 2 cm below and above than the reference for synthetic data generation.

6.4. Number of random realizations

All the inverse runs of the parameter identifiability analysis presented so far were performed by generating a single set of synthetic data. The identifiability analysis was repeated for several sequences of random noisy data to study whether the conclusions derived for a sequence of random data are linked to the particular sequence of random numbers used or whether they are independent of the random sequence. Hence, the $D_{e//}$ and the $D_{e-|}$ of the undisturbed clay and the $D_{e//}$ of the EdZ were estimated from 10 additional realizations of HTO dilution and overcoring data having $\sigma_C = 0.02$.

The estimation errors for each realization of random errors are shown in Figure 9. This figure shows also the mean estimation errors for an increasing number of realizations. Parameter estimates are within a rather narrow range (10 to 16% of estimation error) and the mean estimates get stable after 5 realizations. It can be concluded that the general sequence of random noise is not relevant for the conclusions.

7. DISCUSSION

The simultaneous use of dilution and overcoring data improves the identifiability of the diffusion and sorption parameters for HTO and $^{22}Na^{+}$. Our results have been compared with those from Samper et al. (2010) who used either one or the other type of data.

For HTO, the $D_{e//}$ of the undisturbed clay is close to its true value when it is estimated from only noisy dilution data. Its estimation error for $\sigma_c = 0.02$ is of 7%. Overcoring data do not introduce valuable information in this case. On the other hand, the $D_{e//}$ of the clay and the $D_{e//}$ of the EdZ cannot be estimated simultaneously using only noisy dilution data because these parameters are strongly correlated. By using overcoring data allows one their estimation even when data contain a large noise. Furthermore, estimates are good and estimation errors are similar when the $D_{e-|}$ of the clay is also estimated (Figure 4). Diffusion anisotropy cannot be estimated from dilution data, but it can be derived from dilution and overcoring data. Errors when these three parameters are estimated simultaneously from only noisy dilution data ($\sigma_c = 0.02$) are shown along the y axis of the Figure 4, to illustrate the improvement of the parameter estimates when overcoring data are available.

The K_d and the $D_{e//}$ of the undisturbed clay for $^{22}Na^{+}$ cannot be estimated simultaneously using only dilution data with $\sigma_c > 0.02$ because they are strongly correlated ($\rho = -0.95$). Overcoring data introduces valuable information that allows one the estimation of both parameters simultaneously regardless the noise. The joint estimation of the K_d, $D_{e//}$ and the $D_{e-|}$ of the undisturbed clay is also possible when overcoring data are used. Similar to HTO, the diffusion anisotropy cannot be estimated from dilution data, but it can be from dilution and overcoring data.

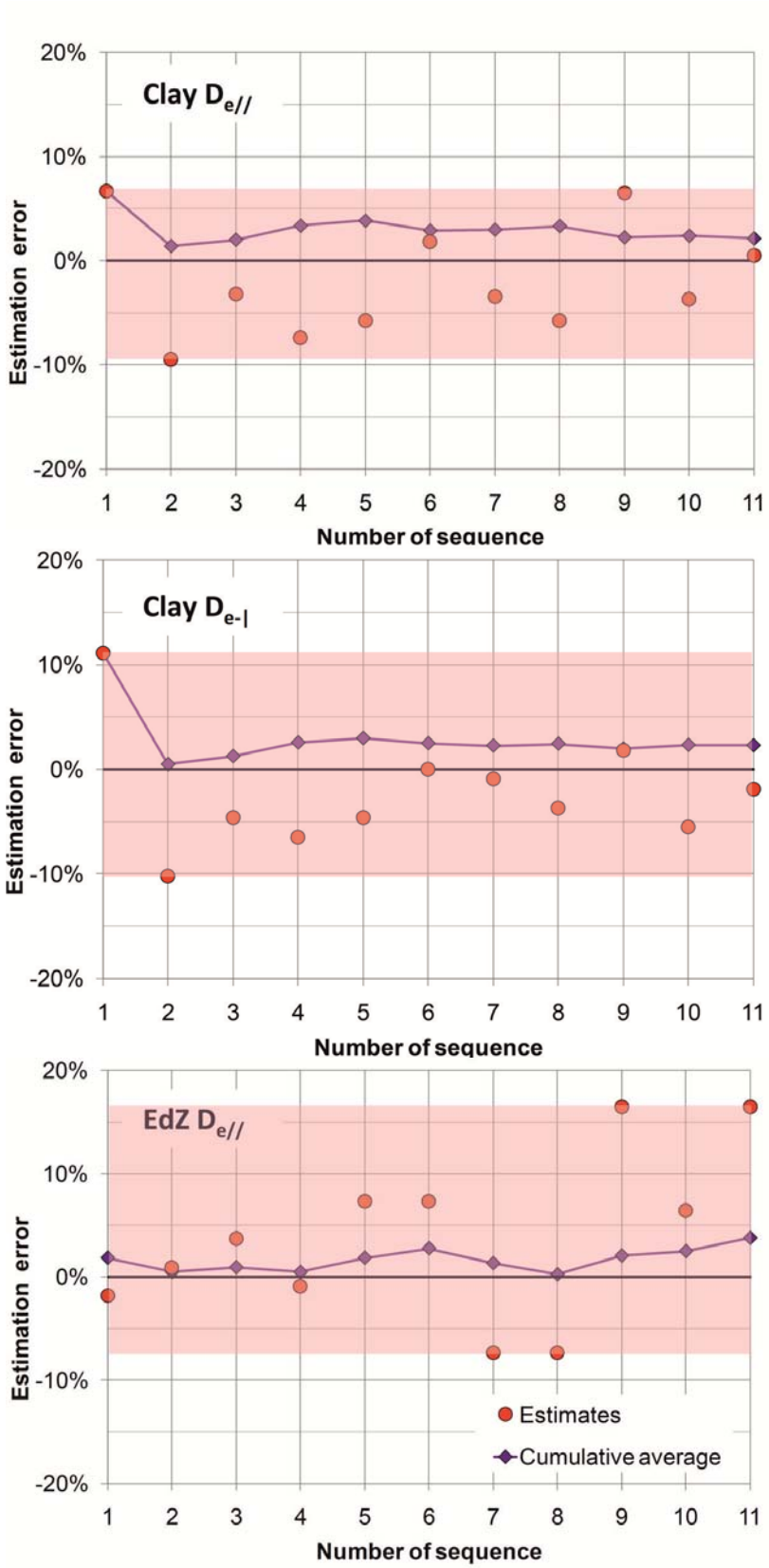

Figure 9 Estimation errors of the $D_{e//}$ and the $D_{e-|}$ of the undisturbed clay and the $D_{e//}$ of the EdZ derived from 11 different sequences of HTO synthetic dilution and overcoring data with random noise of $\sigma_C = 0.02$ (dots). The range of estimation errors is shadowed and the cumulative mean estimation error with an increasing number of runs is also presented for each parameter.

The conclusions about the effect of the uncertainties in the volume of water of the injection system and the existence of the EdZ are similar for the estimation with only dilution data or with dilution and overcoring data. On the other hand, the uncertainties in the value of the D_e of the filter affect very strongly the estimates derived from only dilution data and their effect drastically decreases when overcoring data are available. Inverse runs performed with only dilution data and with a D_e of the filter twice its true values show that parameter estimates deviate from their true values (Samper et al., 2010). Conversely, such effect is negligible when they are performed from dilution and overcoring data

8. CONCLUSIONS

Synthetic experiments generated with known parameters have been interpreted automatically with INVERSE-CORE^{2D}. Then, they have been used to study the parameter identifiability for HTO and $^{22}Na^{+}$ in the presence of random measurement errors and to evaluate model uncertainties. The previous analysis presented by Samper et al. (2010) with either dilution or overcoring data has been extended by using both types of data simultaneously. Moreover, the analysis presented here accounts for the actual position of the overcoring samples in the rock instead of assuming generic profiles. The standard deviation of the noise added to synthetic data has been derived from real data of the DR experiment and other similar experiments. It has been found that the conclusions of the parameter identifiability analysis are not affected by the particular sequence of random numbers. Overcoring data contain additional information to that provided by dilution data. Therefore, the identifiability of the diffusion and sorption parameters improves and the effect of the uncertainties on estimates is reduced when both types of data are used simultaneously.

Estimation errors of the $D_{e//}$ and $D_{e-|}$ of the EdZ and the undisturbed clay for HTO are negligible when the estimation is performed with noise-free data. Noise in the data introduces a bias in the parameter estimates. These two parameters cannot be estimated simultaneously only from noisy dilution data. Accounting for overcoring data allows one to estimate simultaneously the $D_{e//}$ and the $D_{e-|}$ of the clay and the $D_{e//}$ of the EdZ. On the contrary, the $D_{e-|}$ of the EdZ cannot be estimated from HTO noisy synthetic data.

For $^{22}Na^{+}$, the K_d, the $D_{e//}$ and the $D_{e-|}$ of the undisturbed clay and the $D_{e//}$ of the EdZ can be estimated without errors from noise-free data. These parameters cannot be estimated simultaneously from only noisy dilution data. Overcoring data introduces valuable information that allows the joint estimation of the K_d, $D_{e//}$ and the $D_{e-|}$ of the undisturbed clay from noisy data. Good estimates of the $D_{e//}$ of the EdZ cannot be derived when data contain noise.

It has been found also that a good fit of the model to synthetic data does not necessarily ensure good estimates of diffusion parameters.

Small errors in the volume of the circulation system do not affect significantly the estimates of the clay parameter. Good estimates and fits to data are obtained in the identifiability runs performed with noisy dilution and overcoring data with a D_e of the filter twice its true value. Overcoring data, which are less sensitive to the D_e of the filter than dilution data, prevents deviations from the true values that occur when only dilution data are available. The proper interpretation of the experiment requires assuming the right hypothesis about the EdZ existence. A wrong hypothesis leads to large estimation errors. Uncertainties in the exact depth of the overcoring profiles may introduce large errors on parameter estimates. Therefore, attention should be paid to minimize the errors in positioning the depth of the samples.

The conclusions of this identifiability analysis can be extrapolated directly to the interpretation of the actual data of the DR experiment.

9. ACKNOLEDGEMENTS

This work was supported by the Mont Terri Consortium and the Spanish Ministry of Science and Technology through a FPI Research Scholarship awarded by the Spanish Ministry.

10. REFERENCES

Aertsens, M., De Cannière, P., Lemmens, K., Maes, N., Moors, H., 1998. Overview and consistency of migration experiments in clay. *Physics and Chemistry of the Earth* 1, 2-4.

Appelo, C.A.J., Wersin, P, 2007. Multicomponent diffusion modeling in clay systems with application to diffusion of tritium, iodide and sodium in Opalinus Clay. *Enviromental Science and Technology*, 41, 50002-5007.

Bear, J., 1972. Dynamics of Fluids in Porous Media. Elsevier, New York.

Dai, Z., Samper, J., 2004. Inverse problem of multicomponent reactive chemical transport in porous media: formulation and applications. *Water Resource Research* 40, W07407.

De Cannière, P., Moors, H., Lolivier, P., De Preter, P., Put, M., 1996. Laboratory and in situ migration experiments in the Boom Clay. European Commission, Luxembourg, Report EUR 16 927 EN.

Dewocnk, S., Blin, V., Radwan, J., Filippi, M., Landesman, C., Ribet, S., 2010. Long term in situ tracer diffusion tests in the Callovo-Oxfordian clay: Results and modeling. In: *Clays In Natural & Engineered Barriers for Radioactive Waste Confinement 4th International Meeting* in March 2010, Nantes, France.

Fierz, T., 2006. Diffusion and retention (DR) experiment. Field activities phase 11: instrumentation and tracer injection. *Mont Terri Project Technical Note* TN 2006-18.

Gimmi, Th., Soler, J.M., Samper, J., Naves, A., Yi, S., Leupin, O.X., Wersin, P. Van Loon, L.R. , Eikenberg, J., Dewonck, S., Wittebroodt, Ch., 2010. Insights from modelling the Diffusion and Retention experiment at the Mont Terri URL. In: *Clays In Natural & Engineered Barriers for Radioactive Waste Confinement 4th International Meeting* in March 2010, Nantes, France.

Leupin, O.X., Wersin, P., Gimmi, Th., Soler,J. M., Dewonck, S., Wittebroodt, C, Van Loon, L., Eikenberg, J., Baeyens, B., Samper, J., Yi, S., Naves, A., 2010. Diffusion and retention experiment at the Mont Terri underground rock laboratory in St. Ursanne. In: *Clays In Natural & Engineered Barriers for Radioactive Waste Confinement 4th International Meeting* in March 2010, Nantes, France.

Palut, J.M., Montarnal, Ph., Gautschi, A., Tevissen, E., Mouche, E., 2003. Characterisation of HTO diffusion properties by an in situ tracer experiment in Opalinus Clay at Mont Terri. *Journal of Contaminant Hydrology* 61, 203-218.

Pearson, F.J., Arcos, D., Bath, A., Boisson, J.-Y., Fernández, A.M., Gäbler, H.-E., Gaucher, E., Gautschi, A., Griffault, L., Hernán, P., Waber, H.N., 2003. Geochemistry of water in the Opalinus clay formation at the Mont Terri Rock Laboratory. *Reports of Federal Office for Water and Geology*, Bern, Geology Series No. 5, Switzerland.

Samper, J., Yang, C., Naves, A., Yllera, A., Hernández, A., Molinero, J., Soler, J.M., Hernán, P., Mayor, J.C., Astudillo, J., 2006. A fully 3-D anisotropic numerical model of the DI-B in situ diffusion experiment in the Opalinus Clay formation. *Physics and Chemistry of the Earth* 31, 531-540.

Samper, F.J., Dewonck, S., Zheng, L., Yang, Q., Naves, A., 2008a. Normalized sensitivities and parameter identifiability of in situ diffusion experiments on Callovo–Oxfordian clay at Bure site. *Physics and Chemistry of the Earth* 33, 1000–1008.

Samper, J., Yang, Q., Yi, S., García-Gutiérrez, M., Missana, T., Mingarro, M., Alonso, U., Cormenzana, J.L., 2008b. Numerical modeling of large-scale solid-source diffusion experiments in Callovo-Oxfordian clay. *Physics and Chemistry of the Earth* 33, S208-S215.

Samper, J., Yi, S., Naves, A., 2010. Analysis of the parameter identifiability of the in situ diffusion and retention (DR) experiment. *Physics and Chemistry of the Earth* 35, 207-216.

Soler, J.M., Samper, J., Yllera, A., Hernández, A., Quejido, A., Fernández, M., Yang, C., Naves, A., Hernán, P., Wersin, P., 2008. The DI_B in situ diffusion experiment at Mont Terri: Results and modeling. *Physics and chemistry of the Earth* 33, S196-S207.

Tevissen, E., Soler, J.M., Montarnal, Ph., Gautschi, A., Van Loon, L.R., 2004. Comparison between in situ laboratory characterization of HTO and halides diffusion in Opalinus Clay at the Mont Terri URL. Radiochimica Acta 92, 781-786.

Van Loon, L., Soler, J.M., Jakob, A., Bradbury, M.H., 2003. Effect of confining pressure on the diffusion of HTO, $^{36}Cl^-$ and $^{125}I^-$ in a layered argillaceous rock (Opalinus Clay): perpendicular to the fabric. *Applied Geochemistry* 18, 1653-1662.

Van Loon, L.R., Wersin, P., Soler, J.M., Eikenberg, J., Gimmi, T., Hernán, P., Dewonck, S., Savoye, S., 2004a. In-situ diffusion of HTO, $^{22}Na^+$, Cs^+ and I^- in Opalinus clay at the Mont Terri underground rock laboratory. *Radiochimica Acta* 92, 757–763.

Van Loon, L.R., Glauss, M.A., 2008. Effective Diffusion Coefficient of Several Tracers in Teflon Filters. *PSI Technical Note*, Switzerland.

Wersin, P., Van Loon, L.R., Soler, J.M., Yllera, A., Eikenberg, J., Gimmi, Th., Hernán, P., Boisson, J.-Y., 2004. Long-term diffusion experiment at Mont Terri: first results from field and laboratory data. *Applied Clay Science* 26, 123-135.

Wersin, P., van Dorp, F., 2005. Diffusion and retention (DR) experiment in borehole BDR-1 Phase 11 (1 July 2005-30 June 2006): radiation protection and working plan. *Mont Terri Project Technical Note* 2005-47.

Wersin, P., Baeyens, B., Bossart, P., Cartalade, A., Dewonck, S., Eikenberg, J., Fierz, T., Fisch, H.R., Gimmi, T., Grolimund, D., Hernán, P., Möri, A., Savoye, S., Soler, J.M., van Dorp, F., Van Loon, L., 2006. Long-term diffusion experiment (DI-A): Diffusion of HTO, I^-, $^{22}Na^+$ and Cs^+. Field activities, data and modeling. *Mont Terri Technical Report* TR 2003-06.

Wersin, P., Soler, J.M., Van Loon, L., Eikenberg, J., Baeyens, B., Grolimund, D., Gimmi, Th., Dewonck, S., 2008. Diffusion of HTO, Br^-, I^-, Cs^+, $^{85}Sr^{2+}$ and $^{60}Co^{2+}$ in a clay formation: results and modeling from an in situ experiment in Opalinus Clay. *Applied Geochemistry* 23, 678-691.

Yllera, A., Hernández, A., Mingarro, M., Quejido, A., Sedano, L.A., Soler, J.M., Samper, J., Molinero, J., Barcala, J.M., Martín, P.L., Fernández, M., Wersin, P., Rivas, P., Hernán, P., 2004. DI-B experiment: planning, design and performance of an in situ diffusion experiment in the Opalinus Clay formation. *Applied Clay Science* 26, 181-196.

APPENDIX 9

IN SITU DIFFUSION EXPERIMENTS: EFFECT OF WATER SAMPLING ON TRACER CONCENTRATIONS AND PARAMETERS

This appendix presents a paper presented at the international conference MIGRATION07 which took place in Munich (Germany) in August 2007 and was also published in Physics and Chemistry of the Earth in 2008.

All the modeling tasks were performed by the author of this dissertation under the supervision of her advisor Javier Samper and Sarah Dewonck, her co-advisor during her stay at the Meuse/Haute-Marne Underground Research Laboratory (France).

Physics and Chemistry of the Earth 35 (2010) 242–247

Contents lists available at ScienceDirect

Physics and Chemistry of the Earth

journal homepage: www.elsevier.com/locate/pce

In situ diffusion experiments: Effect of water sampling on tracer concentrations and parameters

A. Naves [a,*], S. Dewonck [b], J. Samper [a]

[a] *ETSEICCP Universidad de Coruña. Campus de Elviña, 15192 A Coruña, Spain*
[b] *ANDRA, Laboratoire souterrain de recherche de Meuse/Haute-Marne, 55290 Bure, France*

ARTICLE INFO

Article history:
Received 26 October 2009
Received in revised form 12 March 2010
Accepted 10 April 2010
Available online 24 April 2010

Keywords:
Diffusion
Sorption
Numerical model
Sampling
Aliquoting
In situ diffusion experiments

ABSTRACT

In situ diffusion experiments are performed at underground research laboratories (URL) in clay formations to overcome the limitations of laboratory diffusion experiments and investigate scale effects. Tracers are monitored in the circulation system by aliquoting the solution at selected times. The extracted samples may be replaced with the same volume of synthetic unspiked water as it is done in the Bure URL (France). Sampling with replacement induces the tracer dilution. In the sampling method used in the Mont Terri URL (Switzerland), on the other hand, sampling volumes are not replaced. In this case, there is no tracer dilution, but the volume in circulation decreases progressively. Water sampling is commonly disregarded in the numerical interpretation of such experiments. However, water sampling may induce changes in the tracer concentrations and errors in the estimated diffusion and sorption parameters. Such errors have been analyzed here with a numerical model which accounts for sample extraction, sample replacement and the changes in the volume of the circulation system. These errors have been analyzed for HTO, $^{36}Cl^-$, $^{22}Na^+$ and $^{134}Cs^+$ in the DIR2003 and EST 208 experiments at the Bure URL and for HTO, HDO, Br^-, $^{22}Na^+$, $^{85}Sr^{2+}$, $^{133}Ba^{2+}$ and $^{137}Cs^+$ in the DR experiments at the Mont Terri URL. The effect of water sampling on the relative tracer concentrations depends on the sampling method and frequency, the volume of the sample and the volume of the circulation system. Water sampling causes minor differences in relative tracer concentrations in the DR experiments and its effect can be disregarded. In the DIR2003 experiment, however, the differences induced by aliquoting cannot not be neglected. $^{36}Cl^-$ is the tracer most affected by sampling and $^{134}Cs^+$ is the least influenced. The identifiability analysis of the EST208 experiment reveals that failing to account for the effect of water sampling may lead to a significant overestimation of diffusion and sorption parameters, especially for $^{36}Cl^-$. The results of our analysis indicate that the effects of the water sampling should not be neglected without a careful in-depth analysis.

1. Introduction

Argillaceous rocks have been selected in many countries to host repositories for the disposal of radioactive waste. The diffusion and retention of radionuclides through such rocks are relevant for assessing the performance of repositories. Most of the experimental work in this field has focused on laboratory experiments performed on small samples. *In situ* diffusion experiments are performed at underground research laboratories (URL) in clay formations to overcome the limitations of laboratory diffusion experiments and to investigate possible scale effects. Such experiments have been performed in Opalinus clay in Switzerland (Palut et al., 2003; Tevissen et al., 2004; Wersin et al., 2004; van Loon et al., 2004; Yllera et al., 2004; Samper et al., 2006; Soler et al., 2008) and Callovo-Oxfordian clay at Bure in France (Dewonck, 2007; Delay et al., 2007a).

In situ diffusion experiments in clay media involve several steps (Palut, 2001). First, tracers are diluted in a synthetic solution with a chemical composition similar to that of the formation porewater. Such water comes into contact with the clay formation in the injection chamber consisting of a borehole section isolated by packers. The injection chamber is located far enough from the gallery surface so that the test is performed on saturated clay not significantly disturbed by the construction of the gallery. In order to avoid physical perturbations in the injection section, the hydraulic pressure is fixed to a value similar to the measured interstitial pressure of the formation. The tracers are let to diffuse in the rock. Tracer activities are monitored at the circulation system by aliquoting samples at selected times. After this step, the rock around the borehole where tracers have diffused is overcored. Rock samples are taken and analyzed. Tracer diffusion and sorption parameters are derived from tracer dilution and overcore concentration data.

* Corresponding author.
E-mail address: anaves@udc.es (A. Naves).

1474-7065/$ - see front matter © 2010 Elsevier Ltd. All rights reserved.
doi:10.1016/j.pce.2010.04.009

Generally the effect of water sampling on the interpretation of *in situ* diffusion experiments is neglected when the total volume of the water samples is much smaller than the volume of the circulation system. Water samples extracted from the circulation system decrease the tracer mass, which may affect the evolution of relative tracer concentrations in a non negligible manner. Existing analytical and numerical methods for the interpretation of these experiments usually neglect water sampling. In some cases such as the DIR experiments at Bure URL the total volume of the samples is not negligible (CEA, 2008). Failing to account for the effect of the water sampling may induce errors in the estimated diffusion and sorption parameters. Such errors are analyzed here with a numerical model which accounts for sample extraction, sample replacement and the changes in the volume of the circulation system. The paper starts by describing the *in situ* diffusion experiments and the numerical methods used for their interpretation. The effect of water sampling on the DIR2003 experiment of Bure URL is described. Then, different sampling methods are compared for the conditions of the DIR2003 experiment. The relevance of the sampling volume and frequency is analyzed afterwards. Then, the effect of water sampling on the estimated parameters is discussed. Finally, the main conclusions are presented.

2. DIR and DR *in situ* diffusion experiments

The French National Agency for radioactive waste management (ANDRA) has undertaken an extensive characterization program at the Bure (Meuse/Haute-Marne) site in order to assess the feasibility of a deep high level waste repository in the Callovo-Oxfordian clay (Delay et al., 2007b). Diffusion of inert and reactive tracers (DIR) is one of such experimental programs which aims at characterizing diffusion and retention of radionuclides in this formation.

Seven *in situ* diffusion experiments were performed in vertical boreholes in the Bure underground laboratory to derive diffusion and retention parameters of selected tracers. Experiments DIR2001, DIR2002 and DIR2003 have been carried out in boreholes drilled from a gallery located at a depth of ~450 m. Experiments DIR1001, DIR1002 and DIR1003 have been carried out in boreholes from a gallery located at ~490 m depth corresponding to the main level of the laboratory. Experiment EST208 is taking place in a 542.5 m depth borehole drilled from the ground surface.

DIR *in situ* diffusion experiments were performed as single-point dilution tests by injecting tracers into a 1 m long packed-off section into the boreholes. The required equipment included downhole and surface instrumentation (Palut, 2001). Downhole instrumentation consisted of a pneumatic packer system with a porous screen made of sintered stainless steel mounted just below the packer at the bottom of the borehole. Surface instrumentation included a stainless steel circuit to circulate the tracer solution and to allow for injection and sampling of tracers. The volume of synthetic water in the circulation system is about 10 L for all the DIR experiments. The tracer activities at the injection section were monitored during approximately 1 year for the following tracers: tritium (HTO), chloride ($^{36}Cl^-$), iodide ($^{125}I^-$), sodium ($^{22}Na^+$), strontium ($^{85}Sr^+$), selenium ($^{75}Se^{2+}$) and cesium ($^{134}Cs^+$). Chloride and iodide are subject to anion exclusion while sodium, strontium, selenium and cesium undergo sorption.

The design of the EST208 experiment differs from that of the DIR experiments because EST208 was performed in a deep borehole drilled from ground surface. Downhole instrumentation consists of a 10 m long packed diffusion interval with a stainless steel porous filter and two hydraulic lines for flux circulation. One allows the circulation from the diffusion chamber to the ground surface. The other ensures the water flow along the surface equipment used for monitoring the geochemical parameters and the extraction of water samples during the experiment. The circulation system contains 192.3 L of synthetic solution containing tritium (HTO), chloride ($^{36}Cl^-$) and cesium ($^{134}Cs^+$).

The injection section is composed of an empty central steel cylinder and a 3 mm thick steel filter between which the fluid containing the tracer cocktail circulates. There is a gap of 3 mm between the filter and the borehole wall. This gap is initially filled with artificial water injected during the hydraulic equilibration period. Later on, water in contact with argillite forms probably a viscous mud.

The DR experiment is an on-going *in situ* diffusion experiment within the Mont Terri Project (Mont Terri URL, Switzerland). This experiment is being performed in a borehole drilled into Opalinus clay normal to the bedding and focuses on the study of tracer retention and diffusion anisotropy. The two 15 cm long injection intervals are isolated by packers installed in the borehole. Each interval is connected to the surface equipment. The fluid circulates continuously such, that the tank water and the downhole water are always well mixed. The circulation system contains 20 L of synthetic porewater. The following tracers are injected in the upper interval: $^{60}Co^{2+}$, $^{137}Cs^+$, $^{133}Ba^{2+}$, $^{152}Eu^{3+}$, HDO. In the lower interval the tracers are HTO, $^{22}Na^+$, $^{85}Sr^{2+}$, I^-, Br^-, $^{75}Se^{4+}$ and ^{18}O. The injection of the tracer cocktails started in April 2006. Overcoring of the experiment took place at the beginning of 2010 (Fierz, 2006; Gimmi et al., 2009).

3. Numerical methods

The numerical interpretation of DIR experiments requires the use of 3D models due to diffusion anisotropy. However, symmetry with respect to the borehole axis allows the use of 2D axi-symmetric models. The relevance of diffusion anisotropy on tracer evolution at the test interval was evaluated by Samper et al. (2008) with a 1D axi-symmetric model. The gap and the filter are taken into account in the model. Therefore, five material zones are considered: the injection zone, the filter, the gap, a 2 cm thick excavation disturbed zone (EdZ) and the undisturbed Callovo-Oxfordian (COx) clay. The values of the effective diffusion, the accessible porosity and the distribution coefficient of each tracer in COx clay were derived from available through-diffusion laboratory experiments (Dewonck, 2007; Descostes et al., 2007). They are listed in Table 1. The distribution coefficient, K_d, for $^{22}Na^+$ in COx clay is assumed to be equal to 0.74 ml/g (Radwan et al., 2005). For $^{134}Cs^+$ a K_d of 50 ml/g was used. The effective diffusion coefficients for other materials were derived from those of undisturbed clay by adopting an Archie's law with an exponent equal to 4/3. The filter porosity is 0.3 (Dewonck, 2007). On the other hand, the porosities of the EdZ and the gap are unknown. As an educated guess, the porosity of the EdZ was assumed to be twice that of the clay while the porosity of the gap was assumed to be 0.6. The undisturbed clay and the EdZ were assumed to have the same distribution coefficient.

The diffusion anisotropy of the Opalinus clay is larger than that of the COx clay. Therefore, a 2D axi-symmetric model is needed to simulate and interpret the concentration of the tracers in the injection section (Samper et al., 2010). Several non-ideal factors must be taken into account such as the existence of the filter (3 mm thick), the gap (2 mm thick) between the filter and the borehole wall and the excavation disturbed zone (EdZ). Therefore, five material zones are considered: the injection system, the filter, the gap, the EdZ and the undisturbed clay. The simulation of the DR experiment is performed for the reference values of the diffusion and sorption parameters of the tracer in the Opalinus clay. These values have been derived from laboratory experiments and previous *in situ* diffusion experiments and are similar to those of the COx clay. However, an anisotropy ratio of 4 has been considered.

Table 1
Reference values of tracer diffusion and sorption parameters in the different materials for the DR experiments. D_e is the horizontal effective diffusion, Φ_{acc} is the accessible porosity and K_d is the distribution coefficient.

	HTO	$^{36}Cl^-$	$^{125}I^-$	$^{22}Na^+$	$^{134}Cs^+$
Clay					
D_e (m/s^2)	4.1×10^{-11}	9.1×10^{-12}	4.4×10^{-12}	6.7×10^{-11}	3.6×10^{-10}
Φ_{acc}	0.18	0.09	0.13	0.18	0.18
K_d (ml/g)	–	–	–	0.74	50
EdZ					
D_e (m/s^2)	10^{-10}	2.3×10^{-11}	1.1×10^{-11}	1.7×10^{-10}	9×10^{-10}
Φ_{acc}	0.36	0.18	0.26	0.36	0.36
K_d (ml/g)	–	–	–	0.74	50
Gap					
D_e (m/s^2)	2×10^{-10}	1.1×10^{-10}	3.4×10^{-11}	3.3×10^{-10}	1.8×10^{-9}
Φ_{acc}	0.6	0.6	0.6	0.6	0.6
K_d (ml/g)	–	–	–	0.74	50
Filter					
D_e (m/s^2)	$8{\cdot}10^{-11}$	$4.5{\cdot}10^{-11}$	$1.3{\cdot}10^{-11}$	$1.3{\cdot}10^{-10}$	$7.1{\cdot}10^{-11}$
Φ_{acc}	0.3	0.3	0.3	0.3	0.3

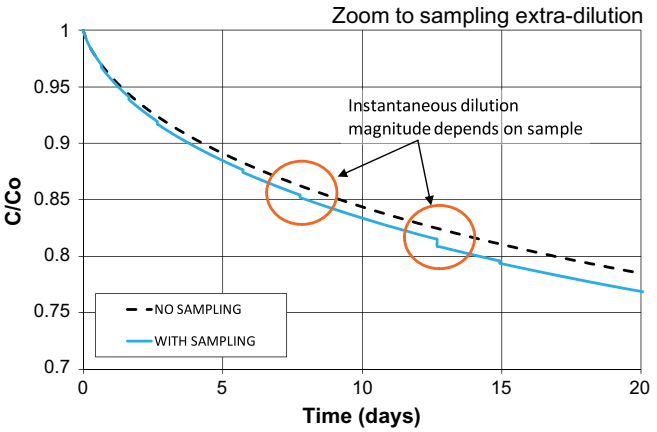

Fig. 1. Comparison of HTO dilution curves computed during the first 20 days of the DIR2003 experiment with and without water sampling. It can be seen the discontinuities associated with the aliquoting and the replacement of the sample volume with untraced synthetic water. The size of the discontinuity depends on the volume of the sample.

4. Effect of sampling on computed concentrations at DIR2003 experiment

Tracers are monitored in the circulation system by aliquoting samples at selected times during the *in situ* diffusion experiment. Extracted samples are replaced with samples of the same volume of synthetic unspiked solution in experiments performed at Bure URL. In this way, the pressure and the volume of water in the circulation system remain unchanged during the experiment. However, a tracer dilution is induced by this replacement.

The tracer mass in the system after sampling, m_f, is equal to the initial mass before the water sampling, m_i, minus the mass contained in the water sample, m_s. Values of m_i and m_s can be expressed in terms of the concentration in the system before sampling, C_i, the total volume of the system, V, and the volume of the sample, V_s, through:

$$M_f = m_i - m_s = C_i(V - V_s) \quad (1)$$

The tracer concentration in the injection interval after water sampling, C_f, can be calculated from m_f and V through:

$$C_f = C_i\left(1 - \frac{V_s}{V}\right) \quad (2)$$

The dilution caused by sampling, ΔC, is given by:

$$\Delta C = C_f - C_i = -C_i\frac{V_s}{V} \quad (3)$$

The dilution depends on the volume of the circulation system, the tracer concentration before sampling and the volume of the aliquot. The effect of water sampling on tracer concentrations, C, is evaluated here in terms of the relative concentrations, $\frac{C}{C_0}$, where C_0 is the tracer concentration at $t = 0$.

Therefore, aliquoting induces an instantaneous decrease of the tracer concentration in the circulation system (Fig. 1). At that time, the tracer concentration in the injection section is smaller than the concentration in the rock at the vicinity of the borehole. Thus, a mass flux from the rock to the borehole takes place during a short period of time until both concentrations reach a similar value. In addition, the decrease of the tracer concentration in the injection interval decreases the concentration gradient between the borehole and the rock and slows down the tracer diffusion from the borehole into the rock. Although the effect of taking several samples is cumulative, the total difference in computed concentrations at the circulation system is not simply equal to the sum of the differences caused by each aliquot. Quantifying the effect of water sampling requires the use of a numerical model accounting for sample aliquoting and replacement.

The relevance of water sampling on relative tracer concentrations for the DIR2003 experiment has been evaluated here by analyzing the differences in relative concentrations computed with simulations which either ignore or take into account the water sampling. Simulations are performed with the same 1D axi-symmetric model used for the interpretation of dilution data (Samper et al., 2008). The simulation is interrupted at each sampling time and relative tracer concentrations are adjusted according to the dilution ΔC of Eq. (3). Aliquots have volumes of either 25 or 75 ml.

HTO was injected at the beginning of the DIR2003 experiment. $^{36}Cl^-$, $^{22}Na^+$ and $^{134}Cs^+$ were injected 434 days later. This feature of the DIR2003 experiment allows us to study the effect on the dilution of HTO of the second injection of tracers and the intensive sampling associated to such injection. Fig. 2 shows the comparison of the dilution curves for the entire experiment and all the tracers computed with and without sampling for each tracer. There is a clear discontinuity in the dilution curve of HTO caused by the large number of samples taken just after the second tracer injection.

The differences in the relative tracer concentrations computed with and without water sampling for the DIR2003 experiment are listed in Table 2. For conservative tracers the differences in computed concentrations increase with time. After 1 year, tracers are not affected in the same way. $^{36}Cl^-$ is the tracer most affected with a difference in relative concentrations of 0.074. For HTO, $^{22}Na^+$ and $^{134}Cs^+$ the differences are equal to 0.033, 0.013 and 0.0002, respectively. The stronger the sorption, the smaller the effect of water sampling. Eq. (3) provides the hints to explain the different effects of sampling on the concentrations of each tracer. Though the volume of the system and the sampling volumes are the same for all the tracers, the concentration in the circulation system before sampling, C_i, is different for each tracer depending on its diffusion and sorption properties. The slower the dilution of a tracer, the larger its concentration before sampling, C_i, and therefore, the larger the effect caused by the water sampling.

5. Comparison of sampling methodologies at DIR2003 experiment

The sampling methodologies used in the *in situ* diffusion experiments in Mont Terri and Bure URL's are different. In Mont Terri water samples are not replaced. The reduction in water pressure

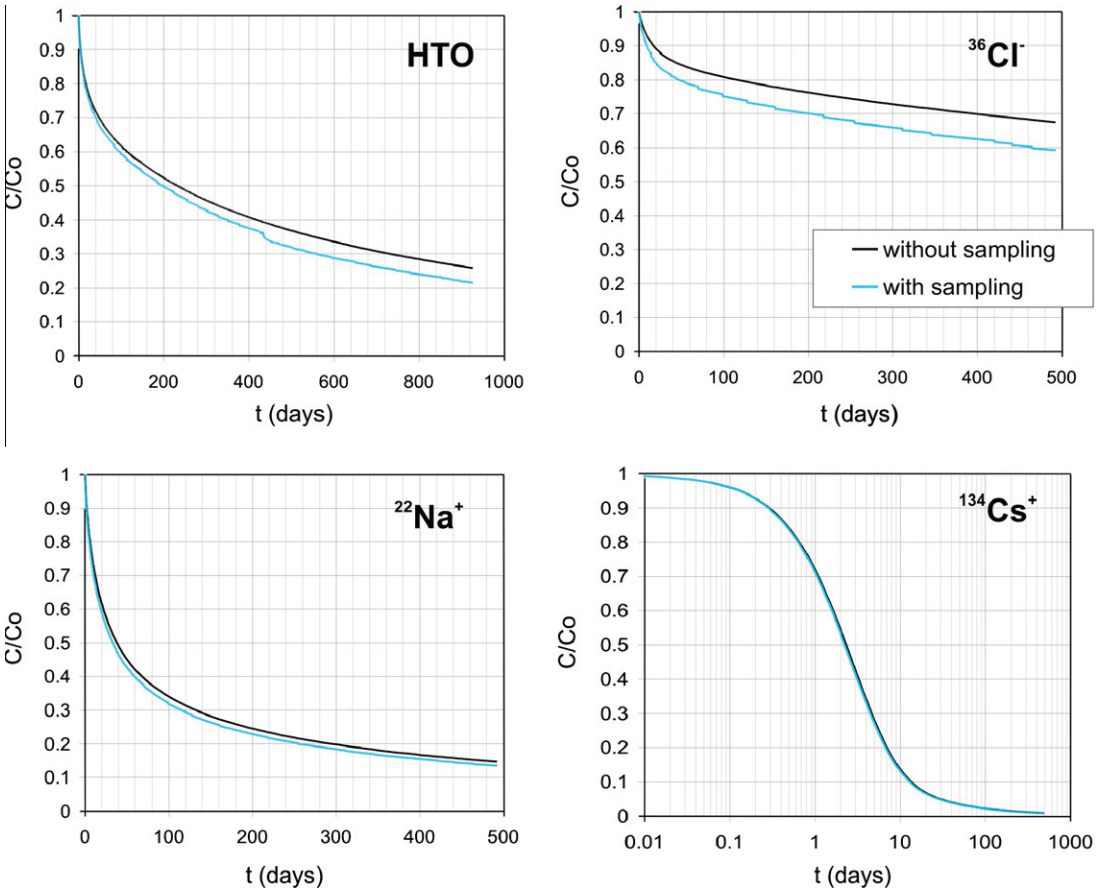

Fig. 2. Comparison of the dilution curves of the DIR2003 experiment computed with and without sampling. The discontinuity in the dilution curve of HTO is related to the second tracer injection.

Table 2
Differences in the relative tracer concentrations computed with and without aliquoting for the DIR2003 experiment.

	HTO	$^{36}Cl^-$	$^{22}Na^+$	$^{134}Cs^+$
10 days	0.01	0.035	0.023	0.009
50 days	0.021	0.046	0.021	0.0005
100 days	0.022	0.057	0.022	0.0008
1 year	0.033	0.074	0.013	0.0002

caused by the decrease of water in the circulation system is equilibrated by injecting gases. In this case, there is no direct tracer dilution, but a progressive reduction of the volume of the circulation system, V, which speeds up the tracer dilution.

Sampling methods with and without replacement have been compared for the conditions of the DIR2003 experiment. The experiment has been simulated by taking into account actual sampling volumes and dates. Fig. 3 shows the computed dilution curves of $^{36}Cl^-$ and $^{22}Na^+$ for: (1) No sampling, (2) sampling with replacement and (3) sampling with no replacement. Table 3 shows the differences in relative tracer concentrations computed with and without sampling at t = 1 year for each type of water sampling procedure (with and without volume replacement). Tracers suffering from anion exclusion are the most affected by the water sampling in both types of methods. On the other hand, water sampling has the smallest effect on the curves of the sorbing tracers. Other things being the same, the replacement of the water samples leads to differences which are larger than those of the no-replacement case for $^{36}Cl^-$ and HTO. For $^{22}Na^+$. However, the difference is larger in the case where the samples are not replaced.

In addition to water sampling, γ-emitter tracers can be monitored online with γ-counting techniques which were successfully tested in the DI-A and DR experiments at the Mont Terri URL (Fierz, 2006; Gimmi et al., 2009). On-line measurement of tracer activities in the circulation system provides a way to reduce the sampling frequency and the effect of the water sampling on tracer dilution data.

6. Relevance of the sampling volume and frequency

Aliquoting affects the relative tracer concentrations in the DIR2003 experiment in a significant manner. The effect of water sampling on tracer concentrations depend on: (1) The diffusion and sorption properties of each tracer, (2) The sampling method (with or without replacement), (3) The sampling frequency, (4) The volume of the samples, and (5) The volume of the circulation system. The first two factors were analyzed in previous sections. Here the influence of the other three is analyzed by analyzing the effect of water sampling in diffusion experiments having different designs such as the DIR2003, the EST208 and the DR experiments.

The EST208 experiment is being performed in a 10 m long packed diffusion interval of a deep borehole. The volume of the circulation system is about 20 times larger than that of the DIR2003 experiment. The sampling frequency is similar for both experiments but the EST208 sample volume is 150 ml which is twice as much as that of DIR2003 experiment. HTO, $^{36}Cl^-$ and $^{134}Cs^+$ are used as tracers. The differences in relative tracer concentrations in the injection interval computed with and without sampling for

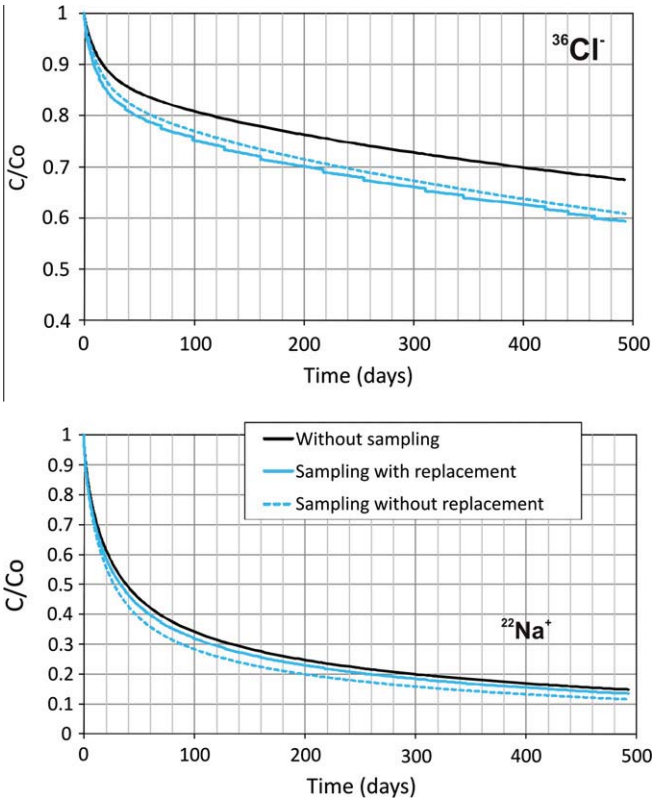

Fig. 3. Comparison of the dilution curves computed: (1) without water sampling, (2) with water sampling and replacement (method used in Bure), and (3) with water sampling and no replacement (Mont Terri method) for $^{36}Cl^-$ and $^{22}Na^+$.

Table 3
Differences in the relative tracer concentrations computed with and without aliquoting for the DIR2003 experiment at $t = 1$ year assuming that the aliquots are replaced or not.

Replacement of aliquots	HTO	$^{36}Cl^-$	$^{22}Na^+$	$^{134}Cs^+$
Yes	0.033	0.074	0.013	0.0002
No	0.013	0.059	0.037	0.002

Table 4
Differences in the relative tracer concentrations at different times computed with and without aliquoting for the EST208 experiment.

	HTO	$^{36}Cl^-$	$^{134}Cs^+$
10 days	0.003	0.003	<0.0001
50 days	0.007	0.009	<0.0001
100 days	0.007	0.009	<0.0001
1 year	0.007	0.011	<0.0001
2 year	0.008	0.014	<0.0001
3 year	0.008	0.016	<0.0001

the EST208 experiment are listed in Table 4. These differences in concentrations are much smaller than those obtained for the DIR2003 experiment. It should be noticed that the ratio V_s/V for the EST208 experiment is much smaller than that of the DIR2003 experiment. Therefore, the dilution caused by water sampling is less relevant for the EST208 experiment than in the DIR2003 experiment. At $t = 3$ years the differences are smaller than 0.02 for all the tracers. On the other hand, $^{36}Cl^-$ is the tracer most affected while $^{134}Cs^+$ is the least influenced.

The effect of water sampling has also been analyzed in the DR experiments where extracted sample volumes are small and are not replaced. The effect of sampling has been neglected in all the previous modelling tasks performed for this experiment because the total volume of the samples is smaller than the volume of the circulation system, $V \sim 20$ L. The effect of water sampling in the relative concentrations has been evaluated for the DR experiments using a numerical model which takes into account the changes in the volume of the circulation system. Dates and sample volumes have been considered for the first 1106 days. The differences in relative concentrations in the injection interval at $t = 3.6$ years computed with and without sampling are listed in Table 5. The differences in relative tracer concentrations caused by sampling are equal or smaller than 0.01 for all the tracers. Such errors are smaller than those computed for the DIR2003 experiment at $t = 1$ year by assuming no water replacement (Table 3). These results are consistent with the values of $\frac{V_s}{V}$ of these experiments. Sample volumes in the DR experiments are smaller than those of the DIR2003 experiment while the volume of the circulation system of the DR experiments is twice of that of the DIR2003 experiment.

7. Effect of sampling on estimated parameters

Synthetic experiments have been used to study parameter identifiability and parameter uncertainties at DIR2001, DIR2002 and EST208. Synthetic data have been generated in order to provide insight on the inverse estimation of diffusion and sorption experiments and to study parameter identifiability. Key diffusion parameters have been estimated from noisy synthetic data generated with a numerical model having known parameters. Here we present the identifiability analysis to evaluate the parameter estimation errors caused by failing to account for the water sampling. A synthetic diffusion experiment having the same geometric properties as the real EST208 experiment was simulated. This model takes into account the water sampling.

Parameters are estimated from synthetic data using a numerical model which neglects sampling. Inverse runs are performed with INVERSE-CORE^{2D} (Dai and Samper, 2004) following a systematic approach according to which: (1) The D_e of the filter and the D_e of the gap are estimated first using early-time data collected during the first 10 days; (2) then, the D_e of the filter and the D_e of the gap are fixed to their estimated values and the D_e of the EdZ and the accessible porosity of the EdZ are estimated using concentration data measured until 50–100 days; and (3) the D_e and the accessible porosity of the undisturbed clay are estimated using all the concentration data while the remaining parameters are fixed to values estimated in steps 1 and 2. Since true values are known and data are free of noise, one can compute the parameter estimation error caused by failing to account for the water sampling. The D_e of the undisturbed clay for HTO is overestimated by 10%. A good fit to $^{36}Cl^-$ data is obtained with values of the D_e of the undisturbed clay and the EdZ which are overestimated by 10–20% and unrealistically too large accessible porosities of the EdZ and the rock (Fig. 4). These large estimation errors for $^{36}Cl^-$ dilution data are caused by the large effect of water sampling on $^{36}Cl^-$ dilution data and by the poor identifiability of the parameters of this tracer when data contain noise (Samper et al., 2008). If accessible porosities are fixed to their true values, the estimation errors of the D_e of the clay and the EdZ are even larger than before.

Table 5
Differences in the relative tracer concentrations at $t = 3.6$ years computed with and without aliquoting for the DR experiment.

HTO	0.006
HDO	0.007
Br^-	0.003
$^{22}Na^+$	0.008
$^{85}Sr^{2+}$	0.009
$^{133}Ba^{2+}$	0.01
$^{137}Cs^+$	0.001

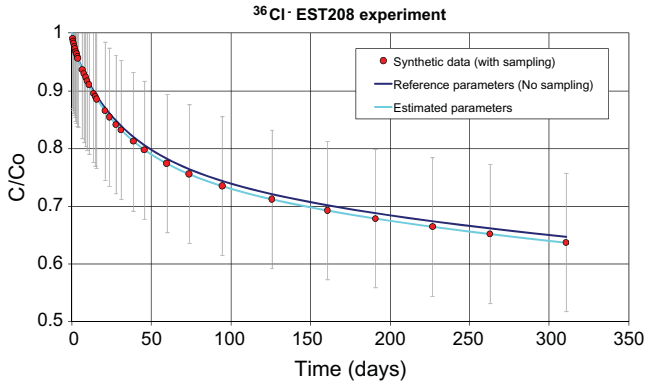

Fig. 4. Synthetic $^{36}Cl^-$ data generated with a model that takes into account water sampling and fit with a model that neglects water sampling. Error bars of synthetic data are similar to those of the real data.

Errors in computed concentrations with and without sampling after 1 year for $^{134}Cs^+$ are smaller than 1%. Therefore, estimation errors of diffusion and sorption parameters are small.

8. Conclusions

The effect of water sampling in relative tracer concentrations in the injection interval of *in situ* diffusion experiments has been analyzed with a numerical model which accounts for sample extraction, sample replacement and the changes in the volume of the circulation system. These effects have been analyzed for HTO, $^{36}Cl^-$, $^{22}Na^+$ and $^{134}Cs^+$ in the DIR2003 and EST 208 experiments at the Bure URL and for HTO, HDO, Br^-, $^{22}Na^+$, $^{85}Sr^{2+}$, $^{133}Ba^{2+}$ and $^{137}Cs^+$ in the DR experiments at the Mont Terri URL. The effect of the water sampling on tracer concentrations depend on: (1) The sampling method (with or without replacement of the volume of the sample); (2) the sampling frequency; (3) the volume of the sample; and (4) the total volume of the circulation system.

It has been found that water sampling in the DR experiments causes minor changes in the relative tracer concentrations. Therefore, its effect can be disregarded. In the DIR2003 experiment, however, the differences induced by the water sampling cannot be neglected. After 1 year, $^{36}Cl^-$ is the tracer most affected by sampling with a difference in relative concentration equal to 0.074. $^{134}Cs^+$ is the least affected with a very small difference. Furthermore, the simulation of this experiment shows that a second injection of tracers and the intensive sampling associated with it generates a clear discontinuity in the dilution trend of the tracer. The identifiability analysis of the EST208 experiment reveals that failing to account for the effect of water sampling may lead to a significant overestimation of diffusion and sorption parameters, especially for $^{36}Cl^-$.

The results of our analysis indicate that the effects of the water sampling should not be neglected without a careful in-depth analysis. They also provide practical guidelines for optimizing the tracer sampling of *in situ* diffusion experiments. Therefore, the effect of sampling can be minimized regardless the sampling method by optimizing the design of the experiment. If the design of the experiment is not optimized, the sampling effect can be reduced by using on-line tracer monitoring techniques.

Acknowledgements

This work was supported by ANDRA and the Spanish Ministry of Science and Technology through the Research Project CGL2006-09080 and a FPI Research Scholarship awarded by the Spanish Ministry to the first author. We are grateful to the two anonymous reviewers for their comments and recommendations which improved the paper.

References

CEA, 2008. Report on first sensitive study of a generic *in situ* tracer injection experiment. FUNMIG Report (Contract no. FP6-516514): PID 3.3.6.

Dai, Z., Samper, J., 2004. Inverse problem of multicomponent reactive chemical transport in porous media: formulation and applications. Water Resour. Res. 40, W07407.

Delay, J., Distinguin, M., Dewonck, S., 2007a. Characterization of a clay-rich rock through development and installation of specific hydrogeoloical and diffusion test equipment in deep boreholes. Phys. Chem. Earth 32, 393–407.

Delay, J., Vinsot, A., Krieguer, J.M., Rebours, H., Armand, G., 2007b. Making of the underground scientific experimental programme at the Meuse/Haute-Marne underground research laboratory, North Eastern France. Phys. Chem. Earth 32, 2–18.

Descostes, M., Blin, V., Radwan, J., Grenut, B., Meier, P., Herbette, M., Claret, F., Latrillen, C., Tevissen, E., 2007. Evaluation des paramètres diffusifs de HTO et 36Cl-sur échantillons des forages DIR2001, DIR2002 et EST207 – Expérience DIR L-04.

Dewonck, S., 2007. Expérimentation DIR. Synthese des résultats obtenus au 01/03/07. Laboratoire de recherche souterrain de Meuse/Haute-Marne. ANDRA Report D.RP.ALS.07-0044.

Fierz, T., 2006. Diffusion and retention experiment field activities phase 11: Instrumentation and tracer injection. Mont Terri Project TN 06-18.

Gimmi, Th., Leupin, O.X., Van Loon, L.R., Wersin, P., Baeyens, B., Eikenberg, J., Soler, J.M., Samper, J., Rübel, A., Dewonck, S., Savoye, S., Yi, S., Naves, A., 2009. A field-scale solute diffusion and retention experiment in Opalinus clay: processes, parameters, sensitivities. Poster Presented at 2009 EGU Meeting in Vienna, Austria.

Palut, J.M., 2001. Spécifications générales – Expérimentation DIR – Essai de Diffusion de Traceurs Inertes et Réactifs. Rapport Andra D.SP.ADPE.01.097.

Palut, J.M., Montarnal, P., Gautschi, A., Tevissen, E., Mouche, E., 2003. Characterisation of HTO diffusion properties by an *in situ* tracer experiment in Opalinus clay at Mont Terri. J. Contam. Hydrol. 61 (1), 203–218.

Radwan, J., Tevissen, E., Descostes, M., Blin, V., 2005. Premiers elements d'interprétation et de modélisation des expériences de diffusion de traceurs inertes et réactifs en laboratoire souterrain de Meuse/Haute-Marne. Note Technique CEA NTDPC/SECR 05-046/A.

Samper, J., Yang, C., Naves, A., Yllera, A., Hernández, A., Molinero, J., Soler, J.M., Hernán, P., Mayor, J.C., Astudillo, J., 2006. A fully 3-D anisotropic model of DI-B *in situ* diffusion experiment in the Opalinus clay formation. Phys. Chem. Earth 31, 531–540.

Samper, J., Dewonck, S., Zheng, L., Yang, Q., Naves, A., 2008. Normalized sensitivities and parameter identifiability of *in situ* diffusion experiments on Callovo-Oxfordian clay at Bure site. Phys. Chem. Earth 33, 1000–1008.

Samper, J., Yi, S., Naves, A., 2010. Analysis of parameter identifiability of the *in situ* diffusion and retention (DR) experiments. Phys. Chem. Earth 35 (6–8), 207–216.

Soler, J.M., Samper, J., Yllera, A., Hernández, A., Quejido, A., Fernández, M., Yang, C., Naves, A., Hernán, P., Wersin, P., 2008. The DI-B in-situ diffusion experiment at Mont Terri: results and modeling. Phys. Chem. Earth 33 (Suppl. 1), S196–S207.

Tevissen, E., Soler, J.M., Montarnal, P., Gautschi, A., Van Loon, L.R., 2004. Comparison between *in situ* and laboratory diffusion studies of HTO and halides in Opalinus clay from the Mont Terri. Radiochim. Acta 92, 781–786.

Van Loon, L.R., Wersin, P., Soler, J.M., Eikenberg, J., Gimmi, Th., Hernán, P., Dewonck, S., Savoye, S., 2004. In-situ diffusion of HTO, $^{22}Na^+$, Cs^+ and I^- in Opalinus clay at the Mont Terri underground rock laboratory. Radiochim. Acta 92, 757–763.

Wersin, P., Van Loon, L.R., Soler, J., Yllera, A., Eikenberg, J., Gimmi, T., Hernan, P., Boisson, J.-Y., 2004. Long-term diffusion experiment at Mont Terri: first results from field and laboratory data. Appl. Clay Sci. 26, 123–135.

Yllera, A., Hernández, A., Mingarro, M., Quejido, A., Sedano, L.A., Soler, J.M., Samper, J., Molinero, J., Barcala, J.M., Martín, P.L., Fernández, M., Wersin, P., Rivas, P., Hernán, P., 2004. DI-B experiment: planning, design and performance of an *in situ* diffusion experiment in the Opalinus clay formation. Appl. Clay Sci. 26, 181–196.

APPENDIX 10

CONCEPTUAL AND NUMERICAL MODELS OF SOLUTE DIFFUSION AROUND A HLW REPOSITORY IN CLAY

This appendix presents the paper *"Conceptual and numerical models of solute diffusion around a HLW repository in clay"* which has been accepted for publication in *Physics and Chemistry of the Earth* in 2011. Previously, it was presented in the *4th International Meeting Clays In Natural & Engineered Barriers for Radioactive Waste Confinement* which took place in Nantes (France) in March 2010.

The paper is the result of a joint research work including the contributions from other researchers. The author participated in the development of the conceptual and numerical models of radionuclide diffusion and sorption of increasing dimensionality, the numerical simulations and the analysis of the model results.

Conceptual and numerical models of solute diffusion around a HLW repository in clay

J. Samper[1], A. Naves[1], C. Lu[2], Y. Li[1], B. Fritz[3] & A. Clement[3]

[1] ETS Ingenieros de Caminos, Canales y Puertos, Universidad de La Coruña, 15071-A Coruña, Spain, *jsamper@udc.es*

[2] Lawrence Livermore National Laboratory, P.O. Box 808, L-223, Livermore, CA 94550, USA, lu25@llnl.gov

[3] Laboratoire d'Hydrologie et de Géochimie de Strasbourg, Université de Strasbourg/EOST, CNRS, 1, rue Blessig, F-67084 Strasbourg Cedex, France, bfritz@unistra.fr.

ABSTRACT

Reactive transport models have been used to simulate solute diffusion, canister corrosion, interactions of the corrosion products with the bentonite and the long-term hydrochemical evolution of porewater composition around radioactive waste repositories. Such models usually rely on simplifications of the geometry and dimensionality of the problem. Detailed three-dimensional flow and transport models, on the other hand, are used which often oversimplify the geochemical reactions. There is a clear need to identify which simplifications and assumptions are admissible. Here we present conceptual and numerical models of radionuclide diffusion and sorption around a HLW repository in clay according to the French reference concept. Models of increasing dimensionality have been performed for: 1) 1D transport perpendicular to the axes of the disposal cells; 2) 1D axisymmetric transport around disposal cells for bounded and unbounded domains; 3) 2D transport through vertical planes; and 4) 1D vertical transport from the disposal cells into the overlying Oxfordian formation. Model results are compared for simulation times up to 10^6 years and for the following radionuclides and tracers: tritium, HTO, which is treated here as an ideal and conservative tracer, $^{36}Cl^-$ which experiences anion exclusion, $^{133}Cs^+$ which sorbs moderately and ^{238}U which shows a strong sorption capacity. Radionuclides are released into the disposal cell either at a fixed concentration or as an instantaneous unit pulse. Model results indicate that the 1D unbounded model is always acceptable for ^{238}U and is valid for $^{133}Cs^+$ for $t < 10^4$ years. It is valid for HTO and $^{36}Cl^-$ only for $t < 10^3$ years. These conclusions hold true for both release modes. Computed concentrations with the 1D parallel and the 1D axisymmetric models are significantly different. Inasmuch as solute diffusion in a radioactive waste repository is expected to show radial symmetry around the cells, the use of the axisymmetric model is strongly recommended for the long-term modeling of radionuclide migration from the repository. The 1D vertical model is valid only for conservative radionuclides released instantaneously and leads always to large errors for all radionuclides for a constant concentration.

Keywords: solute diffusion, Callovo-Oxfordian clay, numerical model

1. INTRODUCTION

Reactive transport models have been used to simulate solute diffusion, canister corrosion, interactions of the corrosion products with the bentonite and the long-term hydrochemical evolution of porewater composition around radioactive waste repositories in clay formations (Samper et al., 2008a; Marty et al., 2010; Lu et al., 2011). Such models usually rely on simplifications of the geometry and dimensionality of the problem. Detailed three-dimensional flow and transport models, on the other hand, generally oversimplify geochemical reactions (Pepin *et al*., 2008). Integrated performance assessment calculations usually rely on simplified models to reduce the computation time. Such simplifications, however, may lead to significant errors. Simplifications in the model geometry of a radioactive waste repository have been analyzed within the framework of European Integrated Projects such as NFPRO by Mathieu et al. (2006) and Samper et al. (2007) and PAMINA by Genty *et al.* (2009). Model results derived from 1D parallel and 1D axisymmetric geochemical models of the near field of a HLW repository in clay show that the penetration into the bentonite buffer of the high pH plume caused by the degradation of the concrete liner after 10^4 years computed with a 1D radial axisymmetric model is larger than that obtained with a 1D parallel model. Solute diffusion in a 1D axisymmetric model is faster than in a 1D parallel model because the diffusive area in radial coordinates depends on the square of the radial distance, *r*, while it does not depend on *r* for a 1D parallel model (Mathieu et al. 2006; Samper et al., 2007).

There is a clear need to study and identify the appropriate assumptions and simplifications for modeling radionuclide migration in a radioactive waste repository. Here we present conceptual and numerical models of radionuclide diffusion and sorption around a HLW repository in clay according to the French reference concept (ANDRA, 2005a, 2005b). The following models of increasing dimensionality are compared: 1) 1D transport perpendicular to the axes of the disposal cells; 2) 1D axisymmetric transport around disposal cells for bounded and unbounded domains; 3) 2D transport through vertical planes; and 4) 1D vertical transport from the disposal cells into the overlying Oxfordian formation. The paper starts with the problem formulation. Then, the numerical model is presented. Model results are discussed later. The paper ends with the main conclusions.

2. PROBLEM FORMULATION

In the French reference concept for vitrified waste (type C) canisters are emplaced in horizontal cells of 70 cm of diameter and 40 m of length (ANDRA, 2005a; 2005b). The spacing between disposal cells is equal to 13 m. Disposal cells have a metal sleeve to enable package handling for their emplacement and possible future retrieval (Figure 1). The excavation damaged zone, *EDZ*, around the cells is deemed to be irrelevant given the small diameter of the cells. Instead

of the EDZ, a micro-fissured zone of a few cm may form due to the mechanical unloading (Genty et al., 2009). Such micro-cracking is expected to close soon after cell closure.

The repository will be emplaced in the Callovo-Oxfordian (C-Ox) clay formation at a depth of 65 m below the overlying Oxfordian limestone formation.

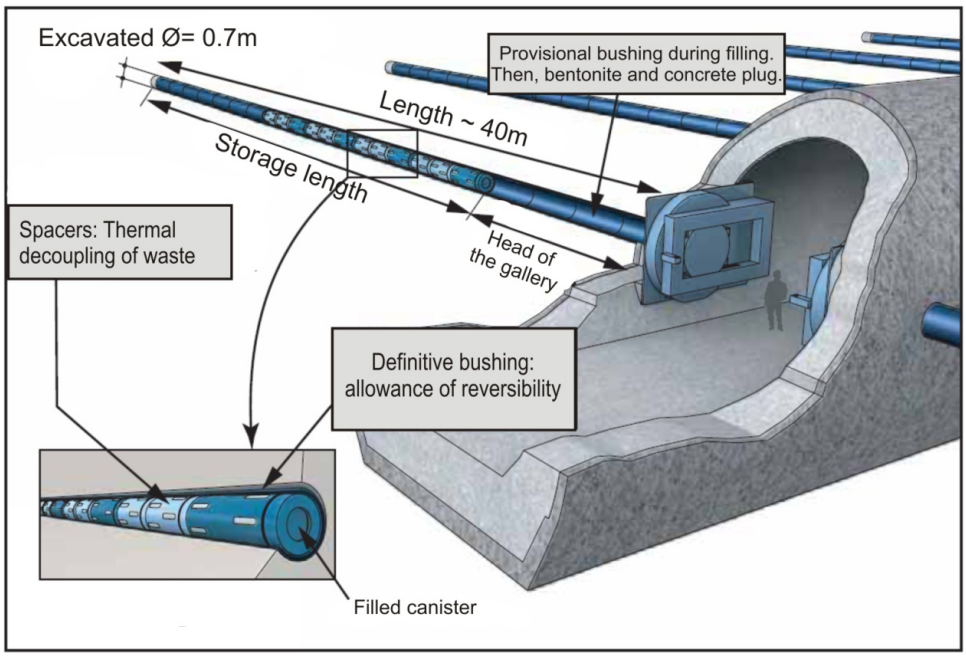

Figure 1 Setup of the repository for wastes type C (modified from ANDRA, 2005a).

Radionuclides are released in the disposal cells. They are free to migrate into the clay formation once the canisters fail. Our model aims at simulating radionuclide migration at that stage of the evolution of the repository when the canisters have failed. At that time, the engineered barriers and the host rock are expected to be resaturated. Simulations are performed over a million years. Given the low hydraulic conductivity of C-Ox clay which ranges from $5{\cdot}10^{-14}$ to $5{\cdot}10^{-13}$ m/s (ANDRA, 2005a), radionuclide transport takes place mostly by molecular diffusion.

HTO is a neutral tracer which is part of the water molecule. In our calculations HTO is assumed to be an ideal and conservative tracer which neither decays nor sorbs. ^{36}Cl is the radioactive isotope of chlorine, *Cl*, which has a half-life of $3.01{\cdot}10^{5}$ years. Given the long simulation time, it has been treated as stable. ^{36}Cl is present mostly as the anion Cl^- which experiences anion exclusion. Caesium, *Cs*, is a fission product that is created in the UO_2 pellets during irradiation in the reactor. Although *Cs* has many isotopes, the stable isotope ^{133}Cs is the most abundant. Dissolved Cs is usually found as Cs^+, except for large Cl^- concentrations when the concentration of CsCl(aq) may be relevant also. Cs^+ sorption onto clay occurs mainly via cation exchange. Cs^+ sorbs rapidly and achieves equilibrium almost instantaneously (Murali and Mathur, 2002; Khan, 2003; Montavon et al., 2006; Samper et al., 2010).

The most abundant isotope of uranium is ^{238}U. Given its very long half-life ($4.47 \cdot 10^9$ years), it can be treated as a stable isotope. In a deep underground radioactive waste repository, the subsurface water has reducing properties in natural conditions. U(IV) has a very low migration ability due to the formation of the poorly soluble hydroxide $U(OH)_4$ (Duro et al., 2006; Omel'yanenko et al., 2007). The dissolved concentration of uranium in subsurface water is usually smaller than 10^{-8} mol/L due to the low solubility of U under near-neutral and reducing conditions (Duro et al., 2006; Omel'yanenko et al., 2007). U sorption occurs by cation exchange and surface complexation. The K_d of U(IV) in bentonite ranges from 3.6 10^3 to 1.113 10^6 L/Kg (Vahlund et al., 2006).

3. NUMERICAL MODEL

3.1. Solute transport equation

The transport equation for a radionuclide which diffuses through a low permeability medium is given by (Bear, 1972):

$$\nabla \cdot (\bar{D}_e \cdot \nabla c) = \alpha \frac{\partial c}{\partial t} \qquad (1)$$

where c [ML^{-3}] is the radionuclide concentration, t [T] is time, α [-] is the capacity factor which is given by:

$$\alpha = \phi_{acc} + \rho K_d \qquad (2)$$

where Φ_{cc} [-] is the accessible porosity which is equal to the total porosity if the radionuclide is not affected by anion exclusion, K_d [L^3M^{-1}] is the distribution coefficient, and ρ [ML^{-3}] is the bulk density. $\bar{D}_e$ [$L^2\,T^{-1}$] is the effective diffusion tensor which in a coordinate system defined along the bedding planes is given by

$$\bar{D}_e = \begin{pmatrix} D_{e//} & 0 & 0 \\ 0 & D_{e//} & 0 \\ 0 & 0 & D_{e\perp} \end{pmatrix} \qquad (3)$$

where $D_{e//}$ and $D_{e\perp}$ are the components of the tensor parallel and normal to the bedding, respectively.

The apparent diffusion coefficient, D_a, takes into account the combined effect of diffusion and sorption and is defined as

$$D_a = \frac{D_e}{f_{cc} + r K_d} \qquad (4)$$

Radioactive decay is neglected here.

3.2. Model domain and spatial discretization

Although radionuclide migration around the repository is fully three dimensional (Genty et al., 2009), radionuclide diffusion exhibits symmetry with respect to the mean horizontal plane of the repository because the repository is located at the middle depth of the Callovo-Oxfordian formation (Figure 2). Therefore, radionuclide migration can be studied in a half of the domain.

Radionuclide migration is assumed to be symmetric with respect to two sets of vertical planes. The first set of symmetry planes contain the axis the disposal cells. The second set of vertical planes pass through the middle point between two adjacent disposal cells. The distance between two adjacent vertical planes of symmetry is equal to the half distance between two adjacent cells which is 6.5 m (ANDRA, 2005b). For a homogeneous formation, radionuclide migration can be studied in a 2D model domain of $65 \cdot 6.5$ m^2 (see Figure 2). The domain is discretized with a finite element mesh of 4550 triangular elements and 2388 nodes. The size of the elements is small near the disposal cell and increases away from the cell (Figure 3).

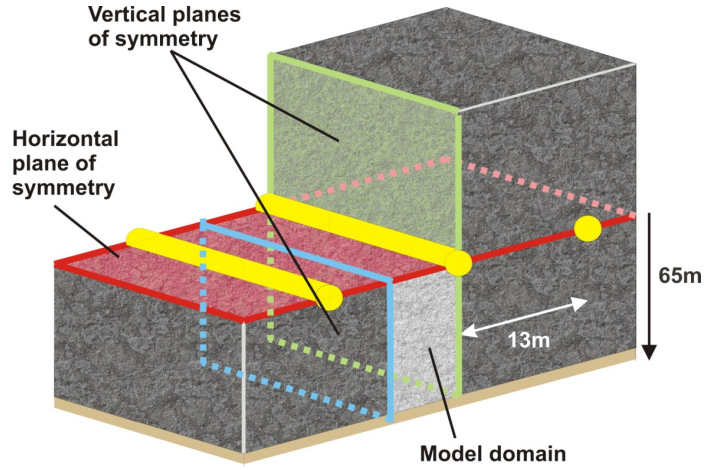

Figure 2 Sketch of the disposal cells layout in the C-Ox clay formation showing the 2D model domain and the following three planes of symmetry: 1) A horizontal plane which divides the cells in two equal parts; 2) A vertical plane that divides the cells vertically in two parts and 3) A vertical plane equidistant to two adjacent cells.

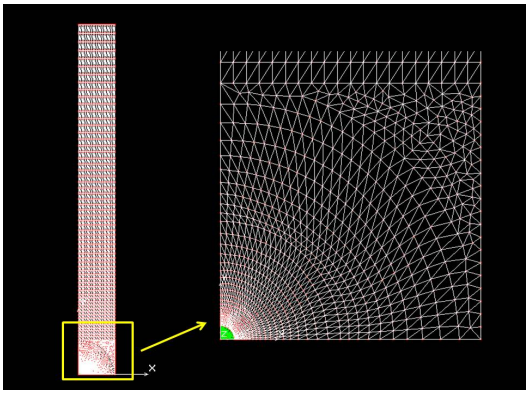

Figure 3 Finite elements mesh of the 2D model which extends over a domain of $6.5 \cdot 65$ m^2. Also shown is a zoom of the area around the disposal cell.

There are several stages in the time evolution of radionuclide migration from the disposal cell to the outflow boundary through the C-Ox clay formation. Radionuclides diffuse from the disposal cell into the C-Ox clay in the first stage in an axisymmetric pattern. This stage lasts for a time t^* such that $0 < t < t^*$, where t^* is the time needed for the radionuclide to arrive at the middle point between two adjacent cells. Axial symmetry vanishes in the second stage when the radionuclides migrate both in the horizontal and the vertical directions. The third stage takes place at late times when radionuclide migration is mostly vertical and can be approximated with a 1D vertical grid. Figure 4 shows the contour plots of computed concentrations of HTO and illustrates the three stages.

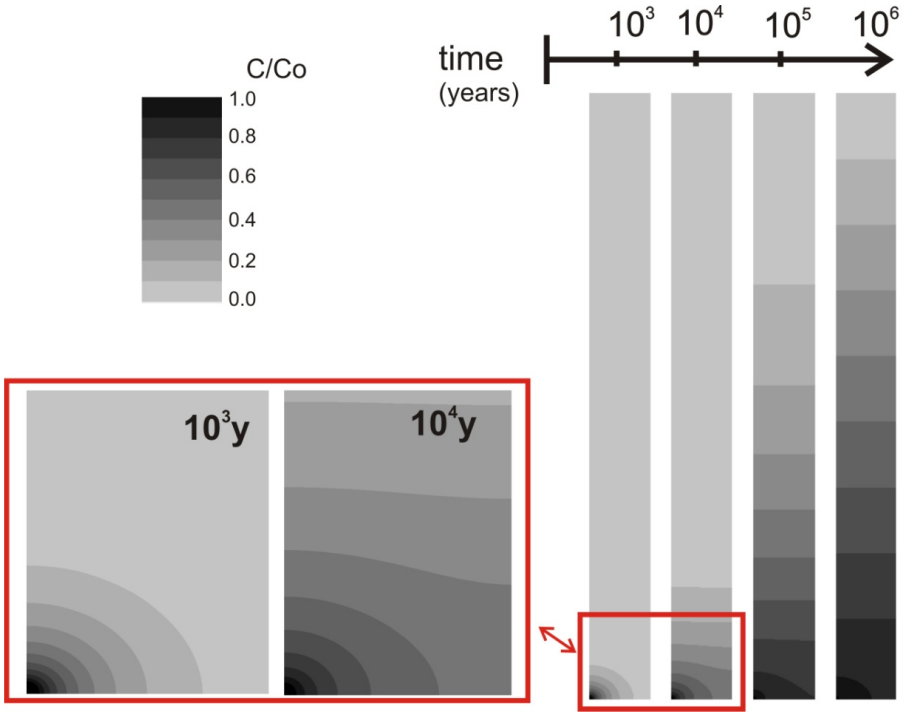

Figure 4 Computed HTO concentrations with a 2D model at 10^3, 10^4, 10^5 and 10^6 years. HTO transport is axisymmetric for $t < 10^3$ years. Transport is 2D for $10^4 < t < 10^5$ years. The diffusive flux at late times is approximately 1D vertical.

The origin of Cartesian coordinate system (x,y) is taken at the center of the disposal cell. The model domain is bounded in the horizontal direction at x = 6.5 m and in the vertical direction at y = 65 m, the vertical distance from the cell to the overlying Oxfordian formation. Radionuclide diffusion during the first stage can be studied with a 1D axisymmetric model around disposal cells. The domain is bounded in the horizontal direction at x = 6.5 m.

1D axisymmetric models sometimes are solved by using 1D parallel grids due to code limitations. Computed results with 1D axisymmetric and a 1D parallel grids have been compared to evaluate the errors committed by adopting a 1D parallel grid for solving a 1D axisymmetric problem. The diffusive area in a 1D axisymmetric model depends on the square of the radial distance, *r*, while the diffusive area is constant for a 1D parallel model (see Figure 5). There are several options to set

the equivalent thickness of the 1D parallel model, *b*. It can be taken equal to the length of the circumference of the disposal cell, L_i, which is equal to $2\pi R_i$ with R_i = 0.35 m. On the other hand, it can be taken equal to $2\pi R_e$, the length of the circumference corresponding to the half-distance between two adjacent cells, L_e, which is given by $2\pi R_e$ with R_e = 6.5 m. The 1D parallel grid has the same water volume as the 1D axisymmetric grid when the thickness b is equal to the average of L_i and L_e, that is $b = \pi (R_e + R_i)$.

The 1D vertical model of the third stage extends from y = 0 to y = 65 m. In this case, radionuclides are released at y = 0.

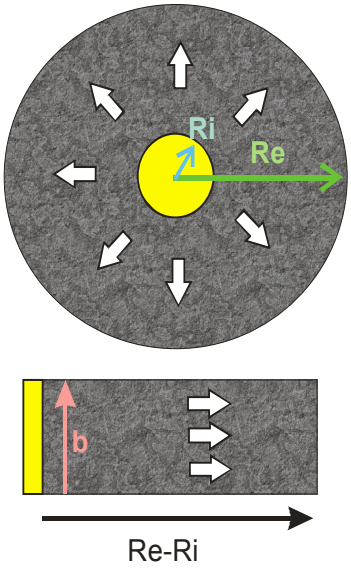

Figure 5 Sketch of the 1D axisymmetric and 1D parallel models. R_i and R_e are the internal and external radii.

3.3. Material zones and boundary conditions

The numerical model considers two material zones: (1) The disposal cell where radionuclides are released and (2) The C-Ox clay formation. The diffusion coefficient for the cell is taken sufficiently large to ensure a homogenous radionuclide concentration within the disposal cell.

The Callovo-Oxfordian formation shows a horizontal stratification with an anisotropic effective diffusion tensor. The horizontal component $D_{e//}$ is 1.56 larger than the vertical component $D_{e\perp}$ (Dewonck, 2007 and Samper et al. 2008b). Transport parameters in the C-Ox clay are radionuclide dependent. The values of the effective diffusion coefficient perpendicular to the stratification, $D_{e-|}$, the accessible porosity, Φ_{cc} and the distribution coefficient, K_d, for HTO, Cl^- and Cs^+ were taken from Dewonck (2007) and were obtained from laboratory experiments. On the other hand, the transport parameters of $^{238}U(IV)$ were taken from Vahlund et al. (2006). The diffusion and sorption parameters of the radionuclides are listed in Table 1.

Table 1 Radionuclide diffusion and sorption parameters in clay: $D_{e\perp}$ and $D_{e//}$ are the vertical and horizontal effective diffusion components, Φ_{cc} is the accessible porosity, K_d is the distribution coefficient, and $D_{a//}$ is the horizontal component of the apparent diffusion.

Radionuclide	$D_{e\perp}$ (m^2/s)	$D_{e//}$ (m^2/s)	Φ_{cc}	K_d (L/Kg)	$D_{a//}$ (m^2/s)
HTO	$2.6\cdot10^{-11}$	$4.1\cdot10^{-11}$	0.18	0	$2.2\cdot10^{-10}$
$^{36}Cl^-$	$6.2\cdot10^{-12}$	$9.7\cdot10^{-12}$	0.06	0	$1.6\cdot10^{-10}$
$^{133}Cs^+$	$2.3\cdot10^{-10}$	$3.6\cdot10^{-10}$	0.18	50	$3.3\cdot10^{-12}$
$^{238}U(IV)$	$1.2\cdot10^{-10}$	$1.9\cdot10^{-10}$	0.18	3000	$2.9\cdot10^{-14}$

The effective diffusion coefficient D_e is taken equal to the horizontal component of the tensor, $D_{e//}$, for 1D transport perpendicular to the axes of the disposal cells while for the 1D vertical model, D_e is taken equal to $D_{e\perp}$.

Background radionuclide concentrations in the clay are assumed equal to zero. Radionuclides are released into the pore space of the disposal cell. Two types of boundary conditions are considered at the disposal cell: a constant concentration and an instantaneous unit pulse. These boundary conditions are imposed at the nodes lying in the disposal cell. The unit mass of the tracer is added instantaneously to the volume of water contained in the disposal cell. Similar to Samper et al. (2009b), it is assumed that disposal cells may contain 100 L of water per meter of cell. The rest of the external boundaries are impervious except for the top outflow boundary at the contact with the Oxfordian limestone where the concentration is prescribed to zero.

Model results are presented in terms of relative concentrations which are normalized by either the boundary or the initial concentrations.

3.4. Computer code

Radionuclide migration has been modeled with CORE^{2D} V4, a general-purpose non-isothermal multicomponent reactive transport code for two-dimensional saturated/unsaturated porous and fractured media (Samper et al. 2003; 2009a; 2011). It can solve simultaneously for groundwater flow, heat transport and multi-component reactive solute transport in saturated or unsaturated steady state or transient groundwater flow under general boundary conditions. CORE^{2D} has been widely used to model laboratory and *in situ* experiments performed for HLW disposal (Molinero and Samper 2006; Samper et al., 2008c; Zheng and Samper, 2008; Zheng et al., 2008, 2010), evaluate the long-term geochemical evolution of radioactive waste repositories in clay (Yang *et al.,* 2008), model the transport of corrosion products and their geochemical interactions with bentonite (Samper et al., 2008a) and evaluate the long-term transport and sorption of radionuclides through the bentonite barrier (Samper et al., 2010). The model results presented here use only the most basic features of CORE^{2D}. Its most advanced features will be used in the next stages of the study.

4. MODEL RESULTS

4.1. 2D model results

Figure 4 shows the contour plots of computed concentrations of HTO at 10^3, 10^4, 10^5 and 10^6 years for a constant concentration at the disposal cell. Contour lines are axisymmetric for t < 10^3 years. In the second stage when HTO reaches the bottom right boundary at (6.5, 0), contour lines are no longer symmetric. The asymmetry of the migration can be observed clearly in the contour plots corresponding at t = 10^4 and 10^5 years. Contour plots become nearly horizontal and the diffusive flux is approximately vertical for t > 10^5 years.

Diffusion patterns are different for each radionuclide because the diffusive rate is proportional to the apparent diffusion coefficient. The diffusive rate of ^{238}U(IV) is two orders of magnitude slower than that of $^{133}Cs^+$ which in turn is two orders of magnitude slower than those of HTO and $^{36}Cl^-$ (see Table 1). The contour line corresponding to a relative concentration of 0.1 for HTO after t = 10^3 years is located at a distance of 3.2 m from the disposal cell. Such distance is 2.7 m for $^{36}Cl^-$. For $^{133}Cs^+$ it is 0.7 m while for ^{238}U(IV) is two orders of magnitude smaller than that of HTO (see Figure 6). Furthermore, diffusion shows axial symmetry until t = 10^4 years for $^{133}Cs^+$ and t = 10^6 years for ^{238}U(IV).

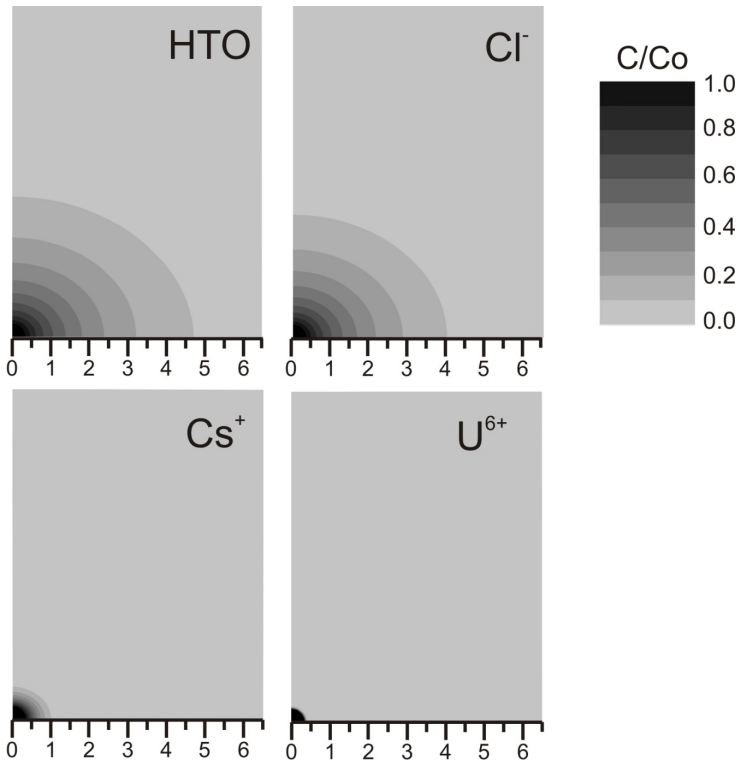

Figure 6 Computed radionuclide concentrations with a 2D model at 103 years considering a constant radionuclide concentration at the disposal cell. Transport is axisymmetric for all the tracers at this time. The relative concentration is larger than 0.1 for distances to the disposal cell smaller than 3.2 m for HTO, 2.7 m for $^{36}Cl^-$, 0.7 m for $^{133}Cs^+$ and 0.4 m for $^{238}U^{(IV)}$.

Diffusion patterns are also different depending on the boundary condition at the disposal cell. The radionuclide mass released at the disposal cell with an instantaneous pulse is smaller than the mass injected with a constant concentration. Therefore, concentration gradients with an instantaneous pulse dissipate faster than in the case of constant concentration.

4.2. 1D axisymmetric models

Radionuclide migration through the C-Ox clay formation has been simulated by using two 1D axisymmetric models around the disposal cell. They differ in the position of the outer boundary. The first model is the so-called bounded model in which the outer boundary is located at r = 6.5 m to account for the boundary effect of two adjacent cells. The second model is denoted here as the "unbounded model". It disregards the effect of the neighbor cell. The outer boundary of this model is located at a distance of 65 m to account for the effect of the top boundary. The results of both models are identical as long as the radionuclides do not reach the location at r = 6.5 m. Later, the radionuclide concentrations for the bounded model at that location are larger than those computed with the unbounded model due to the boundary effect.

The arrival time of a radionuclide to r = 6.5 m is the time needed for the relative concentration of the radionuclide to attain a threshold value greater than zero. Arrival times have been computed for threshold concentrations of 10^{-3} and 10^{-6} (see Table 2). A bounded model is acceptable for $^{238}U(IV)$. It is only acceptable for $t < 8 \cdot 10^3$ years for $^{133}Cs^+$ for a constant concentration and $t < 2.3 \cdot 10^4$ years for an instantaneous pulse. It is acceptable only for t < 120 years for HTO and $^{36}Cl^-$.

Table 2 Arrival times of the radionuclides to the boundary located at the plane of symmetry located at the middle point between two adjacent cells. Results are listed for two threshold relative concentrations $\mathbf{C/C_o}$ and two types of boundary conditions at the disposal cell: constant concentration and instantaneous pulse. Here * means that the radionuclide does not reach this point for the simulation time of 1Ma.

Radionuclide	Arrival times (years)			
	Constant concentration		Instantaneous pulse	
	$C/C_o > 10^{-6}$	$C/C_o > 10^{-3}$	$C/C_o > 10^{-6}$	$C/C_o > 10^{-3}$
HTO	112	273	122	437
$^{36}Cl^-$	157	381	162	463
$^{133}Cs^+$	7648	18650	22930	*
$^{238}U(IV)$	881600	*	*	*

4.3. 1D parallel and axisymmetric models

Model results computed with a 1D parallel model for several values of the thickness b are compared to those calculated with the 1D axisymmetric model. Figure 7a shows the comparison of the breakthrough curves at r = 6.5 m for HTO and $^{133}Cs^{+}$ calculated with the 1D radial and parallel models for a constant concentration at the cell. The results of the 1D parallel model in this case do not depend on the value of b. The concentrations computed with both models are markedly different for all the radionuclides. The 1D parallel model predicts a faster arrival of the radionuclides at the boundary than the 1D axisymmetric model.

In the case of an instantaneous mass pulse, M, the computed concentrations varies with b because the solution depends on the mass per unit thickness, M/b, which decreases when b increases. Therefore, computed concentrations are largest for the minimum b (Figure 7b). The comparison of computed HTO concentrations at the disposal cell and at the external boundary (r = 6.5 m) for several values of b show that the differences between the results of the 1D parallel and 1D axisymmetric models increase with time and are largest for the minimum b (see Figure 7b and 7c). The results of the 1D parallel model for HTO are very inaccurate for the minimum and the maximum values of b. Computed results coincide with those of the 1D axisymmetric after 2000 years for the average value of b. The conclusions for $^{36}Cl^{-}$ are similar to those of HTO. For $^{133}Cs^{+}$ and $^{238}U(IV)$, however, the 1D parallel model deviates significantly from the 1D axisymmetric model regardless the value of b (not shown here).

4.4. Comparison of the 2D and the 1D vertical models

The 1D parallel model in the vertical direction assumes that the radionuclide mass, M, is released instantaneously and uniformly throughout the bottom boundary at z = 0 corresponding to the depth of the disposal cells. The 1D vertical model neglects the horizontal component of the diffusive flux which is especially relevant at intermediate times. Figure 8 shows the comparison of the computed concentrations with the 2D and the 1D vertical models along the vertical line passing through the disposal cell. In the case of a constant concentration at the disposal cell, the concentrations of all radionuclides computed with the 1D vertical model deviate largely from those computed with the 2D model. The results of the 1D vertical model agree with those of the 2D model only after 10^4 years and for conservative radionuclides released instantaneously (Figure 8).

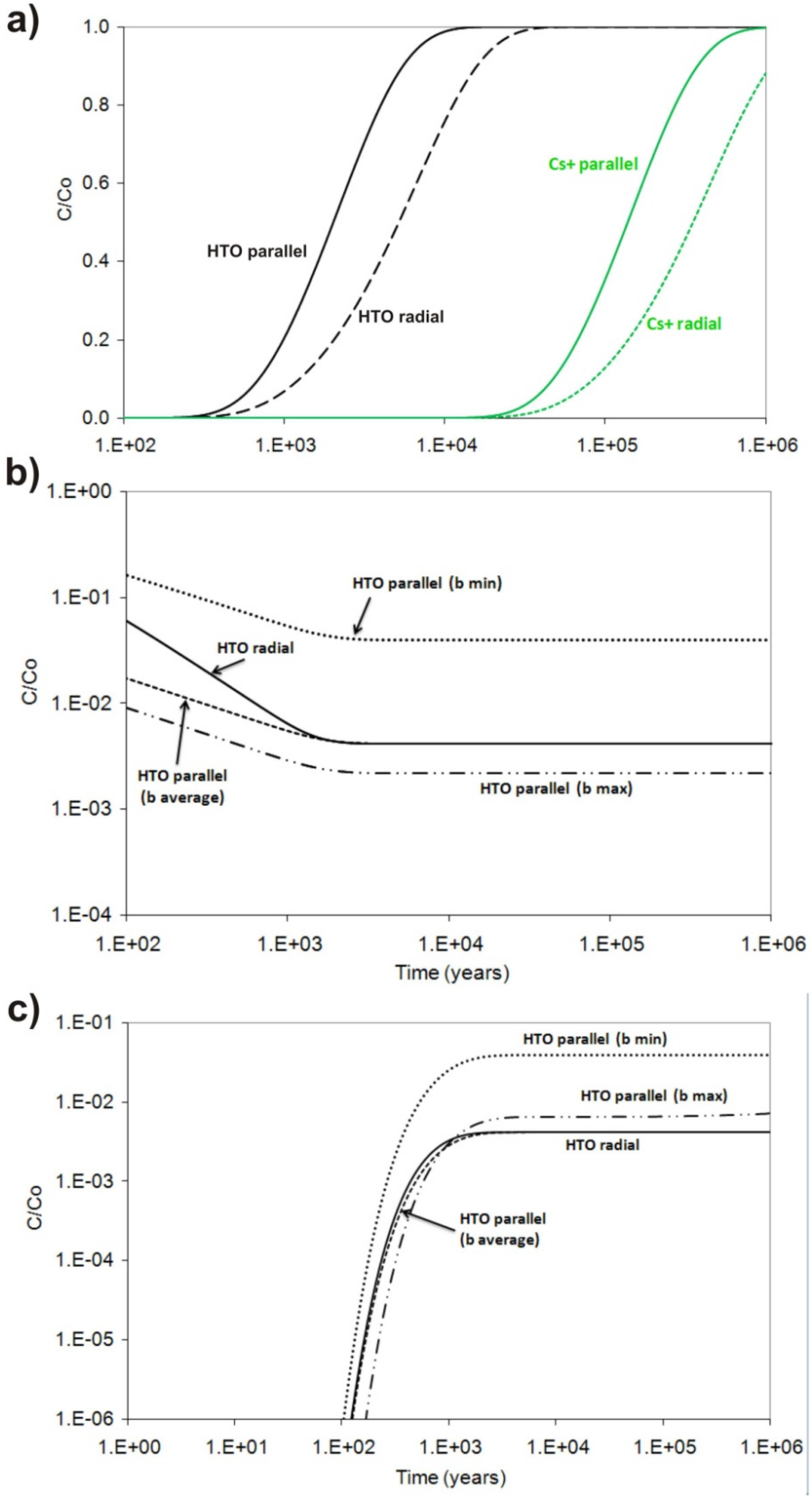

Figure 7 Comparison of the computed concentrations using the 1D axisymmetric and 1D parallel models: (a) Comparison of HTO and $^{133}Cs^{+}$ concentrations at the boundary located 6.5 m from the disposal cell axis for the case of constant concentration at the disposal cell. (b) Comparison of HTO dilution at the disposal cell in the case of an instantaneous pulse for different values of b. (c) Comparison of HTO computed concentrations at the boundary (r = 6.5 m) in the case of an instantaneous pulse for different values of b.

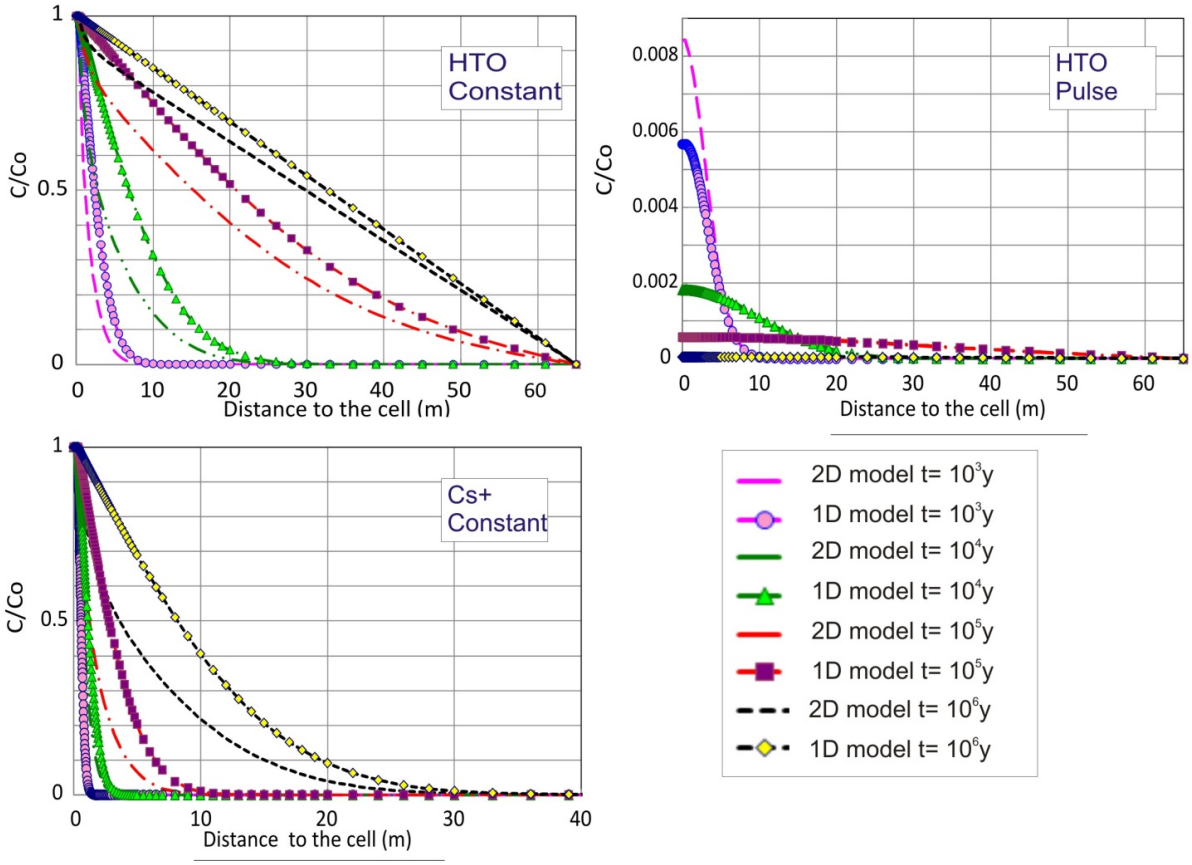

Figure 8 Comparison of the concentration profiles along the left boundary computed with the 2D and the 1D vertical models. Results are presented for HTO considering a constant concentration (top left) and an instantaneous pulse (top right) and for $^{133}Cs^{+}$ (bottom) considering a constant concentration at the cell.

5. CONCLUSIONS

Conceptual and numerical models of radionuclide diffusion and sorption around a radioactive waste repository in clay according to the French reference concept have been presented for HTO, $^{36}Cl^{-}$, $^{133}Cs^{+}$ and ^{238}U (IV). Radionuclides are released into the disposal cell either at a fixed concentration or as an instantaneous unit pulse. Models of increasing dimensionality have been performed for: 1) 1D transport perpendicular to the axes of the disposal cells; 2) 1D axisymmetric transport around disposal cells for bounded and unbounded domains; 3) 2D transport through vertical planes; and 4) 1D vertical transport from the disposal cells into the overlying Oxfordian formation. The results of the 1D unbounded model are always acceptable for ^{238}U. Such model is valid for $^{133}Cs^{+}$ for $0 < t < 10^{4}$ years while it is valid for HTO and $^{36}Cl^{-}$ only for $t < 10^{3}$ years. Computed concentrations with the 1D parallel and the 1D axisymmetric models are markedly different and, therefore, the use of the 1D parallel model for the long-term modeling of radionuclide migration

from the repository should be avoided. The 1D vertical model is valid only for conservative radionuclides released instantaneously and leads always to large errors for all radionuclides for a constant concentration.

Here we have presented the results of the first step of our study for the selection of the most appropriate assumptions and simplifications for the numerical model of the geochemical evolution and radionuclide migration in a radioactive waste repository. The next steps will account for: 1) The decay of radionuclides; 2) The time evolution of the geochemical conditions using reactive transport models; 3) The spatial variability of clay parameters; 4) The uncertainties in the boundary conditions of the CO-x clay formation and the porosity of the disposal cells; and 5) The actual 3D configuration of the repository.

6. Acknowledgements

This work was supported by the European Union through the PAMINA Project ((FP6-036404), the University of A Coruña through a research scholarship awarded to the third author, the Spanish Ministry of Science and Technology through project CGL2006-09080 and a research scholarship awarded to the second author, the Xunta de Galicia (Maria Barbeito Program) through a research scholarship awarded to the fourth author. Parts of this work were performed during the sabbatical stay of Javier Samper at the University of Strasbourg from October 2008 to August 2009 which was supported by the University of A Coruña, the Spanish Ministry of Science and Technology and the University of Strasbourg. We thank also E. Ledoux and Angelo Borrelli for their comments and recommendations which have improved the paper.

7. REFERENCES

ANDRA, 2005a. Dossier 2005 Argile –Synthèse: Evaluation de la faisabilité du stockage géologique en formation argileuse.

ANDRA, 2005b. Dossier Argile –Tome: Arquitecture et gestion du stockage géologique.

Bear, J. (1978) Dynamics of fluids in porous media. Dover, NY, USA

Dewonck, S., 2007. Experimentation DIR: Synthèse des résultats obtenus au 01/03/07. *Rapport ANDRA* D.RP.ALS.07.0044.

Duro, L., Grivé, M., Cera E, Gaona X, Doménech C, Bruno, J., 2006. Determination and assessment of the concentration limits to be used in SR-Can. *SKB Technical report* TR-06-32.

Genty, A., Mathieu, G., Weetjens, E, 2009. Benchmark calculations in clay. *Deliverable 4.2.4 of PAMINA Integrated Project*.

Khan, S.A., 2003. Sorption of the long-lived radionuclides Cesium-134, Strotium-85 and Cobalt-60 on bentonite. *Journal of Radioanalytical and Nuclear Chemistry* 258 (1), 3-6.

Molinero, J., Samper, J., 2006. Modeling of reactive solute transport in fracture zones of granitic bedrocks. *Journal Contaminant Hydrology* 82, 293–318.

Montavon, G., Alhajji, E., Grambow, B., 2006. Study of the interaction of Ni^{2+} and Cs^{+} on MX-80 bentonite: effect of compaction using the "Capillary method". *Environmental Science and Technology* 40, 4672-4679.

Murali, M.S., Mathur, J.N., 2002. Sorption characteristics of Am(III), Sr(II) and Cs(I) on bentonite and granite. *Journal of Radioanalytical and Nuclear Chemistry* 254(1), 129-136.

Lu, C., Samper, J., Fritz, B., Clement, A., Montenegro, L., 2011. Interactions of corrosion products and bentonite: An Extended multicomponent reactive transport model. *Physics and Chemistry of the Earth* (accepted).

Marty, N., Fritz, B., Clément, A., Michau, N., 2010. Modeling the long term alteration of the engineered bentonite barrier in an underground radioactive waste repository. *Applied Clay Science* 47, 1-2, 82-90.

Mathieu, G., Pellegrini, D., Serres, C., 2006. Modeling of cement/clay interactions, gas transport and radionuclide transport. D5.1.9. NF-PRO Project, European Commission.

Omel'yanenko, B.I., Petrov, V.A., Poluektov, V.V., 2007. Behavior of uranium under conditions of interaction of rocks and ores with subsurface water. *Geology of Ore Deposits*. 49, 5, 378-391.

Pepin, G., Plas, F., Nilsson, K.F., Prvakova, S., 2008. Second Benchmark specification for the uncertainty analysis based on the example of the French clay site. Milestone M 4.3.3 of PAMINA Integrated Project.

Samper, J., Yang, C., Montenegro, L., 2003. Users manual of CORE2D version 4: A COde for groundwater flow and REactive solute transport. Universidad de A Coruña, A Coruña, Spain.

Samper, J., Yang, Ch., Montenegro, L., Bonilla, M., Lu, C., Yang, Q., Zheng, L., 2007. Mass and energy balance and flux calculations for radionuclide release and geochemical evolution for SF carbon steel HLW repositories in clay and granite. D5.1.13. NF-PRO Project, European Commission.

Samper, J., Lu, C., Montenegro, L., 2008a. Coupled hydrogeochemical calculations of the interactions of corrosion products and bentonite. *Physics and Chemistry of the Earth* 33, S306-S316.

Samper, J., Yang, Q., Yi, S., García-Gutiérrez, M., Missana, T., Mingarro, M., Alonso, Ú., Cormenzana, J.L., 2008b. Numerical modelling of large-scale solid-source diffusion experiment in Callovo-Oxfordian clay. *Physics and Chemistry of the Earth* 33, S208-S215.

Samper, J., Zheng, L., Fernández, A.M., Montenegro, L., 2008c. Inverse modeling of multicomponent reactive transport through single and dual porosity media. *Journal of Contaminant Hydrology* 98, 3-4, 115-127.

Samper, J., Xu, T., Yang, C., 2009a. A sequential partly iterative approach for multicomponent reactive transport with $CORE^{2D}$. *Computer Geoscience,* doi: 10.1007/s10596-008-9119-5.

Samper, J., Lu, C., Cormenzana, J.L., Ma, H., Cuñado, M.A., 2009b. Benchmark calculations in granite, *Deliverable 4.1.2 of PAMINA Integrated Project.*

Samper, J., Lu, C., Cormenzana, J.L., Ma, H., Montenegro, L., Cuñado, M.A., 2010. Testing K_d models of Cs^{+} in the near field of a HLW repository in granite with a reactive transport model. *Physics and Chemistry of the Earth* 35, 278–283.

Samper, J., Yang, C., Zheng, L., Montenegro, L., Moreira, S., Lu, C., 2011. *$CORE^{2D}$ V4: A code for water flow, heat and solute transport, geochemical reactions, and microbial processes.* Electronic book on Reactive Transport Modelling. Chapter 7.

Vahlund, F.J., Andersson, J.A., Streamflow, A.B., Löfgren, M., 2006.Data report for the safety assessment. SR-Can. *SKB Technical Report TR-06-25.*

Yang, C., Samper, J., Montenegro, L., 2008. A coupled non-isothermal reactive transport model for long-term geochemical evolution of a HLW repository in clay. *Environmental Geology* 53, 1627–1638.

Zheng, L., Samper, J., 2008. Coupled THMC model of FEBEX mock-up test. *Physics and Chemistry of the Earth* 33, S486–S498.

Zheng, L., Samper, J., Montenegro, L., Mayor, J.C., 2008. Flow and reactive transport model of a ventilation experiment in Opallinus clay. *Physics and Chemistry of the Earth* 33, 14-16, 1009-1018.

Zheng, L., Samper, J., Montenegro, L., Fernández, A.M., 2010. A coupled THMC model of a heating and hydration laboratory experiment in unsaturated compacted FEBEX bentonite. *Journal of Hydrology,* doi: 10.1016/j.jhydrol.2010.03.009.